ARAB ACADEMY FOR SCIENCE, TECHNOLOGY AND MARITIME TRANSPORT

College of Engineering and Technology

Department of Mechanical Engineering

PERFORMANCE ANALYSIS OF A CENTRIFUGAL PUMP WITH VARYING BLADE NUMBER AND ANGLES UNDER STABLE AND UNSTABLE EMULSION FLOWS: EXPERIMENTAL, ANALYTICAL, AND NUMERICAL APPROACHES

By

MOHAMED ELSAYED MOHAMED ABDELAAL NOURELDIN

A thesis submitted to AASTMT in partial

Fulfillment of the requirements for the award of the degree of

DOCTOR OF PHILOSOPHY

in

MECHANICAL ENGINEERING

Supervisors

Prof. Hassan A. Elgamal
College of Engineering
Alexandria University
Egypt

Prof. Ahmed A. Hanafy
College of Engineering and Technology, AASTMT
Alexandria, Egypt

Prof. Rola S. Afify
College of Engineering and Technology, AASTMT
Alexandria, Egypt

2026

Abstract

The hydraulic performance of a centrifugal pump operating with water and oil-water emulsions is investigated in this thesis using an integrated experimental, theoretical, and numerical approach. Experimental tests are conducted at a constant rotational speed to evaluate pump head, efficiency, and power consumption under varying flow rates, oil volume fractions, and emulsion stability conditions. A theoretical performance model based on Euler pump theory and loss analysis is developed to assess the influence of impeller blade number and blade inlet and outlet angles on pump head and efficiency. In parallel, three-dimensional computational fluid dynamics (CFD) simulations are performed using ANSYS Fluent to resolve the internal flow field within the impeller and volute, enabling detailed analysis of velocity distributions, pressure fields, and flow separation characteristics. The numerical framework employs a steady-state rotating reference frame and evaluates multiple turbulence models, with the shear stress transport (SST) k-ω model providing the best agreement with experimental measurements. Grid independence is established, and numerical predictions are validated against experimental pump performance curves. The results demonstrate that increasing oil concentration leads to a reduction in pump head and efficiency due to increased effective viscosity and internal hydraulic losses. Moreover, stable emulsions consistently exhibit superior hydraulic performance compared to unstable emulsions at the same oil concentration. Parametric investigations reveal that impeller geometry has a dominant influence on pump performance, where increasing blade number enhances pump head but may reduce efficiency due to increased hydraulic losses, while an optimal combination of blade inlet and outlet angles yields improved overall performance. The findings of this research

provide physical insight into the mechanisms governing centrifugal pump operation with emulsions and offer practical guidance for impeller design and performance optimization in applications involving contaminated or multiphase working fluids.

Table of Contents

Page No.

Table of Contents (Cont'd)

Page No.

Table of Contents (Cont'd)

Page No.

NOMENCLATURE

Symbols

A	Area, cross section [m^2]
Ac	Volute throat area [m^2]
a	Distance between vanes [m]
b	Width of vane [m]
C	Coefficient
$C_{fr,La}$	The impeller friction loss coefficient
C_{sh}	The shock loss coefficient (0.5 – 0.7)
c	Absolute velocity[m/s]
c_{1u}	The circumferential components of absolute velocity at inlet [m/s]
c_{2u}	The circumferential components of absolute velocity at outlet [m/s]
c_{ax}	Axial velocity in gap [m/s]
d	Diameter [m]
e	The blade thickness [m]
g	Gravitational acceleration [m/s^2]
H	Head [m]
k	Rotation factor
kw	Influence of impeller inlet diameter on slip factor
$L_{sh,La}$	Impeller loss [m]
l	Length [m]
le	The blade length [m]
n	Rotational speed [rpm]
P	Pressure [Pa]
P	Power [W]
P_{me}	The mechanical power loss due to the axial thrust losses [1%of useful power]
Q	Flowrate [m^3/s]
Qi	The impeller flow [m^3/s]
Q_{La}	Pump flow [m^3/s]
Q_{sp}	Pump internal leakage flow [m^3/s]
Re	Reynolds number ($Re = \rho \, v \, d \, / \, \mu$)
r	Radius [m]
s	Gap width [m]
s_{ax}	Axial distance between impeller shrouds and casing [m]
T	Shaft torque [N.m]
u_1	Circumferential velocities [m/s]
u_2	Circumferential velocities [m/s]
w	Relative velocity [m/s]
y	Geometry
Z	Sum of hydraulic losses [m]
z	Number of blade

Greek Symbols

α	Angle between direction of circumferential and absolute velocity [°]
β	Angle between relative velocity vector and negative direction of circumferential velocity [°]
γ	Slip factor
δ	Deviation angle [°]
ε	Roughness

η	Efficiency
ν	Kinematic viscosity [m^2/s]
ξ_{EA}	Inlet + outlet loss
ρ	Density [kg/m^3]
τ	Blade blockage factor
λ	Friction coefficient
ω	Shaft angular velocity [rad/s]
Φ	Holdup

Subscripts

1	Impeller blade leading edge
2	Impeller blade trailing edge
av	Average
ax	Axial
c	Casing/volute
e	Blade or vane
E	Emulsion
fr	Friction
h	Hydraulic
inf	Infinity
La	Impeller
m	Mechanical component
me	Mechanical
n	Inner diameter of suction nozzle
o	Oil
p	Static pressure created by the impeller
q	Average velocity calculated from continuity (to be distinguished from velocity vector)
r	Real
s	Shaft
sh	Shock
sp	Annular seal, leakage flow
th	Theoretical
u	Circumferential component
w	Water
v	Volumetric

Abbreviation

CFD	Computational Fluid Dynamics
ESP	Electrical Submersible Pumps
LDA	Laser Doppler Anemometry
LDV	Laser Doppler Velocimetry
LES	Large Eddy Simulation
NSE	Navier-Stokes Equations
o/w	oil-in-water
PIV	Particle Image Velocimetry
VR	Viscosity reduction
SDS	Sodium Dodecyl Sulfate
w/o	water-in-oil

Chemical Symbols

$CH_3(CH_2)_{11}OSO_3Na$ Sodium Dodecyl Sulfate

List of Figures

List of Figures (Cont'd)

List of Figures (Cont'd)

List of Figures (Cont'd)

List of Figures (Cont'd)

List of Figures (Cont'd)

CHAPTER FIVE

List of Figures (Cont'd)

List of Figures (Cont'd)

CHAPTER SIX

List of Figures (Cont'd)

List of Figures (Cont'd)

List of Tables

CHAPTER ONE

INTRODUCTION

CHAPTER ONE

INTRODUTION

1.1 INTRODUCTION

One of the important targets of the mechanical engineers and researcher's society is to reduce the energy used for the transportation of fluids through pipelines. As it is well known, the energy is expensive and of an ever growing cost. The major energy loss factor in a pipe line is due to friction in the boundary layer, the engineers and researchers had to come out with a new brilliant idea, applying a mixture of water and oil reduces friction losses and lowers energy consumption. By minimizing these losses and employing more efficient pumps, the overall used energy can be reduced significantly.

1.2 EMULSION FLOW IMPORTANCE

The emulsion is a mixture of two immiscible liquids, one of which is dispersed in the form of small droplets throughout the other. The dispersed liquid is known as the internal or discontinuous phase, whereas the dispersion medium is known as the external or continuous phase. Stable emulsion involves the presence of surfacants that inhibit coalescence of the dispersed droplets. In unstable emulsion, there is no additives (surfacant) added to the mixture, and the drop diameter distribution depends on the rate of drop break-up and coalescence. Emulsions form the basis of a wide variety of natural and manufactured materials, including foods, pharmaceuticals, biological fluids, agrochemicals, petrochemicals, cosmetics, and explosives. The desired rheology and stability of emulsion-based materials varies widely depending on their intended application. Manufacturers of emulsion-based materials must therefore have a good understanding of the factors that determine their rheology and stability in order to create products with the required physical characteristics.

Many advances have been made in the field of emulsions in recent years. Emulsion behavior is largely controlled by the properties of the adsorbed layers that stabilize the oil-water surfaces. The knowledge of surface tension alone is not sufficient to understand emulsion properties, and surface rheology plays an important role in a variety of dynamic processes. The complexity of petroleum emulsions comes from the oil composition in terms of surface-active molecules contained in the crude, such as low molecular weight fatty acids,

naphthenic acids and asphaltenes. The pronounced nonlinear behavior of surface rheology for asphaltene layers might explain differences in behavior between surfactant and asphaltene emulsions. These effects are very important in the case of heavy oils because this type of crude contains a large amount of asphaltene and surface-active compounds.[1]

Energy input through shaking, stirring, homogenizing, or spray processes are needed to initially form an emulsion. Over time, emulsions tend to revert to the stable state of the phases comprising the emulsion, an unstable emulsion will quickly separate unless shaken continuously. Whether an emulsion turns into a water-in-oil emulsion or an oil-in-water emulsion depends on the volume fraction of both phases and on the type of emulsifier.

Emulsions of crude oil and water can be encountered at many stages during drilling, producing, transporting and processing of crude oils and in many locations such as in hydrocarbon reservoirs, well bores, surface facilities, transportation systems and refineries. A good knowledge of petroleum emulsions is necessary for controlling and improving processes at all stages. The two important sets of emulsions are, an oil-in-water emulsion (oil is the dispersed phase) and water-in-oil emulsion (water is the dispersed phase). As crude oil rises from fissures of earth, it passes through narrow openings accompanied by water and agitation by pumping, gives rise to conditions favorable to the formation of water-in-oil emulsions. Emulsions are extremely fire resistant and highly incompressible with good cooling properties.

1.3 PARAMETERS AFFECTING THE CENTRIFUGAL PUMP PERFORMANCE

Centrifugal pumps are turbomachines that move liquids by increasing a given volume flow to a particular pressure. In turbomachines, energy transfer is always based on hydrodynamic processes, where all pressure and energy differences are typically proportional to the square of the rotor's circumferential speed.

A centrifugal pump is illustrated in Figure 1.1; it is mainly composed of a casing with a bearing housing for the pump shaft that drives the impeller. Via the suction nozzle, the fluid will enter the pump and travel to the impeller. Through a connection, a motor powers the overhanging impeller fixed on the shaft. Because the fluid flow takes a curved path, the impeller accelerates the fluid in a circumferential direction, transferring the energy required to move it. This causes the static pressure to rise in accordance with kinetics. To increase the static pressure, the fluid is decelerated in the volute and diffuser after leaving the impeller.

This is done to improve the kinetic energy at the impeller output. To increase the static pressure, the fluid is decelerated in the volute and diffuser after leaving the impeller. This is done to maximize the kinetic energy at the impeller output. The discharge nozzle is formed by the diffuser.

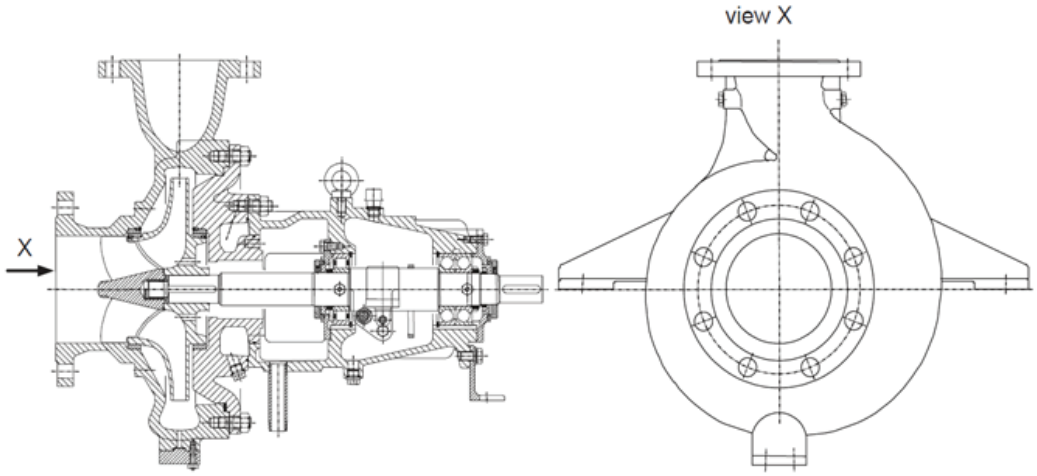

Fig. 1.1 Single-stage volute pump with bearing frame [51]

The impeller can be described by the hub, the rear shroud, the blades transferring energy to the fluid and the front shroud. In some applications the front shroud is omitted. In this case the impeller is termed “semi-open”. [51]

the cross section and the plan view of an impeller is shown in Figure 1.2. The pressure surface is the leading face of the blade of the rotating impeller it is usually subjected to the highest pressure for a given radius. It can also be identified as the pressure surface or pressure side. The suction surface is the opposite blade surface with the lower pressure accordingly it is also identified as the suction side.

Figure 1.2 Also defines the leading edge LE and the trailing edge TE of the blade.

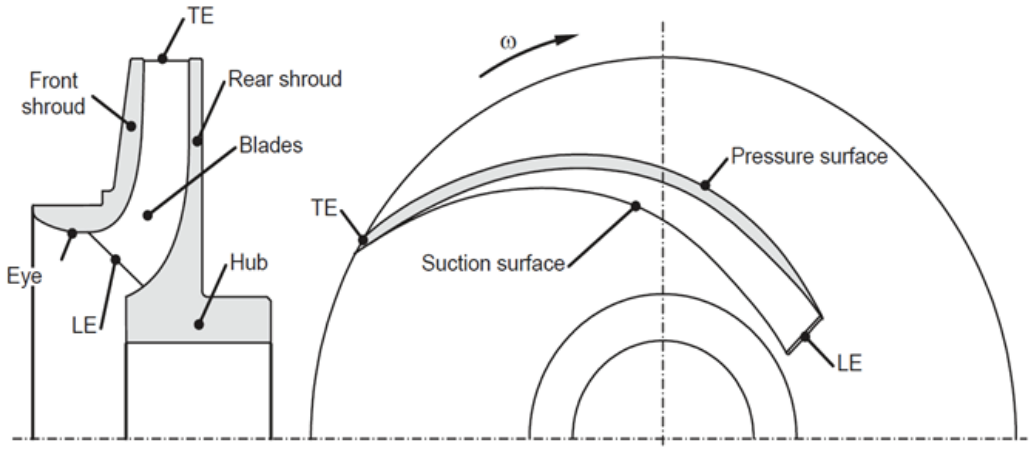

Fig. 1.2 Meridional section and plan view of a radial impeller,
LE: Leading edge, *TE*: Trailing edge [51]

Because impellers, volute casings and diffusers have complicated, three-dimensional curved surfaces, they are usually fabricated by casting. other applications impellers and diffusers require NC-milling, impellers and diffusers made entirely from sheet metal can also be found in some applications and some small pumps in some cases may even be made from plastics. The specific work Y is the total useful energy transmitted by the pump to the fluid per unit of mass. Y is measured between the suction and the discharge nozzle [51]. Y is identical to the total useful (isentropic) enthalpy rise Δh_{tot}. In incompressible flow we have $Y = \Delta h_{tot} = \Delta p_{tot}/\rho$

practically the head $H = Y/g$ is widely used (can also be identified as "total dynamic head"). It can be referred to as specific energy unit (or specific work):

$$Y = \Delta h_{tot} = \frac{p_{2\,tot} - p_{1\,tot}}{\rho} = gH \tag{1.1}$$

The total pressure consists of the static pressure p, the pressure corresponding to the geodetic head $\rho \times g \times z$ and the stagnation pressure $\frac{1}{2} \rho \times c^2$, the total dynamic head of a pump measured between the suction and the discharge nozzles results from the difference of the total pressures expressed as heads $H = H_{discharge} - H_{suction}$.

$$H = \frac{P_d - P_s}{\rho g} + z_d - z_s + \frac{c_d^2 - c_s^2}{2g} \tag{1.2}$$

In this equation all energies are represented as “energy heads”: the static pressure heads p/(g × ρ) measured at the suction or the discharge nozzle, the potential energy z and velocity heads $c^2/(2g)$. Head and specific work are *independent* of the density or the type of the medium. So we can say that theoretically a pump produces the same head when working with any fluid whether it is water, mercury or air. But pressure rise will always be different $\Delta p = \rho \times g \times H$. All pressure differences, powers, forces and stresses are proportional to the density.

The energy transferred per unit mass is represented by the specific work, there for the useful power P_u of a pump can be obtained by multiplying the transported mass flow $m = \rho \times Q$ by the specific work Y:

$$P_u = \rho Y Q = \rho g H Q = Q \Delta p \tag{1.3}$$

The shaft power P needed at the coupling always have greater value when compared to the useful power because all losses of the pump is included and accounted for. The ratio of both values is the pump’s efficiency η:

$$\eta = \frac{P_u}{P} = \frac{\rho g H Q}{P} \tag{1.4}$$

1.4 PUMP CHARACTERISTICS

changing the flow rate of a pump, leads to a change in the head, the power consumption and the efficiency too. Plotting these quantities against the flow rate we obtain the “pump characteristics”, Fig. 1.3. The “best efficiency point” (BEP) is where the pump reaches its maximum value at a certain flowrate. Pumps are usually designed for this BEP which defines Q_{opt}, H_{opt}, P_{opt} and η_{opt} at a certain speed.

The operation point of a pump is invariably where the head generated by the pump equals the head required by the plant: $H = H_A$. In other words, it is at the intersection of the pump characteristic with the system characteristic, [51].

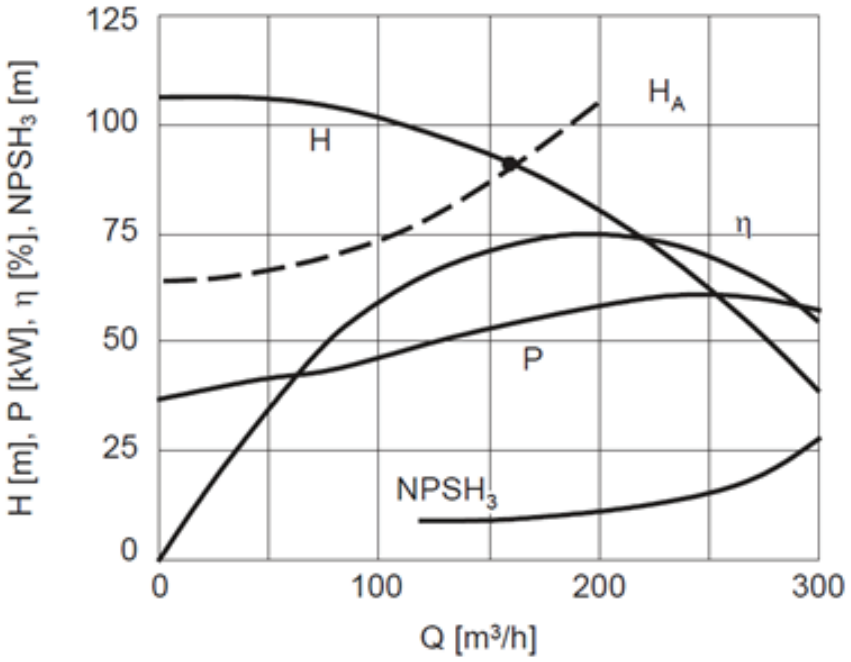

Fig. 1.3 Pump characteristics and system characteristic H_A (broken curve)

1.5 INDUSTRIAL APPLICATIONS OF LOW- CONCENTRATION EMULSION

This particular concentration range (Φ = 0.05%–0.2%), under consideration in this thesis, is typical of crucial industrial applications:

• Industrial Dust Suppression (emulsion concentration (0.05%–0.2%) and flow Rate (Up to 50 l/min)): Due to high surface tension, water alone frequently fails to capture fine dust in mining, building, and bulk material handling. By adding surfactants or oil-based emulsions at these incredibly low concentrations, water's surface tension is lowered, enabling it to moisten and "trap" dust particles.

• Precision Metalworking with Micro-Lubrication (emulsion concentration (0.01%–0.2%) and flow Rate (50 l/min)): Maximum cooling with minimal chemical waste is the aim of several high-speed grinding and light-duty machining procedures.

• Accurate Farming Spraying (emulsion concentration (0.1%–0.2%) and flow Rate (50 l/min)): Highly diluted oil-in-water emulsions are frequently used for large-scale crop protection or nutrient delivery. A lot of contemporary pesticides and "adjuvants" that aid in the spray's adhesion to leaves are designed to work well at these low concentrations.

$$\Phi = \frac{V_o}{V_o + V_w} = \frac{V_o}{V_E} \tag{1.5}$$

1.6 RESEARCH PROBLEM

Surveying of the reported literatures on various types of pumps reveals that the studies on centrifugal pumps handling single fluid are available in considerable numbers in open literatures but literatures for centrifugal pumps handling emulsions are less in number and detailed flow measurements methodologies for these pumps are very limited in the open literatures, there is a dearth of research that simultaneously evaluates the impact of altering the blade number, inlet and outlet blade angles when working with extremely low-concentration emulsions ($\Phi = 0.05\%$ to 0.2%), particularly in both stable and unstable stages.

THESIS ORGANIZATION

In the following chapters of this thesis, chapter two gives a literature review of centrifugal pump design parameters and stable and unstable o/w emulsion flow. Chapter three deals with the experimental model and procedures. Chapter four present the Experimental results. Chapter five deals with the theoretical model. Chapter six deals with the numerical model and. Finally, the main conclusions drawn from this study and recommendations for future research are brought together in chapter seven.

CHAPTER TWO

LITERATURE REVIEW

CHAPTER TWO

LITERATURE REVIEW

2.1 INTRODUCTION

Centrifugal pumps are extensively employed in industrial systems due to their simple construction, operational reliability, and wide operating range. However, pump performance can deteriorate significantly when handling contaminated fluids and oil-water emulsions, which are frequently encountered in petroleum, chemical, and process industries. Understanding the combined influence of fluid properties, emulsion stability, and impeller geometric parameters on pump performance remains a challenging task, particularly due to the complex interaction between turbulence, viscous effects, and internal flow structures.

2.2 LITERATURE SURVEY

In order to clarify the objective of this thesis, this survey has been performed to scan the interesting researches in the fields of single-phase flow, emulsion flow in centrifugal pumps in the period between 1968 and 2025.

2.2.1 Emulsion flow

Langevin et al. [1] found that dispersing heavy oil in water is a highly effective method for reducing the viscosity of an emulsion. Consequently, creating an oil-in-water (o/w) emulsion can be utilized to lower the viscosity of oil flowing through pipelines, which in turn reduces energy losses and the power required for oil transportation. In their study using Omani heavy crude oil, **Al-Wahaibi et al. [2]** observed that the degree of viscosity reduction (VR) increased with higher water content. They noted that at a water content of 30%, a phase inversion occurred, transitioning from an oil-in-water (o/w) emulsion to a water-in-oil (w/o) emulsion. Additionally, they found that VR was inversely related to both the temperature and the concentration of silica nanoparticles. **Halboose et al. [3]** studied the effect of water content and temperature on the stability of crude oil emulsion. They prepared the emulsion was by mixing the crude oil and desired content of water and shaking by hand. They tested emulsions of (10, 20, 30, 40, 50, 60) percent water volume to oil emulsion volume, and temperatures of (20, 30, 40, 50) $^{\circ}$C. They found that, increasing the water concentration decreases the emulsion stability, and that the emulsions became more unstable while

increasing the temperature. **Achour et al. [4]** investigated analytically the degradation of the centrifugal pump performance when pumping emulsion fluid using computational fluid dynamic (CFD) models, they considered the emulsion to be continuous and homogeneous single-phase fluid exhibiting shear thinning behavior for the modeling purpose, they noticed that the CFD simulations pump head curves have a steeper drop at higher flow rates while handling an oil-in-water emulsion, which is consistent with the literature results, they also concluded that modeling the emulsion as a homogeneous single phase fluid with appropriate rheology can be used to estimate the overall pump performance rather than considering the multiphase topology of the fluid.

2.2.2 Stable and unstable emulsion effect on pressure drop and losses

The laminar and turbulent flow behaviors of stable oil-in-water (o/w) emulsions in horizontal pipeline were experimentally studied by **Pal and Rodes [5]**. They noticed that the emulsions are Newtonian for a dispersed phase concentration up to 55.14% by volume. And for concentration of 65.15% o/w emulsions are non-Newtonians fluids. They concluded that the friction factor for stable o/w emulsions follows the usual equations of single phase Newtonian and non-Newtonian fluids with averaged properties. They also pointed out that for dispersed phase concentration more than 50% stable o/w emulsions show drag reduction in turbulent flow, i.e. the experimental friction factors fall somewhat below the single-phase equation. **Pal [6]** studied experimentally the laminar and turbulent flow behaviors of stable and unstable water-in-oil (w/o) and oil in water (o/w) emulsions. He concluded that the pipeline flow behavior of stable o/w and w/o emulsions could be predicted reasonably well using the usual equations of a single phase because they exhibit relatively little drag reduction, while the unstable o/w emulsions exhibit drag reduction behavior in the turbulent regime depending upon the nature of the oil and the holdup of the dispersed phase. Also the unstable w/o emulsion exhibits a much stronger drag reduction activity than the unstable o/w emulsions. **Ismail [7]** examined two explanations for the decrease in drag: the processes of breaking and coalescence, and the ability of the dispersed phase to dampen turbulence. He identified two correlations that explain the relationships among Sauter mean diameter, holdup, and overall diameter. For inlet water fractions between 10% and 20%, **Nadler and Mewes [8]** experimentally studied the flow of two immiscible liquids (oil-water mixture) in a horizontal pipe. They concluded that, the maximum pressure drop for the flow are found in the phase inversion region which is observed for input water fraction between 10 and 20%. They didn't observe any significant temperature effect on the flow characteristics.

Furthermore, **Khalil et al. [9]** studied oil-in-water emulsion flow through pipeline using image analysis technique and They found that, increasing emulsion holdup (ratio of oil volume to mixture volume) causes, an increase in emulsion viscosity, an increase oil droplet diameter, a decrease in discharge coefficient and an increase in energy loss coefficient. They concluded that the o/w emulsion is Newtonian for a holdup lower than 50% and non-Newtonian for more than that. Additionally, **Khalil and Kassab. [10]** demonstrated that the pipe friction factor decreases as emulsion holdup increases. **Turian et al. [11]** investigated non-Newtonian suspension flow through bends and valves and found that as the Reynolds number increased in laminar flow, the resistance coefficient decreased, eventually approaching constant values in a fully developed turbulent flow. The flow of two-phase oil/water mixtures through sudden expansion and contractions was experimentally measured by **Hwang and Pal[12].** They determined the energy losses by measuring the pressure profiles upstream and downstream. They found that the loss coefficients of the emulsions are independent on the emulsion type. **Pal and Hwang [13]**, studied experimentally the loss coefficients for surfactant stabilized emulsions flow through expansions and contractions. They revealed that emulsions are only Newtonian at low to moderate concentrations of dispersed phase (oil concentration up to 46.9%). They also concluded that the frictional losses can be successfully correlated as loss coefficient versus Reynolds number. **Nasr [14]** measured the hydraulic resistance of emulsion (oil-in-water) flow across sudden contraction and sudden enlargement. She performed an experimental study to compare pressure drops across different geometries under different Reynolds number and several oil weight concentrations. She concluded that for the same flow Reynolds number, increasing the oil concentration causes an increase in the energy losses. For the same oil concentration, increasing the flow Reynolds number decreases the energy loss coefficient A computational approach on the pressure drop caused by two-phase flow of oil/water emulsions through sudden expansions and contractions was studied by **Roul and Dash [15]**. They found that, the contraction and expansion loss coefficients are obtained from the pressure loss and velocity data for different concentrations of oil–water emulsions. The loss coefficients for the emulsions were found to be independent of the concentration and type of emulsions. **Balakhrisna et al [16]**. Measured experimentally the pressure drop of oil-in-water emulsion flow through sudden contraction and sudden expansion in a horizontal pipe. They concluded that, the flow phase distribution is affected strongly by the sudden change of the area. And the loss coefficient is independent on the flow pattern. They also found the contraction and expansion loss coefficients of the oil-in-water emulsion flow have a lower value than the

pure water flow through the same test rigs. **Buhidma and Pal [17]** investigated the performance of oil-water (o/w) emulsions using wedge meters and segmental orifice meters of various sizes and shapes. They concluded that across a wide range of Reynolds numbers, both types of meters exhibited a constant discharge coefficient. The energy loss of oil-in-water emulsions flow through pipe fittings was measured using image processing by **Khalil et al [18]**. They concluded that the energy loss coefficient is inversely proportional to the flow Reynolds number, and also the energy loss coefficient increases as the holdup increases and the flow rate decreases. **Perissinotto et al [19]** investigated experimentally the formation of oil-water emulsion in the transparent impeller and volute of an electrical submersible pump (ESP) prototype. The behavior of oil drops injected in water at different flowrates and rotation speed was monitored. They stated that the reduced performance at low water flowrates is due to the accumulation of oil drops in the impeller as a result of vortices and water recirculation. They also noted that the large velocity fluctuations at the impeller and volute boundary causes the oil drops rotation, deformation and fragmentation at high water flow rates. Additionally, **Bulgarelli et al. [20]** analyzed experimentally the Electrical Submersible Pumps (ESP) lift capacity and phase inversion for two different emulsion systems, both stable with and without emulsifier. They compared the results to experimental data of ESP operating with the unstable emulsion, they concluded that Surfactants in the emulsion flow within the ESP provoke intense viscous degradation due to an increase of the emulsion effective viscosity, they observed the opposite behavior while testing the unstable emulsion system.

2.2.3 Using numerical simulations

R. Zhang et al [21] proposed a new kind of centrifugal pump impeller with slot in order to improve the cavitation performance of a pump, the slot is located on the shroud near the suction side of the blade leading edge in an attempt to drain fluids with high energy from the impeller front side chamber to the lowest area, they tested the pump's inner flow for 5 different slot sizes by means of numerical simulation, and compared the hydraulic performance result with those of the prototype pump, they stated that at low flow rates the slot jet can suppress the reverse flow remarkably leading to improvement of the pump efficiency and the pump cavitation performance , the results also imply that the smaller slots had better cavitation performance, they concluded that the slot impellers is proven to be effective in suppressing the cavitation leading to improvement in the available net positive suction head. **X. Li et al [22]** investigated the effect of the loading distribution on head,

radial force and pressure pulsation of a low specific-speed centrifugal pump with cylindrical impeller blades, they obtained blade shapes using the method of 1D inverse design, they conducted the simulation using Three-dimensional URANS method with the shear stress transport (SST) *k-ω* turbulence model to analyze the flow patterns. They validated the numerical results by comparing to experimental data with acceptable agreement, they stated that the well-designed blade loading curve, like the fore-loading impeller, effectively reduce the pressure pulsation amplitude and the radial force. They also concluded that the pressure and velocity distributions at different slopes of the blade loading curves show that a more uniform flow is produced by the fore-loading impeller compared to that of the pump with aft-loading impeller, leading to a reduction of the radial force and pressure pulsation of the pump. Solution and mesh generation algorithms were presented by **Barth and D. Jespersen [23]** for solving the Euler equations on unstructured meshes consisting of triangle and quadrilateral control volumes, they developed cell-centered and mesh-vertex upwind finite-volume schemes that uses multi-dimensional monotone linear reconstruction procedures, they presented numerical results in two dimensions. **Chorin [24]** introduced a new finite-difference method for solving the time-dependent Navier-Stokes equations for an incompressible fluid using pressure and velocity as primitive variables, the presented model can also be used with 2D and 3D problems, he stated that the new method had time dependent results even in 3D problems he also presented an application to a three-dimensional convection problem. Additionally **T.H. Shih et al [25]** proposed a new ***k-e*** eddy viscosity model consisting of a new model dissipation rate equation and a new realizable eddy viscosity formulation, based on the dynamic equation of the mean-square vorticity fluctuation for large turbulent Reynolds number they modified a new dissipation rate equation for the new model, their new eddy viscosity formulation is based on both the positivity of normal Reynolds stresses and the Schwarz' inequality for turbulent shear stresses. They examined different flows including boundary-free shear flows, rotating homogeneous shear flows, a channel flow, and flat plate boundary layers with and without a pressure gradient and backward facing step separated flows, the proposed model performed will for these models and with models, they compared both the new model predictions and the standard ***k-e*** eddy viscosity model with experimental data, they concluded that the new model showed better results compared to the standard ***k-e*** eddy viscosity model. Through numerical analysis, **Bai et al. [26]** studied the effect of both the pressure fluctuations and the unsteady flow patterns on the pump flow channel of three configurations with different

diffuser vane numbers, they found that increasing the number of diffuser vanes gradually increases the amplitude of pressure fluctuation in the diffuser, while reducing the number of diffuser vanes resulted in increasing the static pressure gradually as a result of a weaker pressure fluctuation intensity. Using particle image velocimetry (PIV) and laser Doppler velocimetry (LDV) **Pedersen and Larsen [27]** performed detailed optical measurements of the flow inside the rotating passages of a six-bladed shrouded centrifugal pump impeller, they surveyed the flow at both design load and at severe off-design conditions, their results included instantaneous and ensemble averaged PIV velocity vector maps and also bin-resolved LDV data acquired in the mid plane between hub and shroud of the impeller, they noticed that the mean field of relative velocity is predominantly vane congruent at design load, $Q = Q_d$ without flow separation, while ‘‘two-channel’’ phenomenon consisting of alternate stalled and unstalled passages was observed at quarter-load, $Q = 0.25Q_d$, with large recirculation cell blocking the inlet to the stalled passage with a strong relative eddy dominating the remaining parts of the passage. They described the stall phenomenon as steady, nonrotating and not initiated by the interaction with stationary components. Meanwhile, **Zhang et al. [28]** used the laser Doppler anemometry (LDA) technique to capture velocity signals at different flow rates of a centrifugal pump in an attempt to study the unsteady velocity pulsation characteristics und to understand the effect of the intense rotor-stator interaction on the turbulent flow generation, they found that at low flow rates a prominent hump phenomenon generated within the pump head curve indicating the development of rotating stall in the pump, the result also imply that the discrete blade passing frequency and impeller rotating frequency dominate the velocity and pressure spectra, the root mean square values of velocity signals increase rapidly at off-design flow rates, especially within the rotating stall region, they also observed a similar trend for pressure amplitude at the blade passing frequency.

2.2.4 Number of blades

A numerical investigation was conducted by **Abo Elyamin et al. [29]**, to study the impeller blade number effect on the centrifugal pump performance using three different impellers with 5, 7, and 9 blades are tested numerically in order to determine the optimum blades number at rotational speed of 2800 rpm, they found that the impeller with 7 blades showed the best performance they related that to the decrease of the losses by increasing the blade number due to the reduction of the secondary flow but for a certain limit then the losses increase again due to the friction losses in the impeller and the mixing losses after the

impeller yield an increment in the total losses in the region of the vaneless diffuser, They related that to the increasing number of the impeller channels. Additionally, **Grapsas et al. [30]** developed and tested numerical methodology for hydrodynamic design in centrifugal pumps aiming to maximize the efficiency of the pump impeller through improving its parameters and shape, the simulation was performed with commercial CFD code and the results were compared to the equivalent measurement from laboratory tests of pump impeller, they also carried out a parametric study to test the influence of different blade design parameters on the efficiency and performance of a centrifugal pump impeller like blade length, the inlet height and the leading edge inclination, and combined the parameters that improved the performance in a multi-parametric optimization methodology by means of a stochastic evaluation algorithm software, the final optimum design showed obvious efficiency increase when compared to the original impeller design. The three-dimensional viscous flow field of two centrifugal pumps, having the same volute, design head, design flow rate and rotational speed but with different blade number and the blade shape, referred to as blade load are analyzed by **Xu et al [31]** based on large eddy simulation (LES). They performed the comparisons taking into account the flow field characteristics, hydraulic efficiencies, pressure pulsations and unsteady forces applied on the impellers to find out the effect of the design blade load on hydraulic performance and flow exciting force. They concluded that the efficiency of the pump, the impeller blade of which has larger design load, is improved compared to the lower blade design load. The pressure fluctuation of the pump with high design load is more remarkable. Its coefficient of static pressure maximum amplitude is higher than the latter. They also stated that the blade design load is an important factor on the excitation force in centrifugal pumps.

2.2.5 Centrifugal pump performance

Utilizing ANSYS-CFX, **Djerroud et al. [32]** investigated numerically the effect of the relevant design parameters such as the blade number, the blade height, the blade outlet angle, the blade width and the impeller diameter on the steady state liquid flow in the case of a three dimensional centrifugal pump, they conducted three different case studies: impeller, combined impeller and volute, and combined impeller and diffuser. They validated their results by comparing the numerical simulation results of the combined impeller and diffuser case with experimental results, They concluded that changing the key design parameters have an obvious impact on the performance of the centrifugal pump considering the pump head, the brake horsepower, and the overall efficiency. The performance as a function of

impeller geometry was investigated by **Li and Zm [33]** they tested experimentally and numerically the effect of fluid viscosity on the performance of centrifugal pumps, they concluded that, the high viscosity resulted in sharp increase in the disc friction losses over the outer side of both the impeller shroud and hub, and the obtained results helped in the design and selection of centrifugal oil pumps, while **Cheah et al. [34]** simulated the complex internal flow in a centrifugal pump impeller with six twisted blades by using a three-dimensional Navier-Stokes code with a standard k-e two-equation turbulence model, they used different flow rates at the inlet boundary to study the effect on the pump performance, the study showed that at design point the impeller passage flow is quite smooth and follows the curvature of the impeller blade. However, due to non-tangential inflow condition flow separation takes place at the leading edge. they also concluded that the pressure increases gradually along stream wise direction in the impeller passages and that unsteady flow develop in the impeller passage and the volute casing when the centrifugal pump is operating under off-design flow rate condition. Using theoretical and empirical internal and external energy loss equations **Omar et al. [35]** developed a theoretical procedure to calculate the performance of a centrifugal pump, they implemented the equations in the prediction program and used it to calculate the head, power and efficiency of the pump while varying the fluid properties, rotational speeds and input geometries they used two different experimental rigs with different impeller geometries for the experimental data, that was used for comparison with the theoretical results with good agreement for all impeller geometries and rotational speeds considered with some discrepancies occurring in efficiency and power data due to selected loss equations. **Shojaeefard et al. [36]** proposed a new method to calculate the head, efficiency and input power based on the loss analysis for pumps using industrial oils. They developed a computer code based on the loss analysis method and compared the results to experimental results of a centrifugal pump with good agreement, they observed the sudden rising head from both experimental and numerical results diagrams. Utilizing orthogonal design. **Tang and Kim [37]** investigated the effect of impeller geometrical configurations on crystal particle behaviors by using orthogonal design based on CFD-DEM coupled method to study the inner flow in a pump with crystal particles, their results showed that the blade outlet angle β2 can affect the collisions between particles and blades significantly, the results also imply that a low-speed region at the blade pressure side in the optimal impeller has been reduced, declining the probability of the crystal particles adhering to the impeller. **Williams and Skelley [38]** demonstrated higher pump stage loading with acceptable performance by studying high head unshrouded impeller

technology developed as part of NASA's cost reduction effort for space access, they studied three tip-clearances at on- and off- design conditions, while using a water flow test article to verify the CFD prediction of an advanced unshrouded impeller design. The design succeeded to meets the performance requirements of a 3- stage shrouded fuel pump while using a 2-stage unshrouded fuel pump. **Sugiyama et al. [39]** conducted an experiment measuring the overall pressure and velocity distribution at both the inlet and outlet plane**s** of a diffuser. **Ayada et al. [40]** studied the effect of semi-open centrifugal pump side clearance on the inception of cavitation, they tested he input pressure values from 80 to 16 KPa and pump side clearance values from 1 to 3 mm for impeller rotational speed of 1530 rpm the results showed that both the static pressure inside the impeller and the total pressure in stream wise direction decreased as the total input pressure decreased, and the pump head is constant with the reduction of the total input pressure until reaching the cavitation they also concluded that head is reduced in closed impeller with a percent of 1.5% while it is reduced with a percent of 0.5% for pump side clearance of 1mm , that the cavitation inception in the pump had been affected and delayed with the increase of the pump side clearance.

2.2.6 Blade inlet and exit angles

One of the important parameters in the hydraulic design of the centrifugal pump impeller is the slip factor, using CFD computational results **Li. [41]** estimated the slip factor and how it is affected by the liquid viscosity and the flow rate by means of two approaches: the velocity triangles at the impeller outlet and the other is due to the impeller theoretical head of 3D turbulent viscous fluid, the results were validated with LDV (laser Doppler Velocimetry) results for the best efficiency point, he concluded that the slip factors are significantly dependent of flow rate and the liquid viscosity appear to have less effect on them. He also stated that at the outlet of impeller at low flow rates the volute is responsible for reduction in tangential velocity of fluid and that for impeller with large exit blade angle the slip factor is not sensitive to flow rate. **Li [42]** studied the effects of pumped fluid viscosity and blade exit angle on flow steadiness, by exploring the unsteady flow in an experimental centrifugal pump with two different blade exit angles when the pump handles the liquids with different viscosities using CFD code Fluent, he compared the heads estimated using the unsteady flow model with experiments at two viscosities. Ha also clarified the effects of mesh density and turbulence model on the fluid velocity and pressure profiles behind the impeller, the results were validated with LDV (laser Doppler Velocimetry) results for the velocity profiles, he found that at the inlet and outlet of the impeller the fluctuation in flow variables decreases

by increasing the viscosity of fluid, he also noticed a remarkable fluctuation in the flow variables for larger blade exit angle. **Li [43]** tested numerically by means of CFD software FLUENT the performance of an experimental pump working with both water and viscous oils in both cases of part-loading and the best efficiency points he noticed that the hydraulic performance of the impeller without volute was remarkably different from that of the impeller with volute, on the other hand The effect of the relative position between the volute tongue tip and the blade trailing edge on the performance was not significant. He concluded that the volute has more hydraulic losses compared to the impeller and that the sudden rising head effect is due to the high viscosity and a certain level of roughness. Additionally, The steady three-dimensional and turbulent flows in the impeller without volute and in an experimental centrifugal pump was investigated numerically with CFD by **Li. [44]** he tested different fluid viscosities (water) and 48mm2/s (oil), for roughness of 100 μm, he compared the computational flow fields with that measured by using LDV and found The CFD results of the flow in the impeller and volute are in agreement with that measured by means of LDV, he also indicated that the flow is axi-symmetrical in the impeller without volute, but it isn't in the impeller with volute. The large "dead water" area in the individual passage of impeller is due to combining the peak in the impeller theoretical head curve and the increase in slip factor at low flow rate. **Shojaeefard et al. [45]** investigated numerically some geometric characteristics of the impeller and volute of a centrifugal pump in order to enhance the performance of the pumps during working with viscous fluids , They simulated different cases with changes made to the outlet angle and passage width of the impeller and validated the results by comparing to experimental results, the result showed that changing the outlet angle and the passage width has a significant effect on the pump head and efficiency increases due the changes of the losses arising from the generation of eddies in the passage and outlet of the impeller. According to an experiment conducted by **Liu et al. [46]**, the leading and trailing vane exit angles of the front and back shrouds, along with the blade wrap angle, are critical factors affecting the centrifugal pump's performance. They emphasized that the blade wrap angle has a particularly significant effect on pump efficiency. **Wang et al. [47]** stated that the SST k-ω model combines the benefits of near-wall treatments from a k-ω model with the capability to solve the outer region characteristics of a k-ε model. This model accounts for turbulent shear stress transportation, providing detailed predictions of flow separation under various pressure gradient conditions. **Wilcox [48]** Updated the classical k-ω and added a cross-diffusion term and modified the built-in stress limiter. This significantly enhanced both boundary layer and free surface simulations, as well as

decreased the intrinsic sensitivity of k-ω models to shear flows, he noted that the SST *k-ω* model is effective for predicting high rotational speeds and strong separated flows, emphasizing the high precision and credibility of this approach. **Munson et al. [49]** mentioned that the blade angle (β_o) for real pumps typically ranges from 15° to 35°, with a common range of $20° < \beta_o < 25°$ and $15° < \beta_i < 50°$. Backward-curved blades are characterized by $\beta_o < 90°$, while forward-curved blades have $\beta_o > 90°$. Since forward-curved vanes can lead to unstable flow conditions, they are generally not employed in pump design.

2.3 CONCLUSIONS OF THE LITERATURE SURVEY

The previous abridged literature review on emulsion flow through pipe and fittings and single-phase flow in centrifugal pumps shows that:

1. The emulsion fluid flow (oil-in-water) through centrifugal pumps has not received a sufficient consideration in the previous researches.
2. The formation of oil-in-water emulsion can be used to reduce the viscosity in pipelines and hence to reduce the energy losses and the required power to transmit the oil in pipelines.
3. Increasing emulsion holdup causes, (1) an increase in emulsion viscosity, (2) increasing oil droplet diameter, (3) decreases discharge coefficient and (4) increases energy loss coefficient.
4. changing the pump impeller key design parameters have an obvious impact on the performance of the centrifugal pump considering the pump head, the brake horsepower, and the overall efficiency.
5. changing the outlet angle and the passage width has a significant effect on the pump head and efficiency increases due the changes of the losses arising from the generation of eddies in the passage and outlet of the impeller.
6. The pressure and velocity distributions at different slopes of the blade loading curves show that a more uniform flow is produced by the fore-loading impeller compared to that of the pump with aft-loading impeller, leading to a reduction of the radial force and pressure pulsation of the pump.

2.4 OBJECTIVES OF THE PRESENT WORK

There is still a large research gap in the combined examination of these aspects, even though the previously cited literature offers a thorough framework for comprehending emulsion and centrifugal pump hydraulics separately. The majority of current research focuses on either isolated geometric parameters of the pump or high-concentration emulsions.

Therefore, the goal of this study is to present a thorough examination of how emulsion properties and impeller shape work together to improve centrifugal pump performance. The following are the precise objectives:

- To examine the Integrated Impact of Blade design parameters: To assess experimentally and numerically how changing the number of blades, the angles of the inlet and outlet blades affects the head, efficiency, and power consumption of the pump.
- To examine Low-Concentration Emulsion Behavior: To ascertain how modified impellers operate when managing oil-water emulsions at incredibly low concentrations (0.05%, 0.1%, and 0.2%), which are frequently disregarded in conventional literature.
- To assess Stability Effects on Hydraulic Losses: To contrast how emulsion stability affects flow characteristics and energy dissipation in the pump stages.
- To create a theoretical and numerical framework to better forecast pump performance in multi-phase applications by correlating the relationship between emulsion holdup, stability, and internal hydraulic losses.

2.5 ORIGINAL CONTRIBUTIONS OF THE THESIS

This Research presents the integrated experimental and numerical study of centrifugal pump performance, taking into consideration the effects of impeller blade number, outlet and inlet blade angles while working with extremely low-concentration emulsions (0.05% to 0.2%), the thesis provides a comparison between stable and unstable emulsions regimes demonstrating their effects on pump. Also showing how minor impeller geometric modifications can enhance energy efficiency in low-concentration emulsions applications.

CHAPTER THREE

EXPERIMENTAL ANALYSIS

CHAPTER THREE

EXPERIMENTAL ANALYSIS

3.1 INTRODUCTION

The experimental data are obtained by conducting experiments using a test setup that allows for testing different pump's impellers with different design parameters while also being able to check for the effect of different working fluids (emulsions) on the pump performance under different pump rotational rpm.

3.2 THE EXPERIMENTAL SETUP

The experimental setup is illustrated in Fig. 3.1. It consists of a mixing tank that serves as the primary reservoir with a capacity of 120 liters, an electrical mixer operating at a rotational speed of 1650 RPM, a centrifugal pump, and a discharge tank with a capacity of 40 liters. The setup also includes a manually operated flow valve, two digital pressure transducers, a frequency converter to adjust the pump's speed by varying the frequency, a power meter, and the necessary piping and fittings. All pipes used have a diameter of 1 inch. Fig. 3.2 presents the test setup designed to experimentally investigate the effects of the impeller blades' input and output angles on the centrifugal pump's performance. The test pump is a centrifugal pump of the Calpeda model (NMM, 1/A), with suction and delivery diameters of 1 inch. It operates at a frequency of 60 Hz and a voltage of 380 volts, with a rotating speed of 1700 RPM and a power rating of 1 HP. Table 3.1 presents the main test pump specifications.

The geometry of the original impeller is as follows: impeller diameter (d) is 150 mm, blade thickness (e) is 4 mm, blade inlet angle (β_1) is 10 degrees, blade outlet angle (β_2) is 30 degrees, and the number of blades (z) is 6.

Two groups of impellers were prepared, each containing three impellers. The first set consists of three impellers that have identical parameters, differing only in the blade inlet angle. The second set also has three impellers with the same parameters, but they differ in the blade outlet angle.

Table (3.1) the centrifugal pump specifications

Model	Volt	Power	frequency	RPM	Max flowrate	Max head	Inlet diameter	Outlet diameter
Calpeda CP 1 hp	240 v	1 hp	50/60 Hz	1700	5.2 m^3/h	20.6 m	25 mm	25 mm

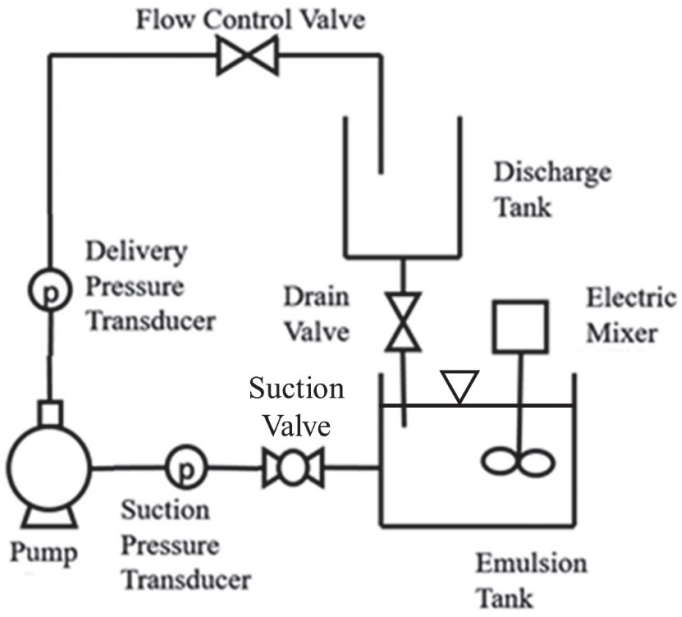

Fig.3.1 The experimental setup

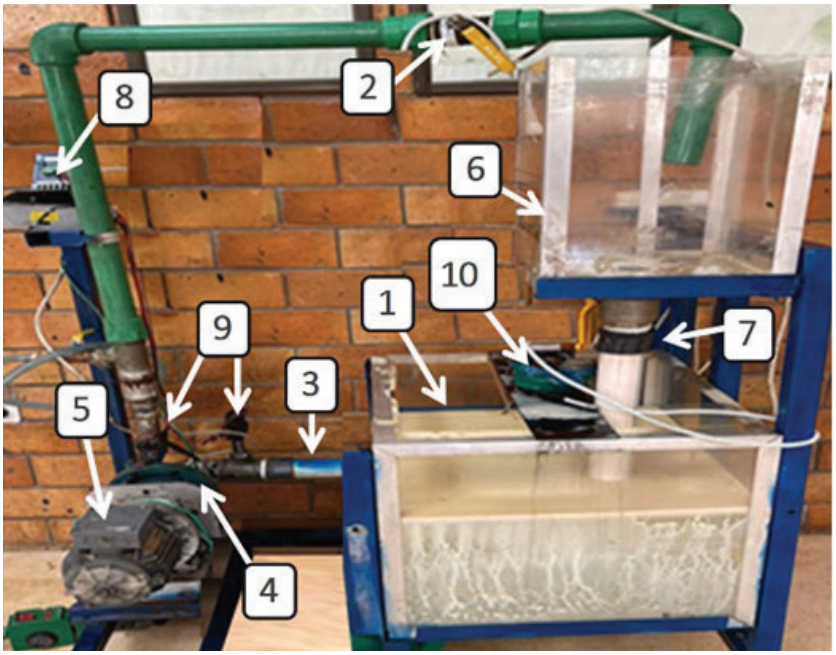

Fig.3.2 The real experimental test setup

1. Mixing tank
2. Flow control valve
3. Pipes
4. Test pump
5. Motor
6. Discharge tank
7. Drain valve
8. Frequency converter
9. Pressure transducer
10. Mixer

3.3 IMPELLERS DESIGN CRITERIA

The impellers were designed by using the original commercial pump's impeller, where the impeller was scanned by 3D scanner then the dimensions were used to redraw the impeller via SolidWorks. The necessary changes were then made to draw the different impellers with the specified parameters, Table 3.2 present the test impellers parameters, the last step was to use 3D printing to produce the test impellers. Figure 3.3 shows an example of the test impellers. In this experiment there are 7 different test impellers, impeller (a) will be considered to be the reference impeller as this is the original impeller of the test pump, and was used to extract all the impellers original parameters. Three sets of impellers were also tested, the first set as shown in figure 3.4 will be impeller (a) alongside impellers (b, c) which have the same blade parameters with different blade number (z). The second set as shown in figure 3.5 will be impeller (a) alongside impellers (d, e) which have the same parameters except for the blade inlet angle (β_1). The final set as shown in figure 3.6 will be impeller (a) alongside impellers (f, g) which have the same parameters except

for the blade outlet angle (β_2). The pump performance is to be analyzed by monitoring the pump head (H), the pump shaft power (P_s) and the pump overall efficiency (η_o) for different flow rate at different pump motor rpm. Figure 3.7 shows the inlet and outlet velocity triangles with the blade inlet and outlet angles.

Table (3.2) The parameters of the test impellers

impeller	Blade number (z)	Blade inlet angle (β_1)	Blade outlet angel(β_2)	Impeller diameter
a	6	10°	30°	150 mm
b	5	10°	30°	150 mm
c	7	10°	30°	150 mm
d	6	20°	30°	150 mm
e	6	30°	30°	150 mm
f	6	10°	25°	150 mm
g	6	10°	20°	150 mm

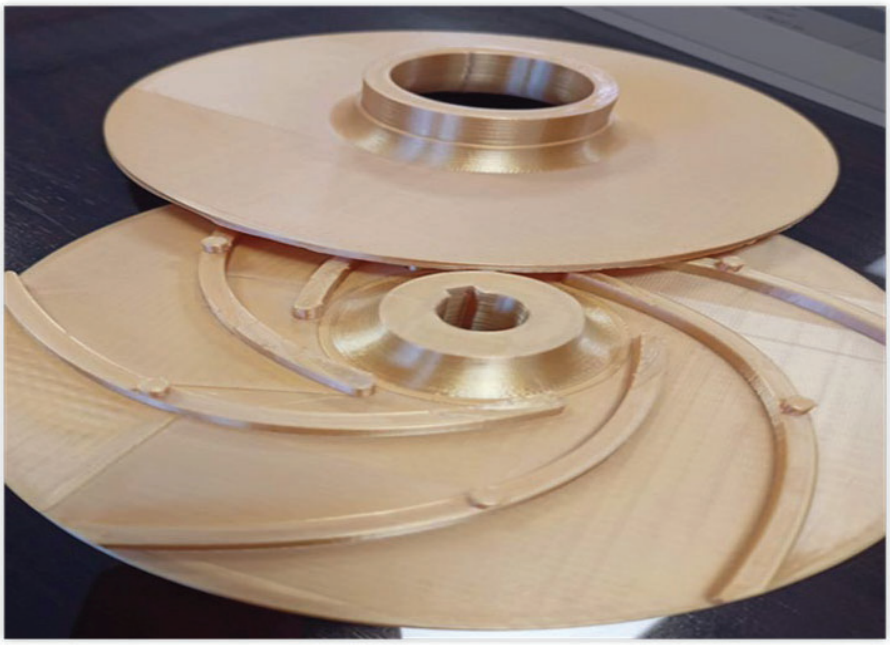

Fig.3.3 Example of the test impellers

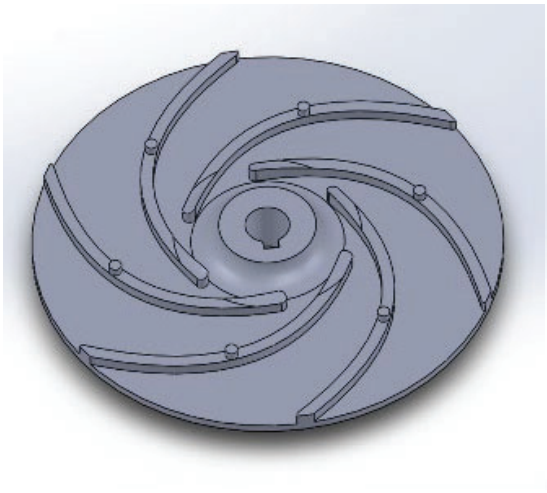

Impeller (a) with (6) blades

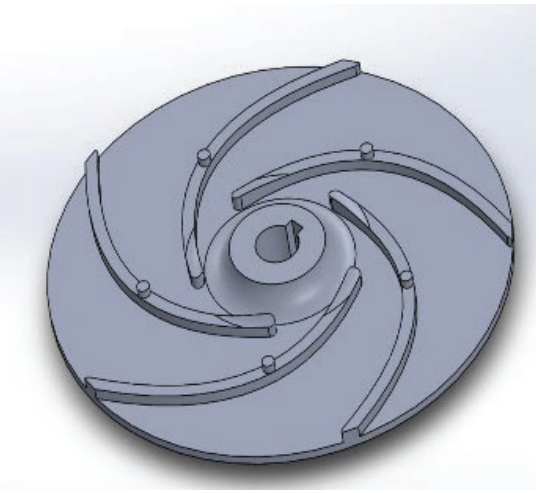

Impeller (b) with (5) blades

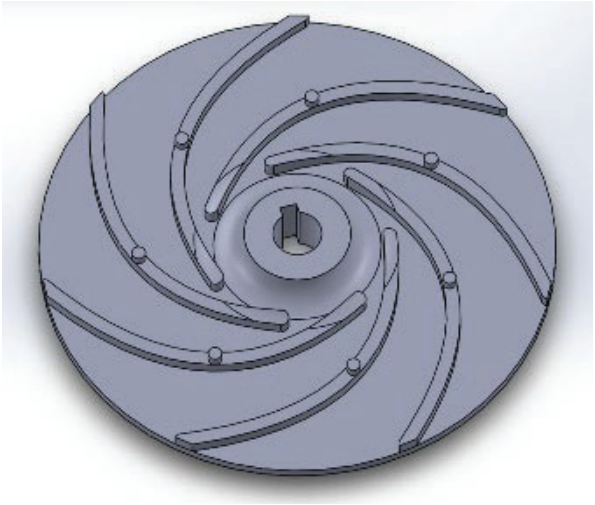

Impeller (c) with (7) blades

Fig.3.4 Test impellers for blade number effect.

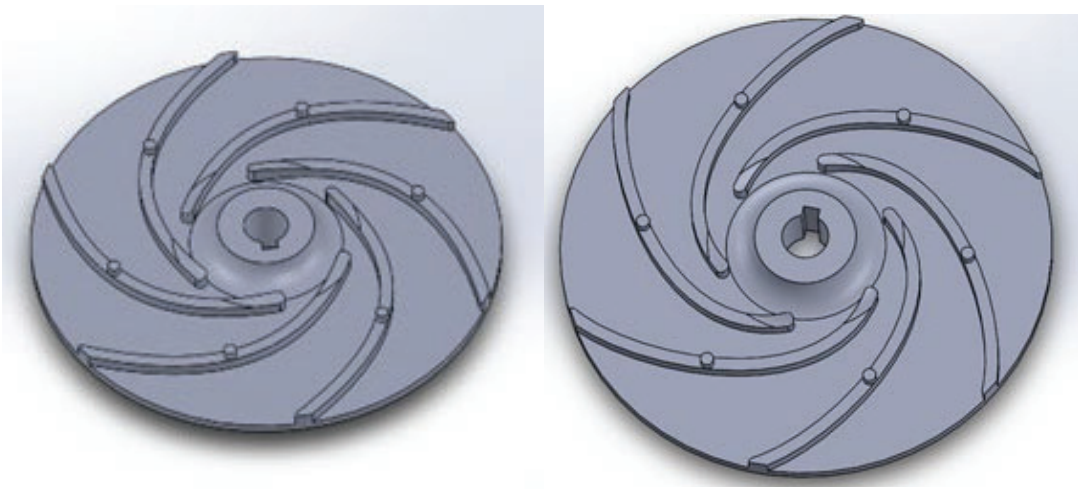

Impeller (a) (β_1= 10^o) Impeller (d) (β_1= 20^o)

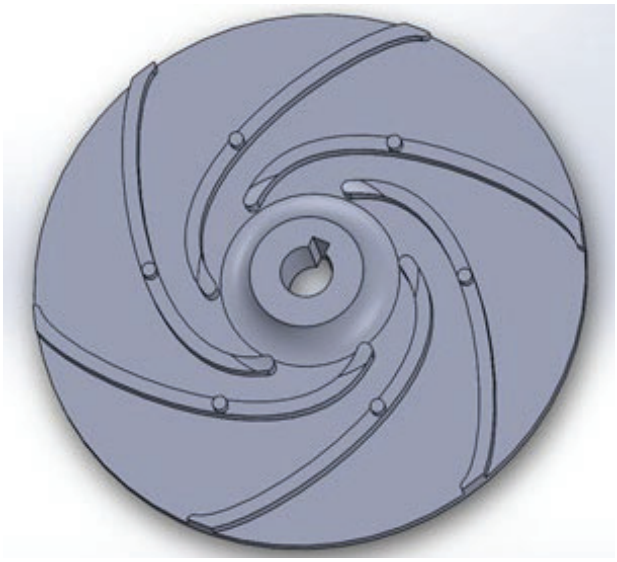

Impeller (e) (β_1= 30^o)

Fig.3.5 Test impellers for inlet angle effect

Impeller (a) (β_2= 30^o)

Impeller (f) (β_2= 25^o)

Impeller (g) (β_2= 20^o)

Fig.3.6 Test impellers for outlet angle effect

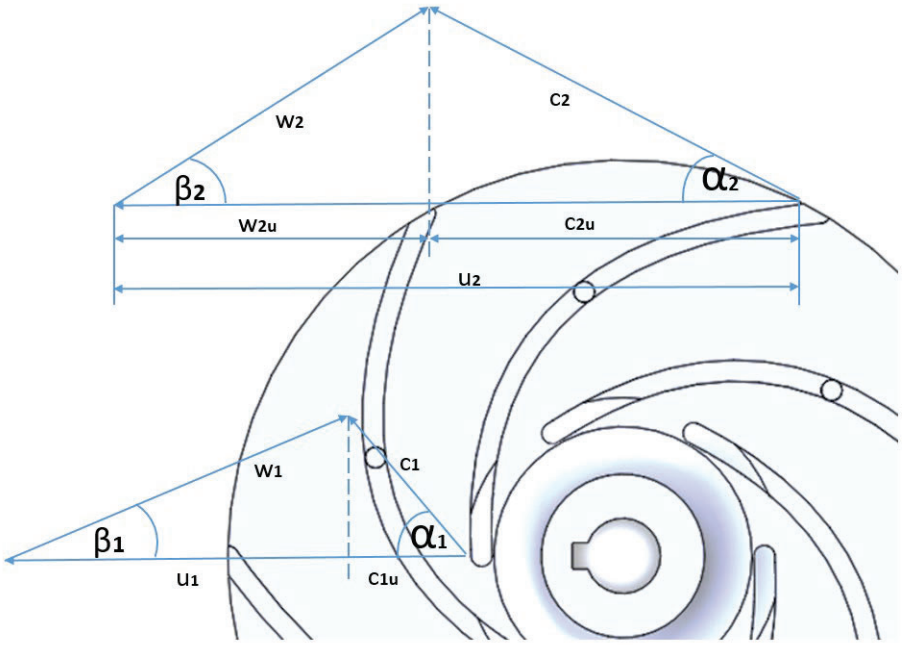

Fig.3.7 Inlet and outlet velocity triangles.

3.4 EMULSION PREPARATION

Two sets of oil-in-water (o/w) emulsions were used in the experiment: an unstable o/w emulsion and a stable o/w emulsion created with sodium dodecyl sulfate (SDS) [$CH_3(CH_2)_{11}OSO_3Na$] as the emulsifier, which was used at a concentration of 1.5% by weight based on the water. This emulsifier helps keep the globules of both liquids suspended in a continuous phase.

Experiments were conducted at various holdup values, specifically at a holdup (Φ) of 0.0% (pure water), 0.05%, 0.1%, and finally 0.2% (representing different oil concentrations by volume). The oil utilized in the experiments was Mobil Special 20W-50, supplied by Mobil Company in Egypt. The oil has a density of 878 kg/m³ at 15°C and a kinematic viscosity of 185 mm²/s at 40°C.

The experiments are conducted on all models with unstable and stable o/w emulsions of holdup,

(Φ = 0.05% and 0.1% and 0.2%) to investigate the effect of emulsion stability on the centrifugal pump performance.

The oil is added to the water in the mixing tank shown in Figure 3.8 with the considered amounts for every holdup ratio and the electric mixer is used to stir the fluid for producing

the emulsion, the mixer motor is 220 V, 0.8 Amp, 105 Watts and have a rotational speed of 1650 RPM.

After testing every working fluid, the tanks were drained in specified jerrycans, rinsed and dried completely before adding the next working fluid.

Fig.3.8 The mixing tank

3.5 MEASUREMENTS AND INSTRUMENTATION

● The pressure is measured using two pressure transducers model QDW90A one at the pump intake pipe and the other at the discharge pipe with sensitivity of ± 0.2 %. Figure 3.9 shows the pressure transducer.

● The flow rate is measured using the discharge tank level marking and a stop watch. Figure 3.10 shows the discharge tank.

● The voltage, current, power consumption is measured via the UNI-T UT230B-EU power meter with sensitivity of ± 1 % . Figure 3.11 shows the power meter.

● The rotor rotational speed is measured by Mastech MS6208B digital tachometer which has laser ray pointed to a reflector stacked on the rotor blade whose speed is to be measured. All the measured rotor speeds are with sensitivity of ±0.1 rpm. Figure 3.12 shows the digital tachometer.

Fig.3.9 The QDW90A pressure transducer

Fig.3.10 The discharge tank

Fig.3.11 The UNI-T UT230B-EU power meter

Fig.3.12 The Mastech MS6208B digital tachometer

3.6 EXPERIMENT PROCEDURES

1. Begin by adding the appropriate test emulsion to the mixing tank. Once added, connect the electric power to the system and turn on the mixer.
2. Close the flow control valve on the discharge line, then open the pump intake valve.
3. Open the drain valve of the discharge tank.
4. Use the frequency converter to set the desired rotational speed of the pump, as indicated by the tachometer.
5. While the flow control valve is fully closed, record the readings from both pressure transducers and the power meter.
6. Adjust the flow control valve to the next position, then record the readings from both pressure transducers and the power meter again.
7. Close the discharge tank drain valve. Measure the time it takes for the emulsion level to move between the markers on the tank to determine the flow rate. To minimize error, calculate the average of three readings when measuring the flow rate.
8. Repeat steps 6 and 7 for each flow control valve position.
9. Repeat steps 5, 6, 7, and 8 for each selected pump rotational speed.
10. Disconnect the electric power, remove the test emulsion from the system, and store it in a dedicated container. Rinse the system thoroughly with water before introducing the next emulsion.
11. For every test emulsion, repeat the steps from 2 to 10.
12. After testing all the emulsions, rinse the system with water and allow it to dry completely. Disconnect the electric power, open the pump casing, replace the test impeller, and reseal the pump casing.
13. For each new test impeller, repeat the steps from 1 to 12.

3.6.1 Calculations

After the previous measurements are carried out, the following parameter can be calculated

.

$$\eta_o = \frac{Pout}{Pin} = \frac{\rho g H Q}{T\omega} \qquad (3.1)$$

3.7 MEASUREMENTS ACCURACY

To minimize random error and improve measurement accuracy while collecting experimental data, the measuring process was conducted three times for each specific flow rate, and the average of these three values was taken. Additionally, more than six flow rates are considered to exclude out-of-range readings. The values from these measurements were then used to display the pump performance curves. Uncertainty analysis was conducted for the flow rate, Head, and power. They are found to be 3.33%, 1.17%, and 0.29%, respectively. Uncertainty analysis for flow rate is shown in Appendix A. Pressure and power uncertainty analysis are conducted in the same manner.

CHAPTER FOUR

EXPRIMENTAL RESULTS

CHAPTER FOUR

EXPERIMENTAL RESULTS

4.1 INTRODUCTION

In order to have a vision on the effect of the different pump rotational speed, different impeller's design parameters and different emulsion properties on the performance of the centrifugal pump, the data from the experimental work is recorded and was used to extract several diagrams to illustrate the effect of each impeller's design parameter separately as well as the emulsion's properties, the following is a description of the pump behavior noted during the experimental work.

4.2 EFFECT OF PUMP ROTATIONAL SPEED

To have a better understanding of the effect of the pump rotational speed on the performance of the centrifugal pump we have 7 different impellers, as mentioned earlier in paragraph 3.4 with different parameters. The 7 impellers are divided into 3 sets. Each set has the same dimensions while changing one of the impeller's design parameters. Each set is tested at three different pump rotational speed (1420, 1530 and 1650) rpm. The results were monitored and analyzed for each set separately in order to have a clear idea on the effect of the pump rotational speed while pumping water alongside six different emulsions.

Figure 3.4 shows the test impellers with different blade numbers. Each of the mentioned impellers will be tested for performance while pumping water alongside three stable emulsions and three unstable emulsions. They also are to be tested at three different shaft rotational speeds (1420,1530 and1650) rpm.

Examples of the curves expressing the pump head as function of the volume flow rate with rpm as a parameter are presented in figures 4.1 to 4.3. It can be clearly observed that the pump head decreases with increasing volume flow rate due to decreasing liquid pressure, in addition the pump head increases with increasing the pump rotational speed for the different blade numbers.

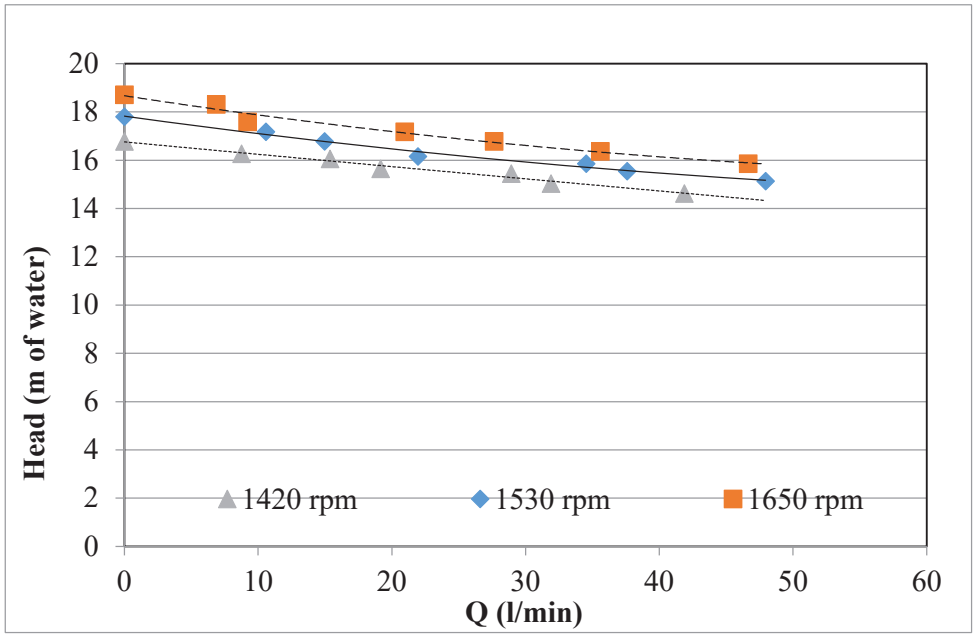

Fig.4.1 Pump rotational speed effect on head with 0.02 unstable emulsion for pump impeller with 7 blades

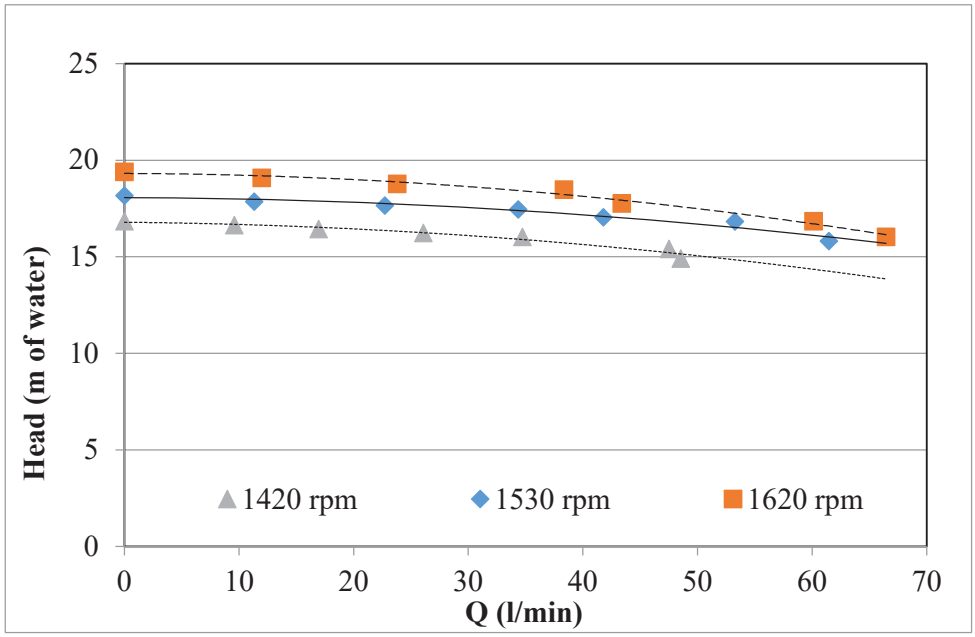

Fig.4.2 Pump rotational speed effect on head with 0.01 stable emulsion for pump impeller with 6 blades.

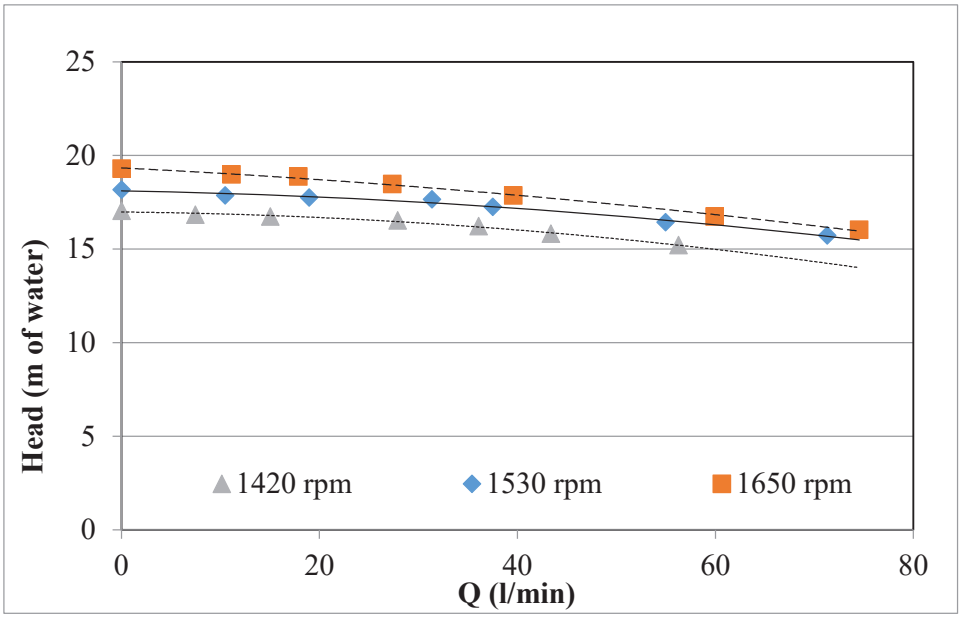

Fig.4.3 Pump rotational speed effect on head with 0.005 stable emulsion for pump impeller with 5 blades.

Figures 4.4 to 4.6 present some examples of the curves representing the shaft power as a function of the volume flow rate while also having the rpm as a parameter. It can be observed that the shaft power increase proportionally with the volume flow rate, also the shaft power increase by increasing the rpm.

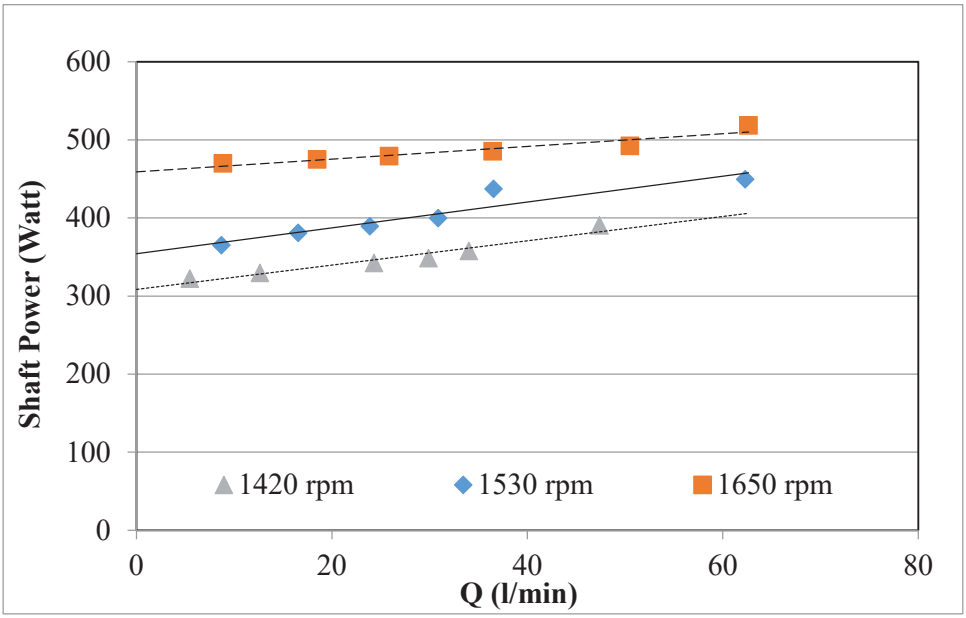

Fig.4.4 Pump rotational speed effect on shaft power with water for pump impeller with 7 blades

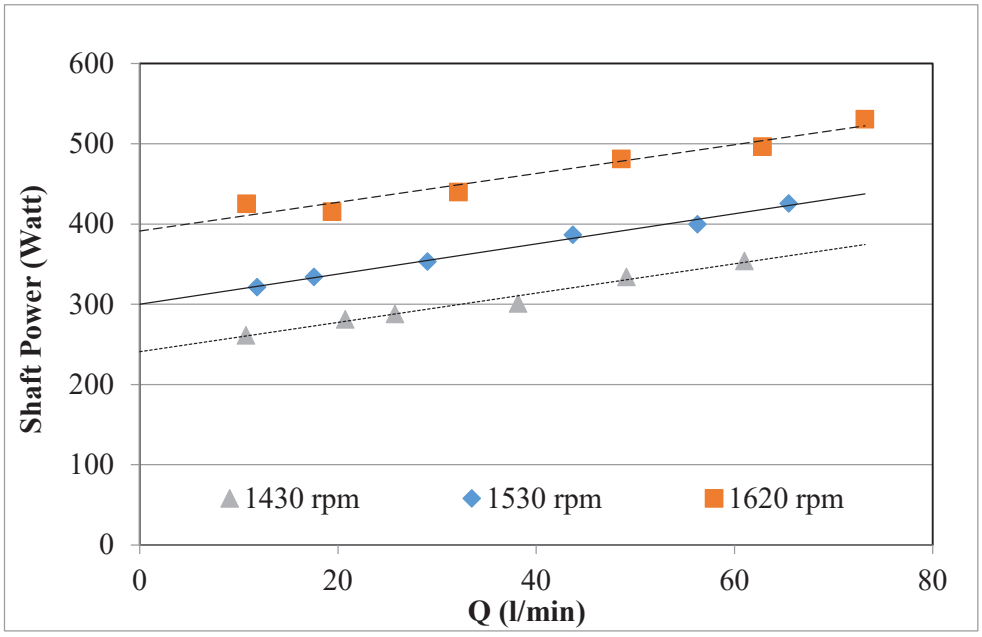

Fig.4.5 Pump rotational speed effect on shaft power with 0.02 stable emulsion for pump impeller with 6 blades

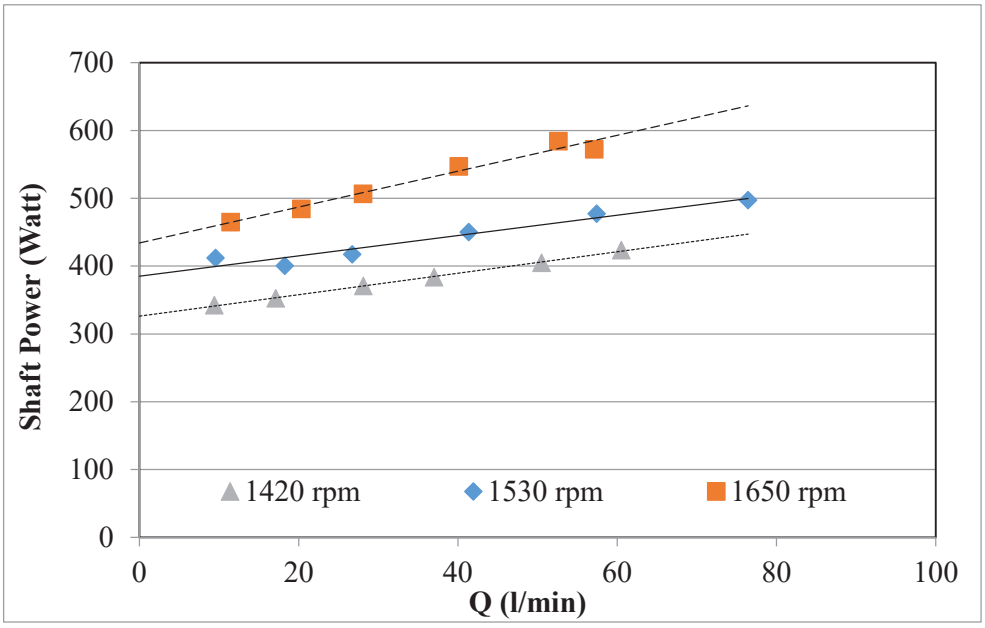

Fig.4.6 Pump rotational speed effect on shaft power with 0.01 unstable emulsion for pump impeller with 5 blades

Figures 4.7 to 4.9 presents three examples of the curves representing the pump efficiency as a function of the volume flow rate while also having the rpm as a parameter. It can be

observed that the pump efficiency increase proportionally with the volume flow rate, it is also observed that the rotational speed of 1420 rpm showed the best pump efficiency, due to less used shaft power.

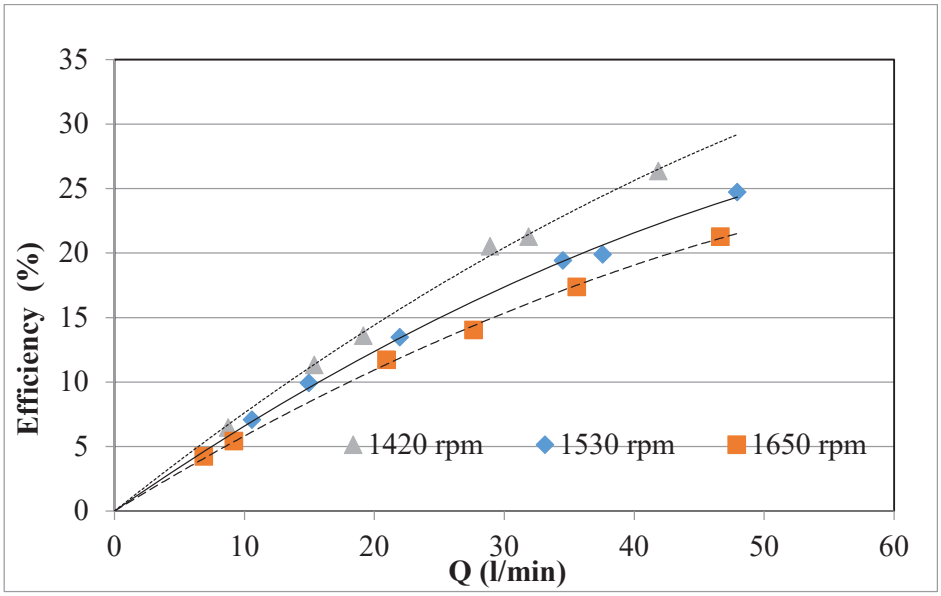

Fig.4.7 Pump rotational speed effect on pump efficiency with 0.02 unstable emulsion for pump impeller with 7 blades

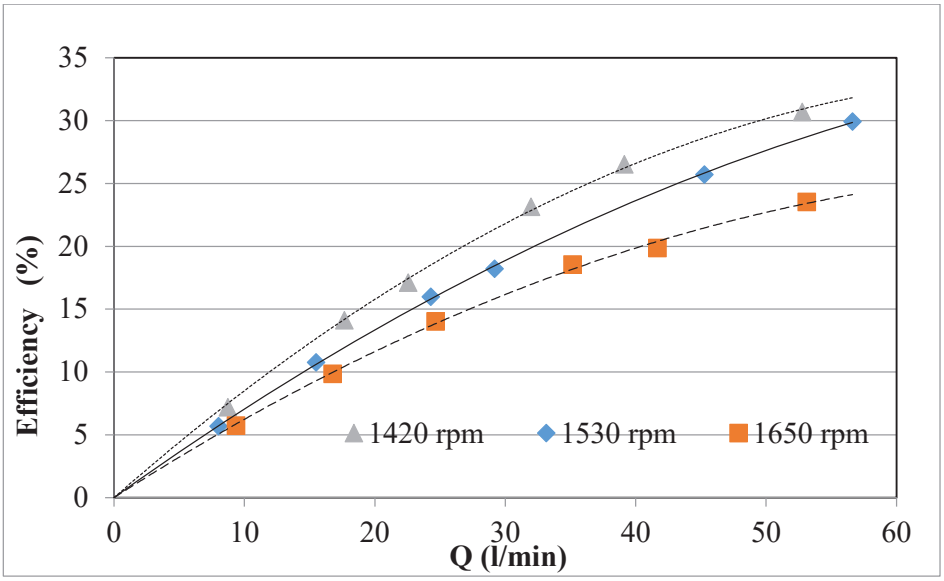

Fig.4.8 Pump rotational speed effect on pump efficiency with 0.02 stable emulsion for pump impeller with 6 blades

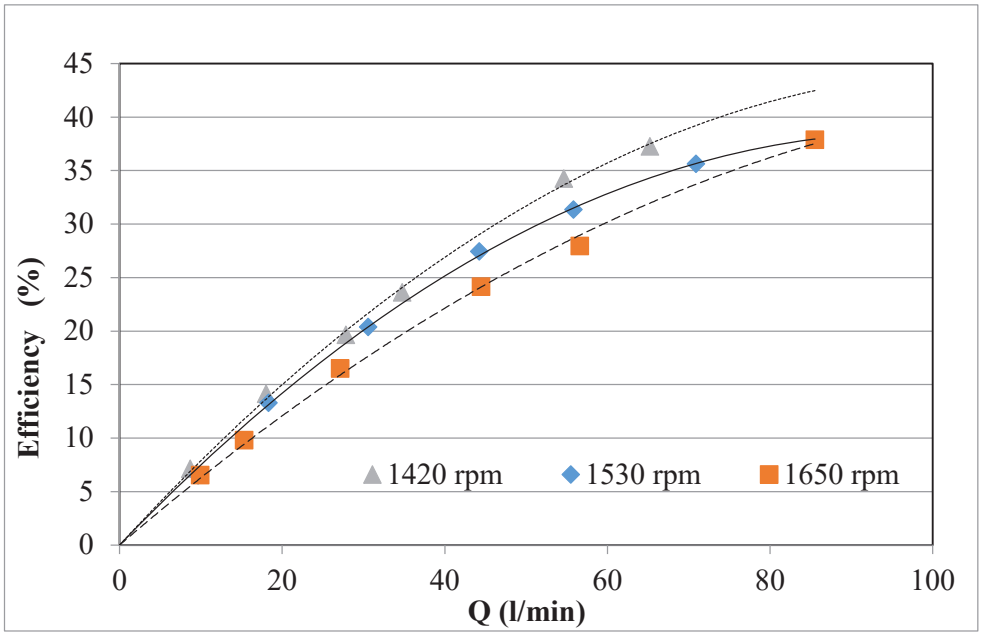

Fig.4.9 Pump rotational speed effect on pump efficiency with water for pump impeller with 5 blades

Figure 3.5 shows the second set of impellers. Each impeller has the same parameters with the same number of blades but with different blade inlet angle (β_1). Impeller (a) has inlet angle of (10°), impeller (d) has inlet angle of (20°) and impeller (e) has inlet angle of (30°). Each of the mentioned impellers is to be tested for performance while pumping water alongside three stable emulsions and three unstable emulsions, and they are also to be tested at three different shaft rotational speed (1420,1530,1650) rpm.

Examples of the curves expressing the pump head as function of the volume flow rate with rpm as a parameter are presented in figures 4.10 to 4.12. It can be clearly observed that the pump head decreases with increasing volume flow rate due to decreasing liquid pressure, in addition the pump head increases with increasing the pump rotational speed for the different blade inlet angels.

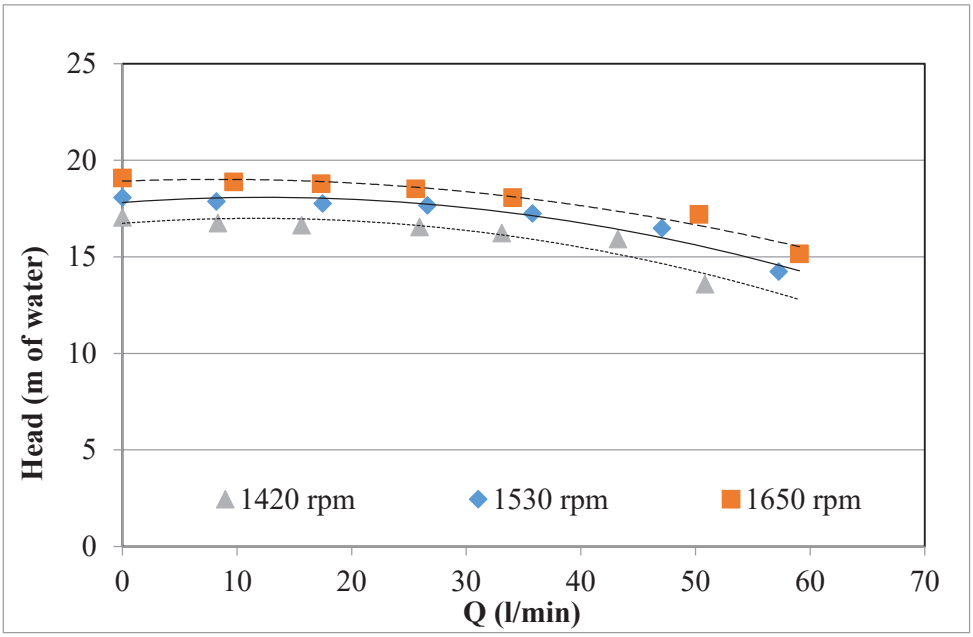

Fig.4.10 Pump rotational speed effect on head with 0.005 stable emulsion for pump impeller with inlet angle 10°

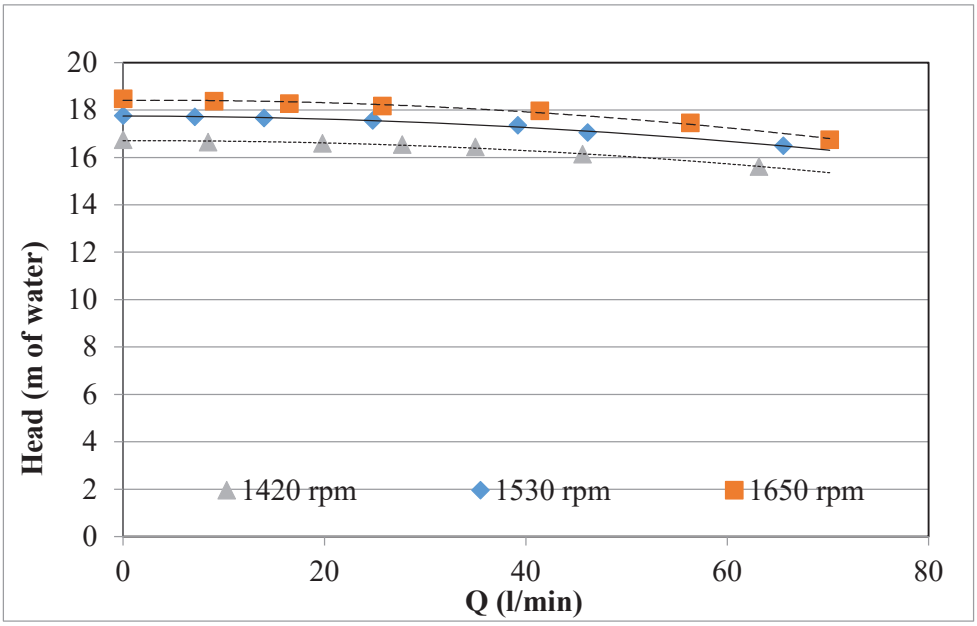

Fig.4.11 Pump rotational speed effect on head with 0.01 stable emulsion for pump impeller with inlet angle 20°

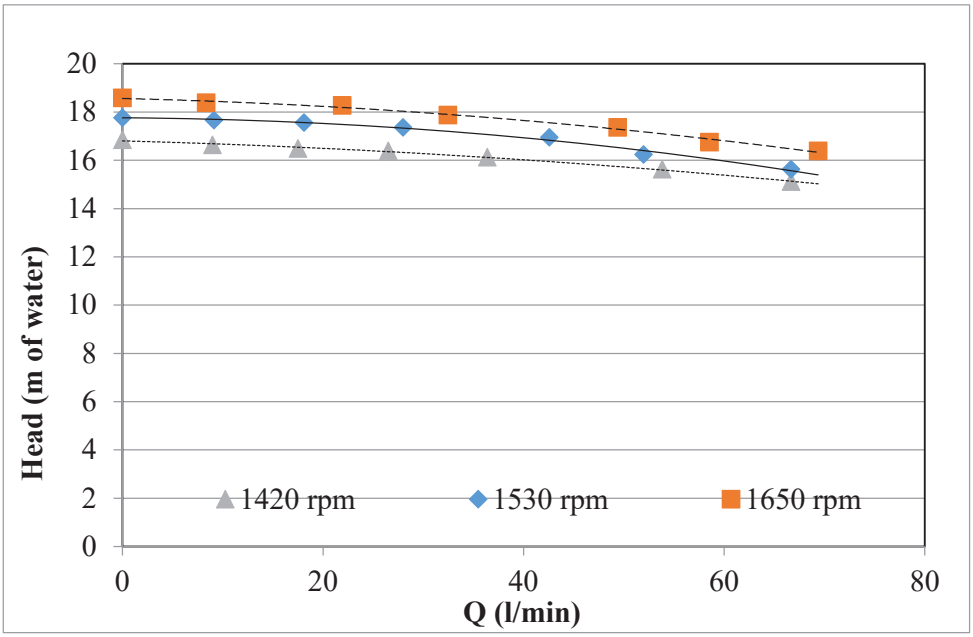

Fig.4.12 Pump rotational speed effect on head with 0.005 unstable emulsion for pump impeller with inlet angle 30°

Figures 4.13 to 4.15 present some examples of the curves representing the shaft power as a function of the volume flow rate while also having the rpm as a parameter. It can be observed that the shaft power increase proportionally with the volume flow rate, also the shaft power increase by increasing the rpm.

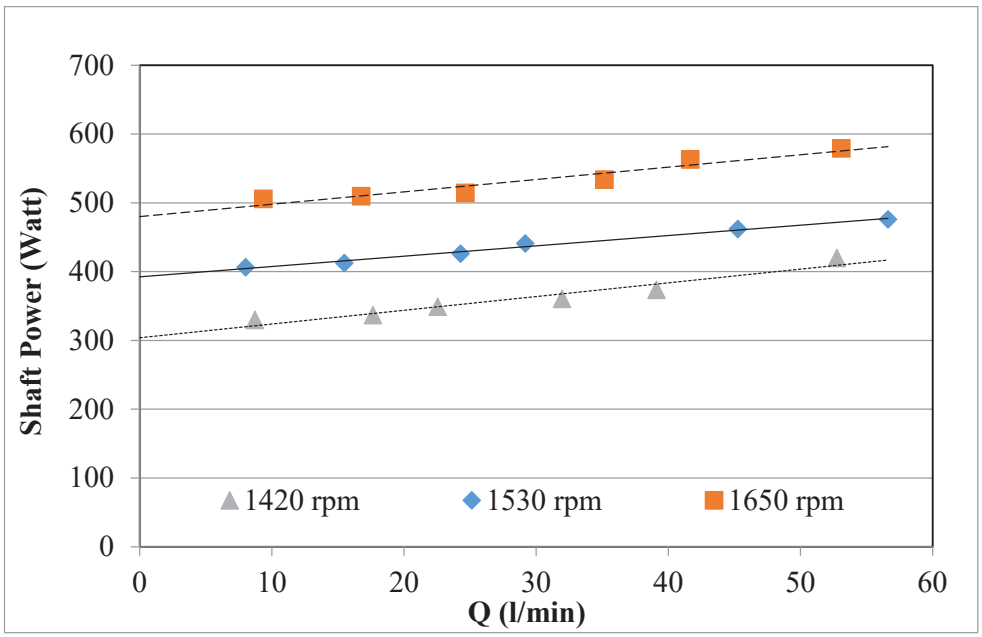

Fig.4.13 Pump rotational speed effect on shaft power with 0.005 unstable emulsion for pump impeller with inlet angle 10°

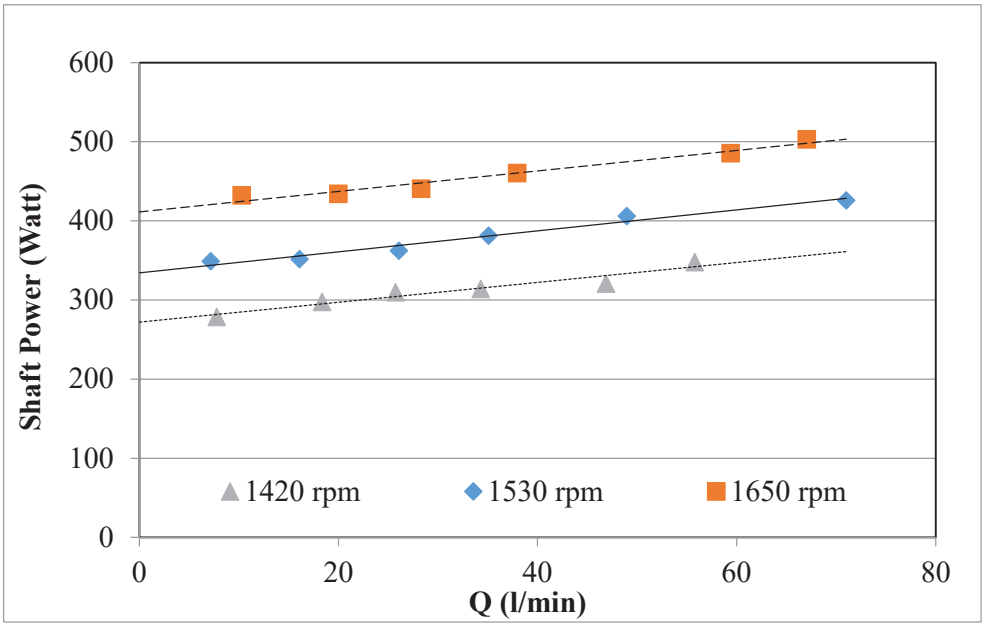

Fig.4.14 Pump rotational speed effect on shaft power with 0.005 stable emulsion for pump impeller with inlet angle 20°

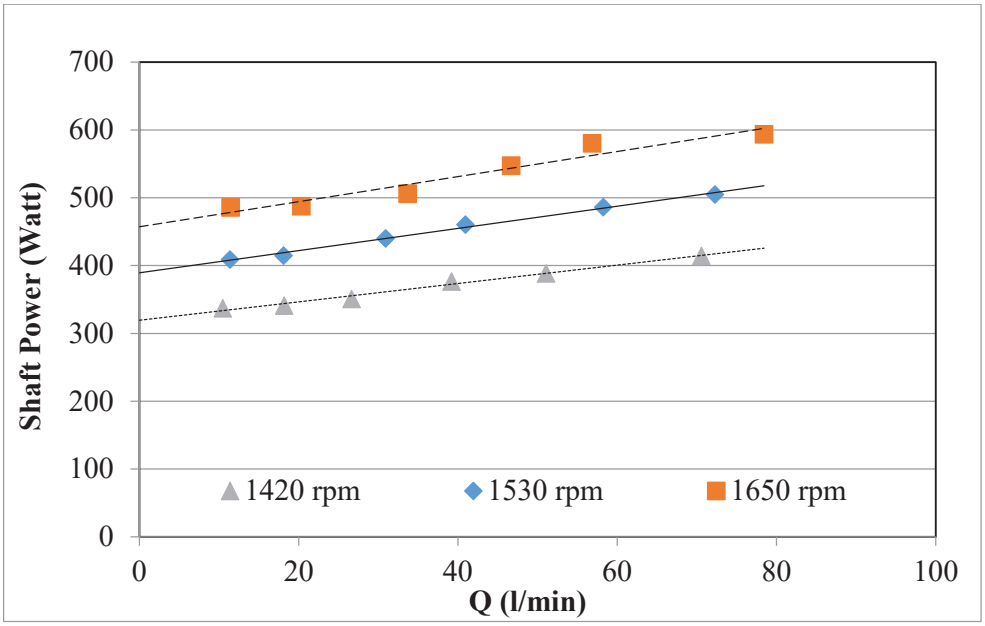

Fig.4.15 Pump rotational speed effect on shaft power with water for pump impeller with inlet angle 30°

Figures 4.16 to 4.18 present three examples of the curves representing the pump efficiency as a function of the volume flow rate while also having the rpm as a parameter. It can be

observed that the pump efficiency increases proportionally with the volume flow rate. It is also observed that the rotational speed of 1420 rpm showed the best pump efficiency.

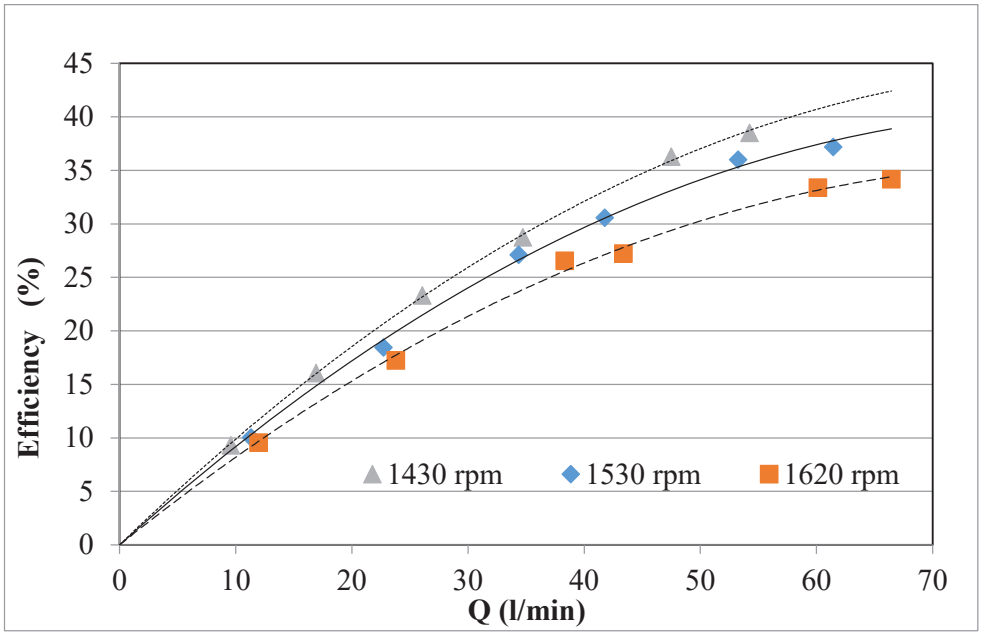

Fig.4.16 Pump rotational speed effect on pump efficiency with 0.01 stable emulsion for pump impeller with inlet angle 10°

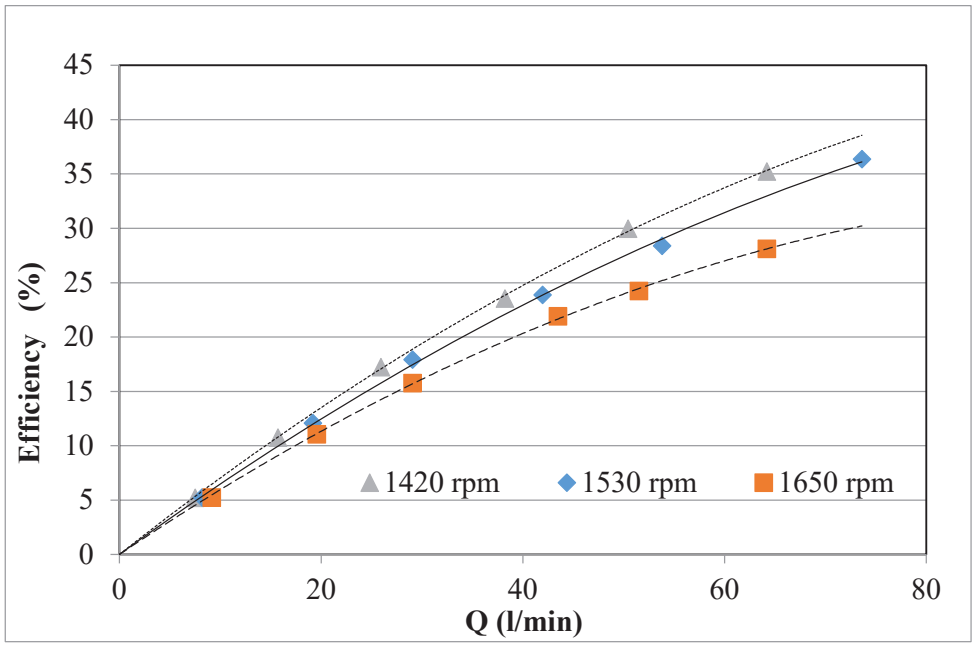

Fig.4.17 Pump rotational speed effect on pump efficiency with 0.005 unstable emulsion for pump impeller with inlet angle 20°

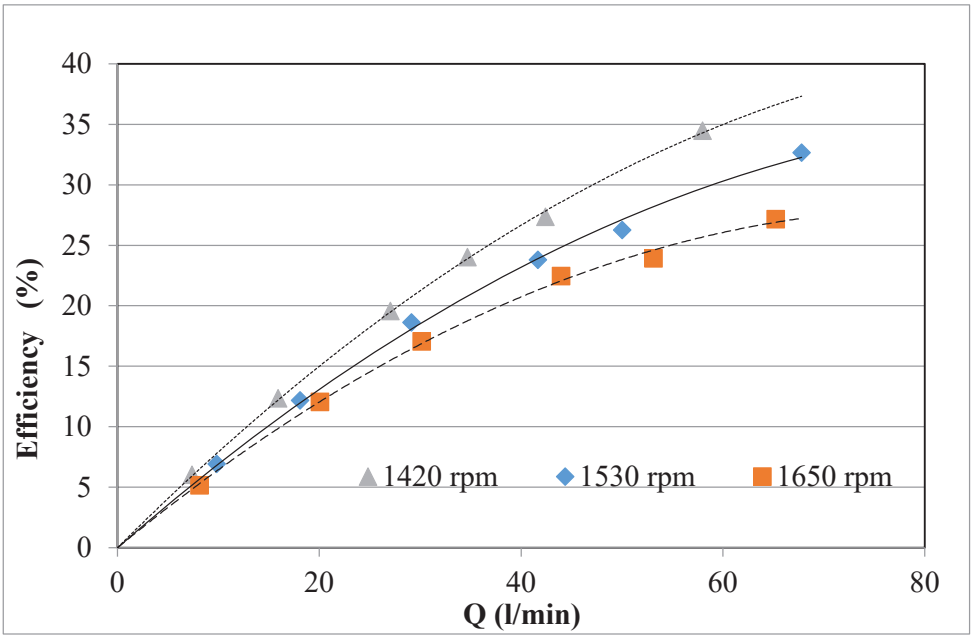

Fig.4.18 Pump rotational speed effect on pump efficiency with 0.02 unstable emulsion for pump impeller with inlet angle 30°

Figure 3.6 shows the third set of impellers. Each impeller has the same parameters with the same number of blades but with different blade outlet angle (β_2). Impeller (a) has outlet angle of (30°), impeller (f) has outlet angle of (25°) and impeller (g) has outlet angle of (20°). Each of the mentioned impellers is to be tested for performance while pumping water alongside three stable emulsions and three unstable emulsions, They also are to be tested at three different shaft rotational speeds (1420,1530,1650) rpm.

Examples of the curves expressing the pump head as a function of the volume flow rate with rpm as a parameter are presented in figures 4.19 to 4.21. It can be clearly observed that the pump head decreases with increasing volume flow rate due to decreasing liquid pressure, in addition the pump head increases with increasing the pump rotational speed for the different blade outlet angels.

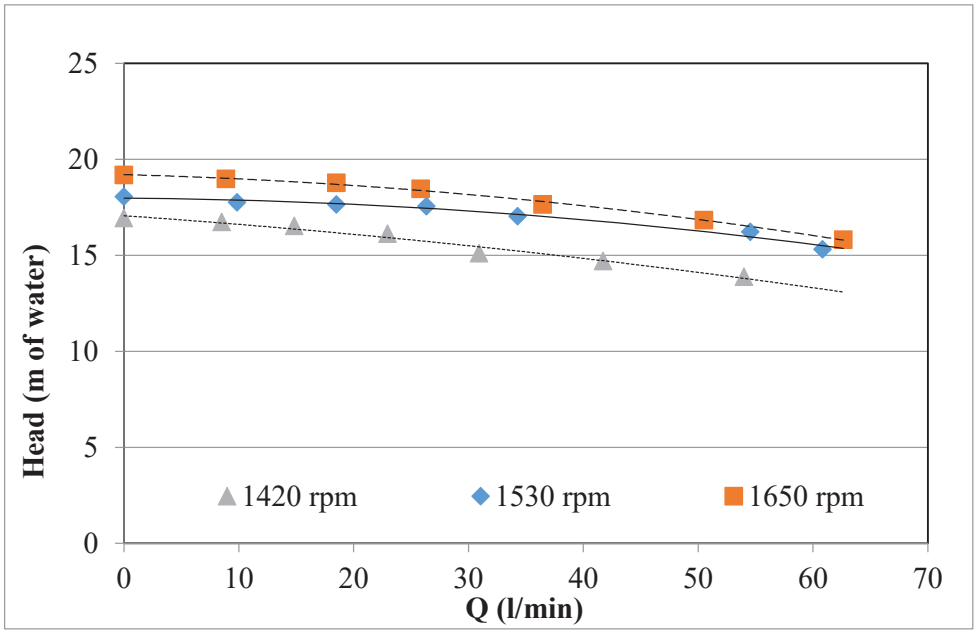

Fig.4.19 Pump rotational speed effect on head with water for pump impeller with outlet angle 30°

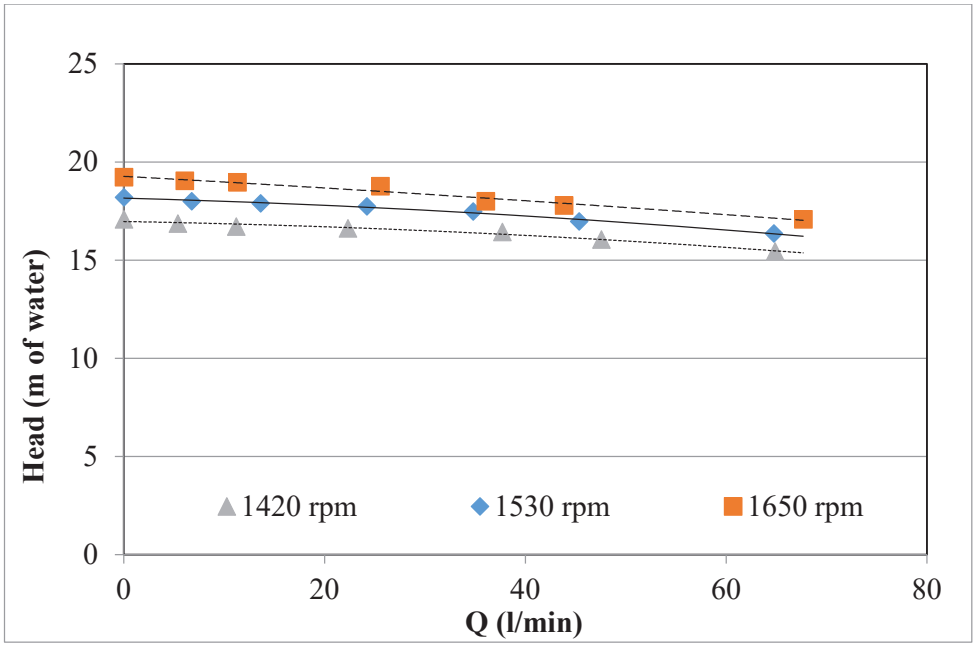

Fig.4.20 Pump rotational speed effect on head with 0.02 unstable emulsion for pump impeller with outlet angle 25°

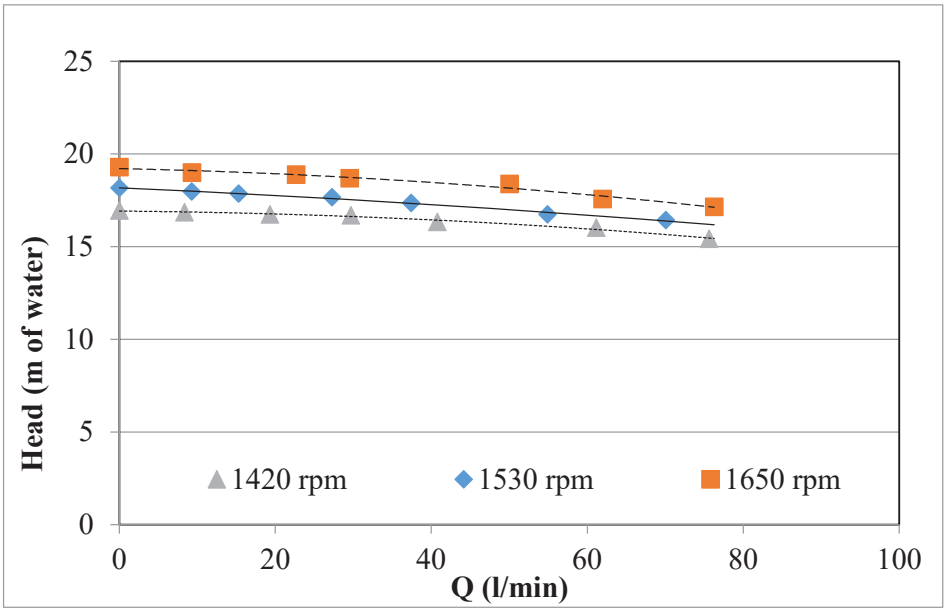

Fig.4.21 Pump rotational speed effect on head with 0.005 unstable emulsion for pump impeller with outlet angle 20°

Figures 4.22 to 4.24 present some examples of the curves representing the shaft power as a function of the volume flow rate while also having the rpm as a parameter. It can be observed that the shaft power increases proportionally with the volume flow rate, and also the shaft power increases by increasing the rpm.

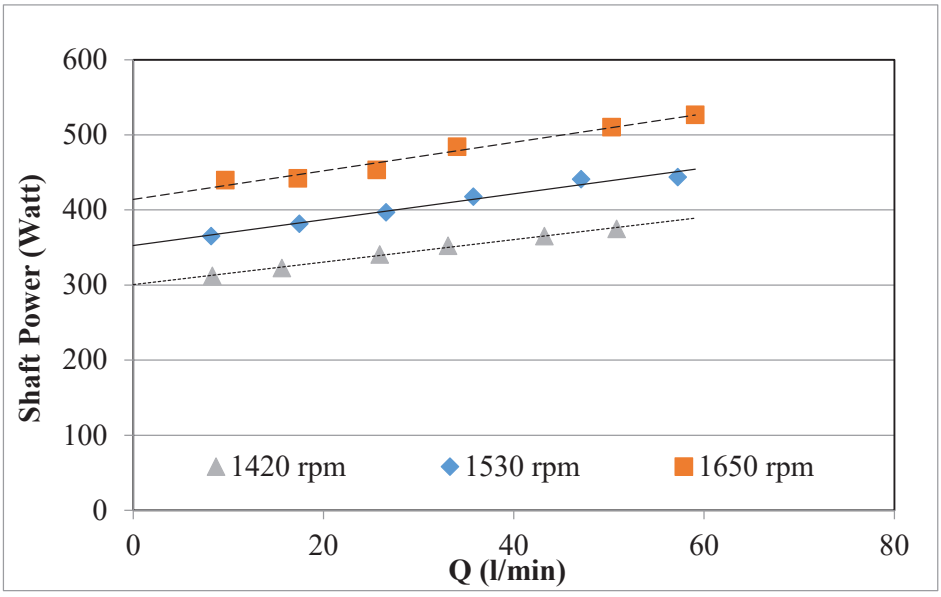

Fig.4.22 Pump rotational speed effect on shaft power with 0.005 stable emulsion for pump impeller with outlet angle 30°

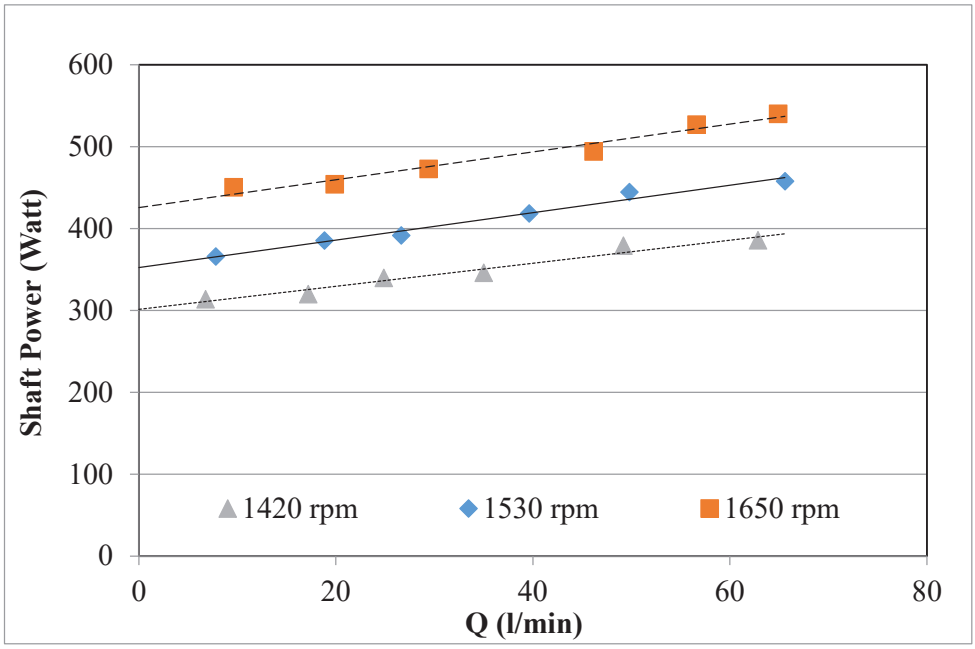

Fig.4.23 Pump rotational speed effect on shaft power with water for pump impeller with outlet angle 25°

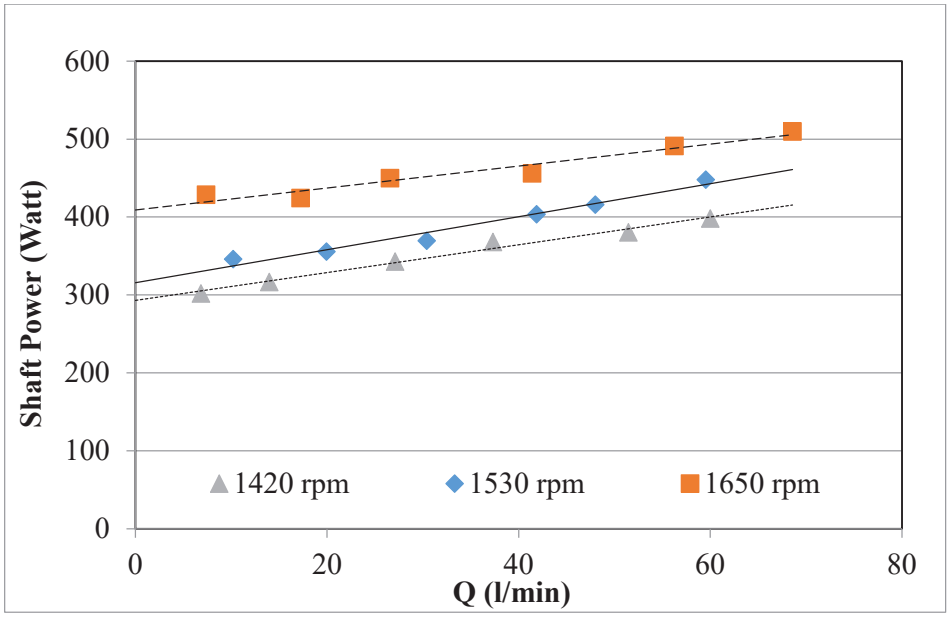

Fig.4.24 Pump rotational speed effect on shaft power with 0.01 unstable emulsion for pump impeller with outlet angle 20°

Figures 4.25 to 4.27 present three examples of the curves representing the pump efficiency as a function of the volume flow rate while also having the rpm as a parameter. It can be

observed that the pump efficiency increases proportionally with the volume flow rate, and it is also observed that the rotational speed of 1420 rpm showed the best pump efficiency.

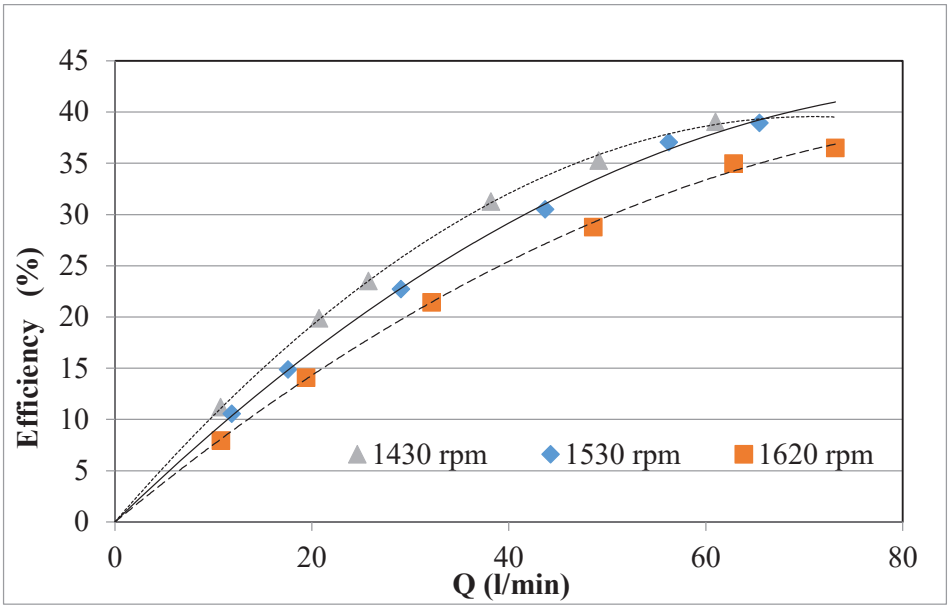

Fig.4.25 Pump rotational speed effect on pump efficiency with 0.02 stable emulsion for pump impeller with outlet angle 30°

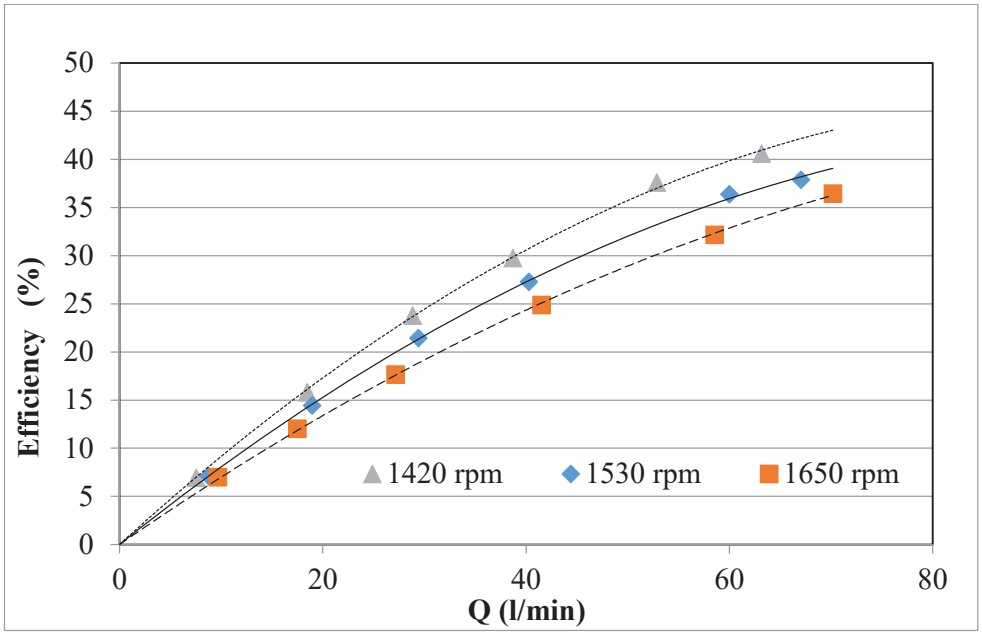

Fig.4.26 Pump rotational speed effect on pump efficiency with 0.005 stable emulsion for pump impeller with outlet angle 25°

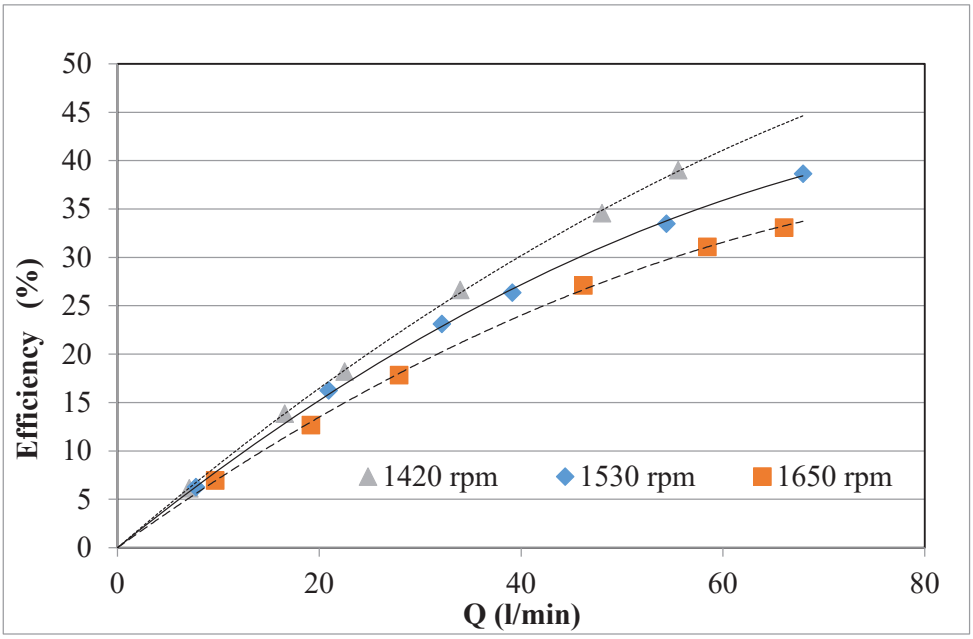

Fig.4.27 Pump rotational speed effect on pump efficiency with 0.02 unstable emulsion for pump impeller with output angle 20°

4.3 EFFECT OF IMPELLER BLADE NUMBER

In order to have a better understanding of the effect of the impellers blade number (z) on the performance of the centrifugal pump we have three different impellers, each has the same parameters except for the number of blades. Impeller (a) has 6 blades, impeller (b) has 5 blades and impeller (c) has 7 blades.

Each of the mentioned impellers shown in Figure 3.4 will be tested for performance while pumping water alongside three stable emulsions and three unstable emulsions. They also are to be tested at three different shaft rotational speeds (1420,1530,1650) rpm.

An example of the curves expressing the pump head as function of the volume flow rate with blade number as a parameter are presented in figure 4.28. It can be clearly observed that the pump head decreases with increasing volume flow rate due to decreasing liquid pressure, in addition the pump head increases with increasing the blade number.

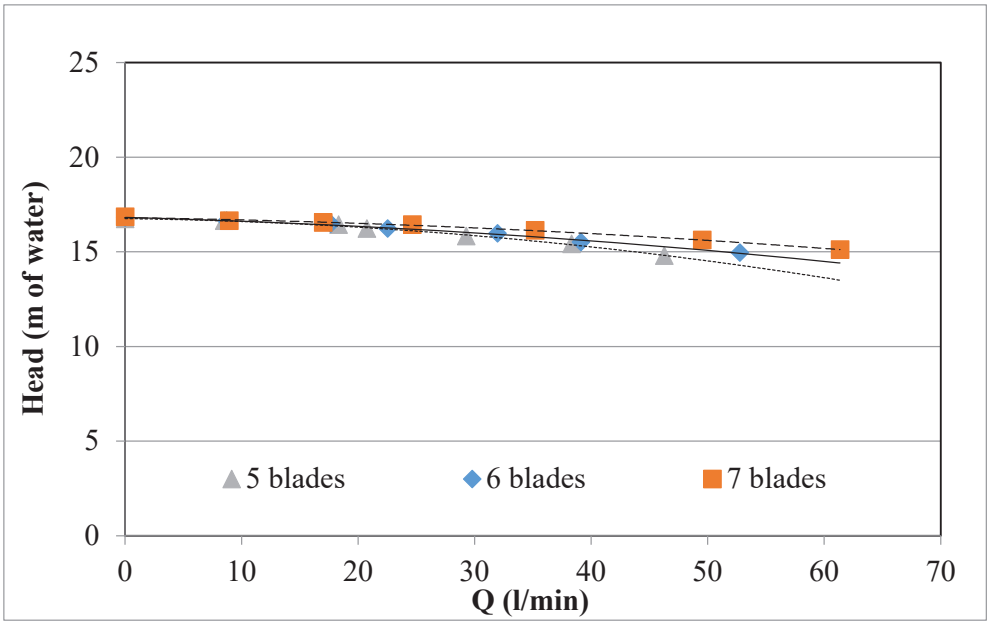

Fig.4.28 Number of blades effect on head for 0.005 unstable emulsion with pump running at 1420 rpm

Figure 4.29 presents an example of the curves representing the shaft power as a function of the volume flow rate while also having the blade number as a parameter. It can be observed that the shaft power increase proportionally with the volume flow rate, also the shaft power increase by increasing the blade number.

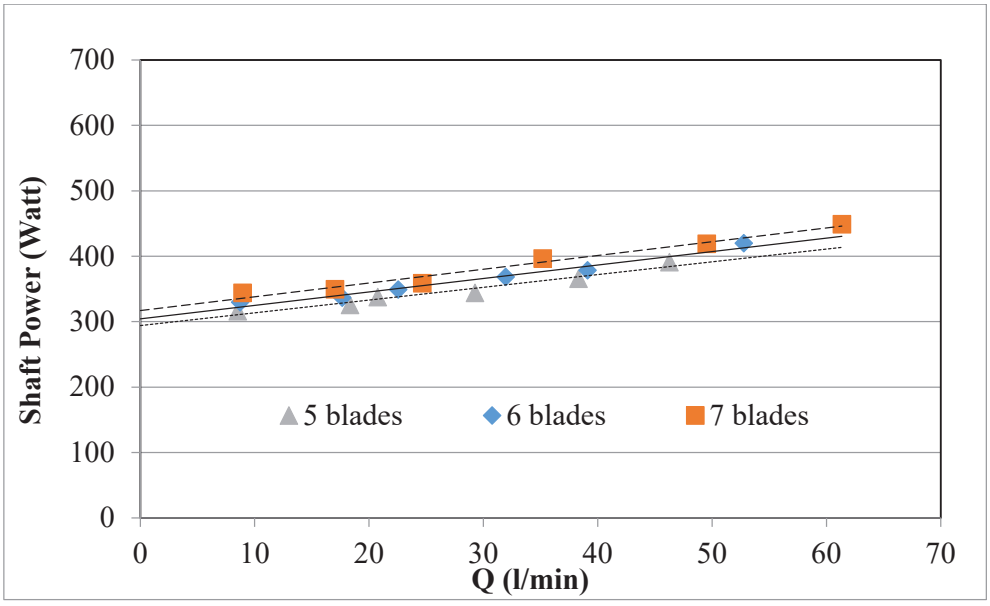

Fig.4.29 Number of blades effect on shaft power for 0.02 stable emulsion with pump running at 1650 rpm

Figure 4.30 presents an example of the curves representing the pump efficiency as a function of the volume flow rate while also having the blade number as a parameter. It can be observed that the pump efficiency increases proportionally with the volume flow rate, it is also observed that the impeller with (5) blades showed the best pump efficiency, this is attributed to the rise of the shaft power as a result of the increased surface friction that results from increasing the blade number.

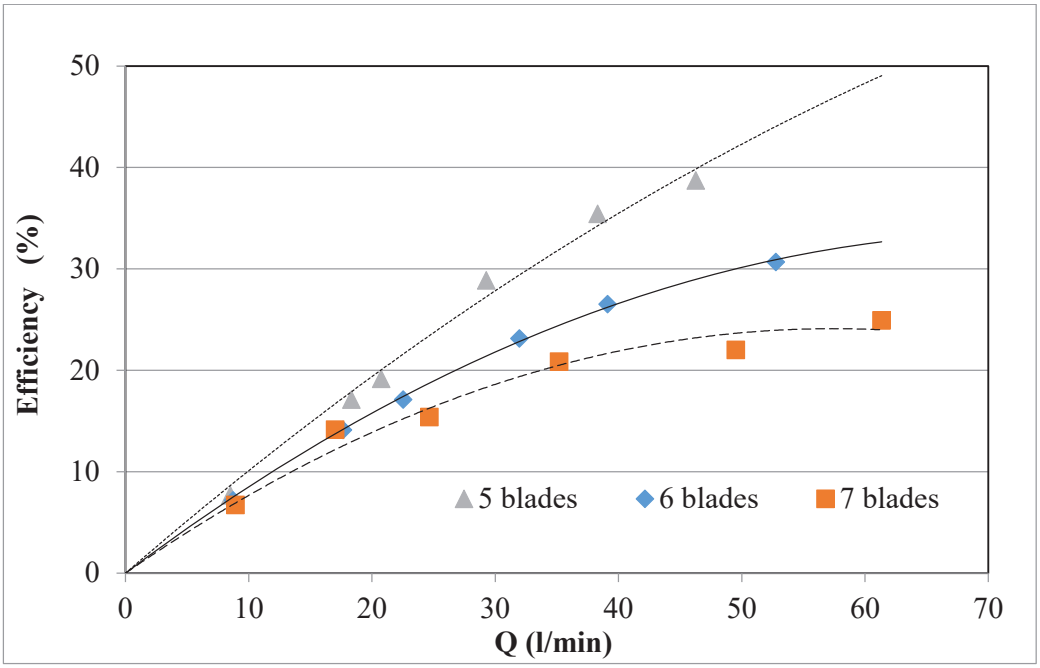

Fig.4.30 Number of blades effect on pump efficiency for 0.005 unstable emulsion with pump running at 1420 rpm

4.4 EFFECT OF IMPELLER BLADE INLET ANGLE

For the purpose of testing the effect of the impellers blade inlet angle, the same method is to be applied as well, for three different impellers, each has the same parameters with the same number of blades but with different blade inlet angle (β_1). Impeller (a) has inlet angle of (10°), impeller (d) has inlet angle of (20°) and impeller (e) has inlet angle of (30°). Figure 3.5 shows the test impellers, each of the mentioned impellers is to be tested for performance while pumping water alongside three stable emulsions and three unstable emulsions, they also are to be tested at three different shaft rotational speed (1420,1530,1650) rpm.

An example of the curves expressing the pump head as function of the volume flow rate with inlet angle as a parameter are presented in figure 4.31. It can be clearly observed that the pump head decreases with increasing volume flow rate due to decreasing liquid pressure similar to the observation in the impellers with different blade number. In addition, the pump head tends to show higher values with the impeller of inlet angle (β_1= 20°).

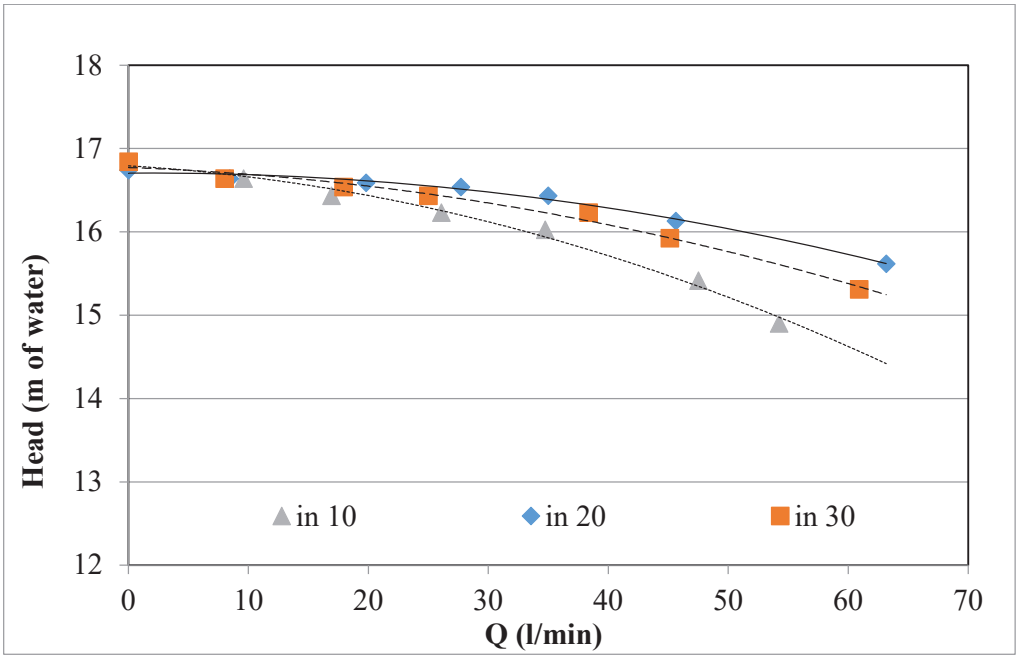

Fig.4.31 Blade inlet angle effect on head for 0.01 stable emulsion with pump running at 1420 rpm

Figure 4.32 presents an example of the curves representing the shaft power as a function of the volume flow rate while also having the blade inlet angle as a parameter. It can be observed that the shaft power increase proportionally with the volume flow rate, also the shaft power increases by increasing the blade inlet angle.

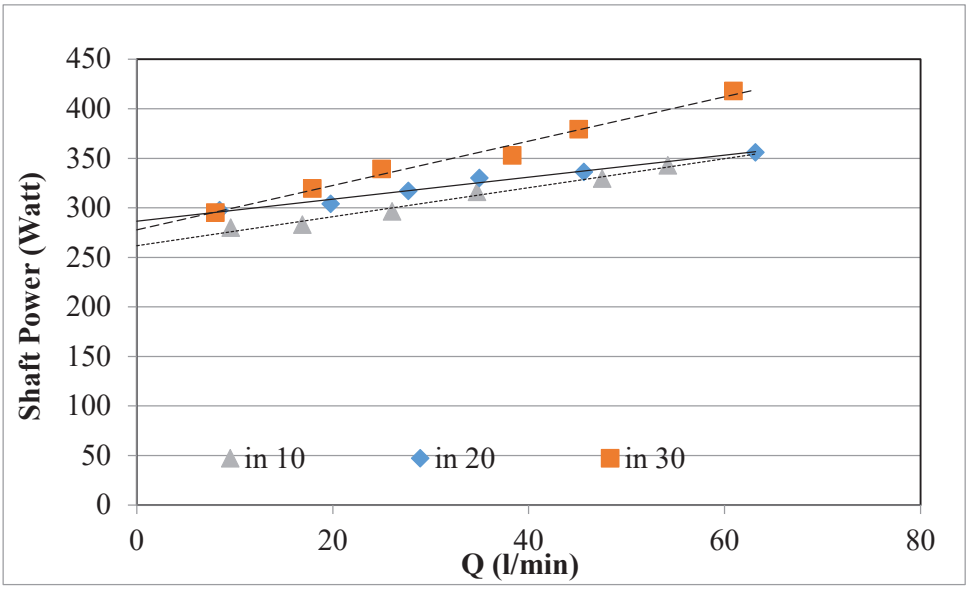

Fig.4.32 Blade inlet angle effect on shaft power for 0.01 stable emulsion with pump running at 1420 rpm

Figure 4.33 Presents an example of the curves representing the pump efficiency as a function of the volume flow rate while having the blade inlet angle as a parameter. It can be observed that the pump efficiency increase proportionally with the volume flow rate, and it is also observed that the impeller with inlet angle (β_1= 10°) showed the best pump efficiency which matches the original factory optimum design as well.

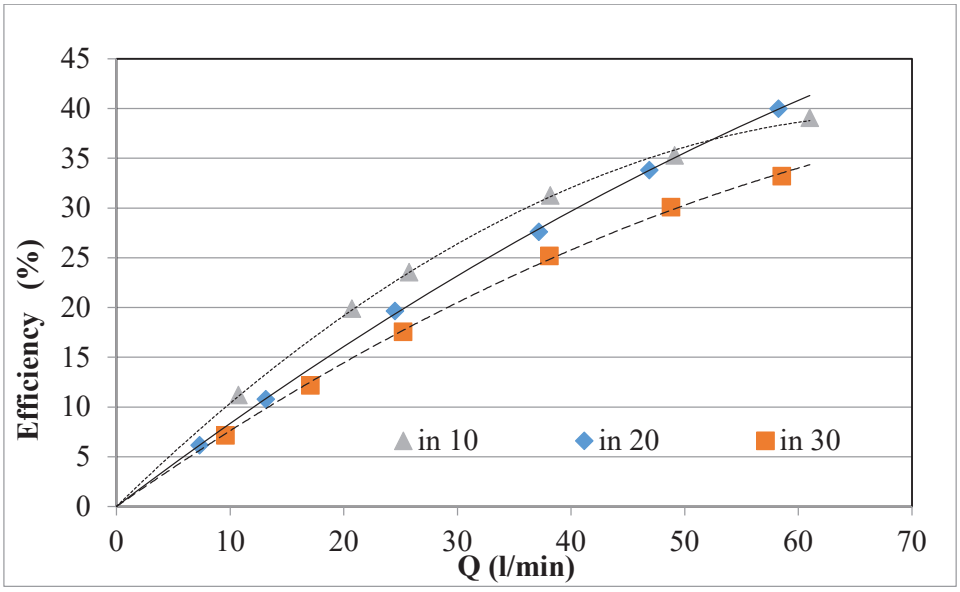

Fig.4.33 Blade inlet angle effect pump efficiency for 0.02 stable emulsion with pump running at 1420 rpm

4.5 EFFECT OF IMPELLER BLADE OUTLET ANGLE

For the purpose of testing the effect of the impellers blade outlet angle, the same method is to be applied as well with three different impellers, each has the same parameters with the same number of blades but with different blade outlet angle (β_2) impeller (a) has outlet angle of (30°), impeller (f) has outlet angle of (25°) and impeller (g) has outlet angle of (20°). Figure 3.6 shows the test impellers, each of the mentioned impellers is to be tested for performance while pumping water alongside three stable emulsions and three unstable emulsions. They are also to be tested at three different shaft rotational speed (1420,1530,1650) rpm.

An example of the curves expressing the pump head as function of the volume flow rate with outlet angle as a parameter are presented in figure 4.34. It can be clearly observed that the pump head decreases with increasing volume flow rate due to decreasing liquid pressure similar to the observation. In the impellers with different blade number. In addition, the pump head tends to show higher values with the impeller of outlet angle (β_2= 25°)

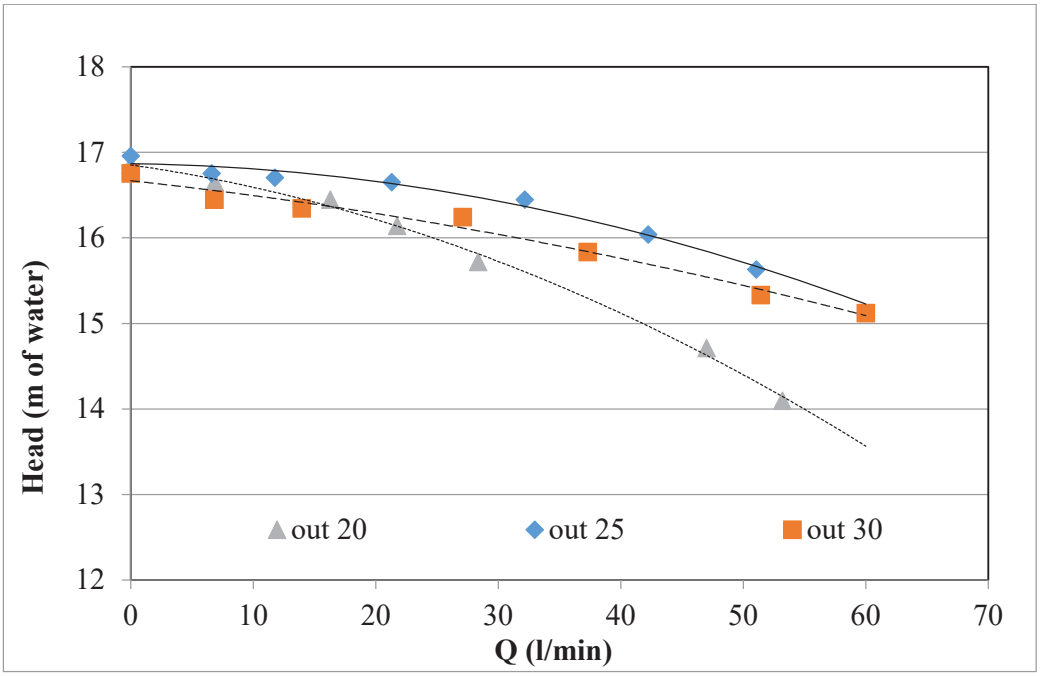

Fig.4.34 Blade outlet angle effect on head for 0.01 unstable emulsion with pump running at 1420 rpm

Figure 4.35 presents an example of the curves representing the shaft power as a function of the volume flow rate while also having the blade outlet angle as a parameter. It can be observed that the shaft power increases proportionally with the volume flow rate, and also the shaft power increase by decreasing the blade outlet angle.

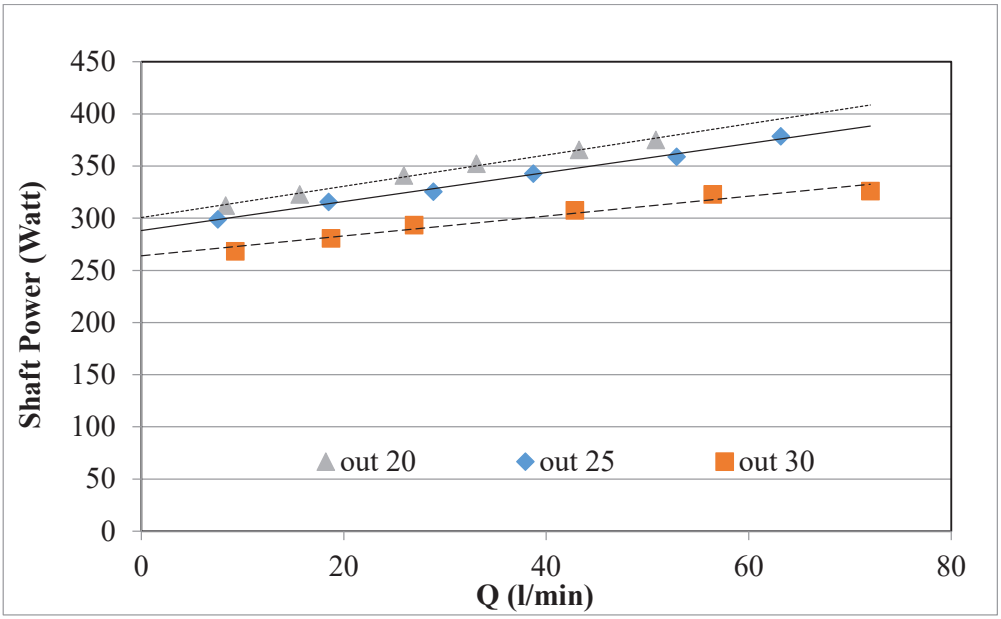

Fig.4.35 Blade outlet angle effect on shaft power for 0.005 stable emulsion with pump running at 1420 rpm

Figure 4.36 presents an example of the curves representing the pump efficiency as a function of the volume flow rate while having the blade outlet angle as a parameter. It can be observed that the pump efficiency increase proportionally with the volume flow rate, it is also observed that the impeller with outlet angle (β_2= 30°) showed the best pump efficiency which matches the original manufacturer's design as well.

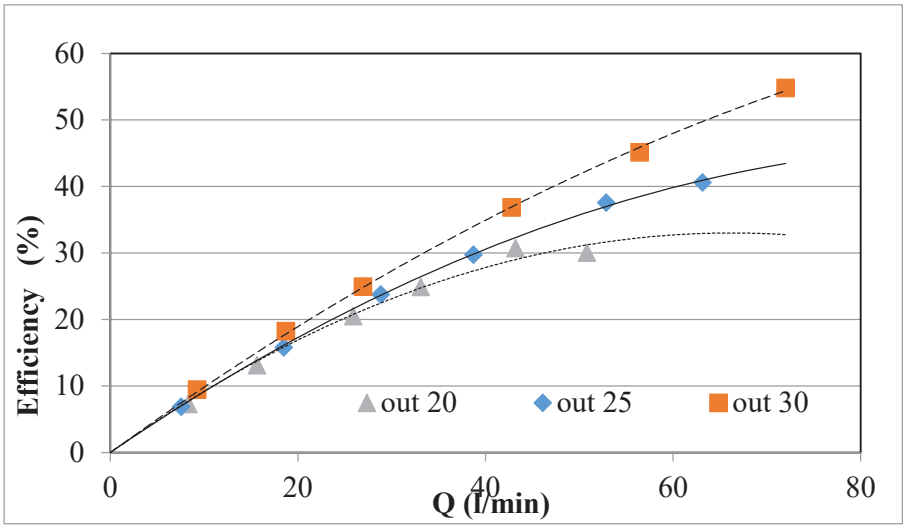

Fig.4.36 Blade outlet angle effect on pump efficiency for 0.005 stable emulsion with pump running at 1420 rpm

4.6 EFFECT OF EMULSION HOLDUP

For the purpose of understanding the effect of the emulsion holdup, water will be used as working fluid alongside 6 different (oil in water) emulsions. The emulsions are divided into two groups (stable and unstable) where each group consists of 3 emulsions with emulsion holdup Φ of (0.005, 0.01 and 0.02).

An example of the effect of the emulsion holdup on the pump head is shown on figure 4.37. It can be noted that increasing the emulsion holdup increases the pump head.

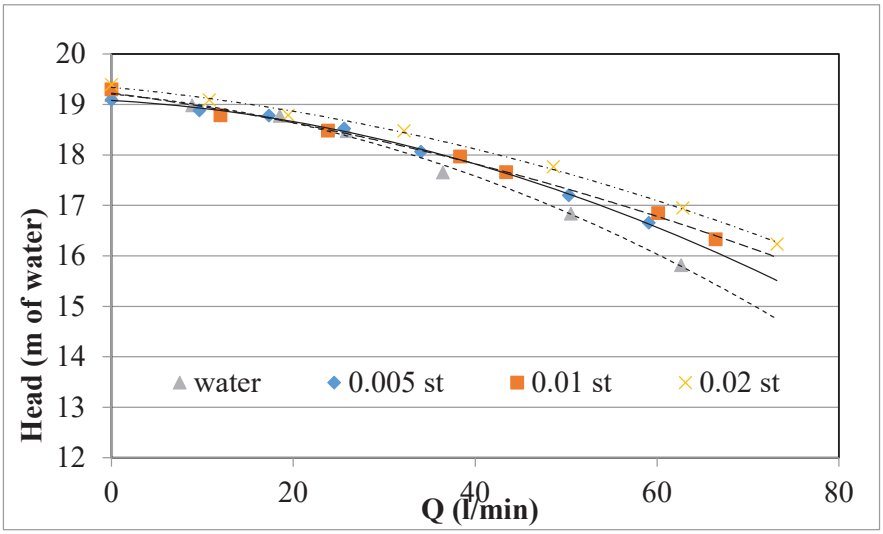

Fig.4.37 Emulsion holdup effect on head for blade inlet angle 10° with pump running at 1650 rpm (stable emulsions)

The effect of the emulsion holdup on the pump efficiency is shown in the example on figure 4.38. It shows that the pump efficiency increases with increasing the emulsion holdup. With emulsions with (Φ = 0.02) the best pump efficiency is shown in most of the cases.

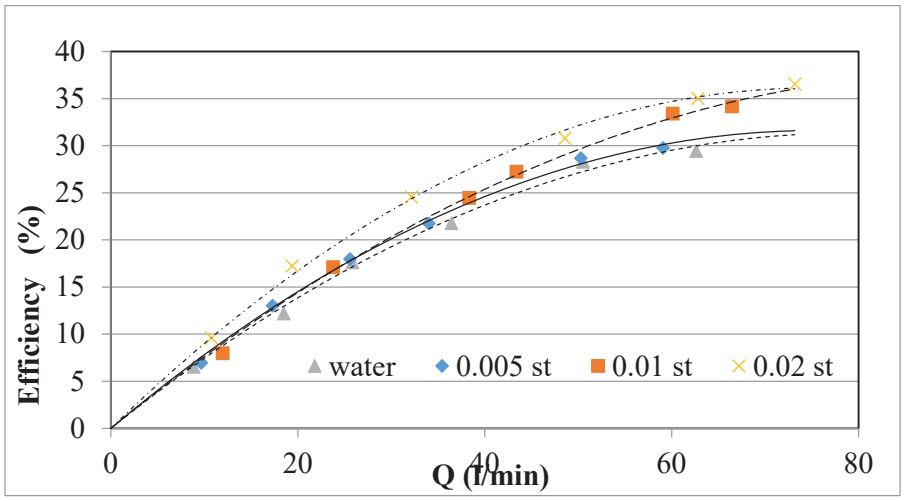

Fig.4.38 Emulsion holdup effect on pump efficiency for blade inlet angle 10° with pump running at 1650 rpm (stable emulsions)

The effect of the emulsion holdup on the consumed shaft power is shown in the example on figure 4.39. It shows that the shaft power decreases with increasing the emulsion holdup. With emulsions with (Φ = 0.02) using less shaft power in most of the cases.

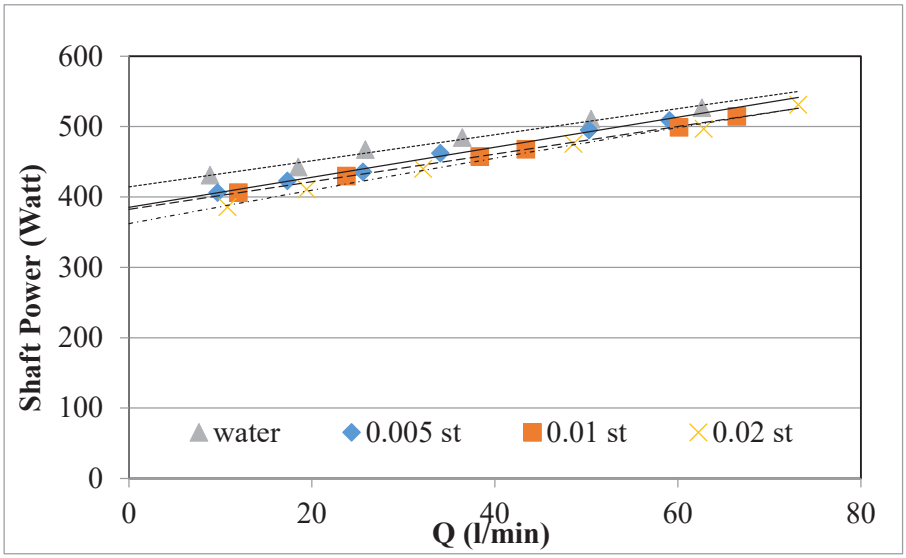

Fig.4.39 Emulsion holdup effect on shaft power for blade inlet angle 10° with pump running at 1650 rpm (stable emulsions)

4.7 EFFECT OF EMULSION STABILITY

The working fluids for the current study is to be the stable emulsions with holdup (0.005, 0.01 and 0.02) and the unstable emulsions are with holdup (0.005, 0.01 and 0.02). The emulsions performances were monitored throughout all the previous trials for parametric changes and at different rpms.

The following paragraphs discuses some samples of the emulsion stability effect on the pump performance.

Figures 4.40 to 4.42 show the emulsion stability effect on the pump head for some examples at different impeller design parameters, it is clear that the stable emulsions showed higher head values at the different test runs.

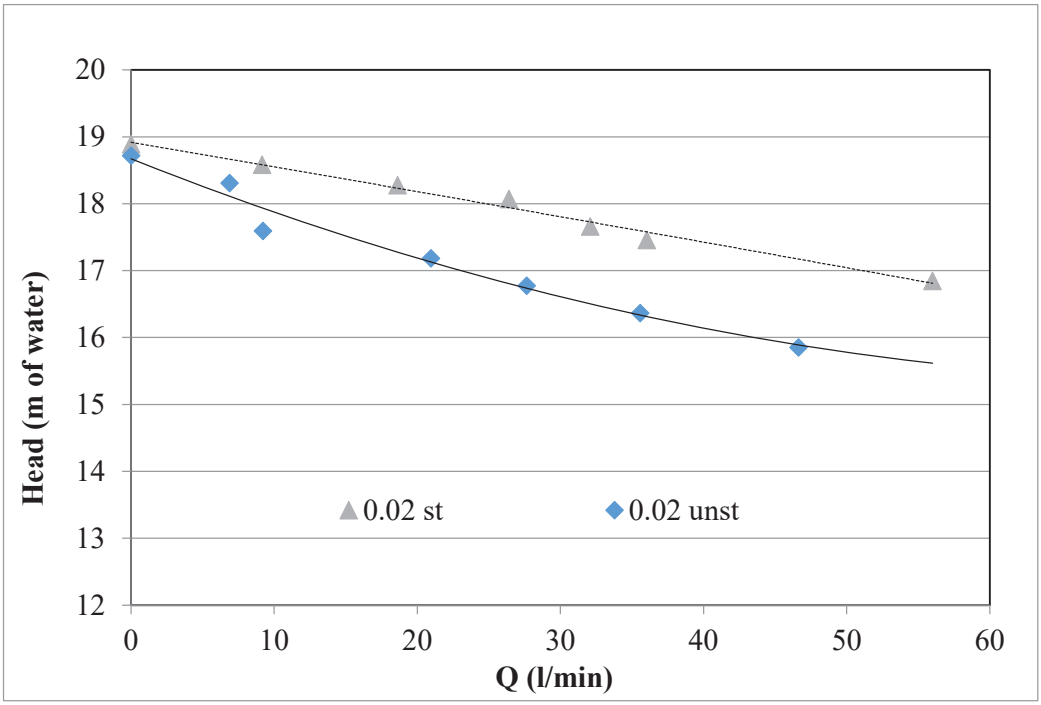

Fig.4.40 Emulsion stability effect on head for blade number (7) with pump running at 1650 rpm for emulsions with holdup ($\Phi = 0.02$)

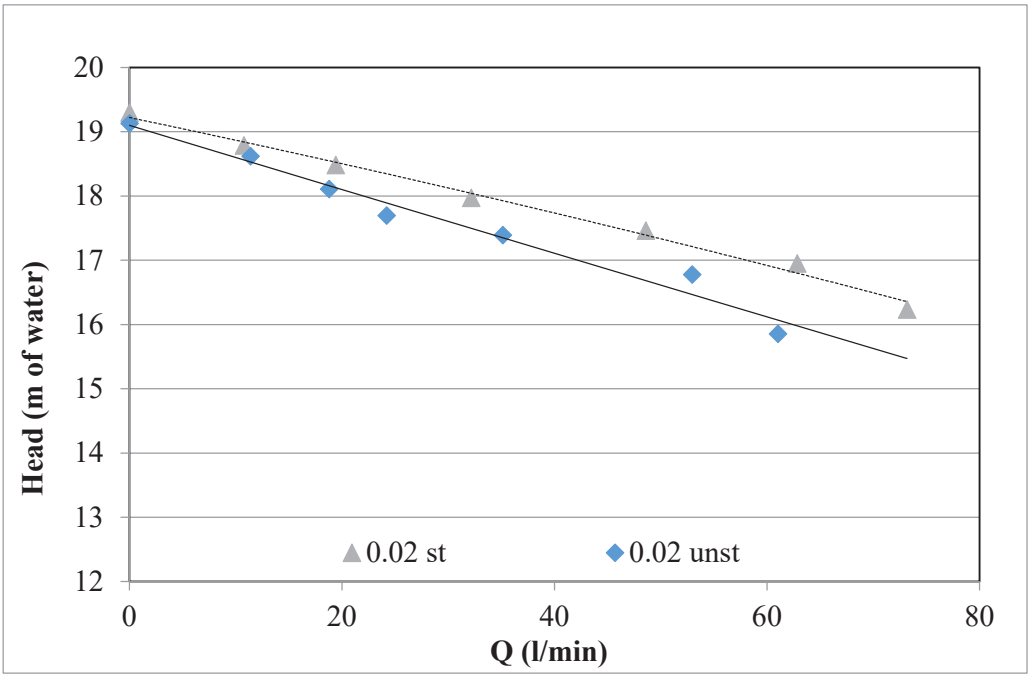

Fig.4.41 Emulsion stability effect on head for blade inlet angle 10° with pump running at 1650 rpm for emulsions with holdup (Φ = 0.02)

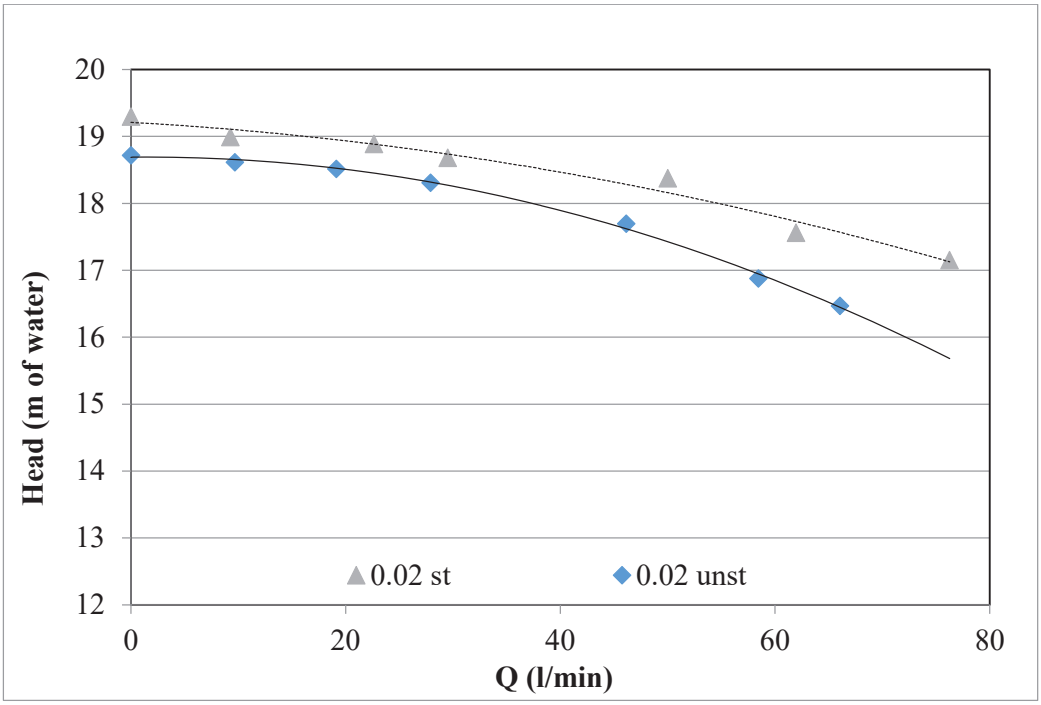

Fig.4.42 Emulsion stability effect on head for blade outlet angle 30° with pump running at 1650 rpm for emulsions with holdup (Φ = 0.02)

Figures 4.43 to 4.45 show the emulsion stability effect on the pump shaft power for some examples at different impeller design parameters. It is to be noted that the stable emulsions consumed lower shaft power values at the different test runs.

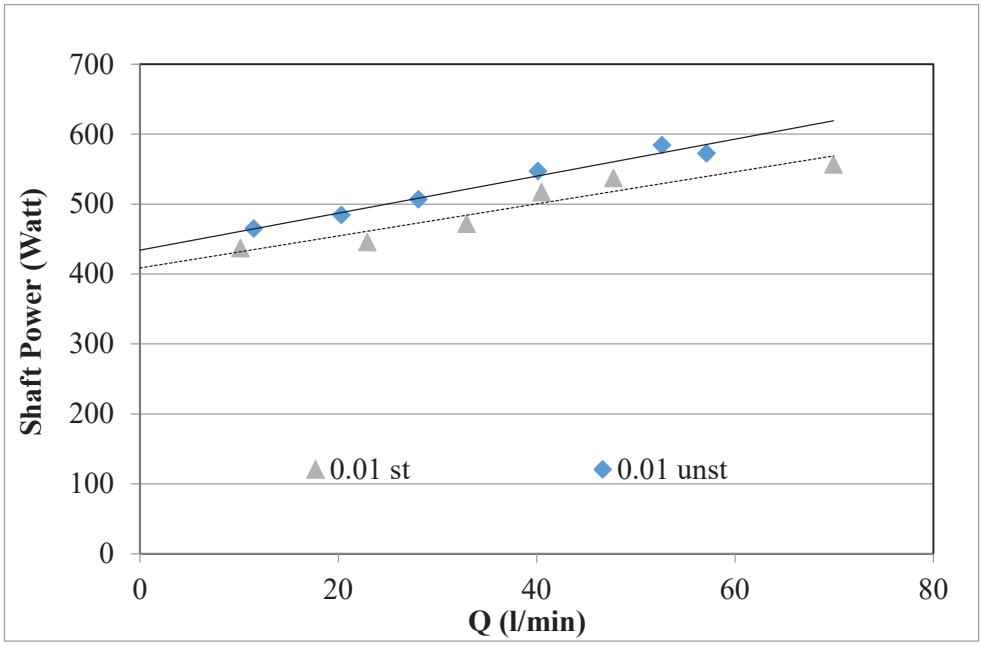

Fig.4.43 Emulsion stability effect on shaft power for blade number (5) with pump running at 1650 rpm for emulsions with holdup ($\Phi = 0.01$)

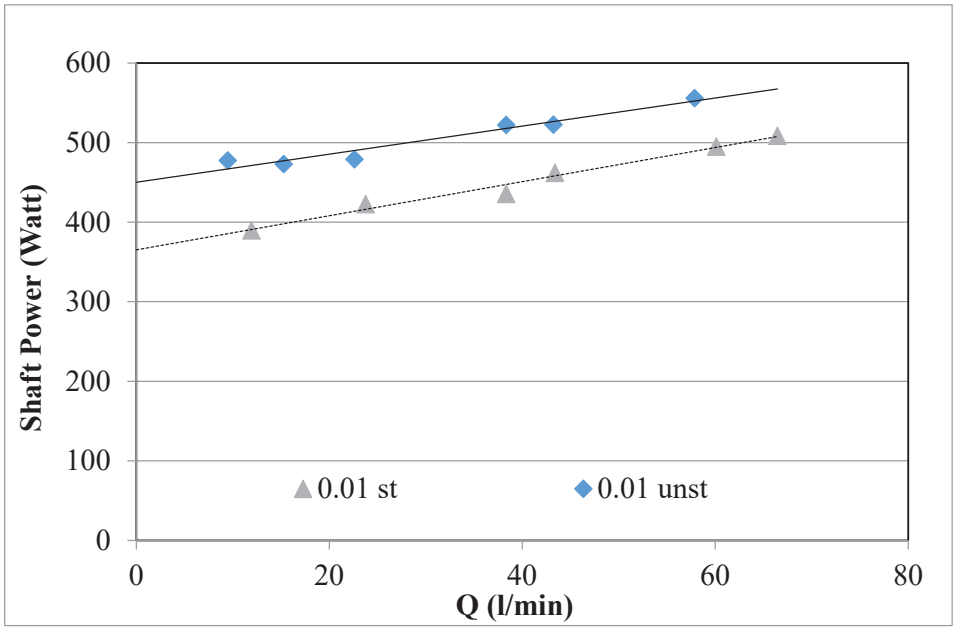

Fig.4.44 Emulsion stability effect on shaft power for blade inlet angle 10^{o} with pump running at 1650 rpm for emulsions with holdup ($\Phi = 0.01$)

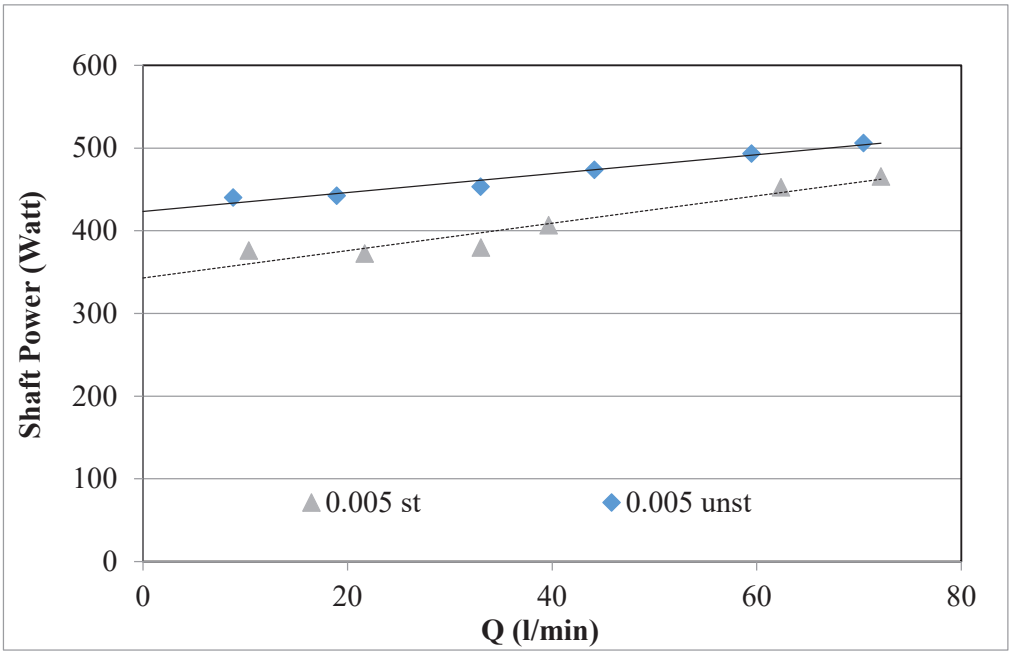

Fig.4.45 Emulsion stability effect on shaft power for blade outlet angle 30º with pump running at 1650 rpm for emulsions with holdup (Φ = 0.005)

Figures 4.46 to 4.48 show the emulsion stability effect on the pump efficiency for some examples at different impeller design parameters. It is to be noted that the stable emulsions were related to the better pump efficiency.

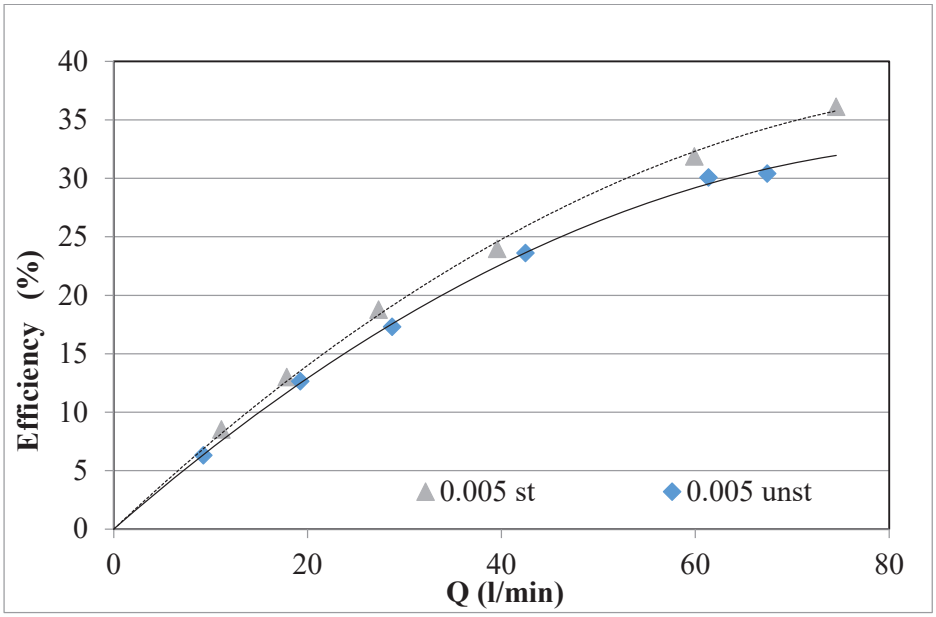

Fig.4.46 Emulsion stability effect on pump efficiency for blade number (5) with pump running at 1650 rpm for emulsions with holdup (Φ = 0.005)

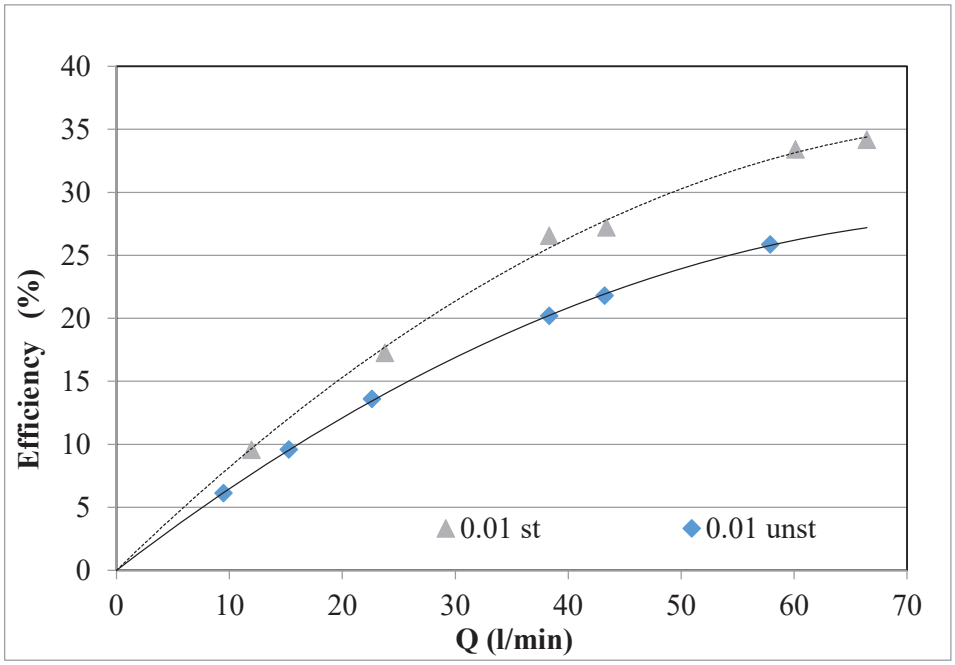

Fig.4.47 Emulsion stability effect on pump efficiency for blade inlet angle 10° with pump running at 1650 rpm for emulsions with holdup (Φ = 0.01)

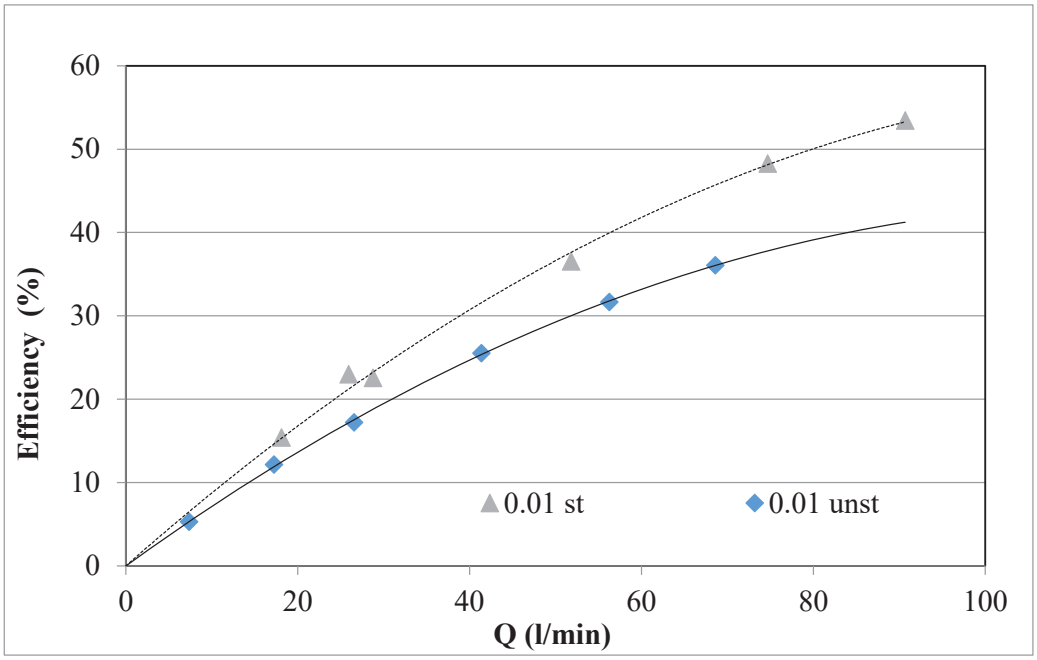

Fig.4.48 Emulsion stability effect on pump efficiency for blade outlet angle 30° with pump running at 1650 rpm for emulsions with holdup (Φ = 0.01)

4.8 THE COMPLETE EXPERIMENTAL RESULTS

All the experimental results obtained in this study is presented in figures 4.49 to 4.97 in the form of pump performance curves comparison while having the pump rotational speed as a parameter, each figure will present a specific impeller operating with one of the working fluids (Emulsions) at three different RPMs.

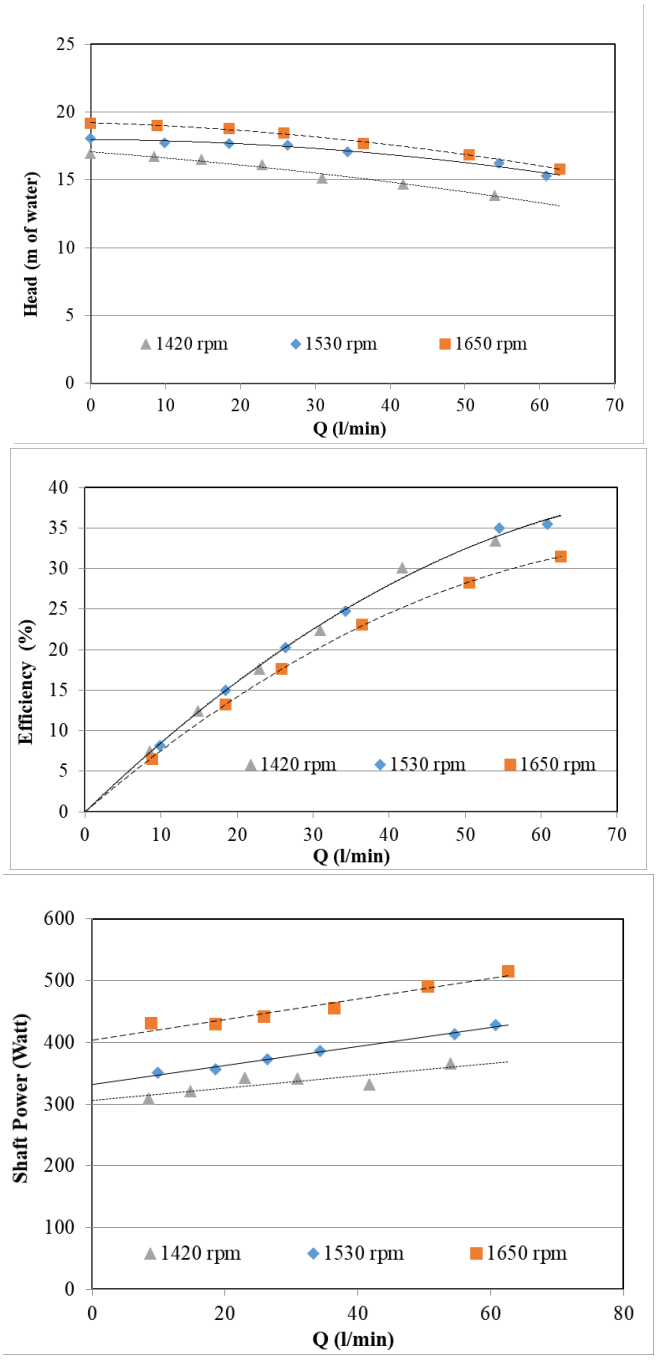

Fig.4.49 Pump performance curves for impeller with 6 blades, blade inlet angle 10° and blade outlet angle 30° for water

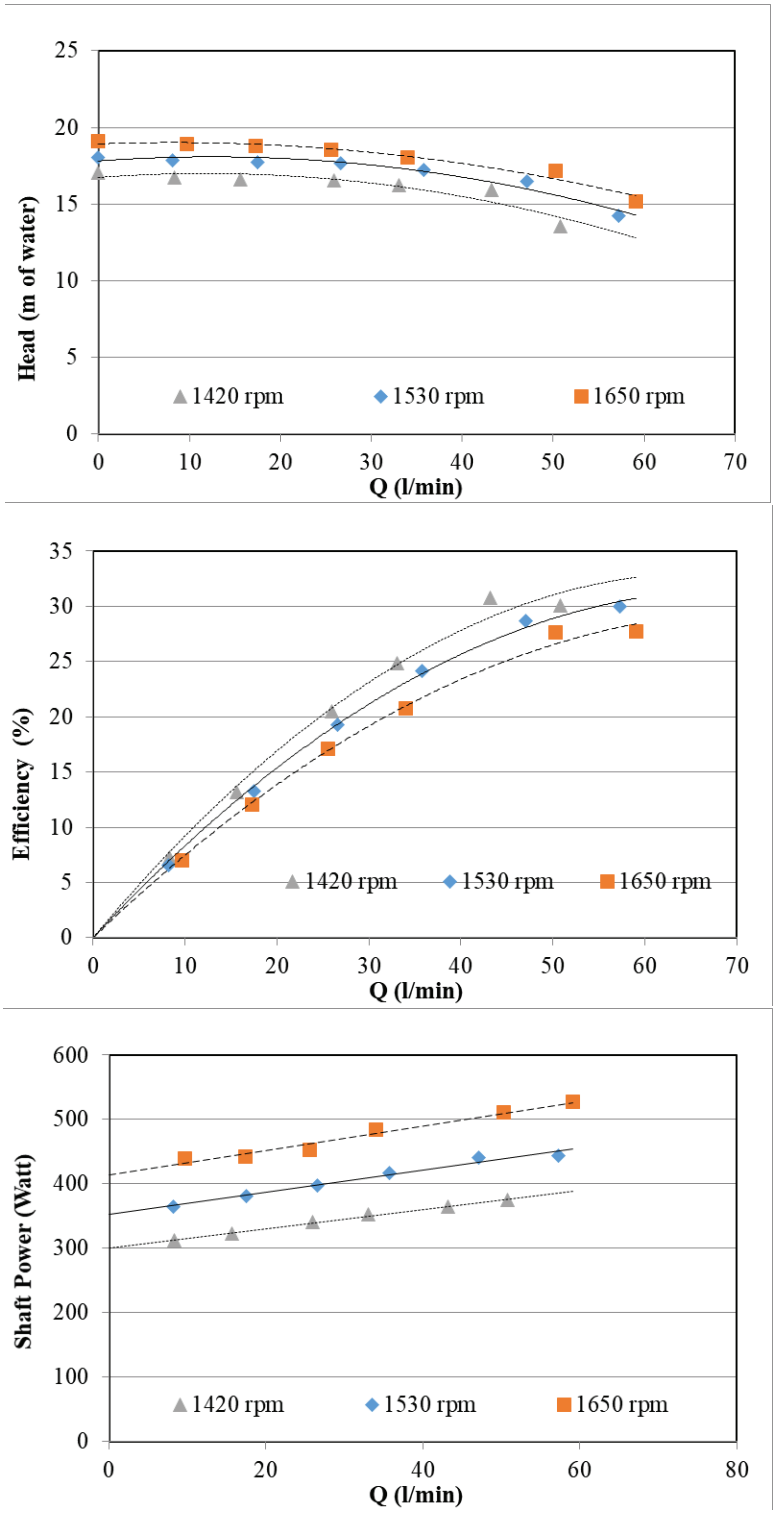

Fig.4.50 Pump performance curves for impeller with 6 blades, blade inlet angle 10° and blade outlet angle 30° for 0.005 stable emulsion

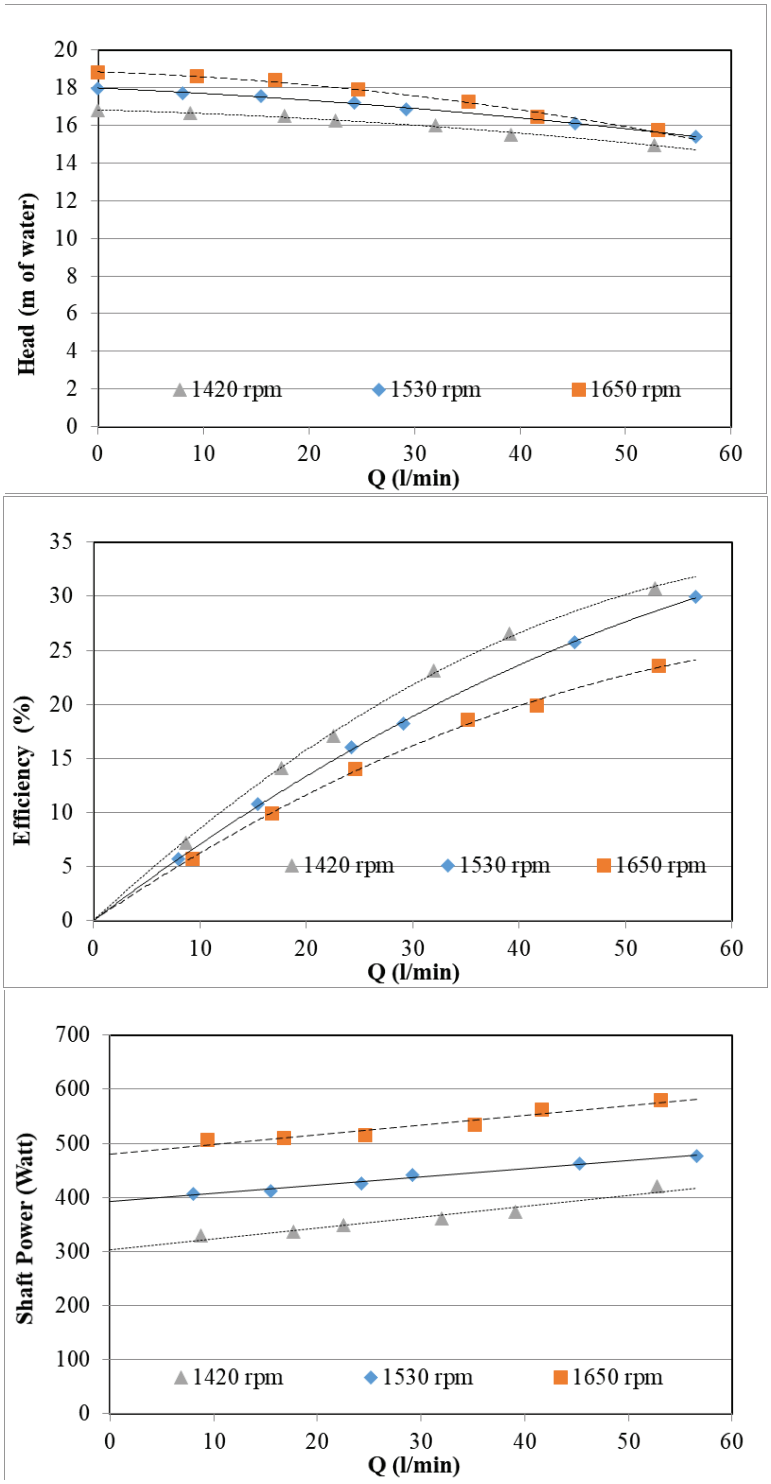

Fig.4.51 Pump performance curves for impeller with 6 blades, blade inlet angle 10° and blade outlet angle 30° for 0.005 unstable emulsion

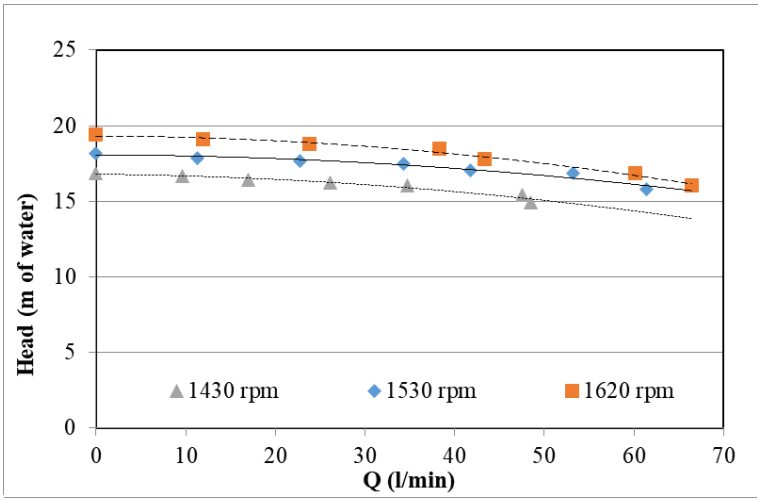

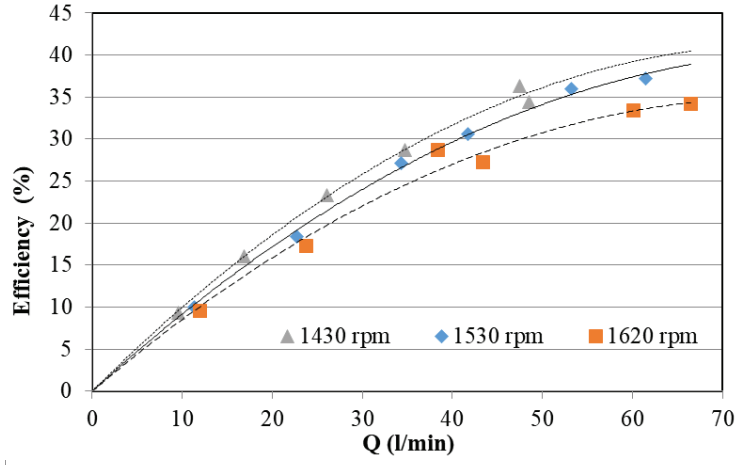

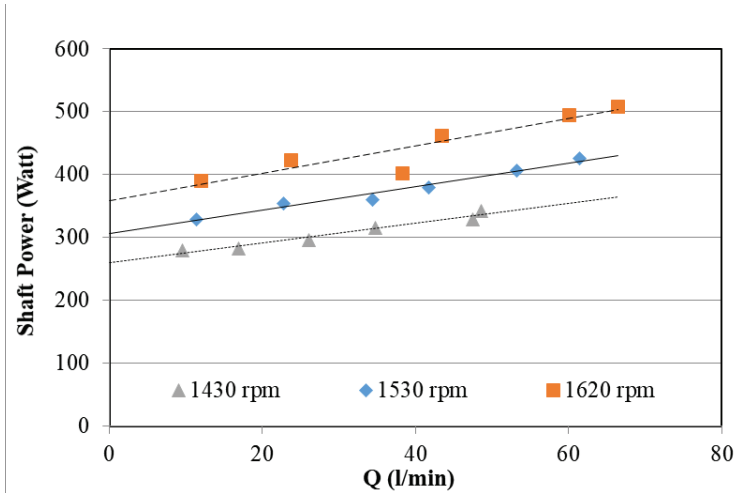

Fig.4.52 Pump performance curves for impeller with 6 blades, blade inlet angle 10° and blade outlet angle 30° for 0.01 stable emulsion

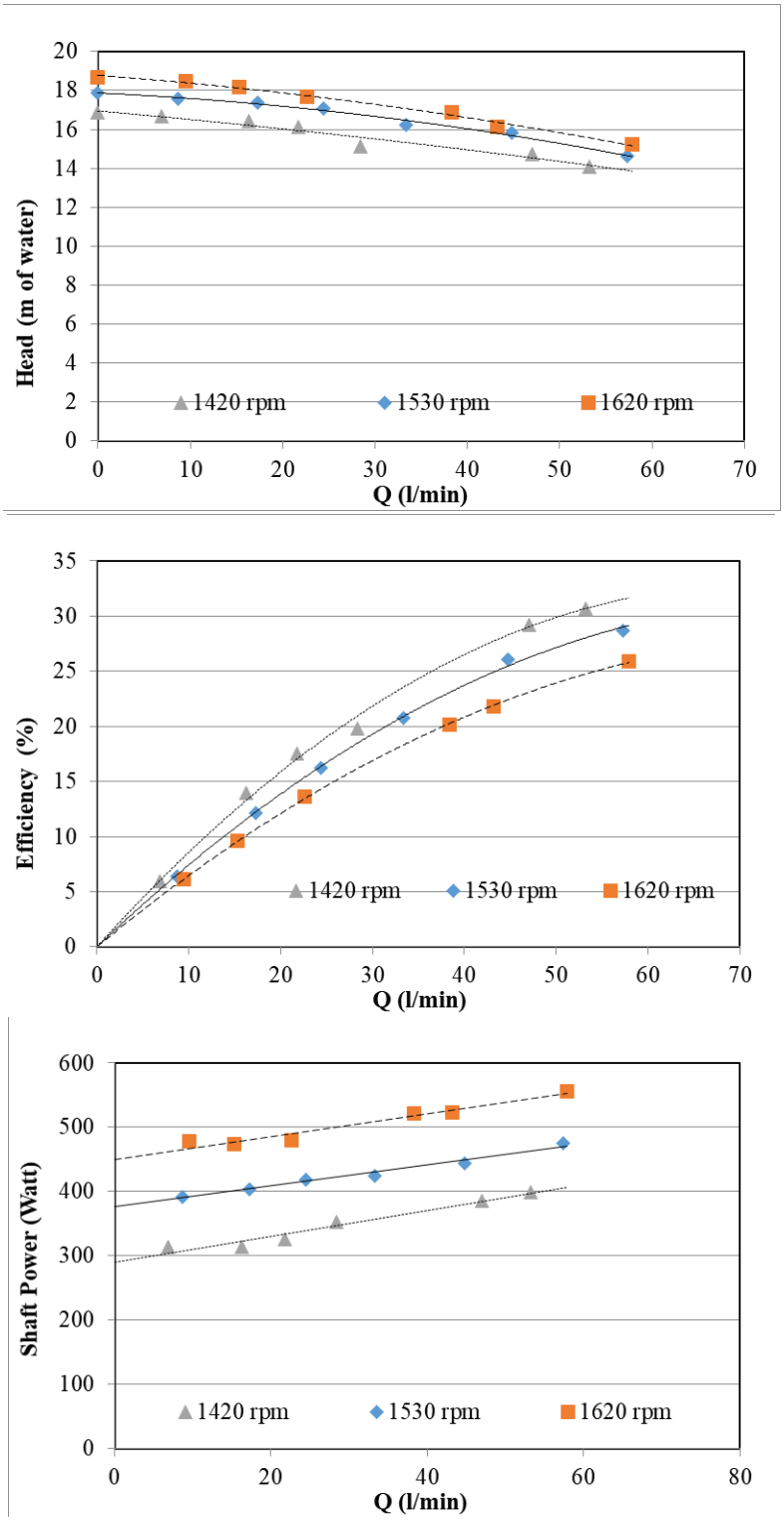

Fig.4.53 Pump performance curves for impeller with 6 blades, blade inlet angle 10° and blade outlet angle 30° for 0.01 unstable emulsion

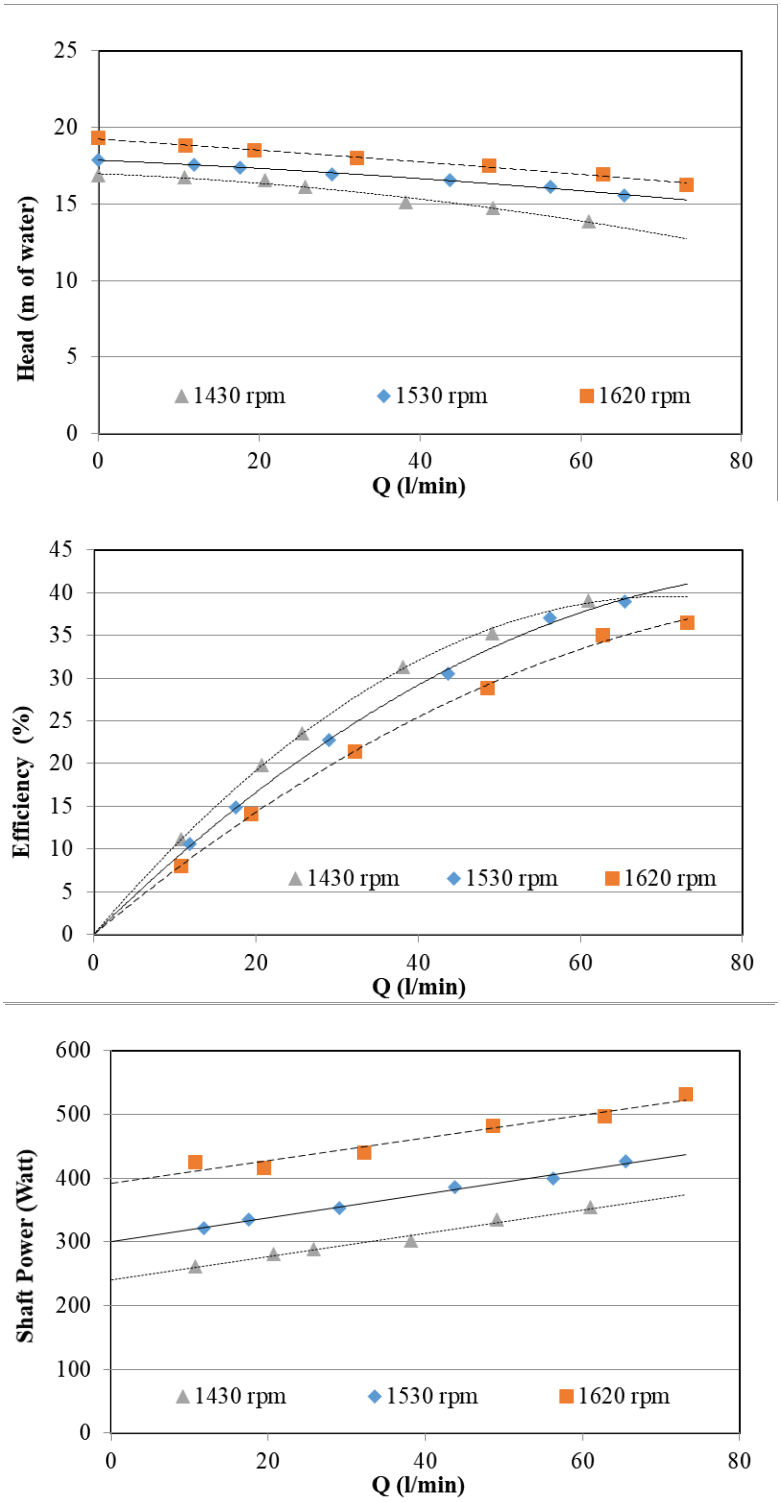

Fig.4.54 Pump performance curves for impeller with 6 blades, blade inlet angle 10° and blade outlet angle 30° for 0.02 stable emulsion

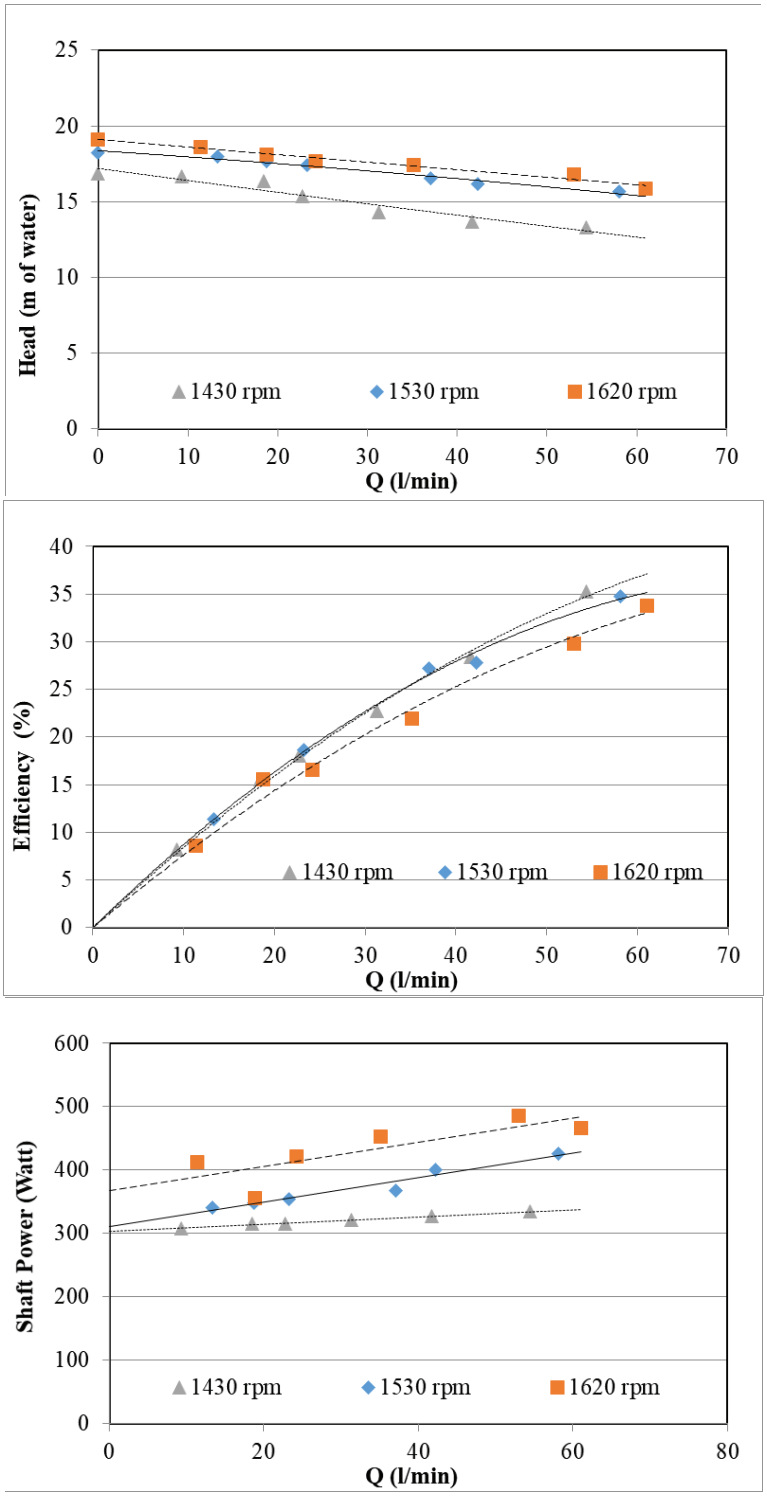

Fig.4.55 Pump performance curves for impeller with 6 blades, blade inlet angle 10° and blade outlet angle 30° for 0.02 unstable emulsion

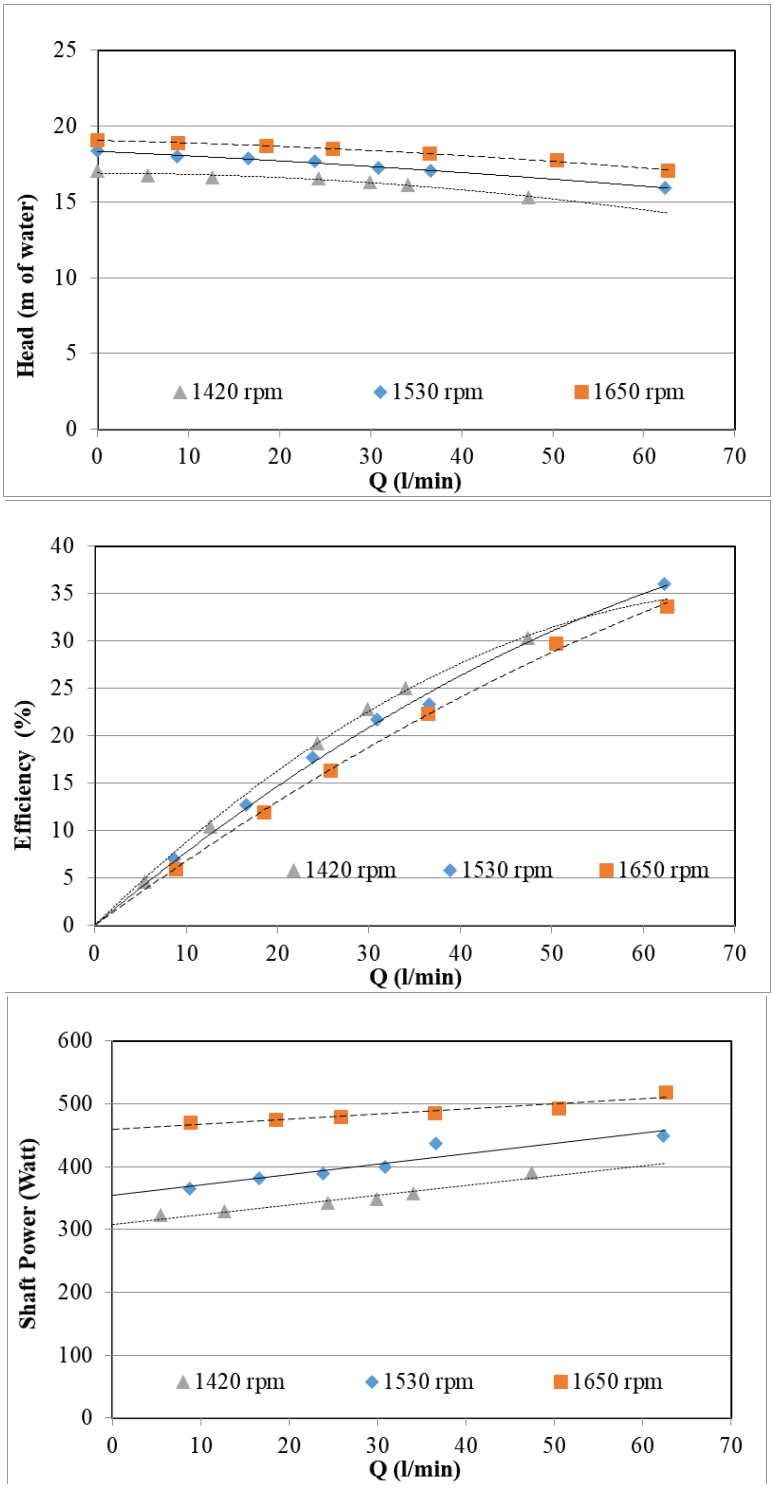

Fig.4.56 Pump performance curves for impeller with 7 blades, blade inlet angle 10° and blade outlet angle 30° for water

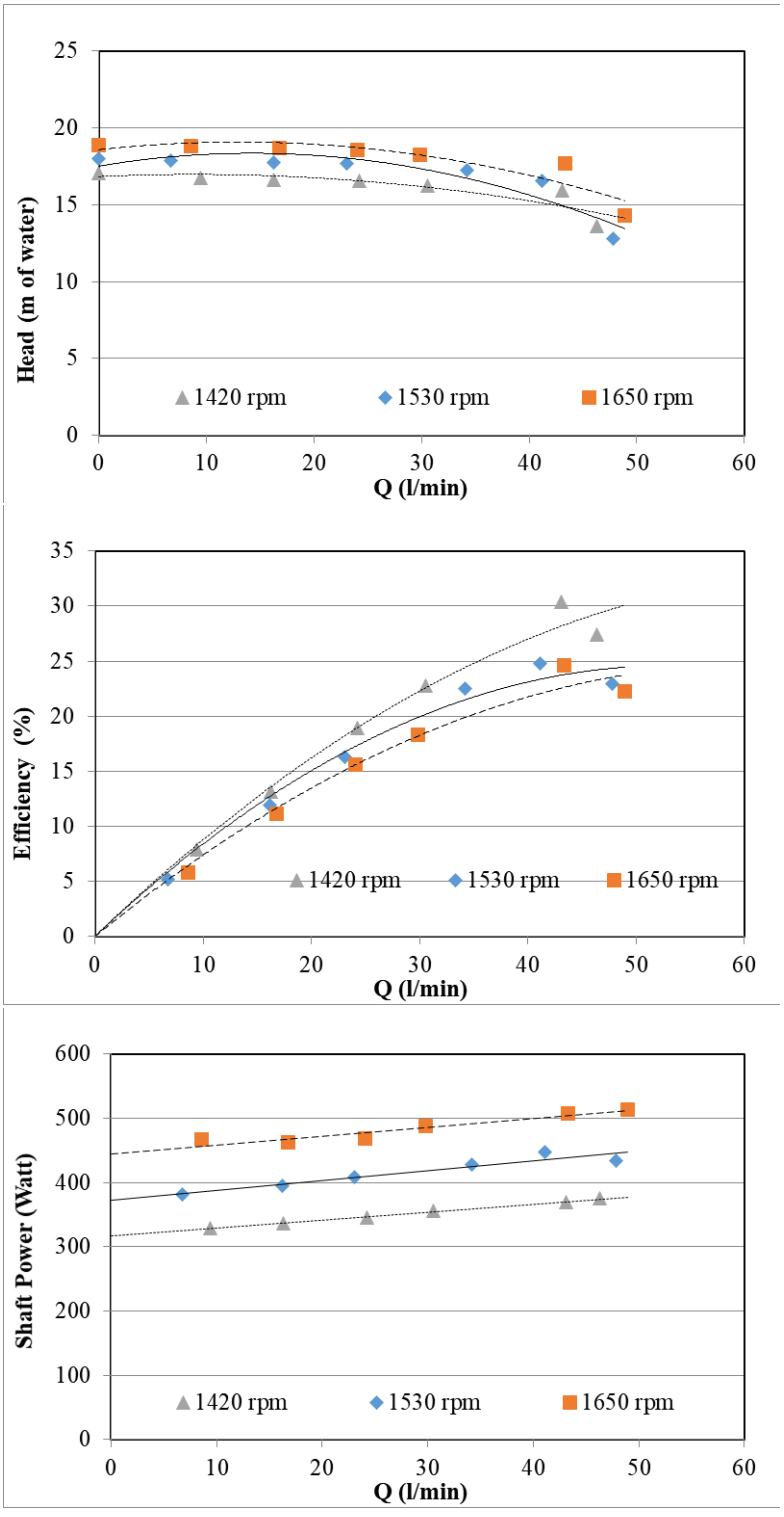

Fig.4.57 Pump performance curves for impeller with 7 blades, blade inlet angle 10° and blade outlet angle 30° for 0.005 stable emulsion

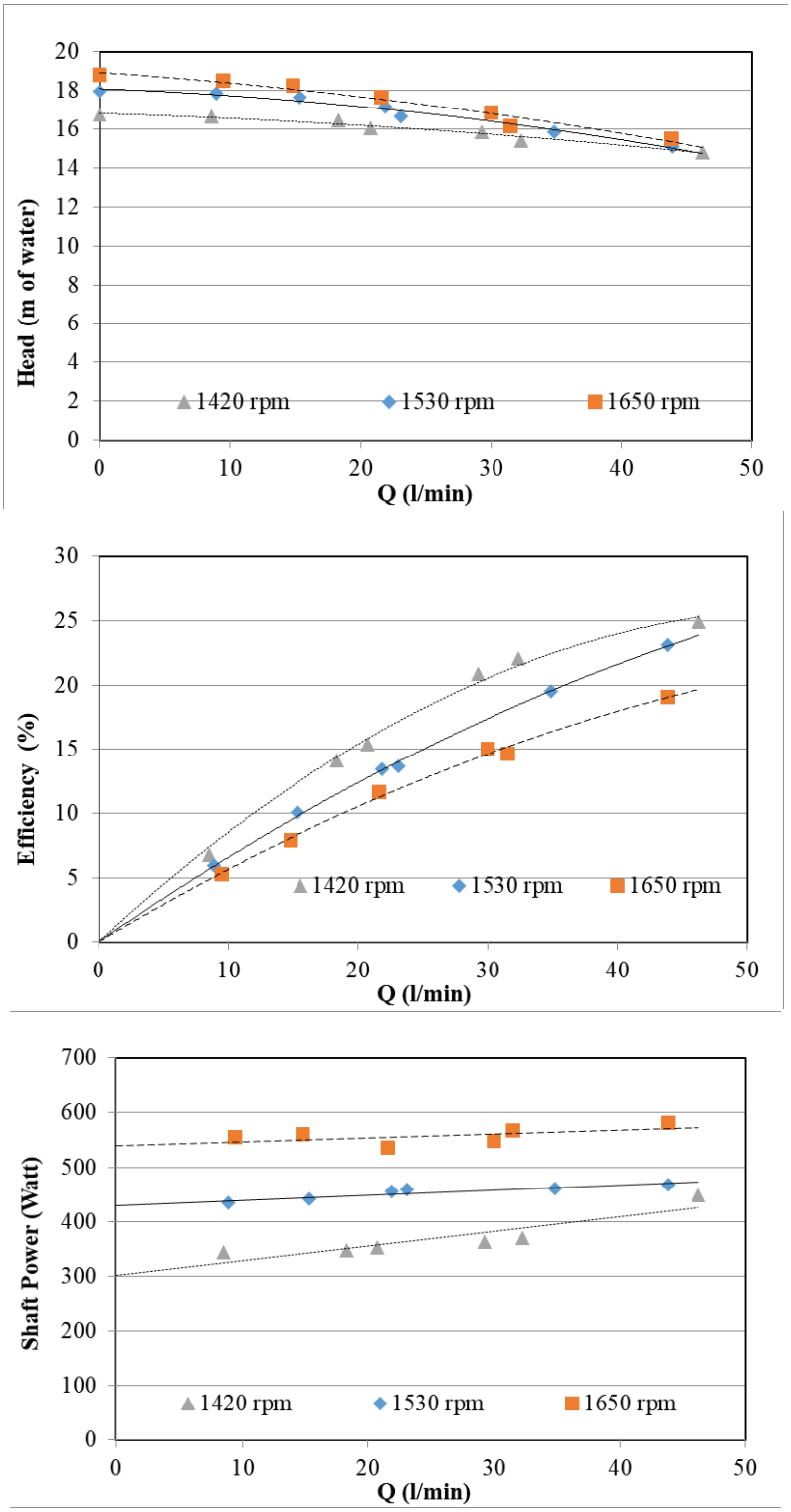

Fig.4.58 Pump performance curves for impeller with 7 blades, blade inlet angle 10° and blade outlet angle 30° for 0.005 unstable emulsion

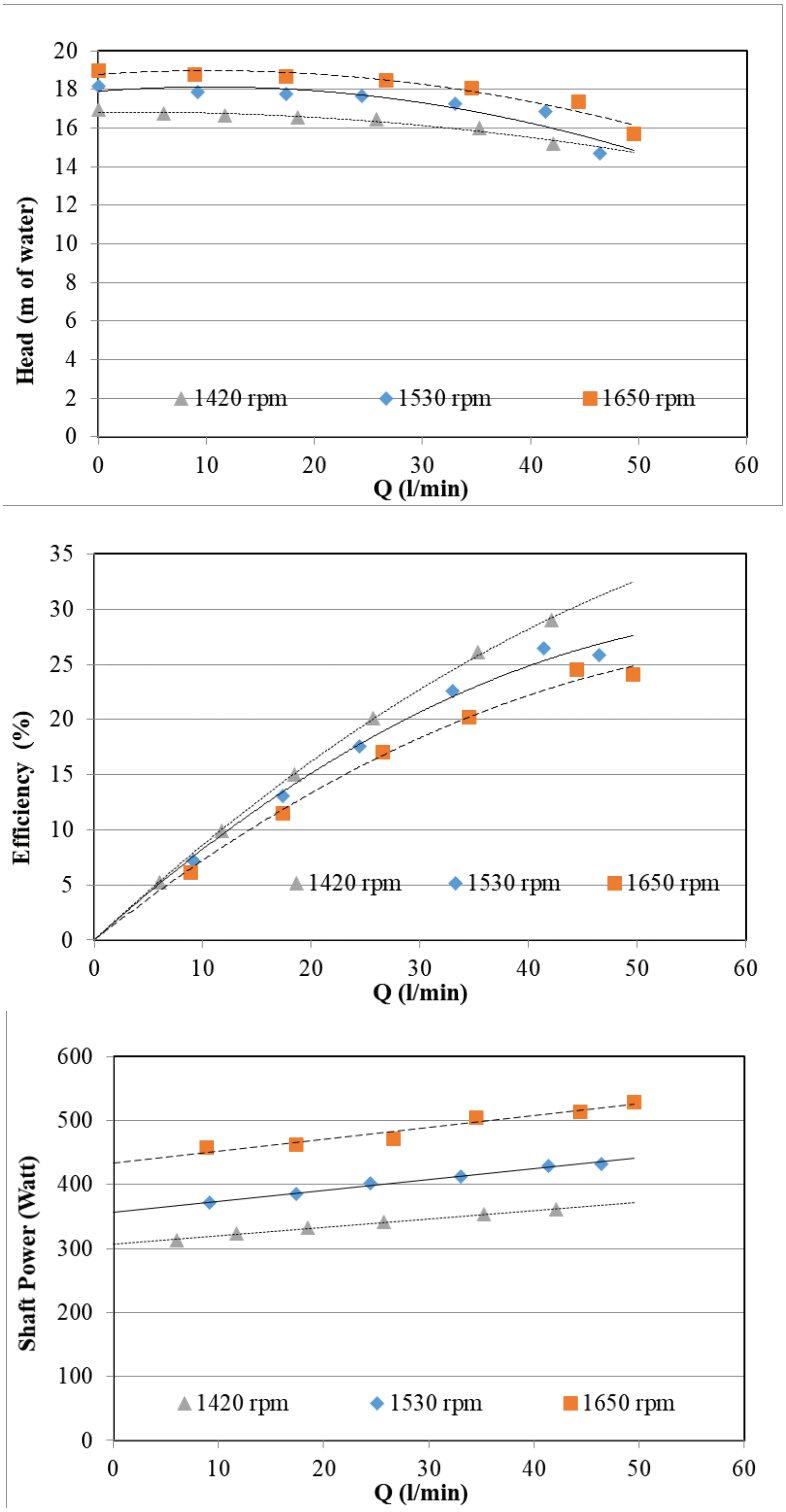

Fig.4.59 Pump performance curves for impeller with 7 blades, blade inlet angle 10° and blade outlet angle 30° for 0.01 stable emulsion

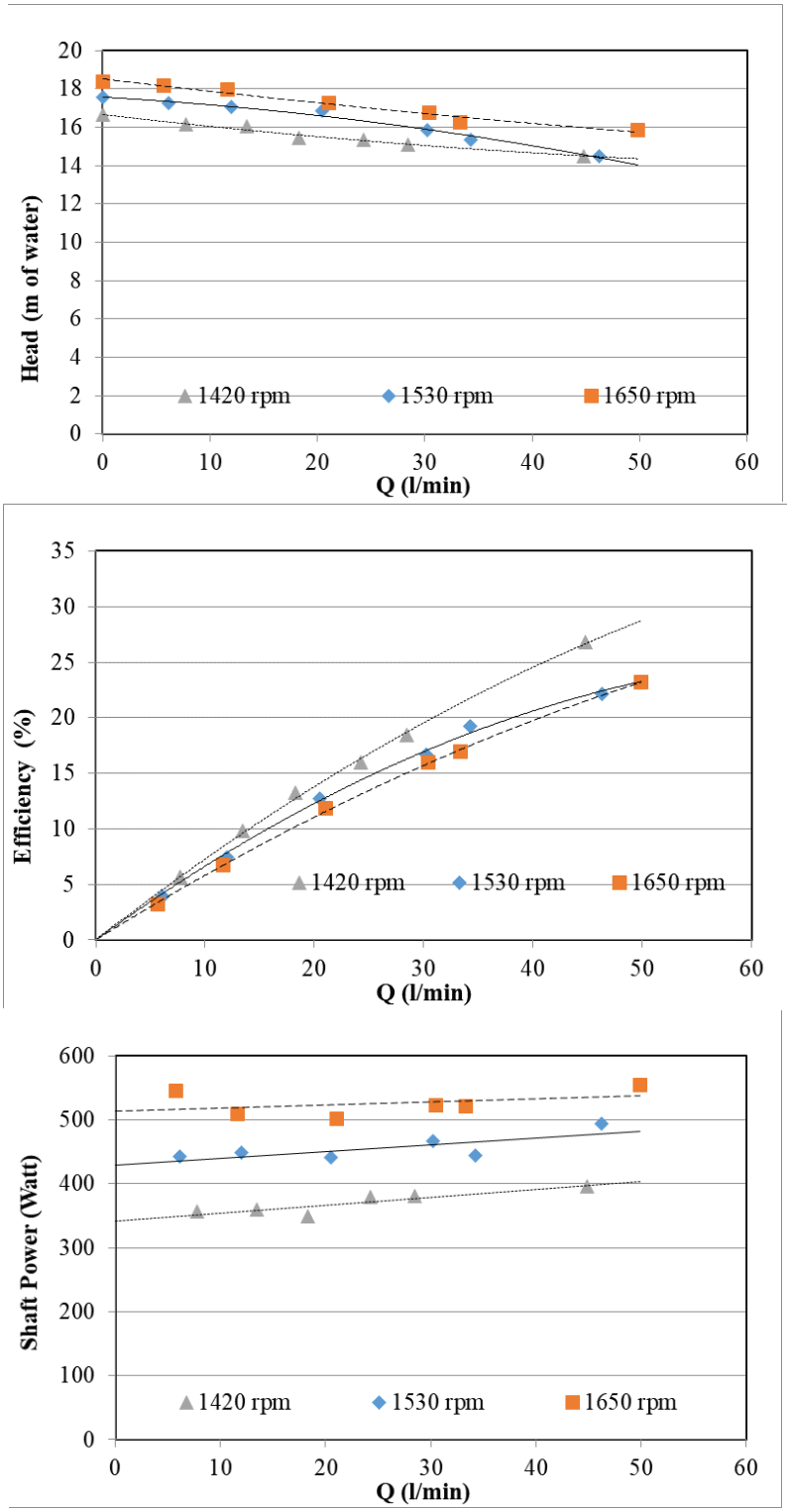

Fig.4.60 Pump performance curves for impeller with 7 blades, blade inlet angle 10° and blade outlet angle 30° for 0.01 unstable emulsion

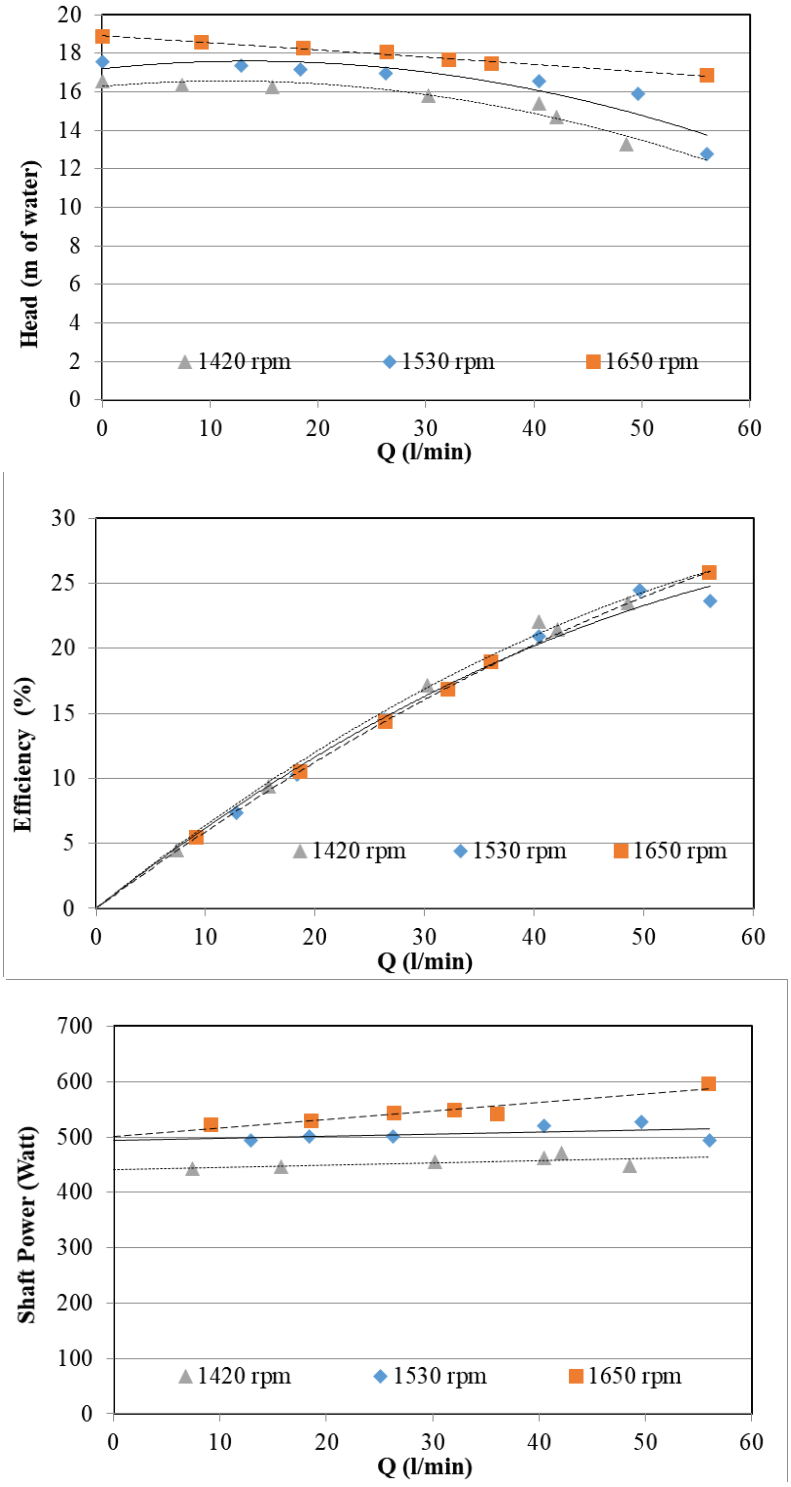

Fig.4.61 Pump performance curves for impeller with 7 blades, blade inlet angle 10° and blade outlet angle 30° for 0.02 stable emulsion

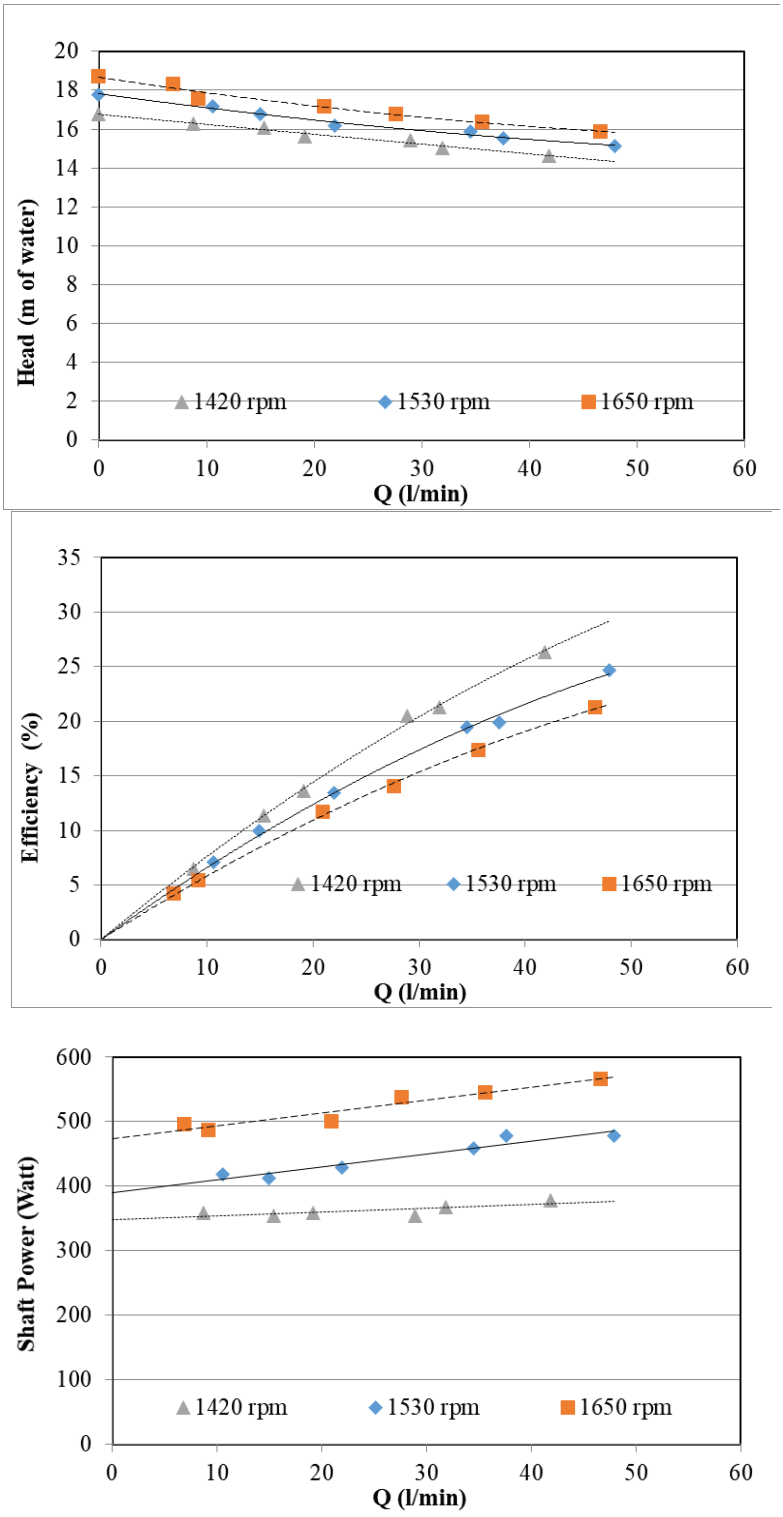

Fig.4.62 Pump performance curves for impeller with 7 blades, blade inlet angle 10° and blade outlet angle 30° for 0.02 unstable emulsion

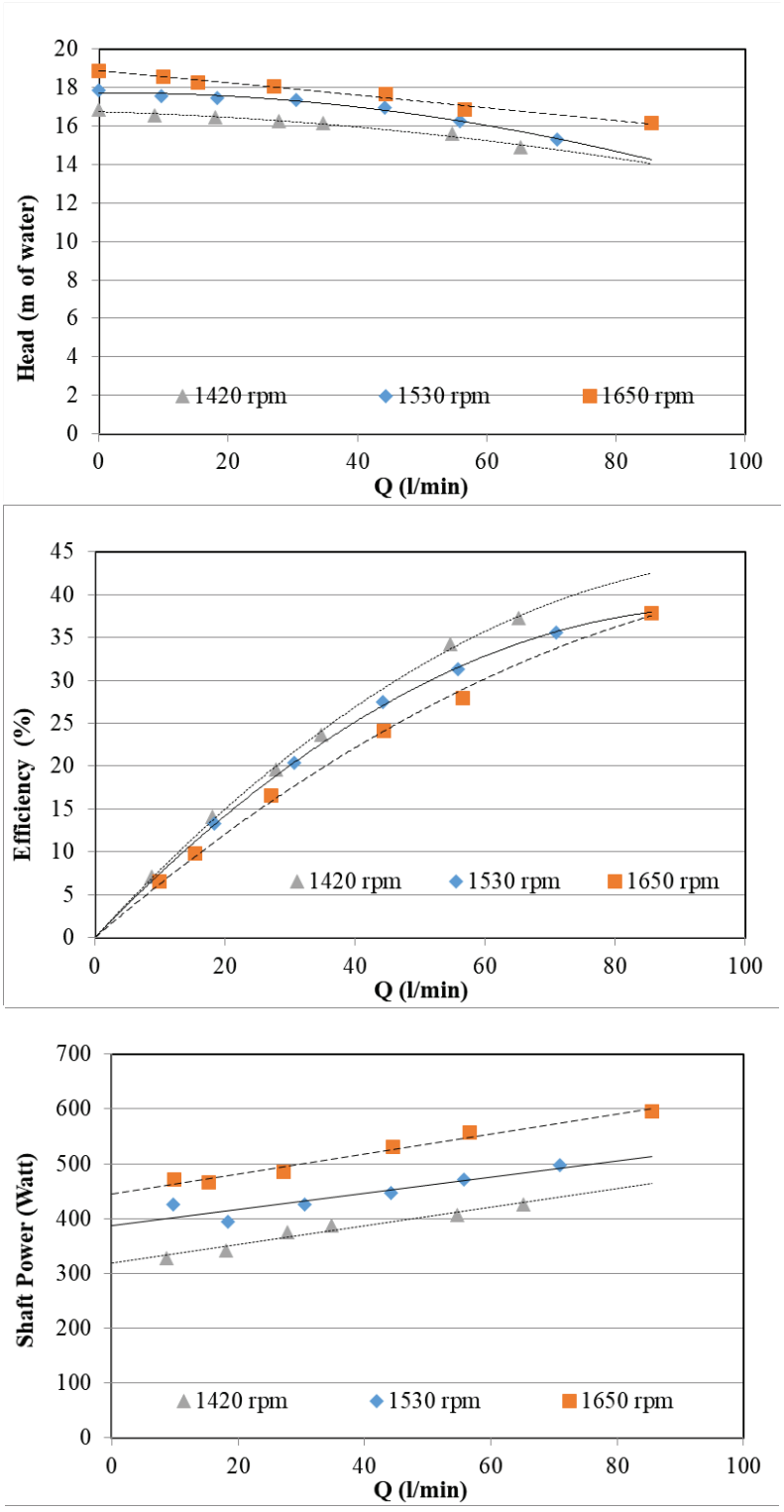

Fig.4.63 Pump performance curves for impeller with 5 blades, blade inlet angle 10° and blade outlet angle 30° for water

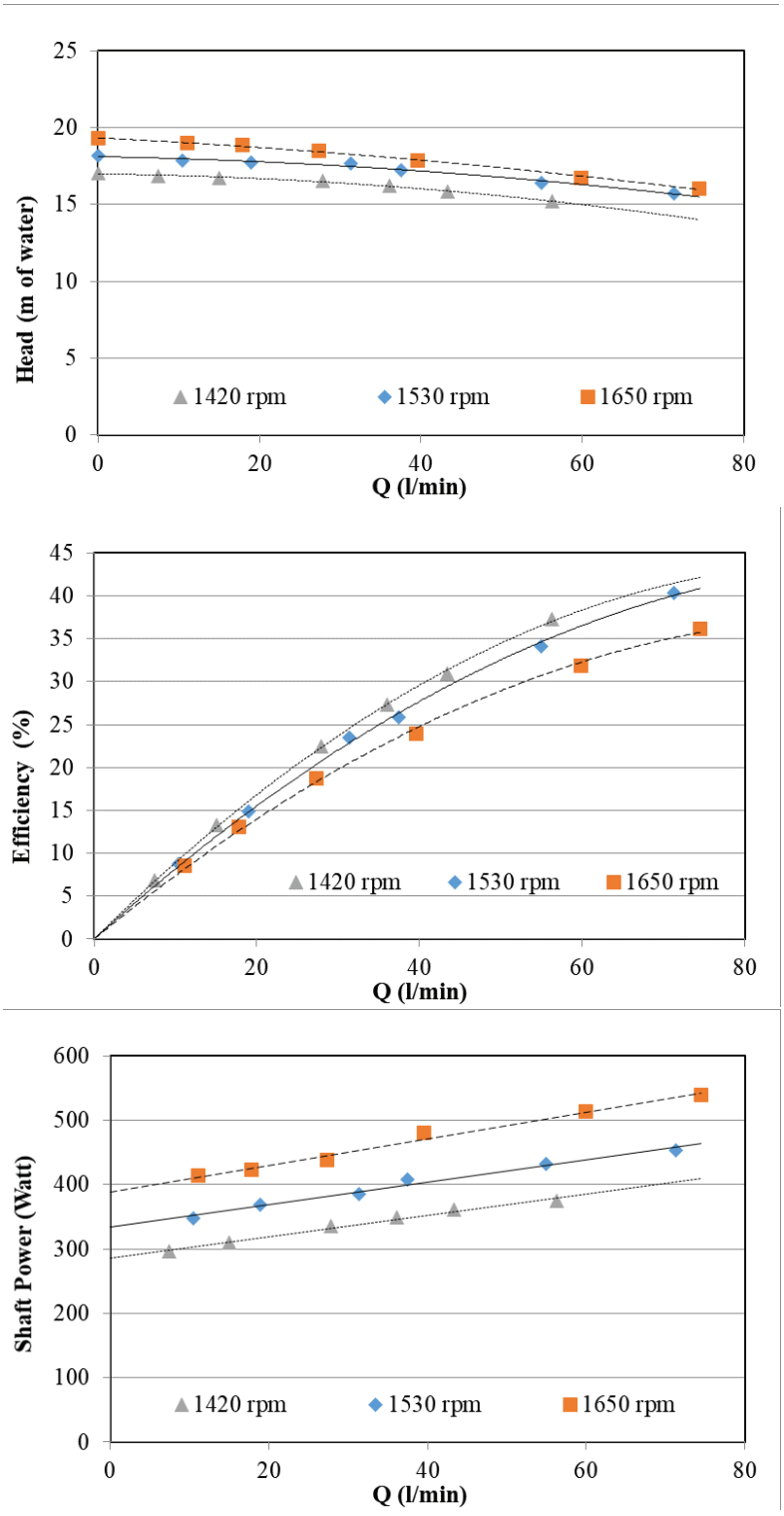

Fig.4.64 Pump performance curves for impeller with 5 blades, blade inlet angle 10° and blade outlet angle 30° for 0.005 stable emulsion

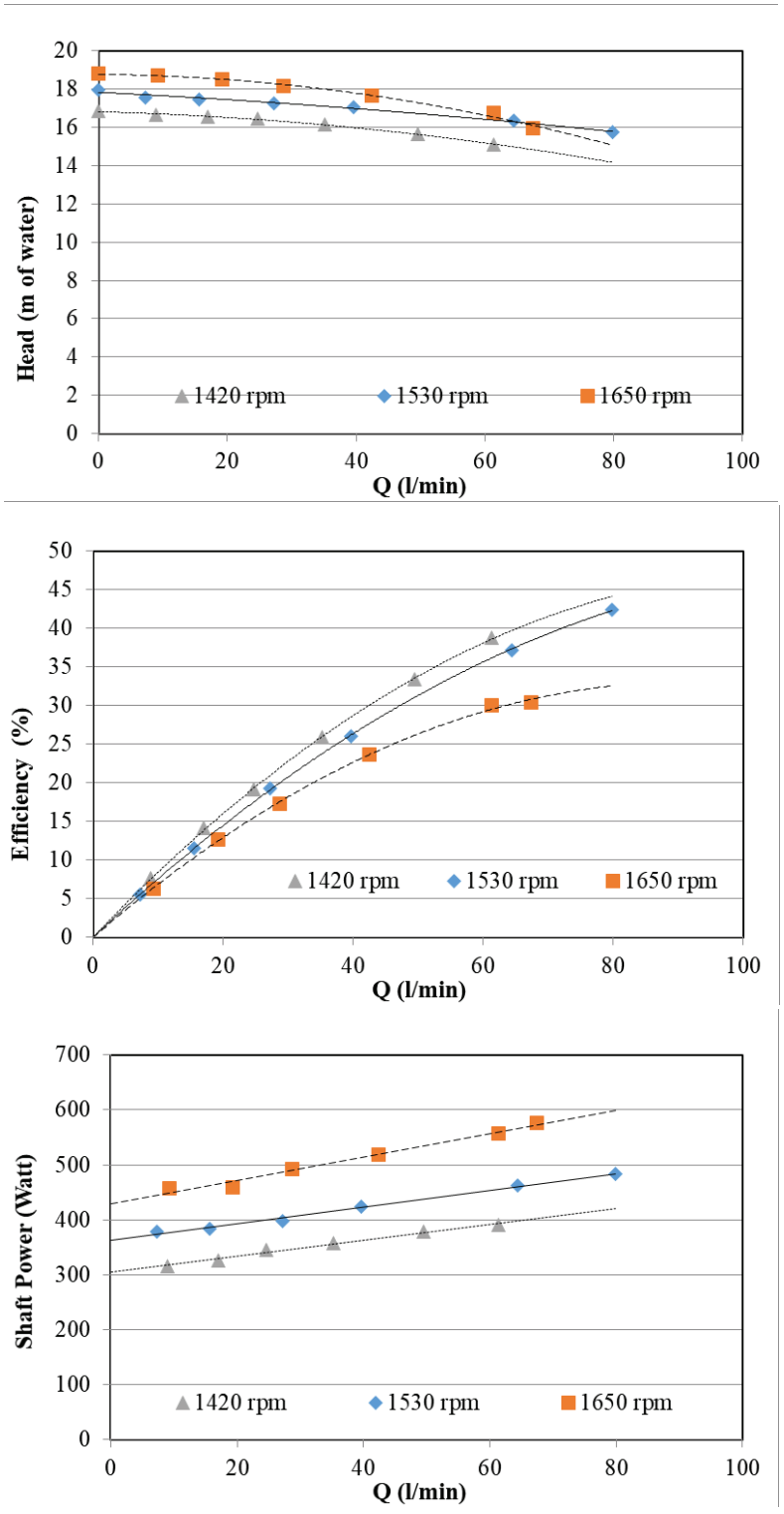

Fig.4.65 Pump performance curves for impeller with 5 blades, blade inlet angle 10° and blade outlet angle 30° for 0.005 unstable emulsion

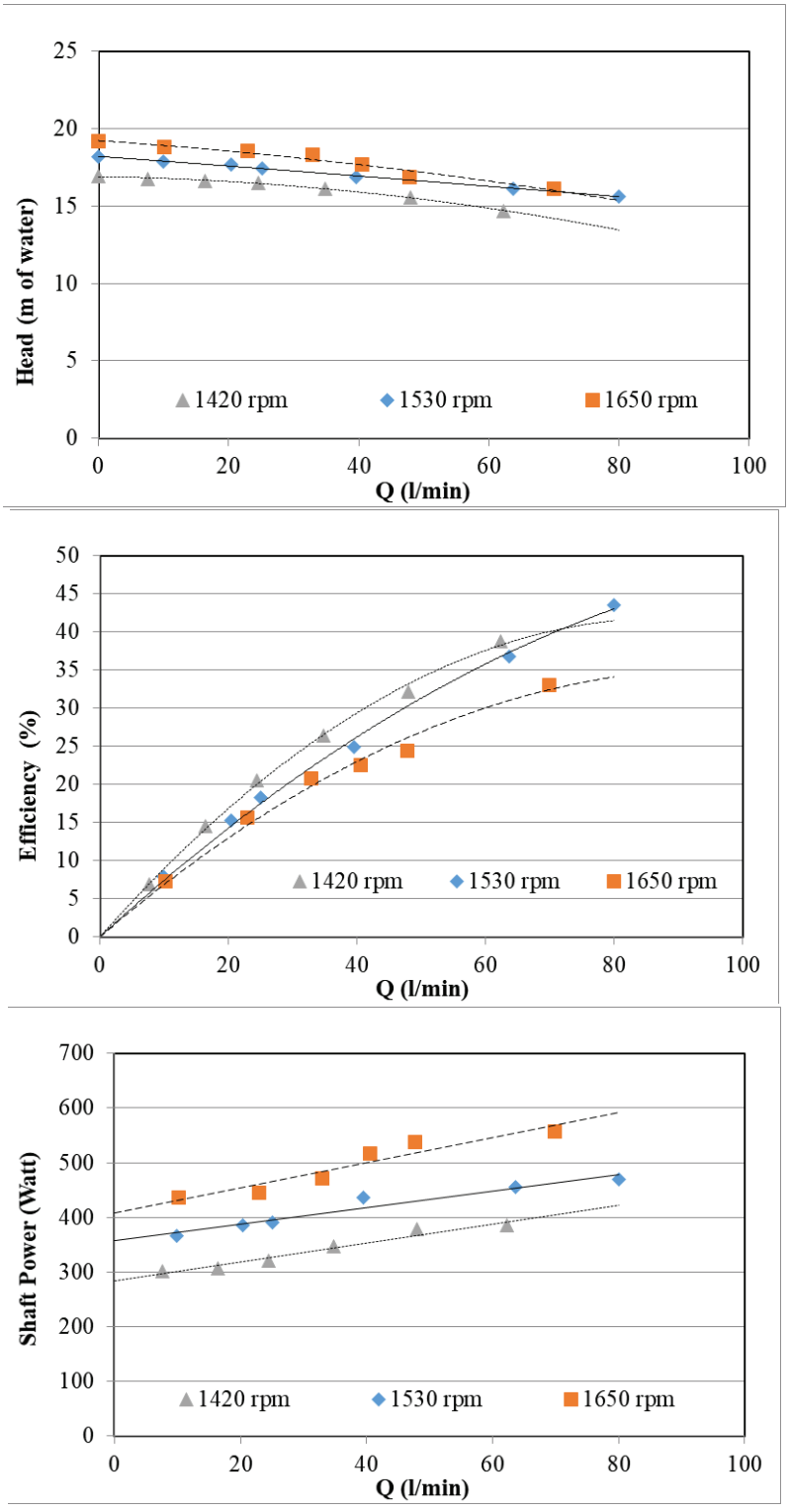

Fig.4.66 Pump performance curves for impeller with 5 blades, blade inlet angle 10° and blade outlet angle 30° for 0.01 stable emulsion

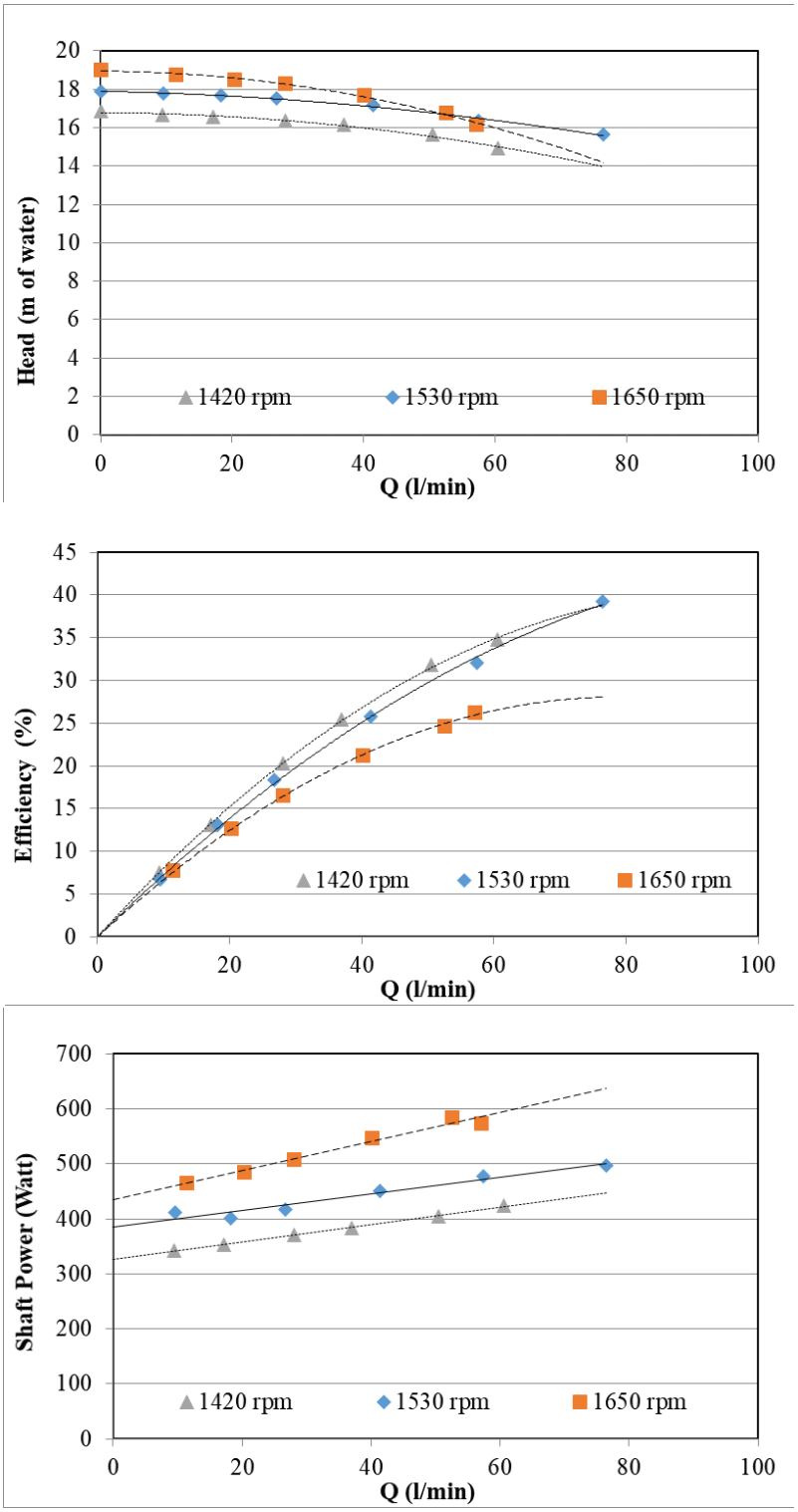

Fig.4.67 Pump performance curves for impeller with 5 blades, blade inlet angle 10° and blade outlet angle 30° for 0.01 unstable emulsion

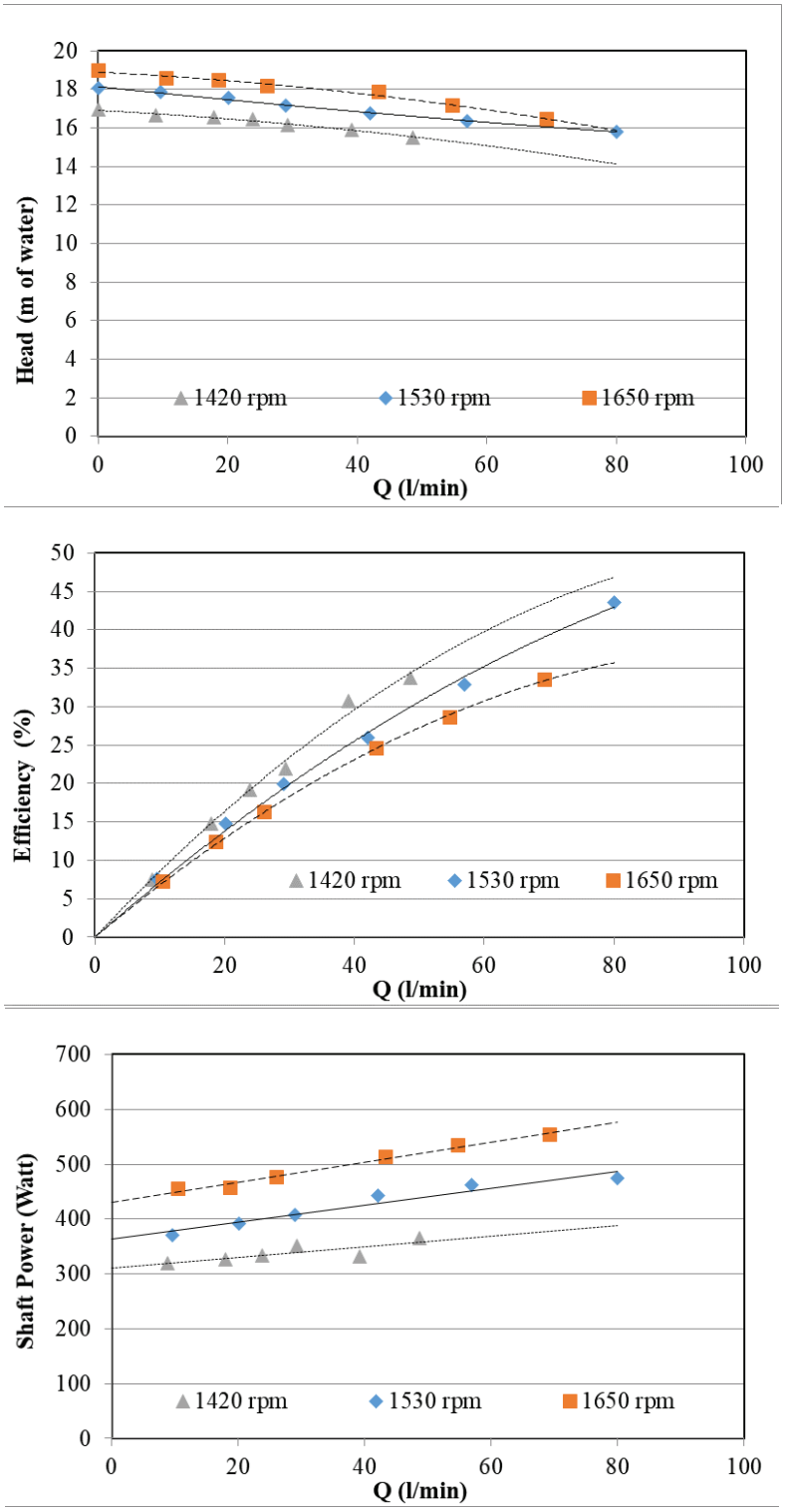

Fig.4.68 Pump performance curves for impeller with 5 blades, blade inlet angle 10° and blade outlet angle 30° for 0.02 stable emulsion

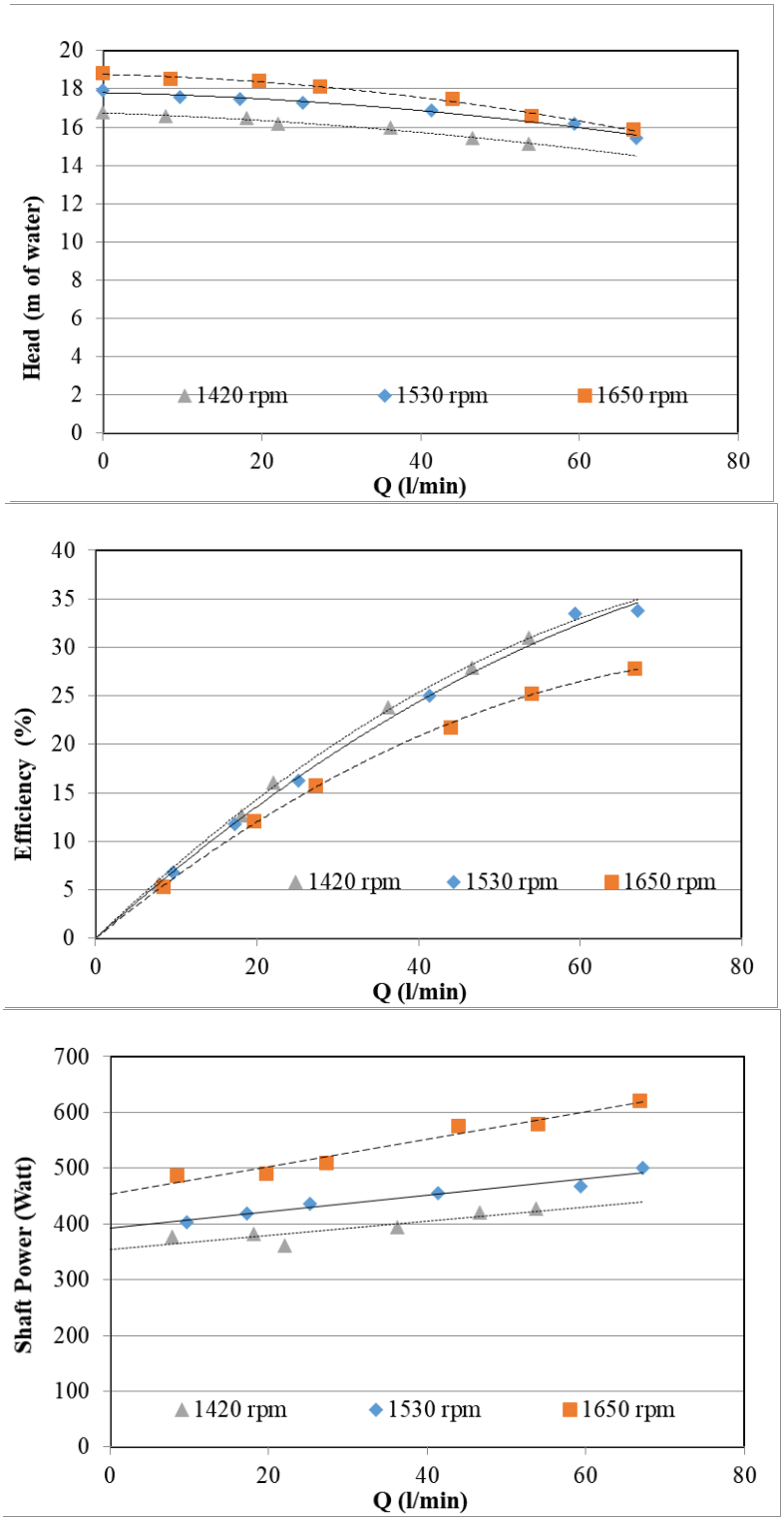

Fig.4.69 Pump performance curves for impeller with 5 blades, blade inlet angle 10° and blade outlet angle 30° for 0.02 unstable emulsion

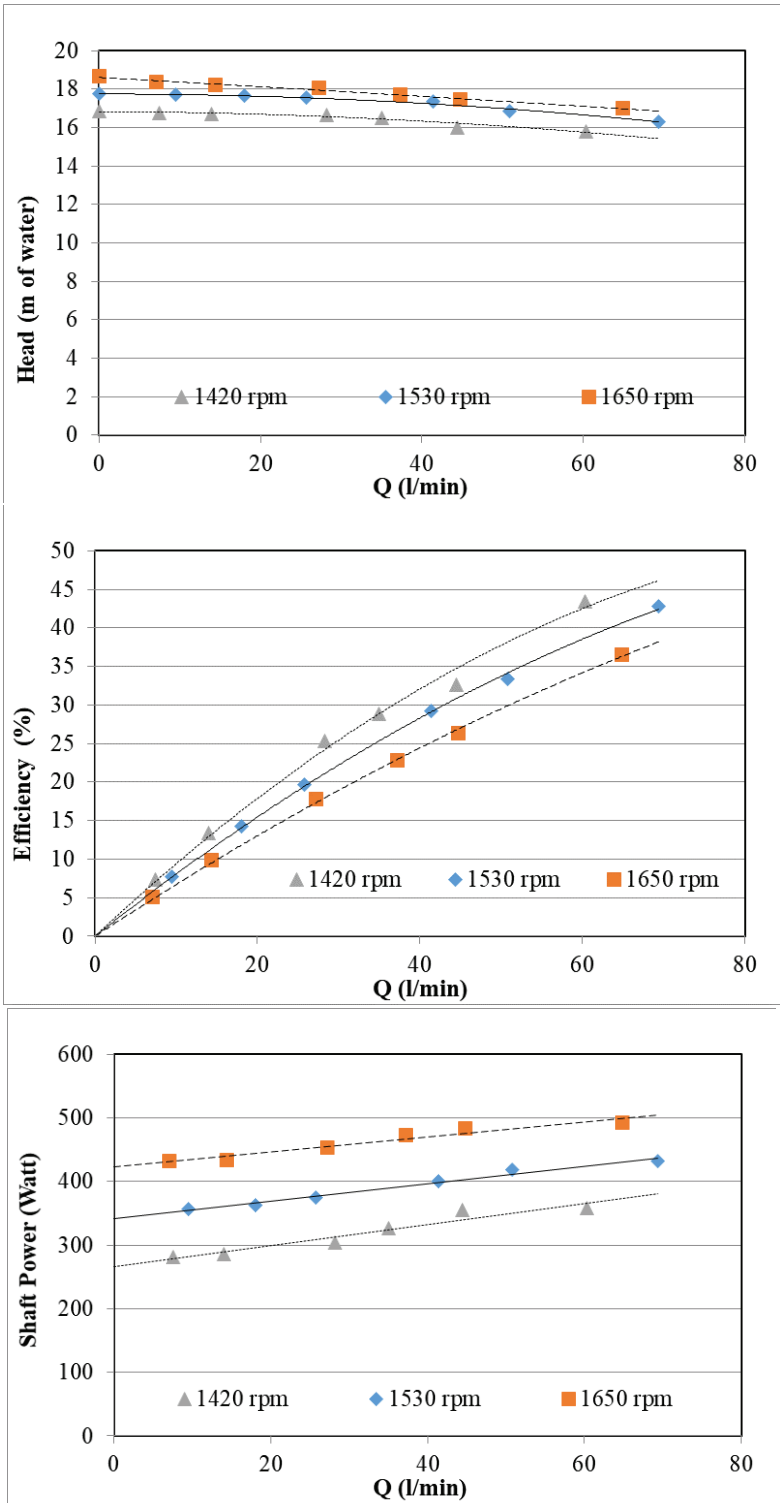

Fig.4.70 Pump performance curves for impeller with 6 blades, blade inlet angle 20° and blade outlet angle 30° for water

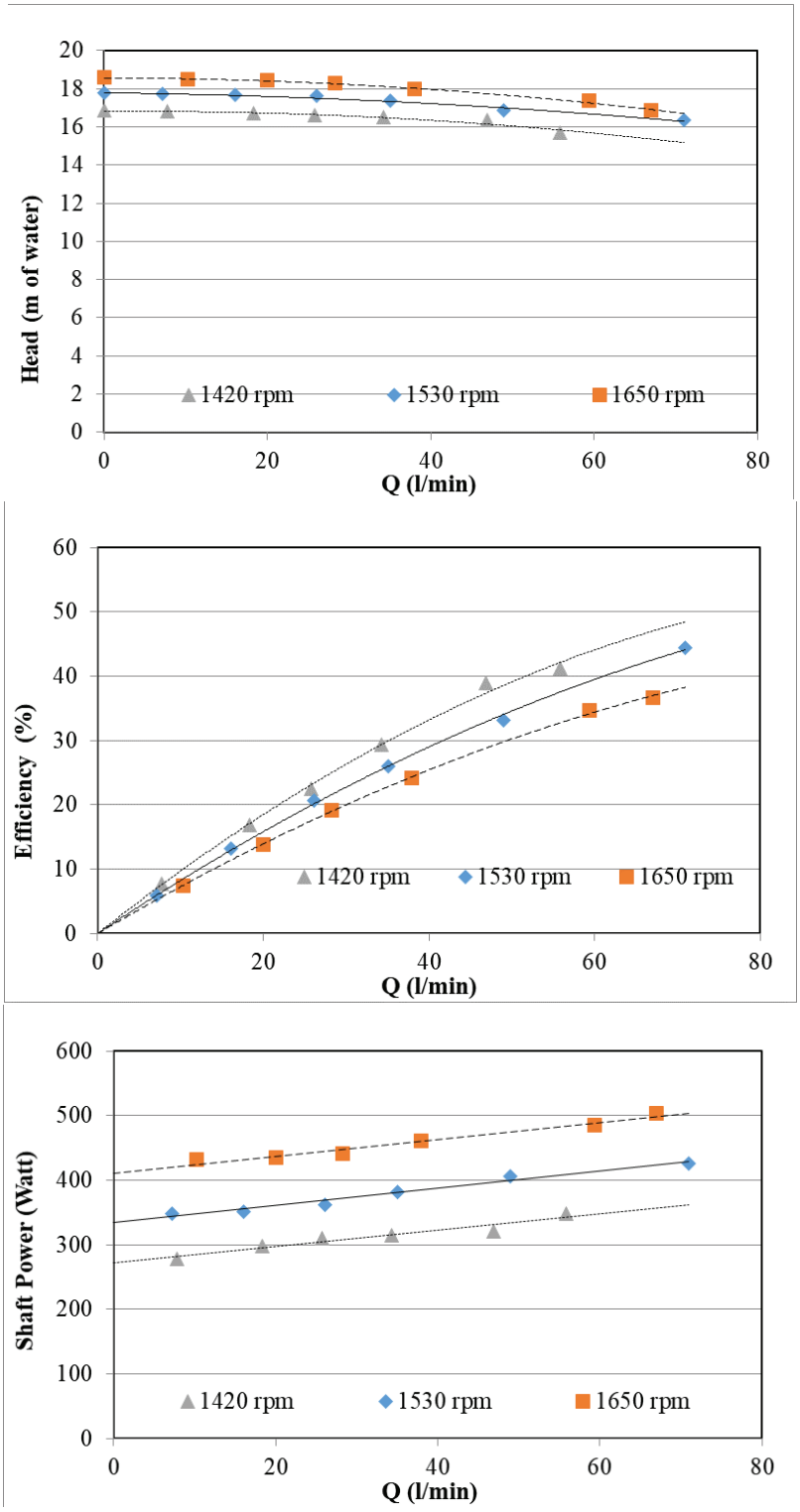

Fig.4.71 Pump performance curves for impeller with 6 blades, blade inlet angle 20° and blade outlet angle 30° for 0.005 stable emulsion

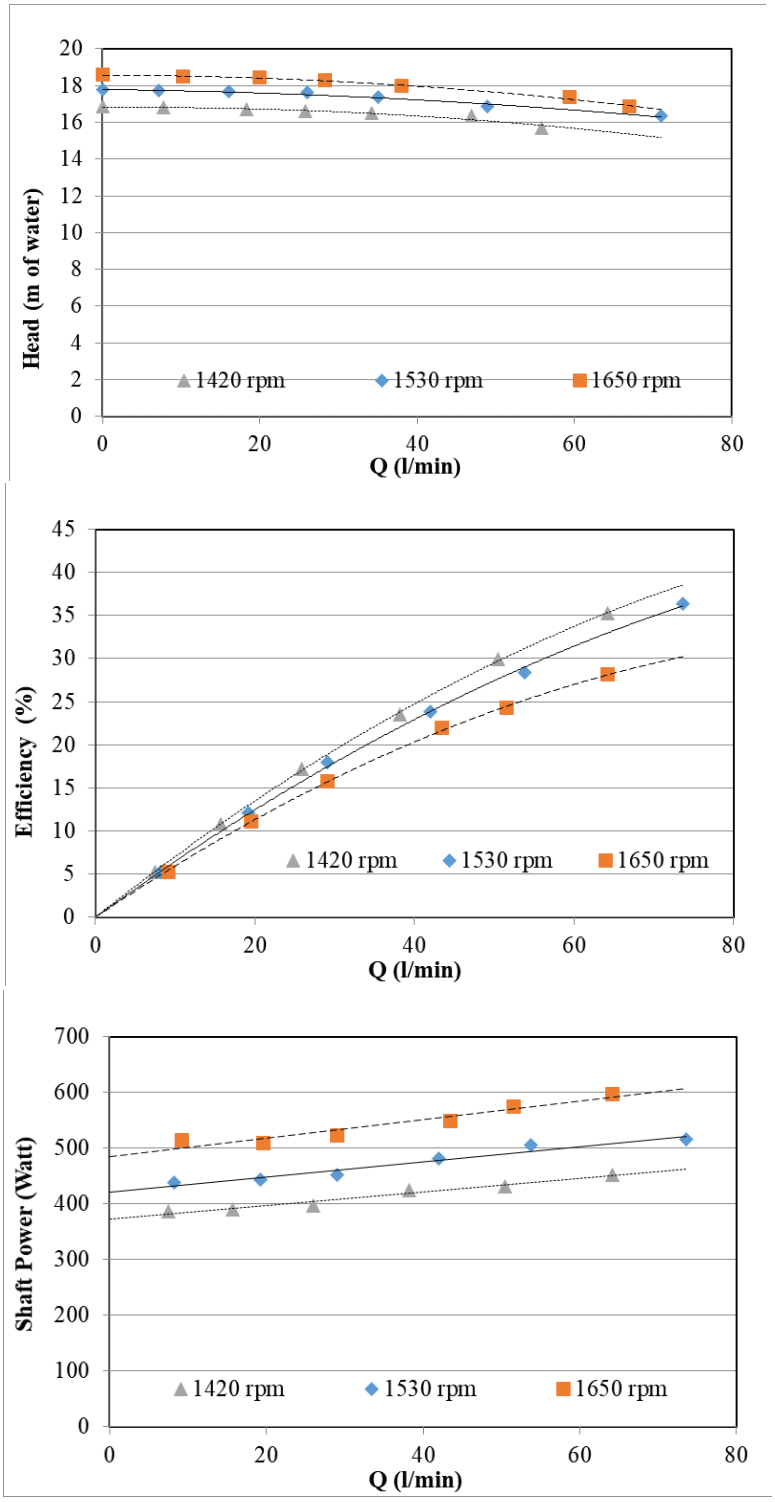

Fig.4.72 Pump performance curves for impeller with 6 blades, blade inlet angle 20° and blade outlet angle 30° for 0.005 unstable emulsion

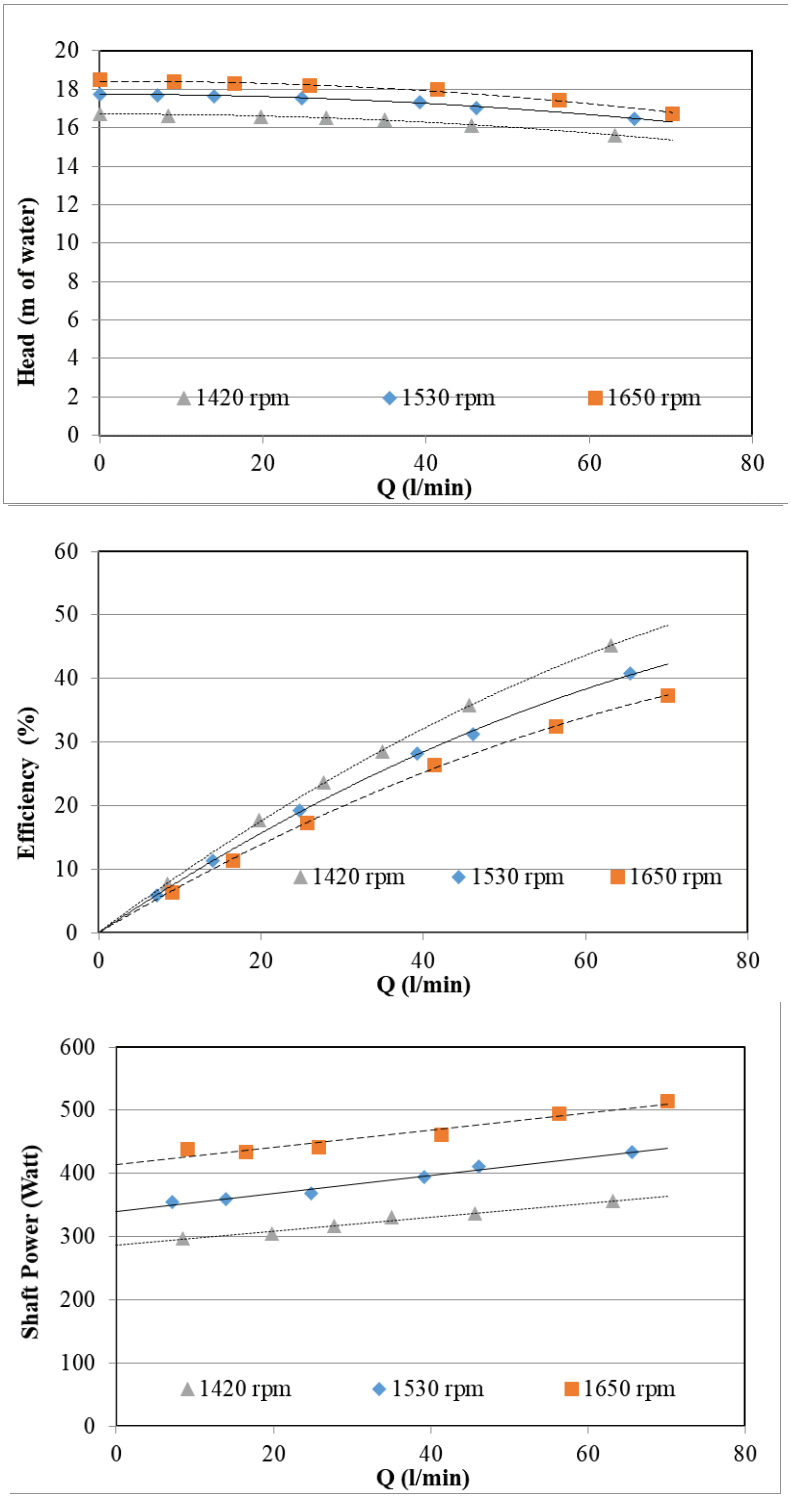

Fig.4.73 Pump performance curves for impeller with 6 blades, blade inlet angle 20° and blade outlet angle 30° for 0.01 stable emulsion

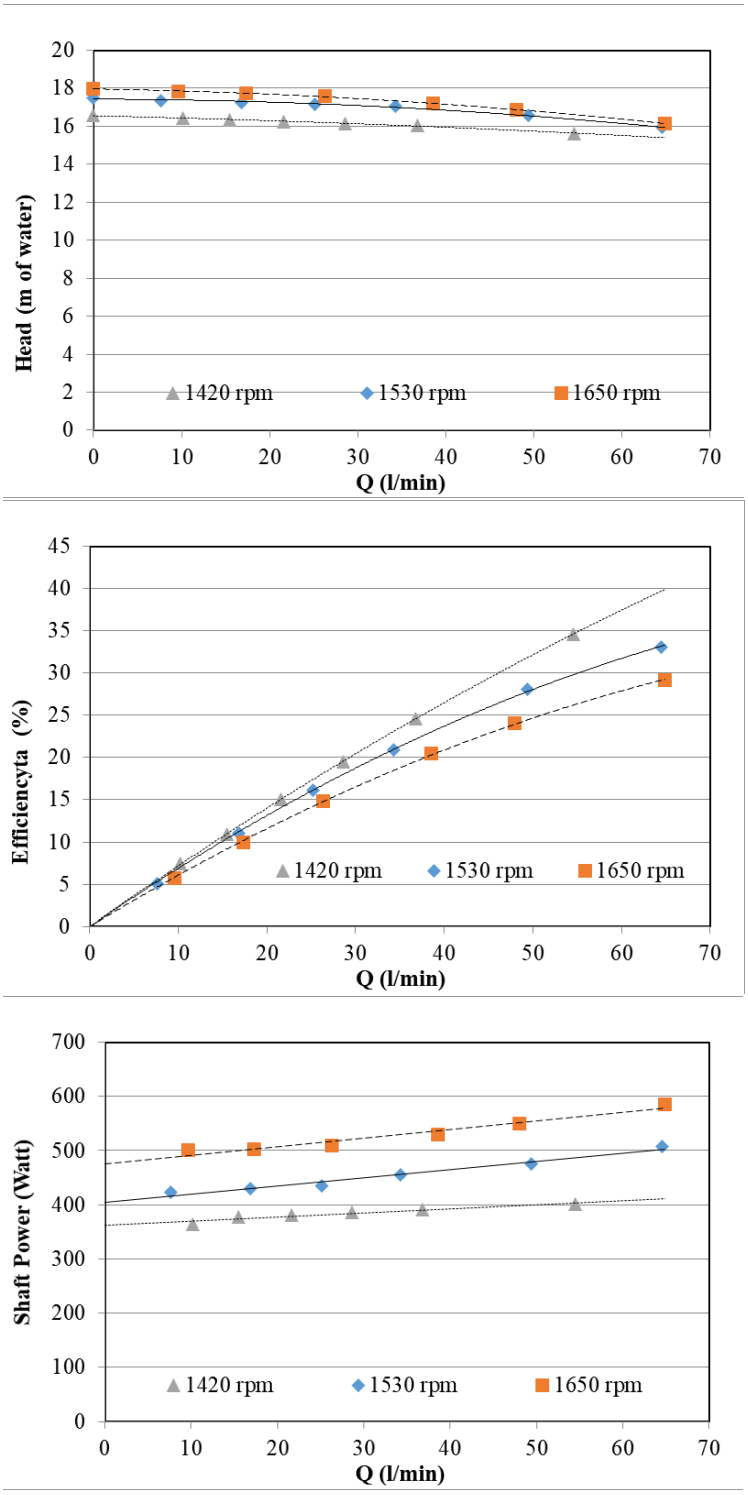

Fig.4.74 Pump performance curves for impeller with 6 blades, blade inlet angle 20° and blade outlet angle 30° for 0.01 unstable emulsion

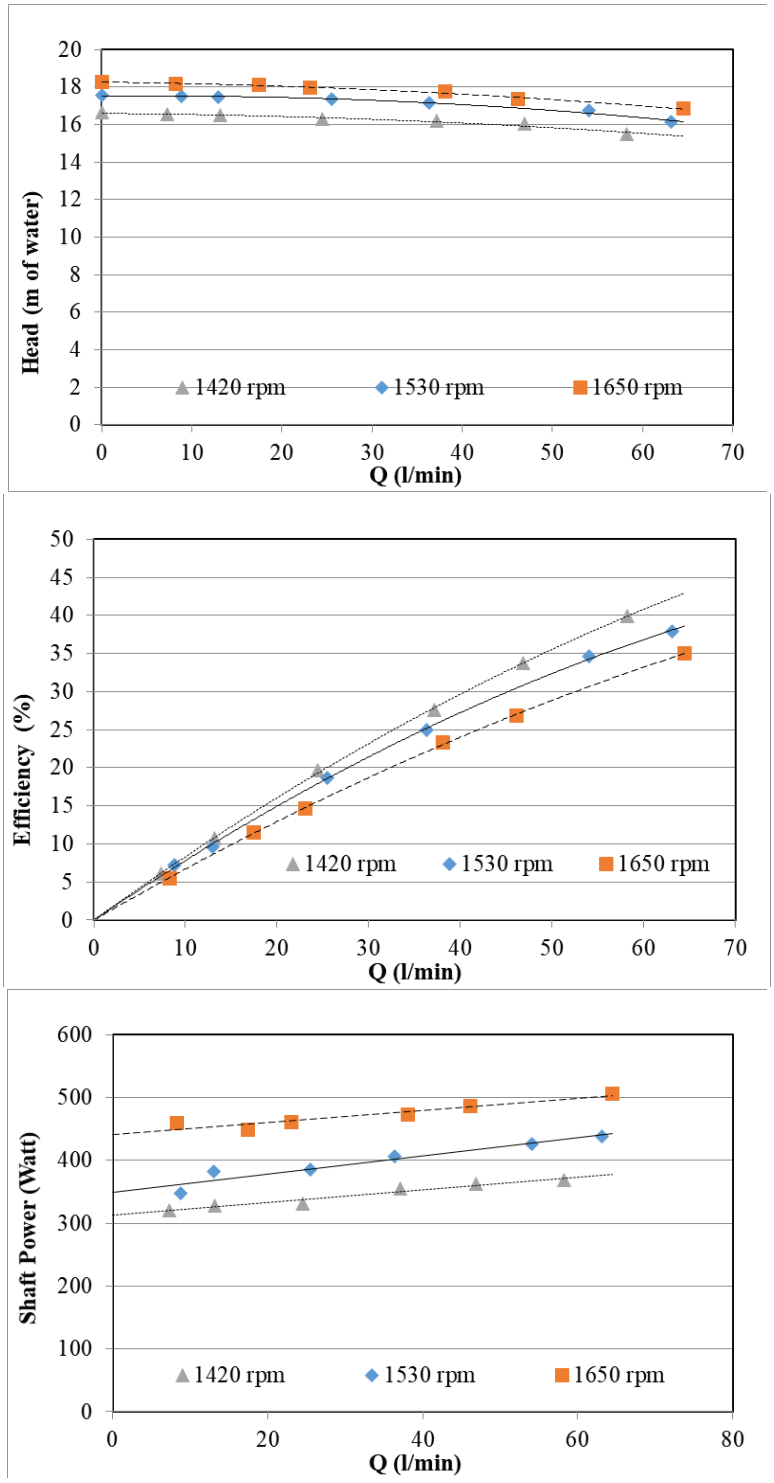

Fig.4.75 Pump performance curves for impeller with 6 blades, blade inlet angle 20° and blade outlet angle 30° for 0.02 stable emulsion

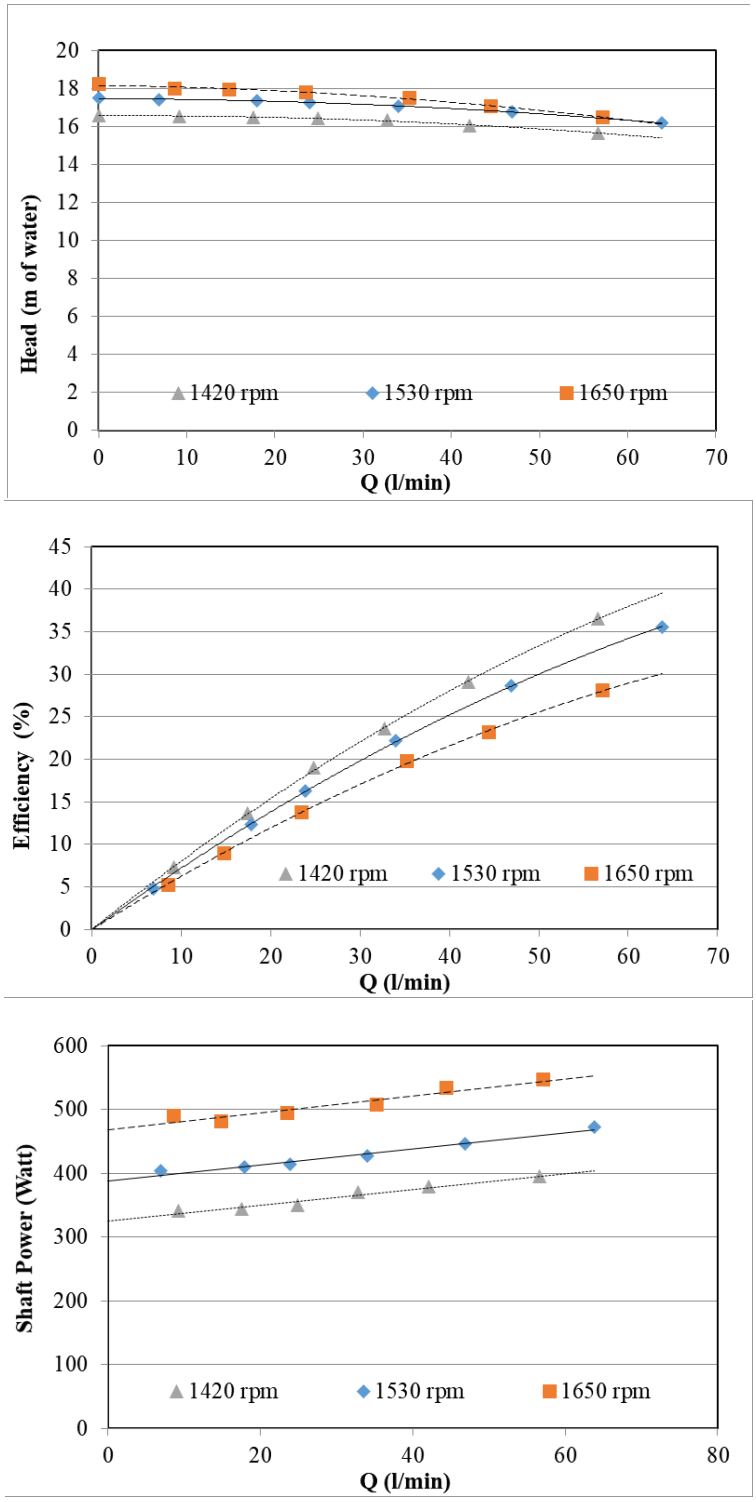

Fig.4.76 Pump performance curves for impeller with 6 blades, blade inlet angle 20° and blade outlet angle 30° for 0.02 unstable emulsion

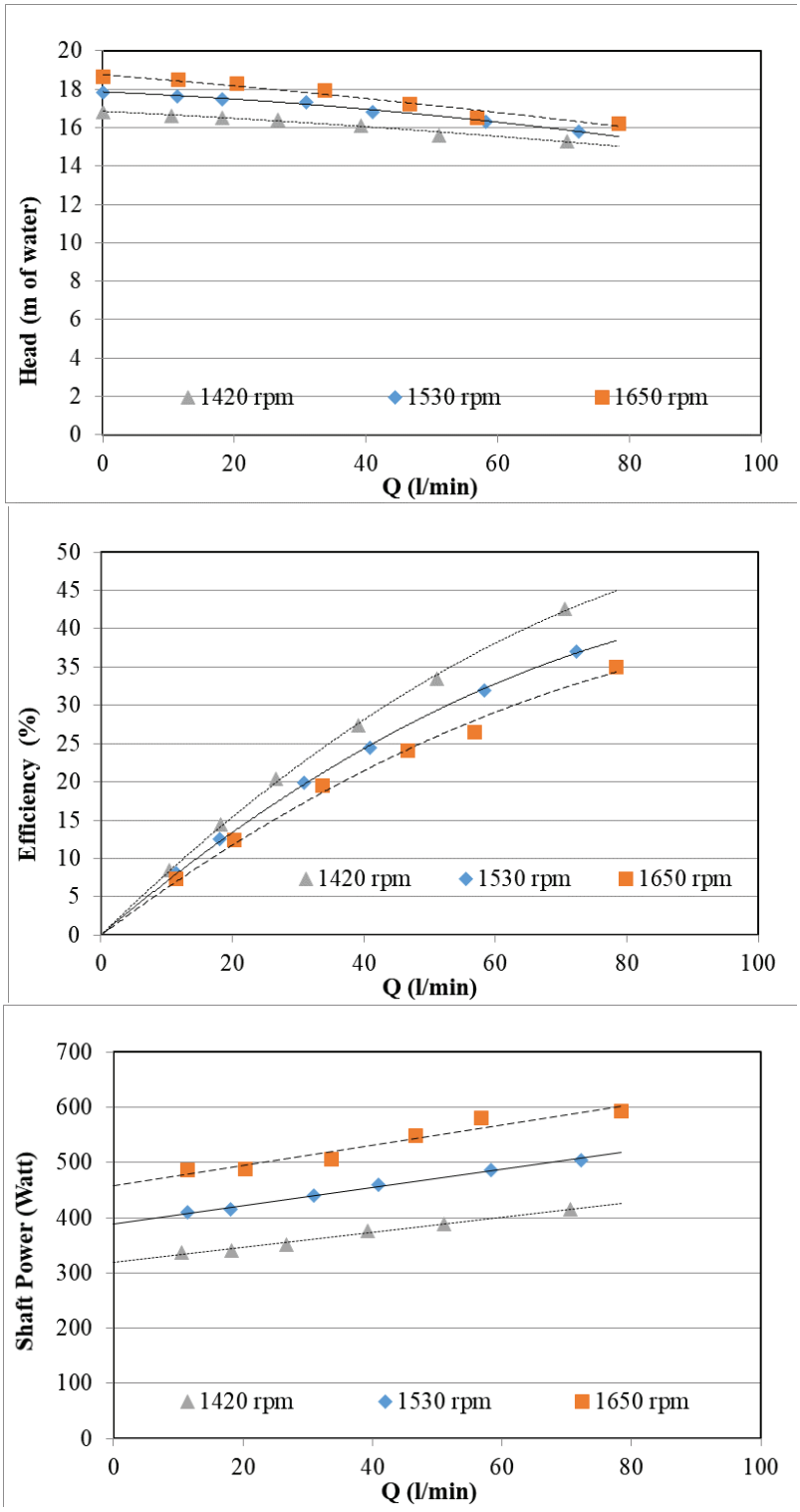

Fig.4.77 Pump performance curves for impeller with 6 blades, blade inlet angle 30° and blade outlet angle 30° for water

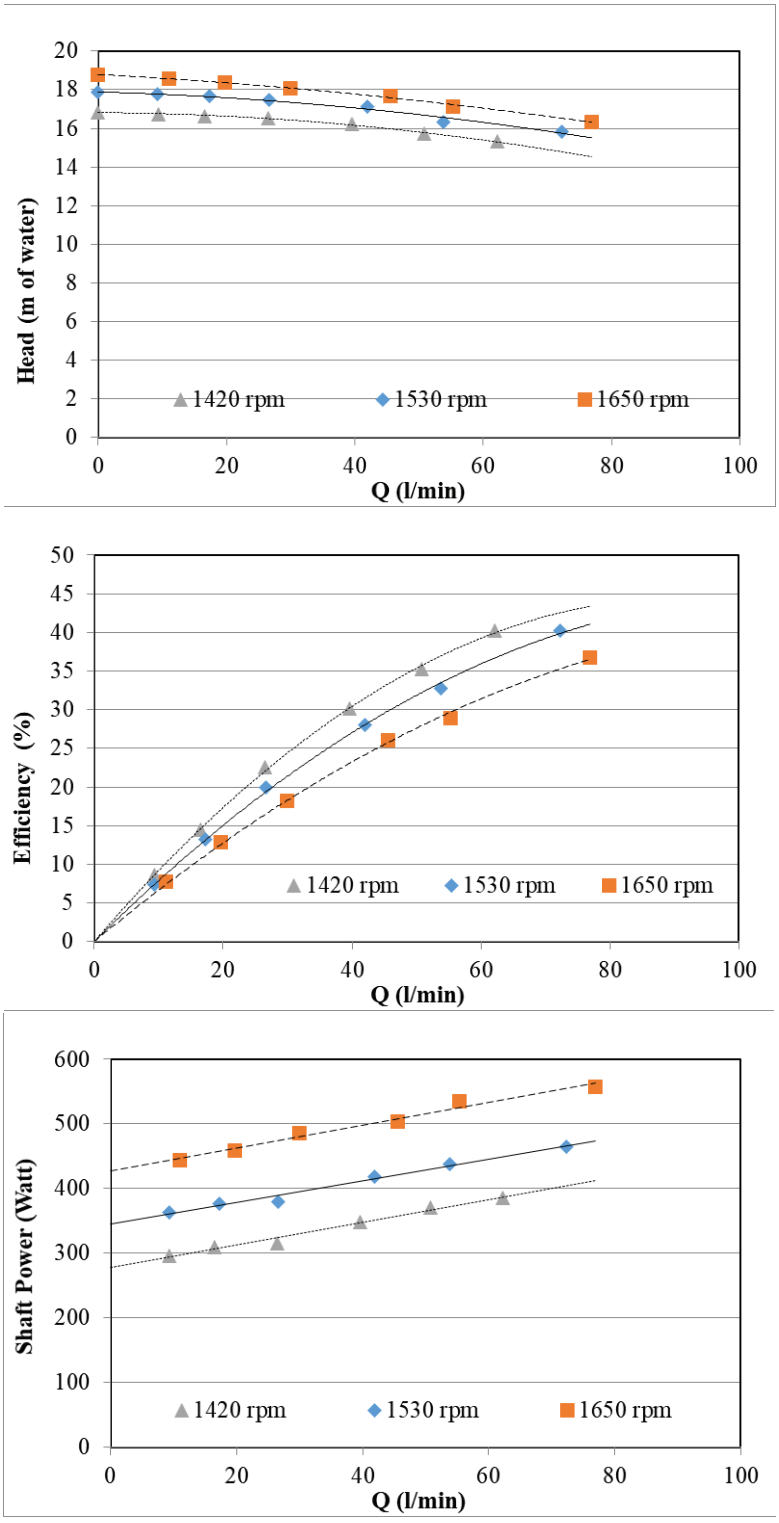

Fig.4.78 Pump performance curves for impeller with 6 blades, blade inlet angle 30° and blade outlet angle 30° for 0.005 stable emulsion

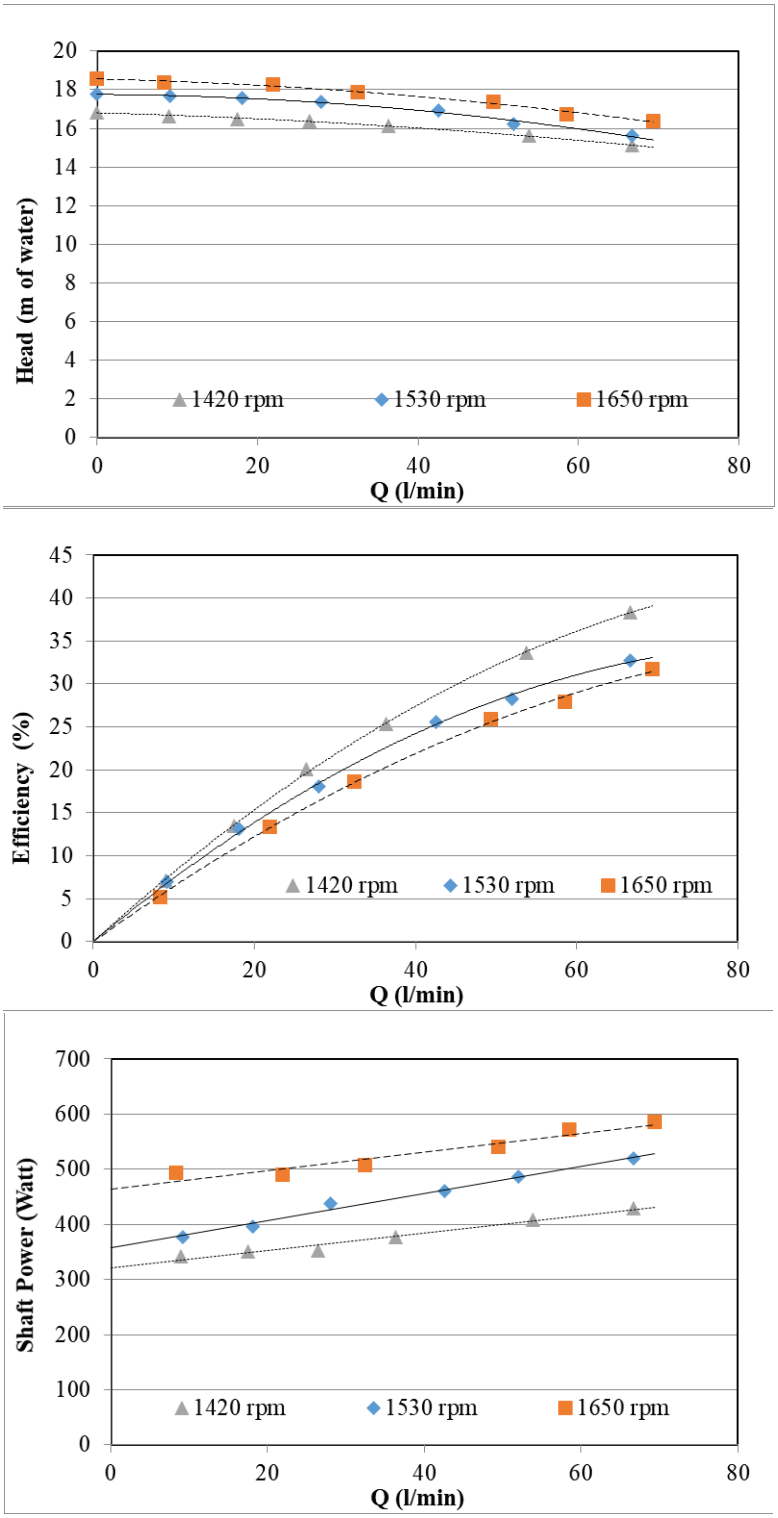

Fig.4.79 Pump performance curves for impeller with 6 blades, blade inlet angle 30° and blade outlet angle 30° for 0.005 unstable emulsion

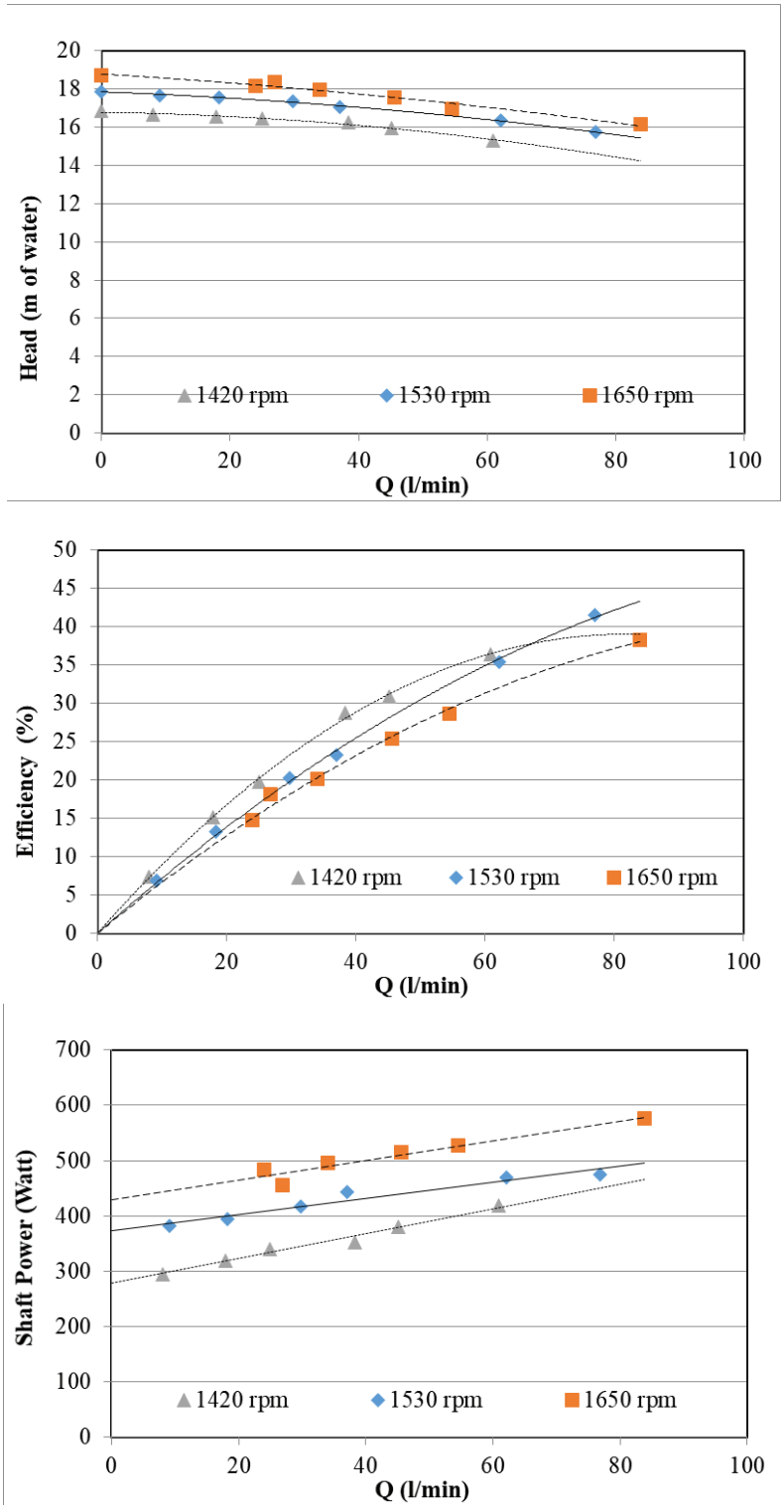

Fig.4.80 Pump performance curves for impeller with 6 blades, blade inlet angle 30° and blade outlet angle 30° for 0.01 stable emulsion

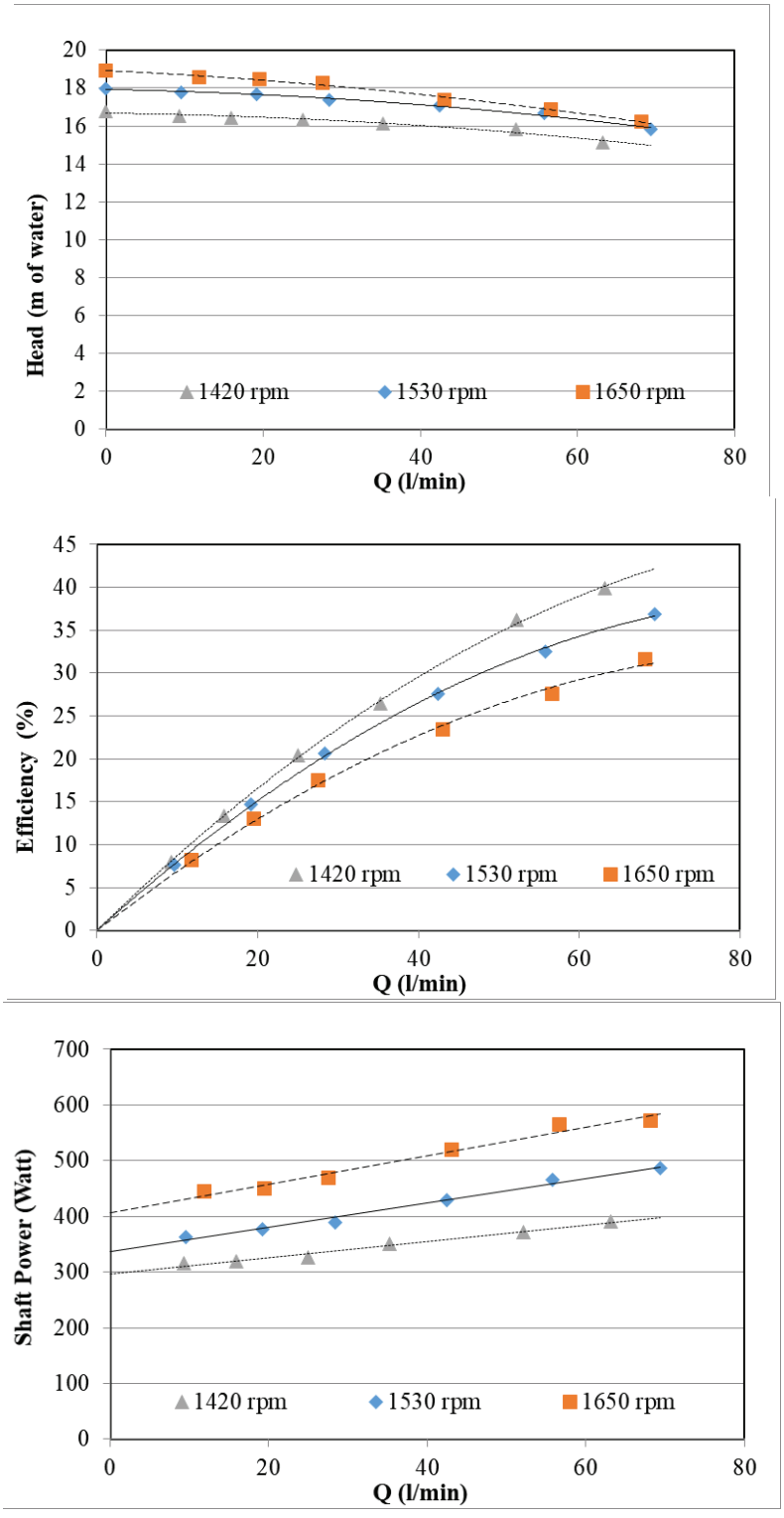

Fig.4.81 Pump performance curves for impeller with 6 blades, blade inlet angle 30° and blade outlet angle 30° for 0.01 unstable emulsion

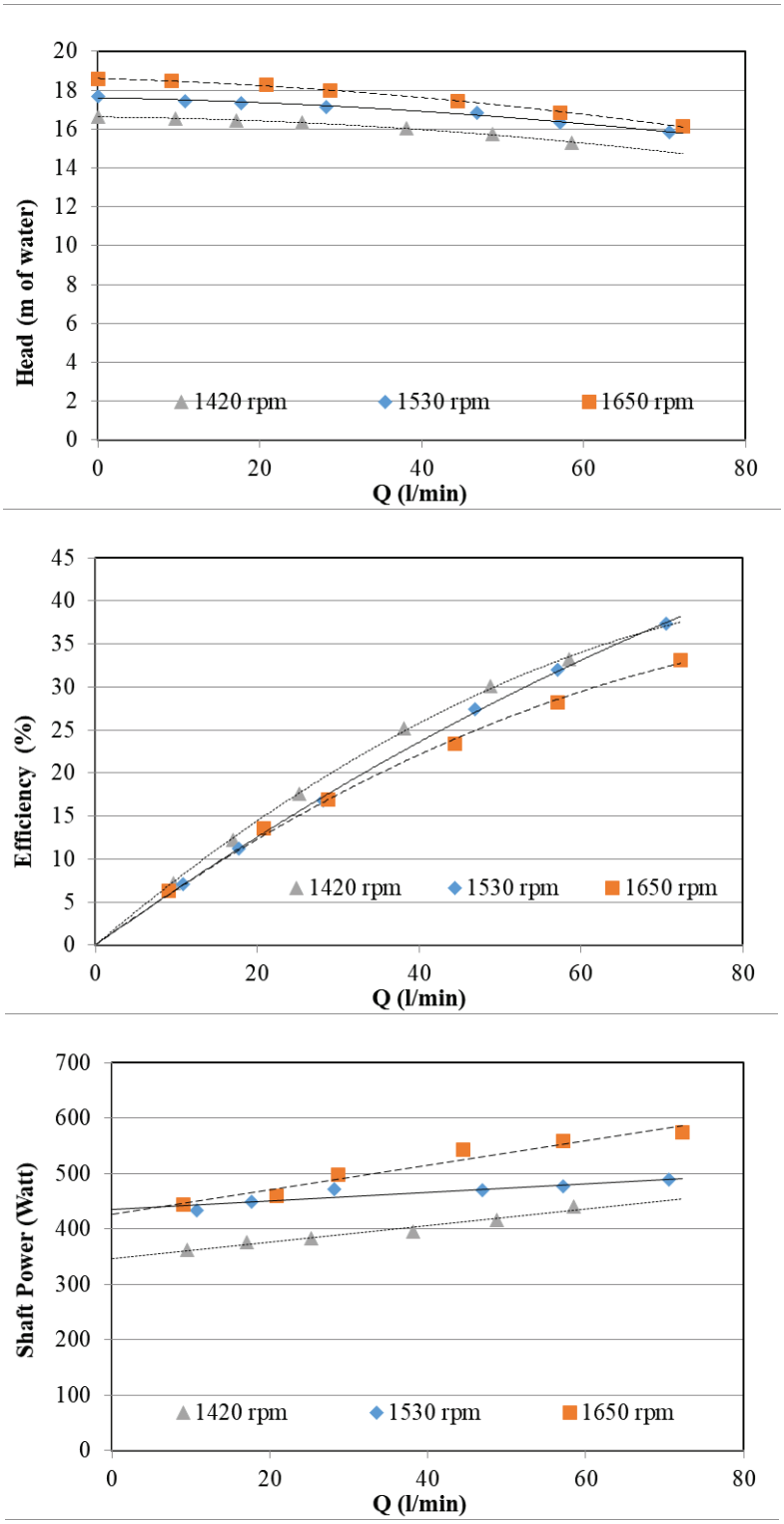

Fig.4.82 Pump performance curves for impeller with 6 blades, blade inlet angle 30° and blade outlet angle 30° for 0.02 stable emulsion

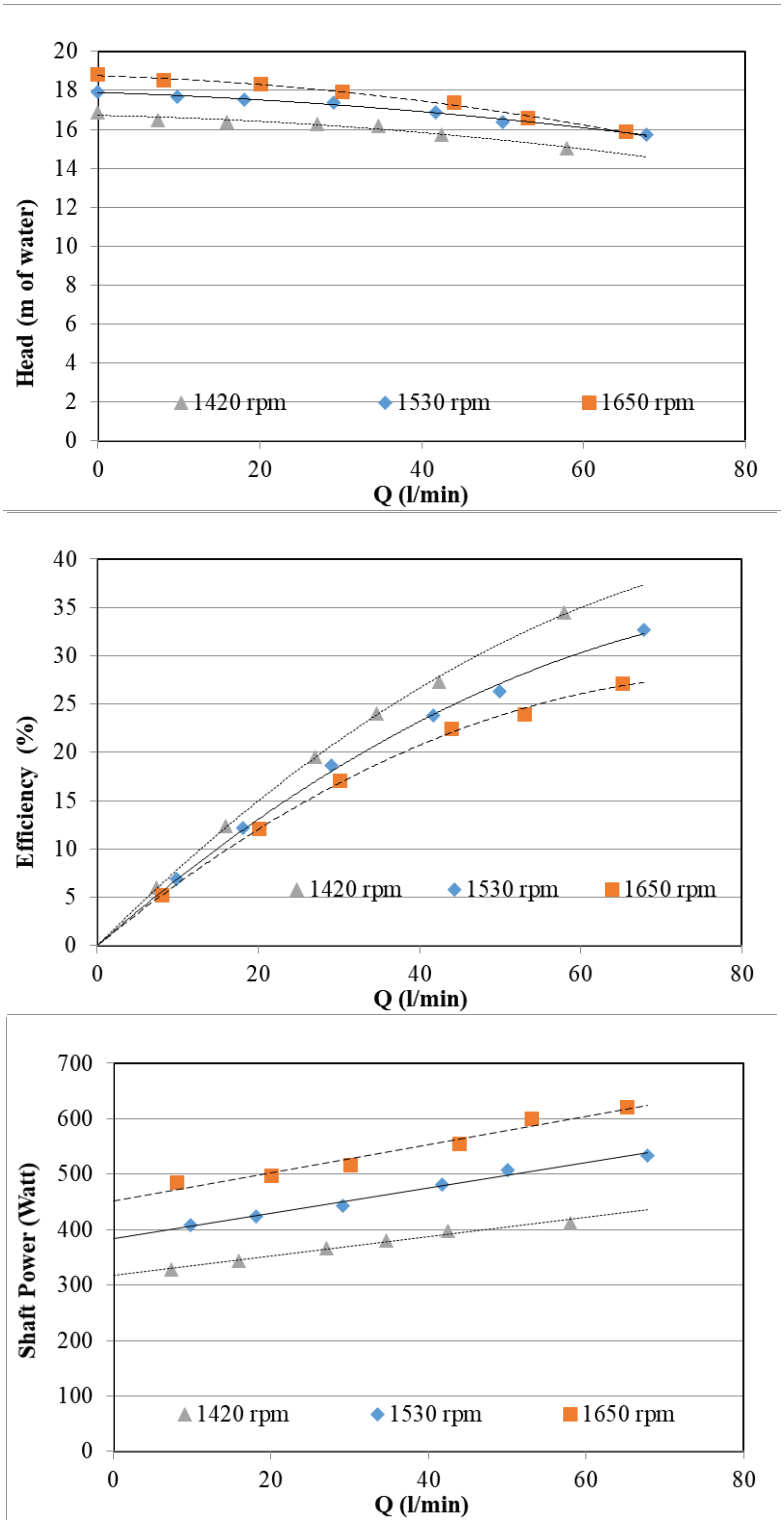

Fig.4.83 Pump performance curves for impeller with 6 blades, blade inlet angle 30° and blade outlet angle 30° for 0.02 unstable emulsion

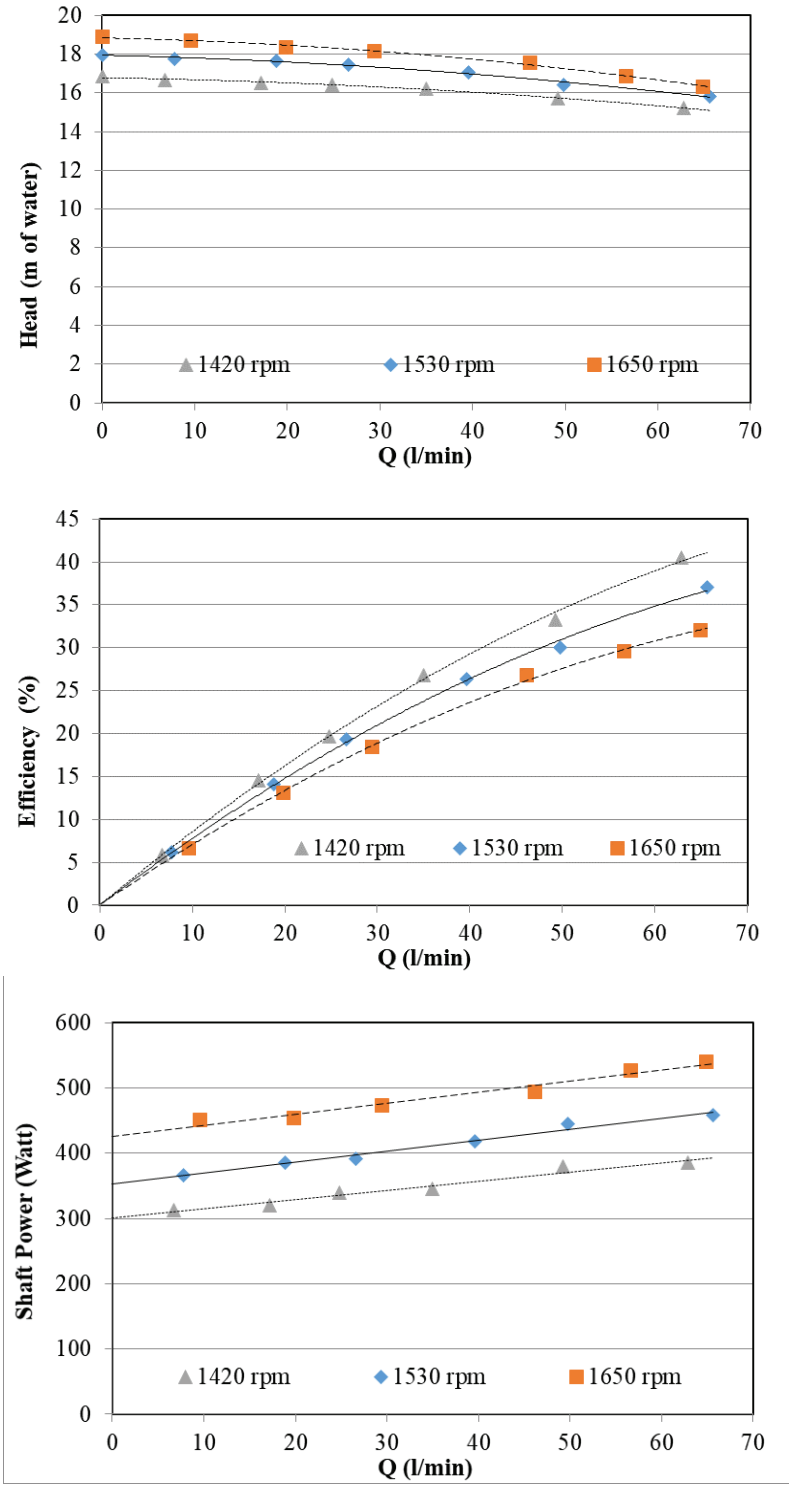

Fig.4.84 Pump performance curves for impeller with 6 blades, blade inlet angle 10° and blade outlet angle 25° for water

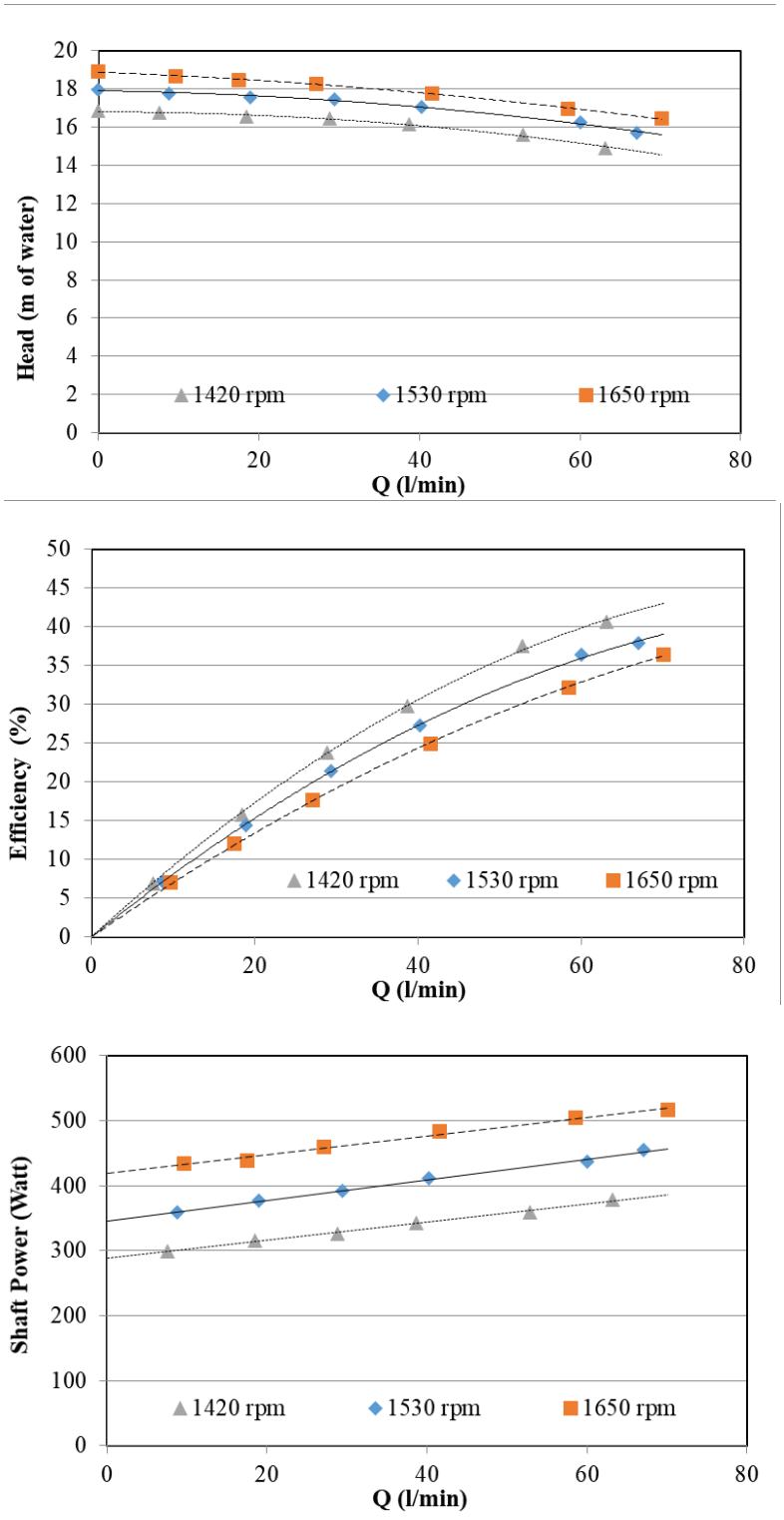

Fig.4.85 Pump performance curves for impeller with 6 blades, blade inlet angle 10° and blade outlet angle 25° for 0.005 stable emulsion

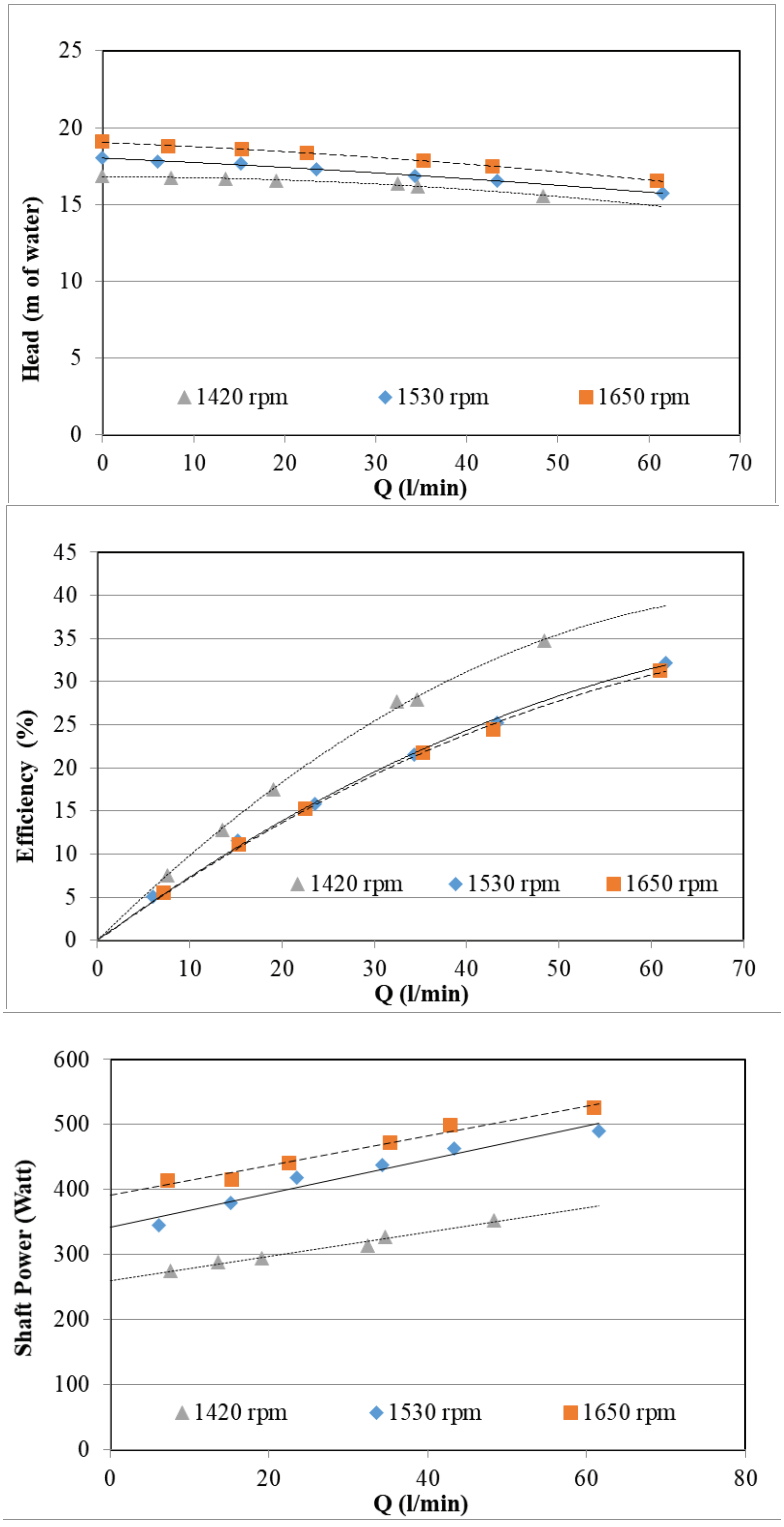

Fig.4.86 Pump performance curves for impeller with 6 blades, blade inlet angle 10° and blade outlet angle 25° for 0.005 unstable emulsion

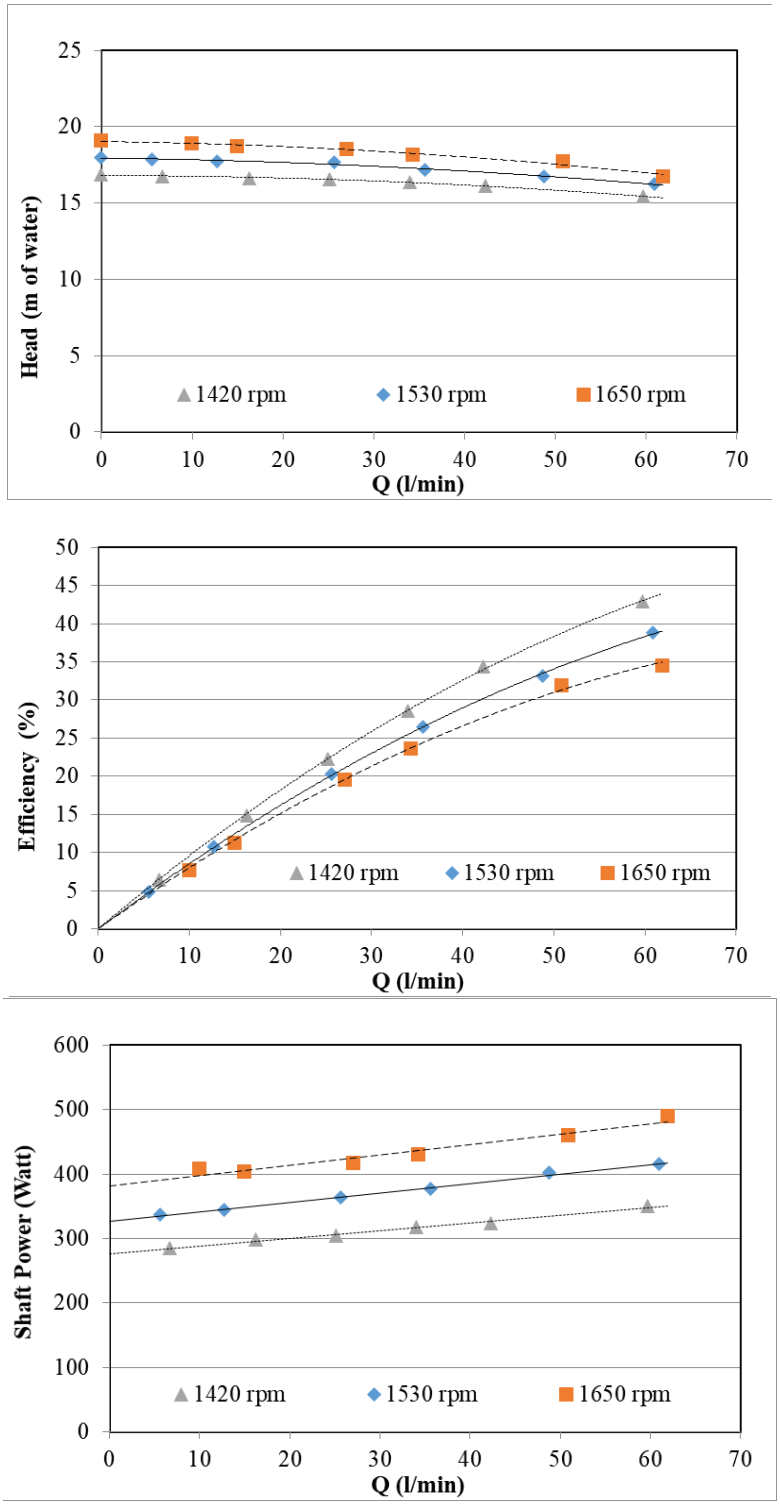

Fig.4.87 Pump performance curves for impeller with 6 blades, blade inlet angle 10° and blade outlet angle 25° for 0.01 stable emulsion

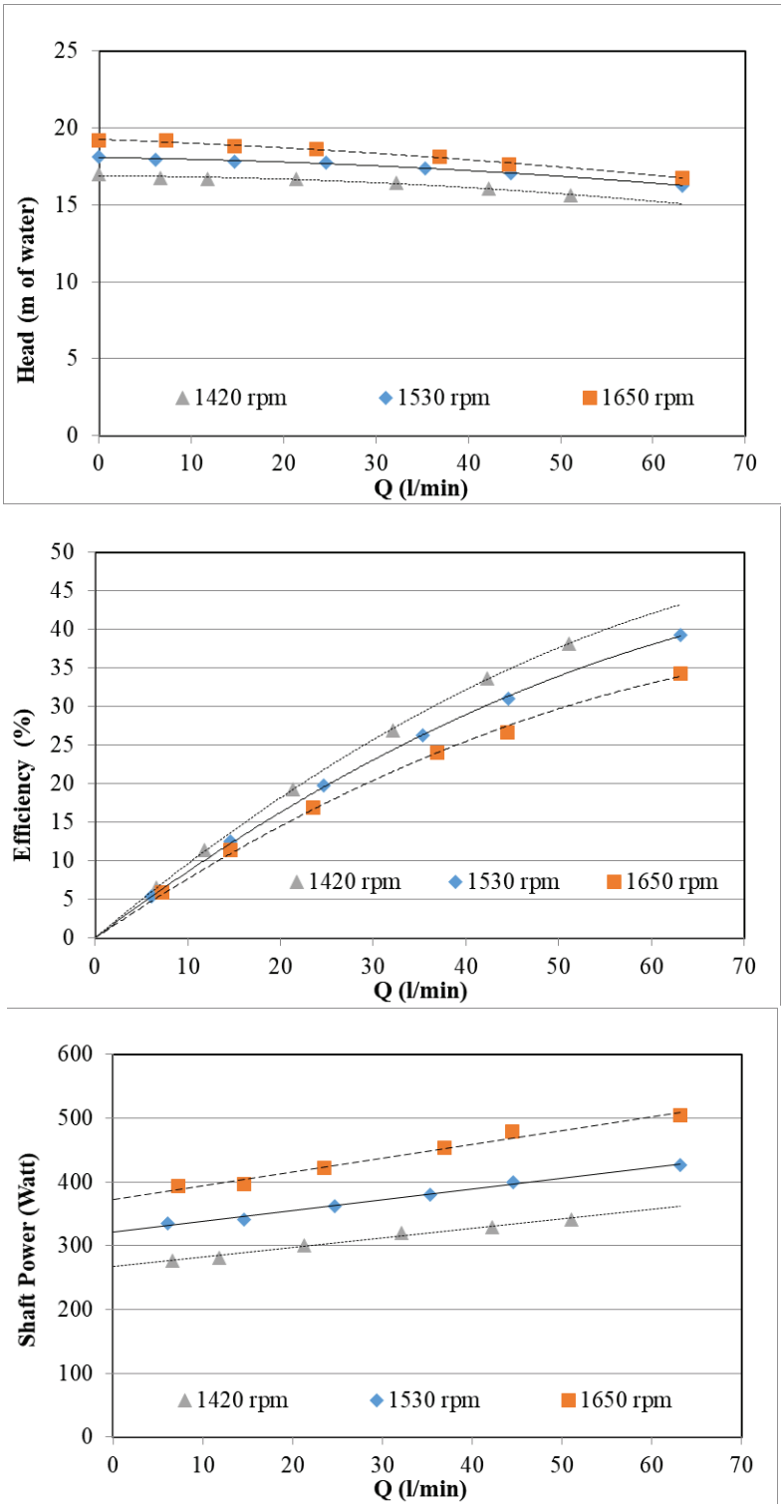

Fig.4.88 Pump performance curves for impeller with 6 blades, blade inlet angle 10° and blade outlet angle 25° for 0.01 unstable emulsion

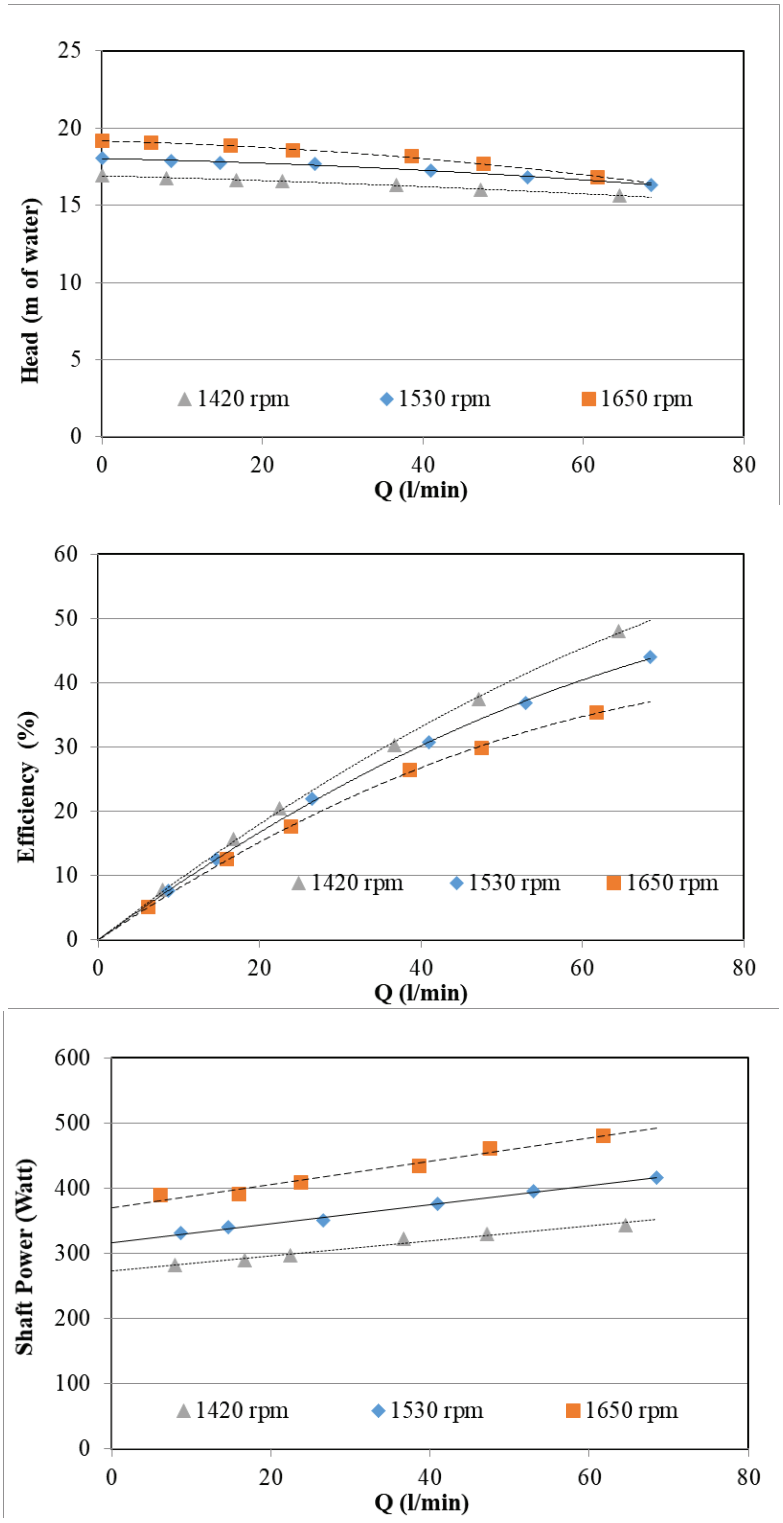

Fig.4.89 Pump performance curves for impeller with 6 blades, blade inlet angle 10° and blade outlet angle 25° for 0.02 stable emulsion

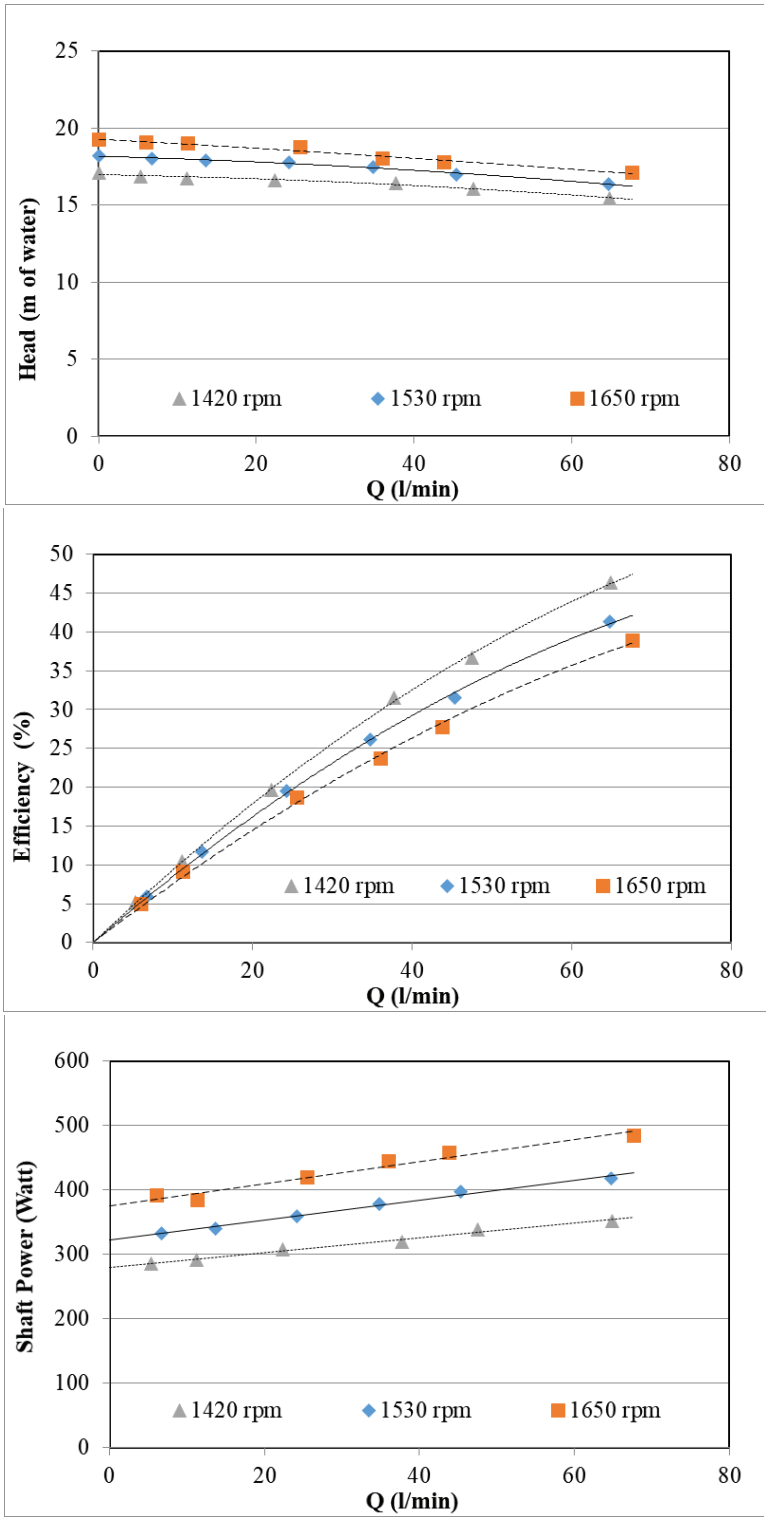

Fig.4.90 Pump performance curves for impeller with 6 blades, blade inlet angle 10° and blade outlet angle 25° for 0.02 unstable emulsion

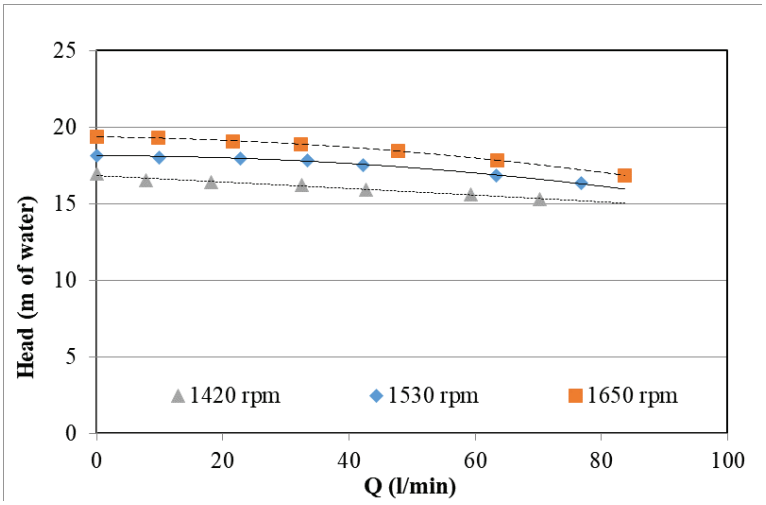

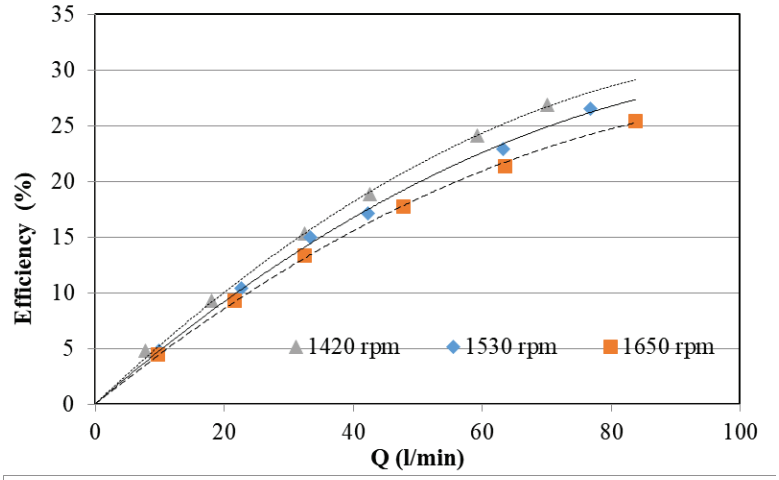

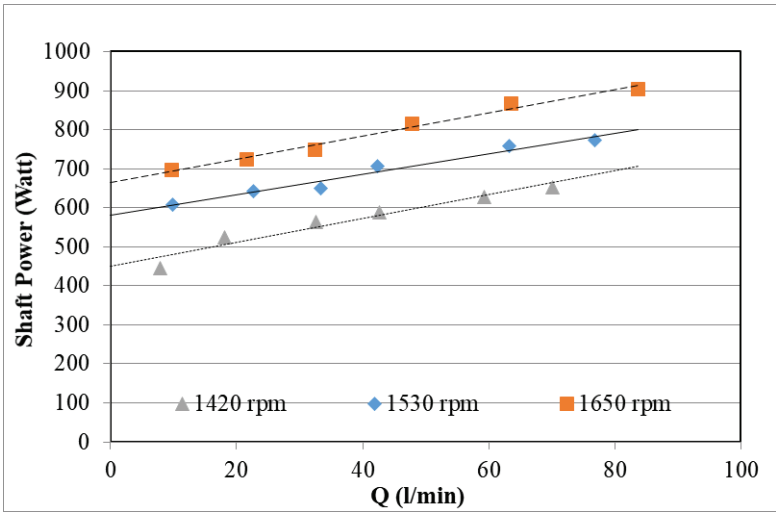

Fig.4.91 Pump performance curves for impeller with 6 blades, blade inlet angle 10° and blade outlet angle 20° for water

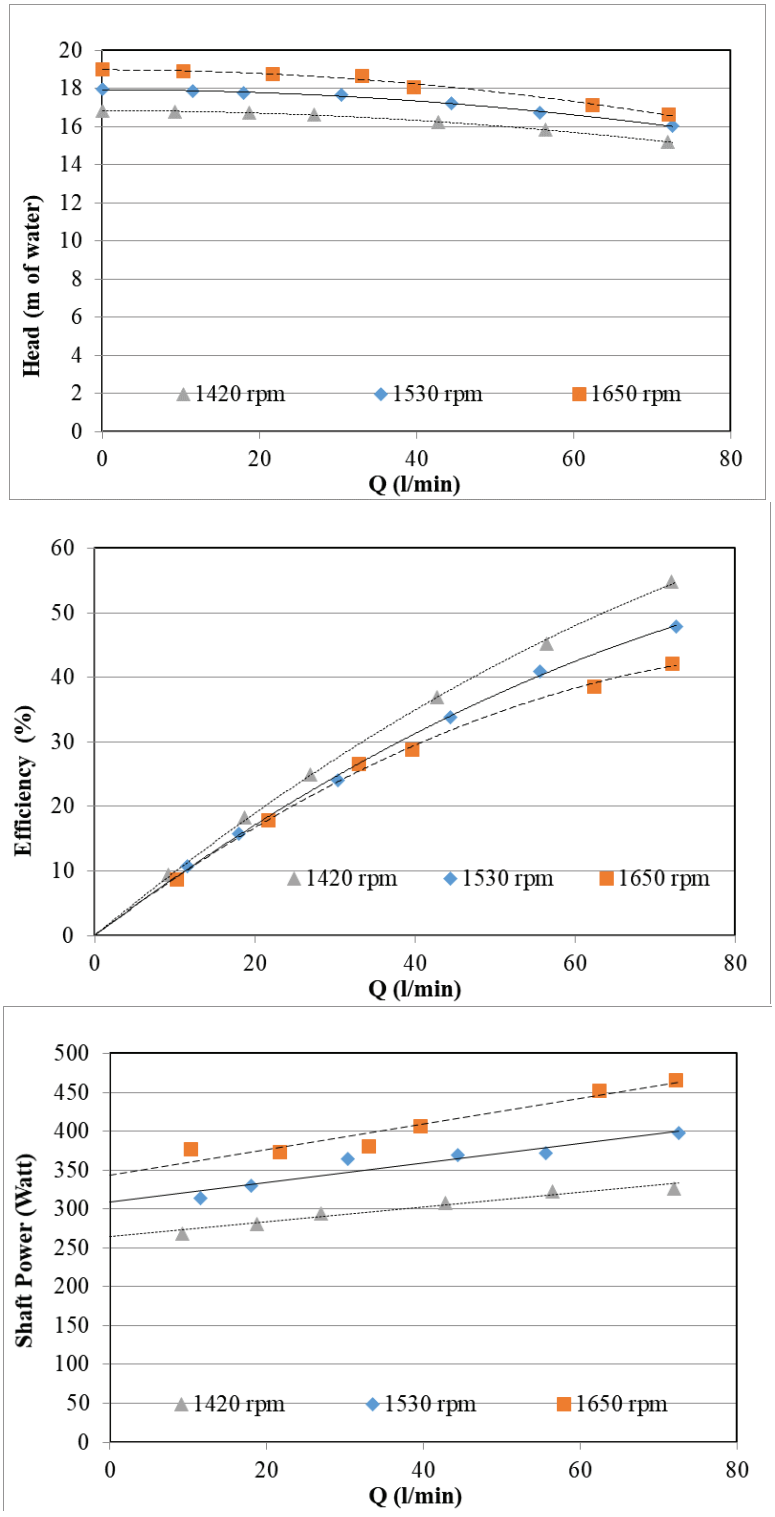

Fig.4.92 Pump performance curves for impeller with 6 blades, blade inlet angle 10° and blade outlet angle 20° for 0.005 stable emulsion

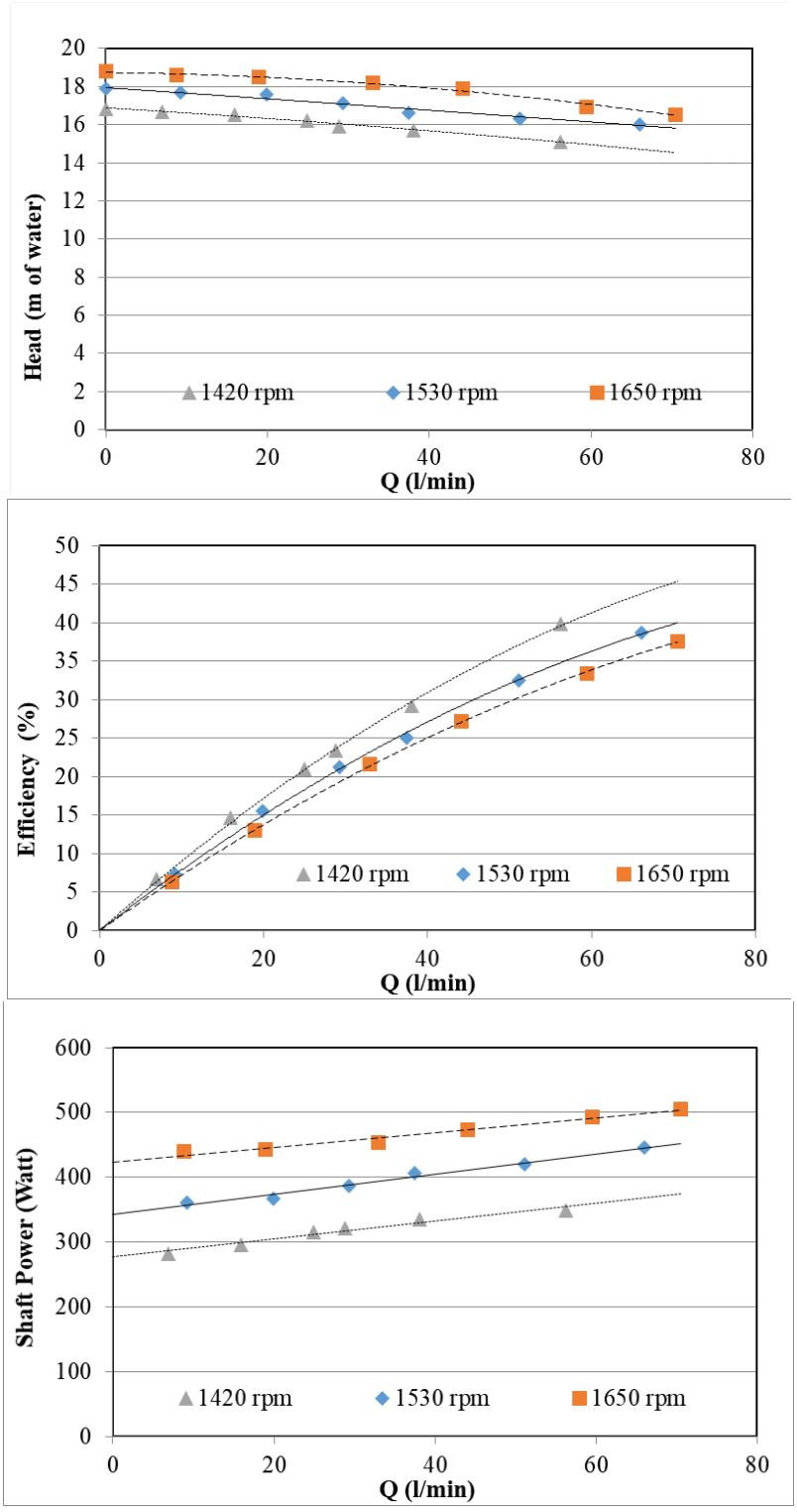

Fig.4.93 Pump performance curves for impeller with 6 blades, blade inlet angle 10° and blade outlet angle 20° for 0.005 unstable emulsion

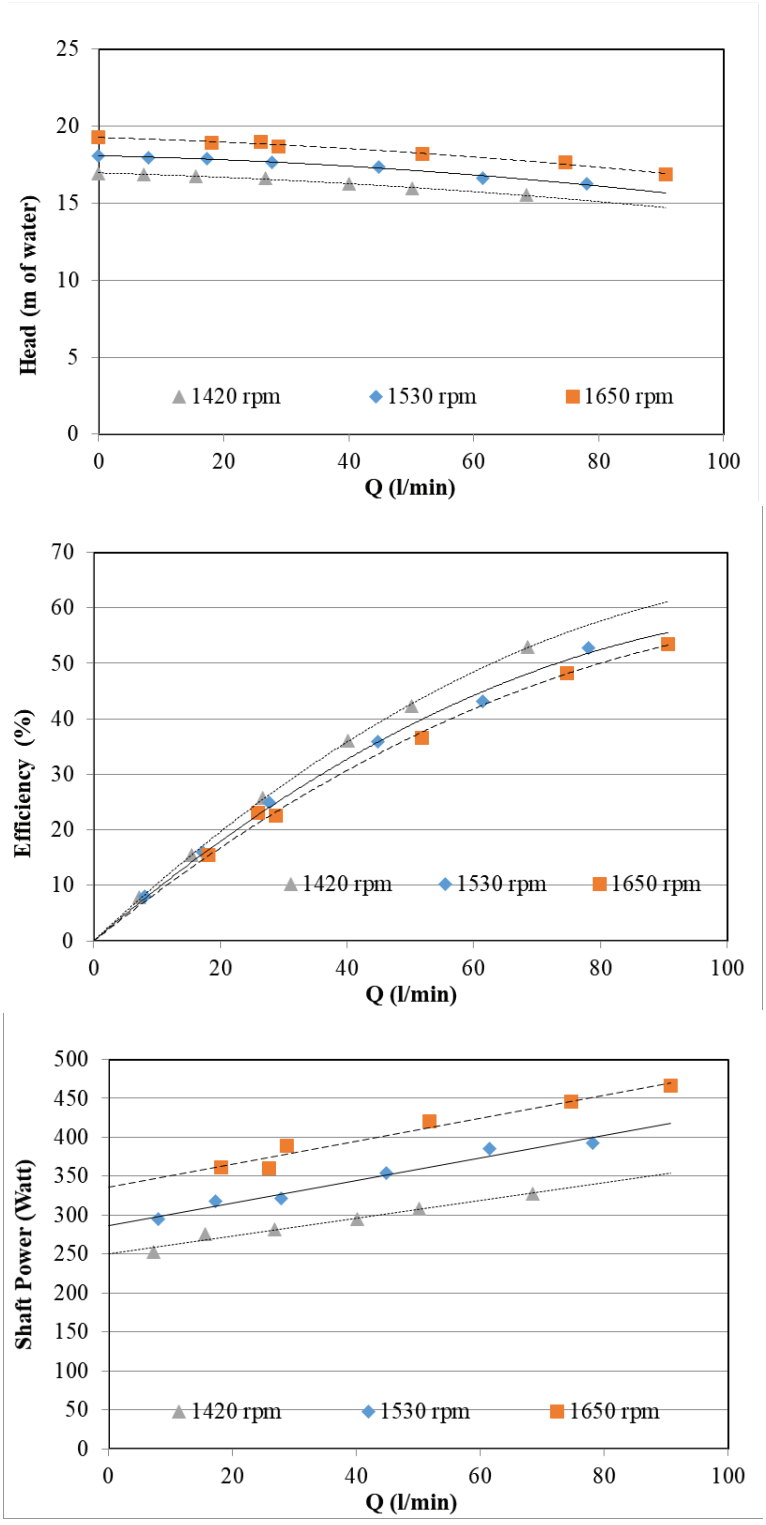

Fig.4.94 Pump performance curves for impeller with 6 blades, blade inlet angle 10° and blade outlet angle 20° for 0.01 stable emulsion

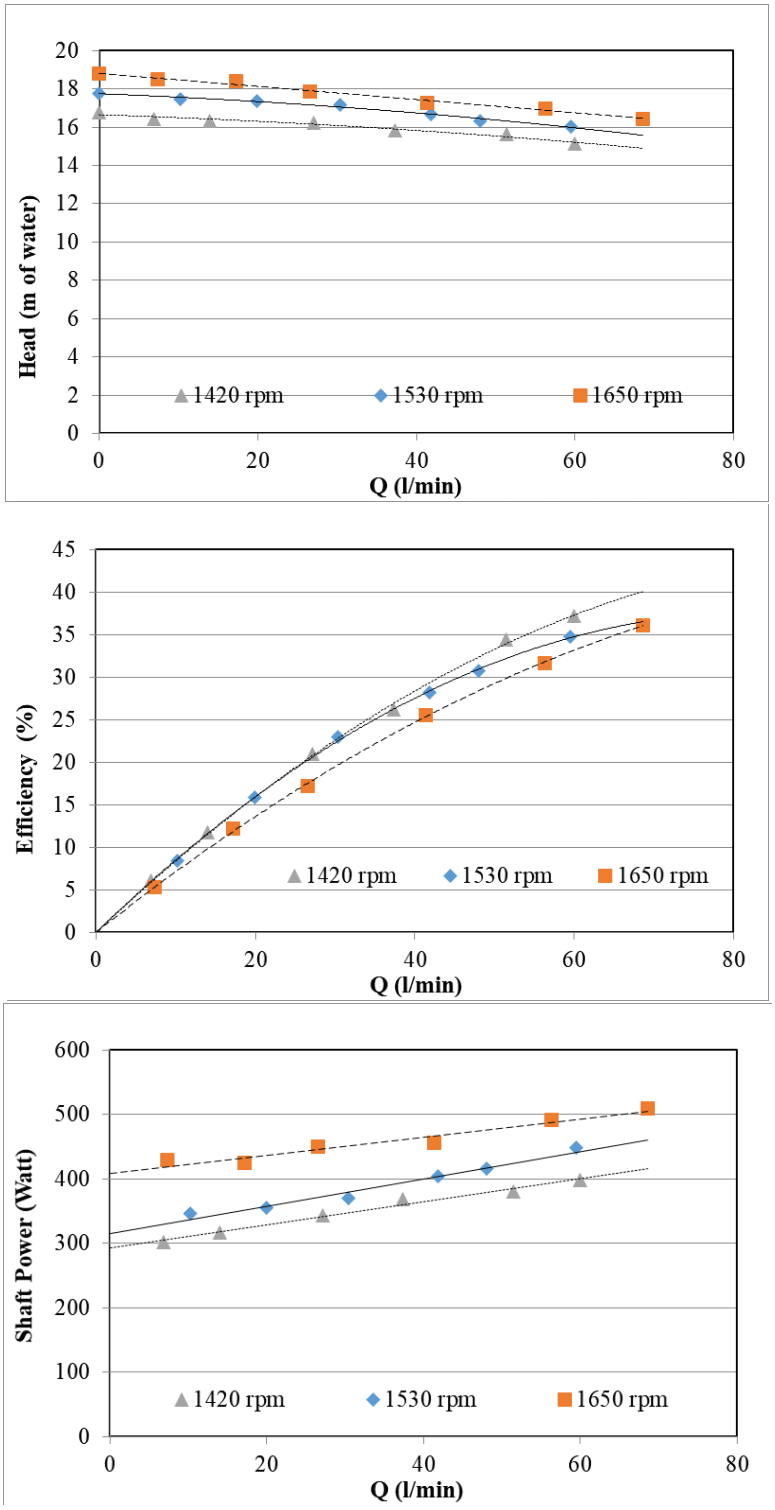

Fig.4.95 Pump performance curves for impeller with 6 blades, blade inlet angle 10° and blade outlet angle 20° for 0.01 unstable emulsion

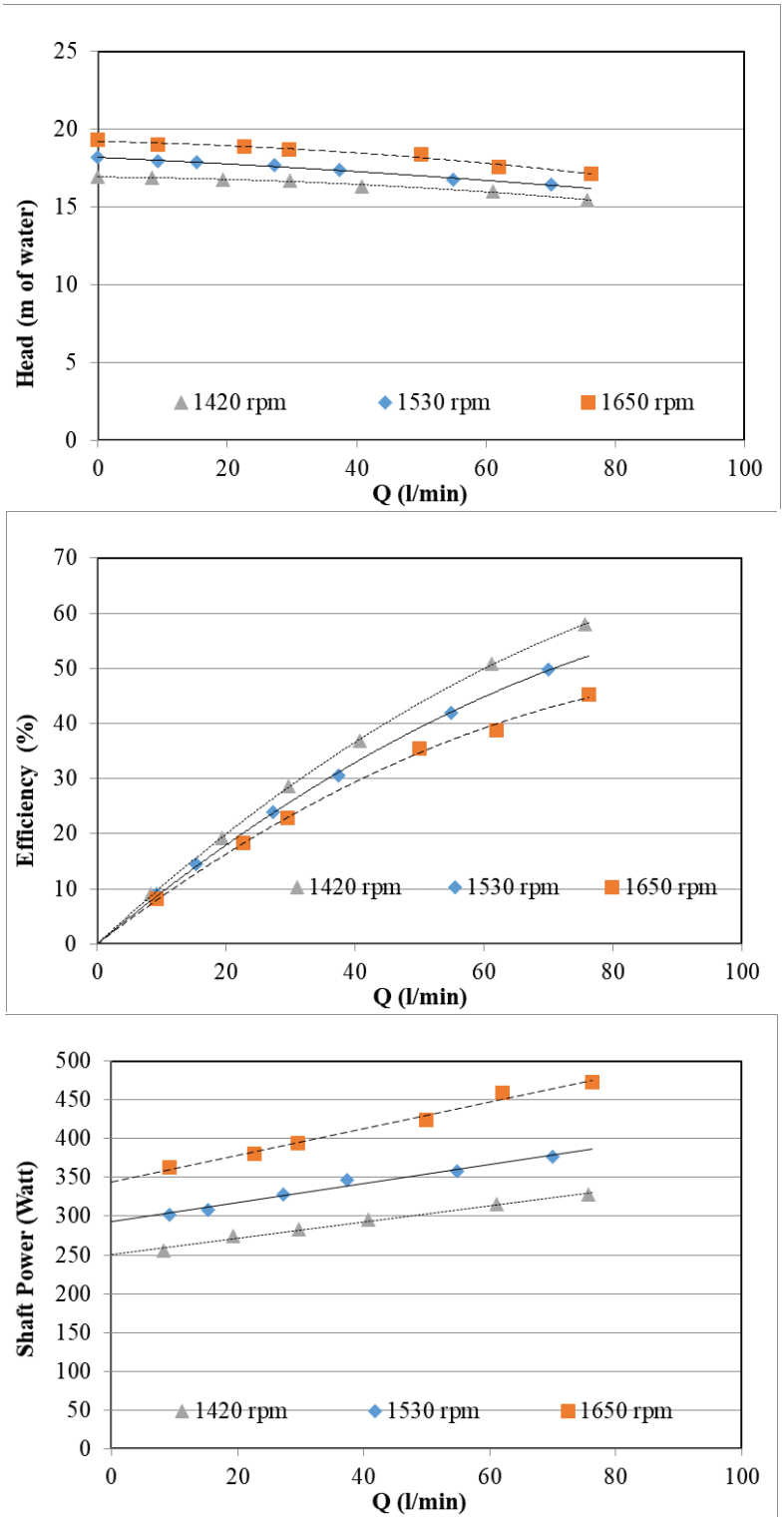

Fig.4.96 Pump performance curves for impeller with 6 blades, blade inlet angle 10° and blade outlet angle 20° for 0.02 stable emulsion

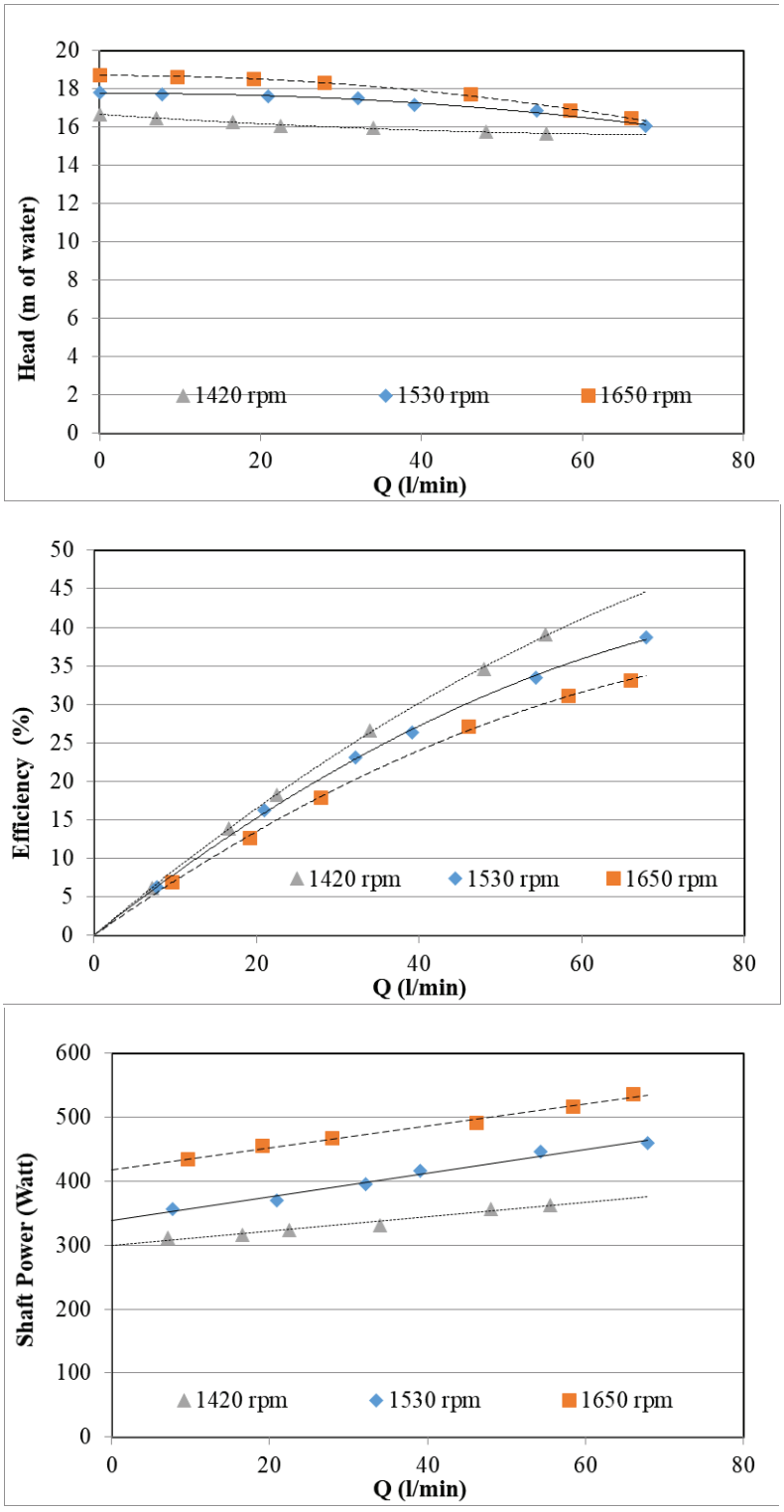

Fig.4.97 Pump performance curves for impeller with 6 blades, blade inlet angle 10° and blade outlet angle 20° for 0.02 unstable emulsion

CHAPTER FIVE

THEORETICAL ANALYSIS

CHAPTER FIVE

THEORETICAL ANALYSIS

5.1 INTRODUCTION

In this chapter the performance of the test pump will be predicted using the energy loss analysis, a theoretical procedure was developed to calculate the performance of a centrifugal pump utilizing theoretical and empirical internal and external energy loss equations. The equations were implemented in an excel sheet and were used to predict the pump head, power and efficiency while varying different impeller geometries, rotational speed and fluid properties. The results were compared to the experimental work in order to validate the accuracy and methodology of the test procedures, the theoretical model is also considered a faster method for predicting the pump performance.

5.2 THEORETICAL ANALYSIS

Euler presented the fundamental equation of turbomachines with infinite blade (without swirl) as [50]:

$$H_{inf} = (u_2 c_{2u} - u_1 c_{1u})/g \qquad (5.1)$$

where u_1 and u_2 are circumferential velocities at the inlet and outlet of the impeller, respectively; c_{1u} and c_{2u} are the circumferential components of absolute velocity at inlet and outlet, respectively as shown in Figure 5.1.

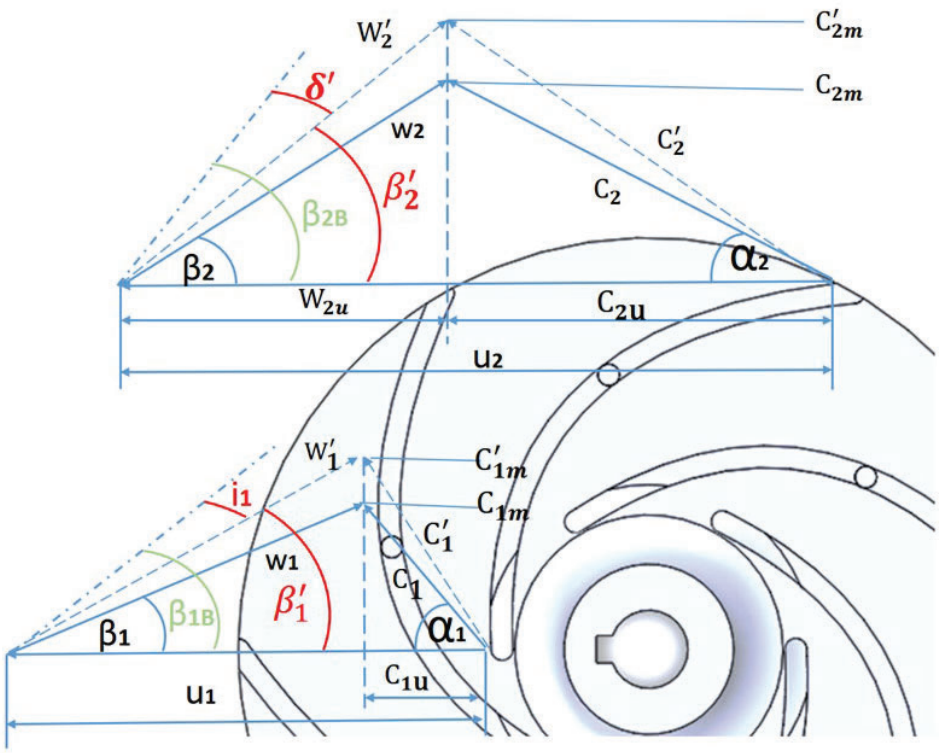

Fig. 5.1 The velocity triangle at blade inlet and outlet

Introducing the slip factor γ and the blade blockage τ_2, to Euler equation present the theoretical head as [51]:

$$H_{the}=\frac{u_2^2}{g}\left\{\gamma-\frac{Q_{La}}{A_2 u_2 \tan\beta_{2B}}\left[\tau_2+\frac{A_2 d_{1m}^{*}\tan\beta_{2B}}{A_1\tan\alpha_1}\right]\right\} \quad (5.2)$$

Where:

$$A_1=\frac{\pi}{4}(d_1^2-d_n^2) \quad (5.3)$$

$$A_2=\pi d_{2b} b_2 \quad (5.4)$$

5.2.1. Velocity triangles

The velocity triangle is a triangle representing the various components of velocities of the working fluid in a turbomachine. It can be drawn in both the inlet and outlet sections of any turbomachine. The vector nature of velocity is used in the triangles and the basic form of velocity triangle consists of the tangential velocity, the absolute velocity and the relative velocity of the fluid making the three sides of the triangle.

The rules of vector addition can be used to obtain the relationship between circumferential impeller speed u, relative velocity w and absolute velocity c which can be illustrated as velocity triangles [51].

5.2.2 Impeller losses

5.2.2.1 *Impeller inlet shock loss*

The difference between relative velocities before and after the blade leading edge determine the magnitude of the shock loss and is calculated using the following model [51]:

$$L_{sh.La} = C_{sh} \frac{(w_1 - w_{1q})^2}{2g} \quad (5.5)$$

where, C_{sh} is the shock loss coefficient at impeller inlet. Its empirical value is set to 0.5–0.7 depending on the size of the recirculation zone after the blade leading edge.

5.2.2.2 *Impeller skin friction loss*

The impeller skin friction relationship is similar to the standard pipe friction model [35]. And because the flow passage across the impeller is irregular, we use hydraulic diameter d_h and average relative velocity w_{av} [51] and given as follows:

$$L_{fr.La} = 4C_{fr.La} \frac{l_e}{d_{h.La}} \frac{w_{av}^2}{2g} \quad (5.6)$$

$$d_{h.La} = \frac{2(a_2 b_2 + A_{q1})}{a_1 + b_1 + a_2 + b_2} \quad (5.7)$$

$$l_e = \frac{r_2 - r_1}{cos\beta_{2B}} \quad (5.8)$$

5.2.2.3 *Impeller diffusion loss*

Due to the separation appearing invariably within the impeller at some point the diffusion loss needs to be taken into account. A portion of the velocity head difference is lost if the ratio of the inlet relative velocity w_1 to the outlet one w_2 exceeds the value of 1.4, [35]:

$$L_{D.La} = 0.25 \frac{W_1^2}{2g} \quad (5.9)$$

5.2.3. Leakage losses

The gaps between the rotating and fixed parts of the pump allows for smaller fluid circulation to pass through leading to leakage losses and as a results a loss in efficiency. To calculate the leakage loss, the pressure difference over the seal at the impeller inlet ΔH_{sp} must be established [51].

$$\Delta H_{sp} = H_p - k^2 \frac{u_2^2}{2g}\left(1 - \frac{d_{sp}^2}{d_2^2}\right) \quad (5.10)$$

with, H_p is the pressure rise given by the impeller and k is the rotation factor of the fluid between impeller and casing and are both given as:

$$H_p = \frac{u_2^2 - u_1^2 + w_1^2 - w_2^2}{2g} - z_{la} \quad (5.11)$$

$$k = 0.9 y_{sp}^{0.087} \quad (5.12)$$

$$y_{sp} = Re_{u2}^{0.3} \frac{s d_{sp}}{d_2^2} \sqrt{\frac{s}{l_{SP}}} \quad (5.13)$$

$$Re_{u2} = \frac{u_2 r_2}{v} \quad (5.14)$$

where, Z_{La} is the sum of losses in impeller, y_{sp} is the seal geometry and Re_{u2} is Reynolds number.

The axial velocity c_{ax} in the annual seal has to be calculated iteratively, and it is given as:

$$c_{ax} = \sqrt{\frac{2g\Delta H_{sp}}{\xi_{EA} + \lambda \frac{l_{sp}}{2s}}} \quad (5.15)$$

where, l_{sp} is the gap length, and λ is the friction coefficient which is calculated in the same way as the friction coefficient in a channel For turbulent flow $4000 < Re_{sp} < 10^8$:

$$\lambda_0 = \frac{0.31}{\left(log\left[A + \frac{6.5}{Re_{sp}}\right]\right)^2} \quad (5.16)$$

which, Re_{sp} is the Reynolds number through the gap and A is the seal surface [35]:

$$Re_{sp} = \frac{2sc_{ax}}{v} \quad (5.17)$$

The effect of the rotation in turbulent flow is covered by an experimentally determined factor λ/λ_0, [51]:

$$\frac{\lambda}{\lambda_0} = \left\{1 + 0.19\left(\frac{Re_{u2}}{Re_{sp}}\right)^2\right\}^{0.375} \quad (5.18)$$

The friction coefficient λ is calculated iteratively [48].Subsequently, the leakage flow is calculated as follows:

$$Q_{sp} = \pi d_{sp}\, s\, c_{ax} \quad (5.19)$$

5.2.4. Efficiencies and powers

5.2.4.1. Volumetric efficiency

The volumetric efficiency is the percentage of the actual fluid flow out of the pump compared to the flow out of the pump without leakage, it can be also described as the percentage of the pump flow compared to the impeller flow:

$$\eta_v = \frac{Q_{la}}{Q_i} = \frac{Q_{la}}{Q_{la}+Q_{sp}} \quad (5.20)$$

where, Q_i is the impeller flow which is the sum of pump flow Q_{La} and pump internal leakage flow Q_{sp}. The impeller flow can be calculated as:

$$Q_i = c_{2m}\pi d_2 b_2 \varepsilon_2 = c_{1m}\pi d_1 b_1 \varepsilon_1 \quad (5.21)$$

where, ε_1 is the blade thickness coefficient at the impeller inlet, ε_2 is the blade thickness coefficient at the impeller outlet [43]. They are given as:

$$\varepsilon_1 = (Z_{la}/\pi)\left(\left(e_1/sin(\beta_{1B})\right)/d_1\right) \quad (5.22)$$

$$\varepsilon_2 = (Z_{la}/\pi)\left(\left(e_2/sin(\beta_{2B})\right)/d_2\right) \quad (5.23)$$

where, e_1 is the blade thickness.

5.2.4.2. Mechanical efficiency

The mechanical efficiency is the ratio between the power available at the impeller to the power at the shaft of the centrifugal pump.

The mechanical efficiency is given as [35]:

$$\eta_{me} = 1/\left(1 + \frac{\eta_v \eta_h (P_{me}+P_{RR})}{pgH_{th}Q_{la}}\right) \quad (5.24)$$

where, P_{me} is the mechanical power loss due to the bearing and axial thrust losses. It is assumed to be 1% of the useful power.

5.2.4.3. Hydraulic efficiency

The hydraulic efficiency is mostly determined from power balance of a measured pump. According to [48] the full equation is given by:

$$\eta_h = \frac{\rho g H_r (Q_{La}+Q_{sp})}{P - P_{RR} - P_m} \quad (5.25)$$

For single stage pump and in the absence of recirculation, power consumption can be expressed in simplified form and Equation (63.A) becomes [48]:

$$P = \frac{\rho g H Q}{\eta_v \eta_h} + P_m \quad (5.26)$$

The actual head H_r is given as:

$$H_r = H_{th} - \left(L_{sh.La} + L_{fr.la} + L_{D.la}\right) \quad (5.27)$$

5.2.4.4. Overall efficiency

The overall efficiency is defined as the ratio of the power output of the pump compared to the power input to the pump

The overall efficiency is the partial efficiencies products [50], given as:

$$\eta = \eta_v \eta_h \eta_m \quad (5.28)$$

5.3 THEORETICAL MODEL VALIDATION

Figure 5.2 presents a comparison between theoretical and experimental results for the pump performance curves at an impeller blade outlet angle of β_2 = 20°, using a 0.02 unstable emulsion while the pump operates at 1420 rpm. Subfigures 9 (a), (b), and (c) illustrate the head, shaft power, and efficiency comparisons. The results indicate that both the theoretical and experimental methods demonstrate similar trends and are in close agreement. Additionally, the patterns observed in Figure 5.2 confirm that the theoretical model accurately predicts the pump performance curves, establishing it as a valid solution model. Table 4.1 presents the average variations between results.

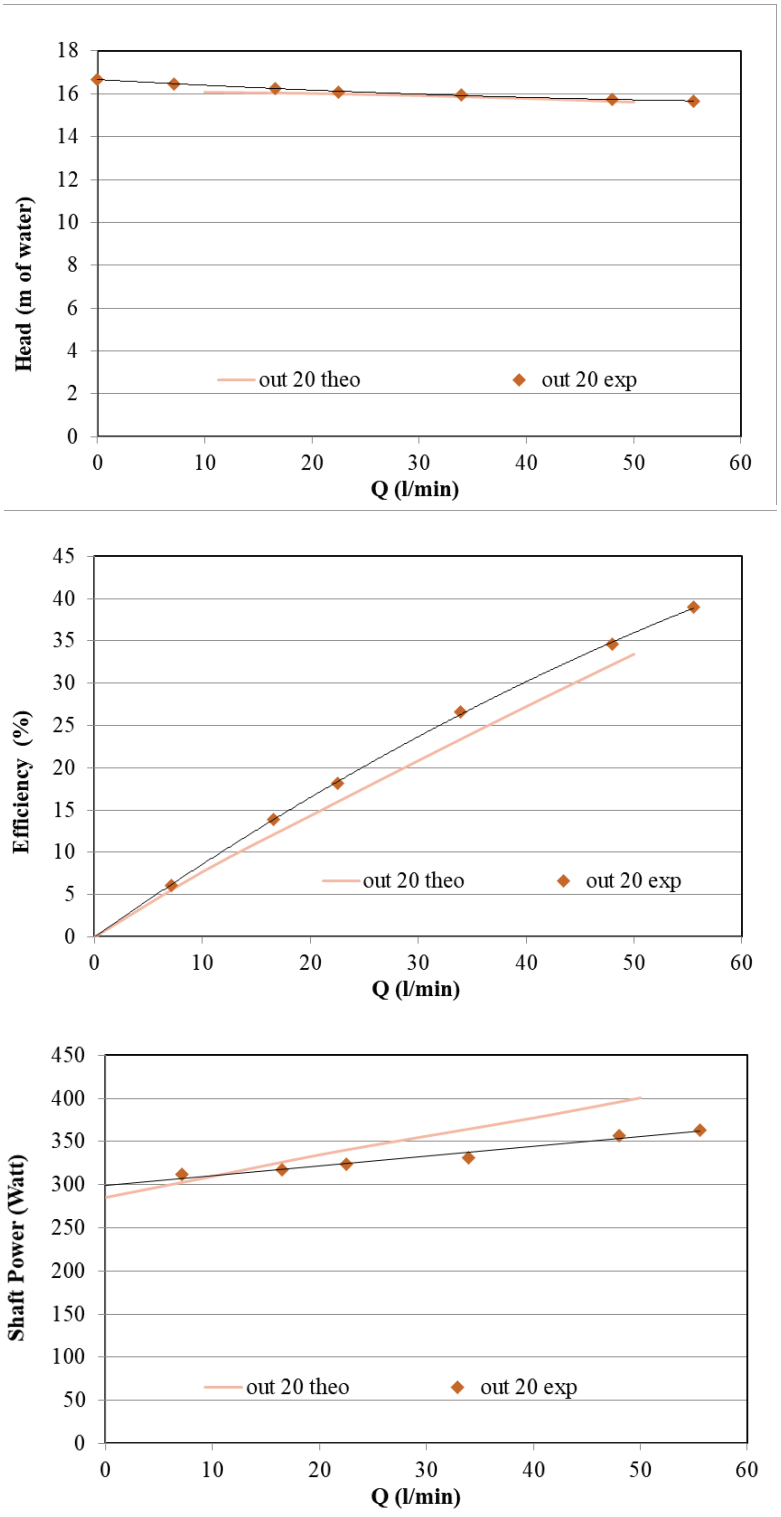

Fig. 5.2. Comparison between theoretical and experimental results of pump performance for blade outlet angle (β_2= 20°) effect with 0.02 unstable emulsion for a pump running at 1420 rpm (a) head-flow rate (b) efficiency-flow rate (c) shaft power-flow rate.

Table 5.1 The average theoretical results variations

Results	Minimum variation	Maximum variation	Average
Head	0	1.5%	0.76%
Efficiency	1.2%	6.3%	3.75%
Shaft Power	0%	9.2%	4.6%

5.4 RESULTS AND DISCUSSION

The theoretical approach in this chapter is used to understand the effect of the different pump rotational speed, different impeller's design parameters and different emulsion properties on the performance of the centrifugal pump, the data from the theoretical work is calculated and was used to extract several diagrams similar to the experimental work in the previous chapter to illustrate the effect of each impeller's design parameter separately as well as the emulsion's properties, the following is a description of the pump behavior noted from the theoretical calculations.

5.4.1 Effect of Pump rotational speed

Following the same monitoring method mentioned earlier in chapter 3, a comparison between the different impeller performance curves extracted from the theoretical calculations is used to form an idea about the effect of the rotational speed on the pump performance, using the impellers design parameters used in the experimental work, again the 7 impellers are divided into 3 sets. Each set has the same dimensions while changing one of the impeller's design parameters. Each set parameters are used in the calculations at three different pump rotational speed (1420, 1530 and 1650) rpm. The results from the calculations were plotted and analyzed for each set separately in order to have a clear idea on the effect of the pump rotational speed while pumping water alongside six different emulsions.

Examples of the curves expressing the pump head as function of the volume flow rate with rpm as a parameter are presented in figures 5.3 to 5.5. It can be clearly observed that the pump head decreases with increasing volume flow rate due to decreasing liquid pressure, in addition the pump head increases with increasing the pump rotational speed for the different blade numbers.

Figures 5.6 to 5.8 present some examples of the curves representing the shaft power as a function of the volume flow rate while also having the rpm as a parameter. It can be observed that the shaft power increase proportionally with the volume flow rate, also the shaft power increase by increasing the rpm.

Figures 5.9 to 5.11 presents three examples of the curves representing the pump efficiency as a function of the volume flow rate while also having the rpm as a parameter. It can be observed that the pump efficiency increase proportionally with the volume flow rate, it is also observed that the rotational speed of 1650 rpm showed the best pump efficiency.

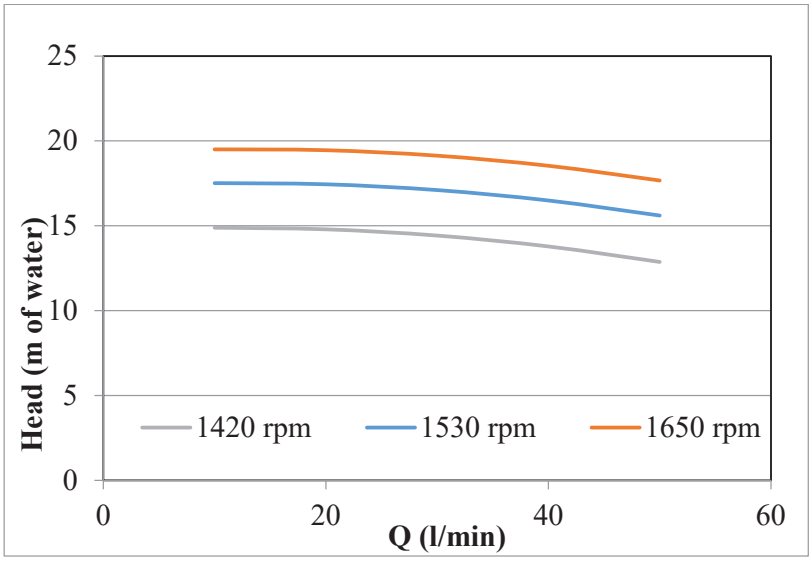

Fig.5.3 Pump rotational speed effect on head with 0.02 unstable emulsion for pump impeller (c) with 7 blades

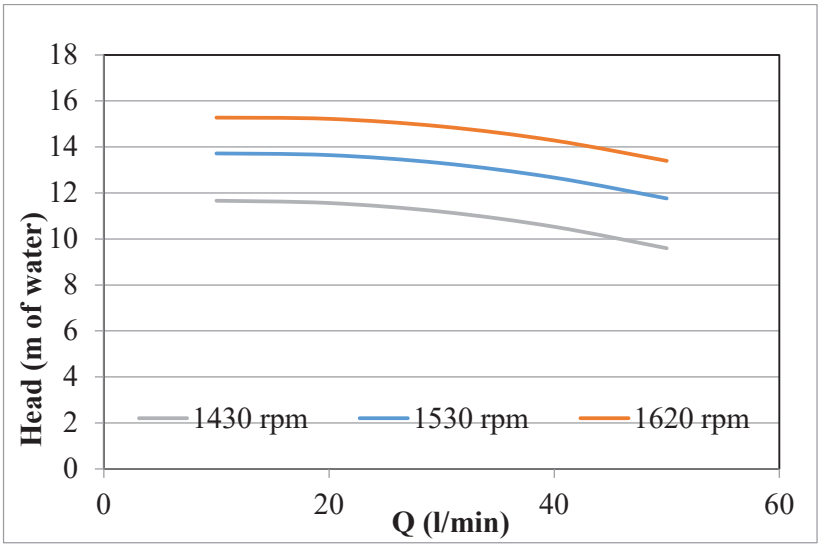

Fig.5.4 Pump rotational speed effect on head with 0.02 stable emulsion for pump impeller (a) with 6 blades.

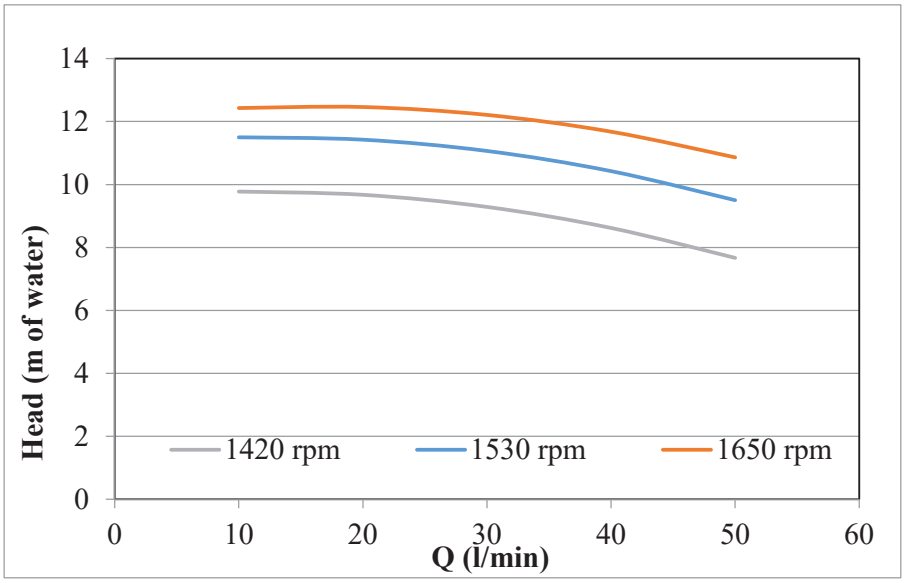

Fig.5.5 Pump rotational speed effect on head with water for pump impeller (b) with 5 blades.

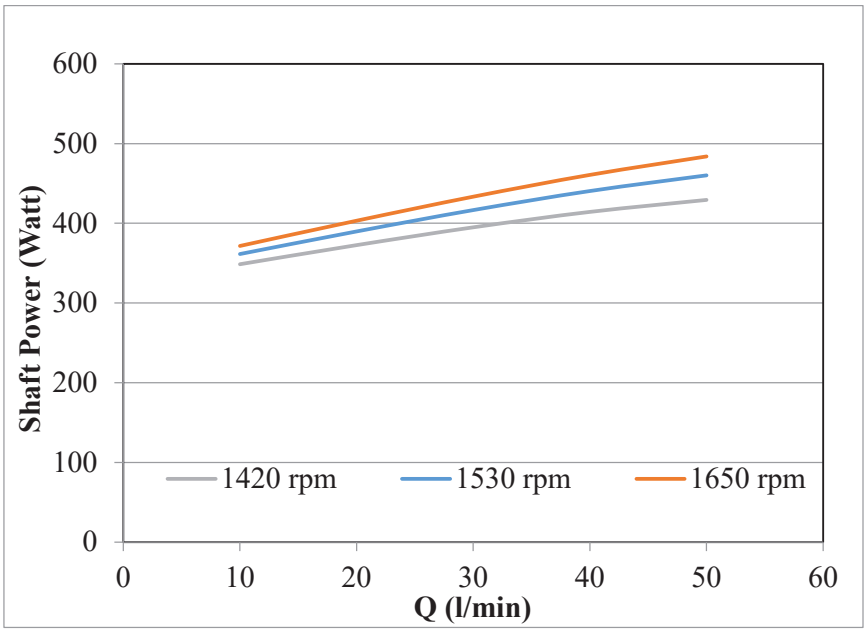

Fig.5.6 Pump rotational speed effect on shaft power with 0.02 unstable emulsion for pump impeller (c) with 7 blades

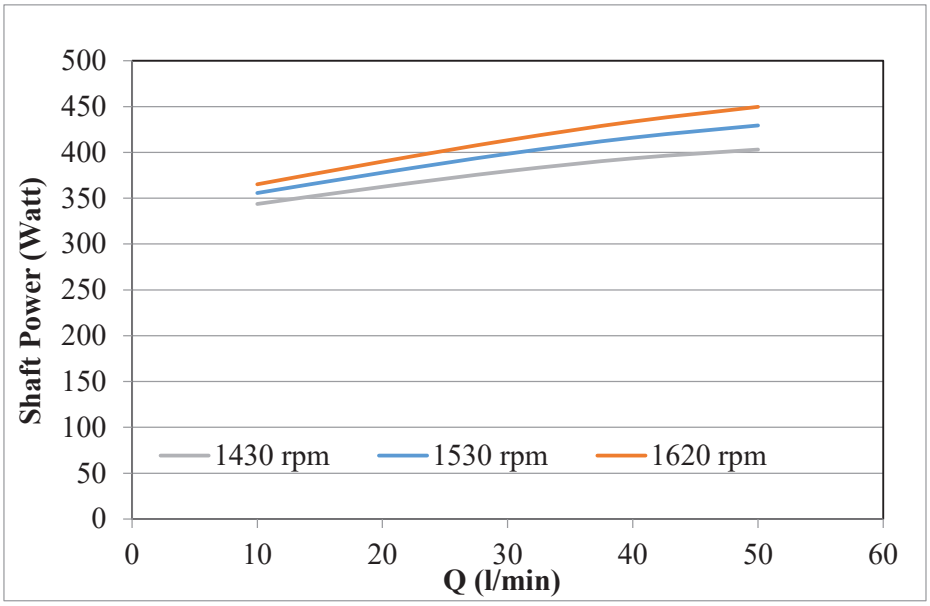

Fig.5.7 Pump rotational speed effect on shaft power with 0.02 stable emulsion for pump impeller (a) with 6 blades

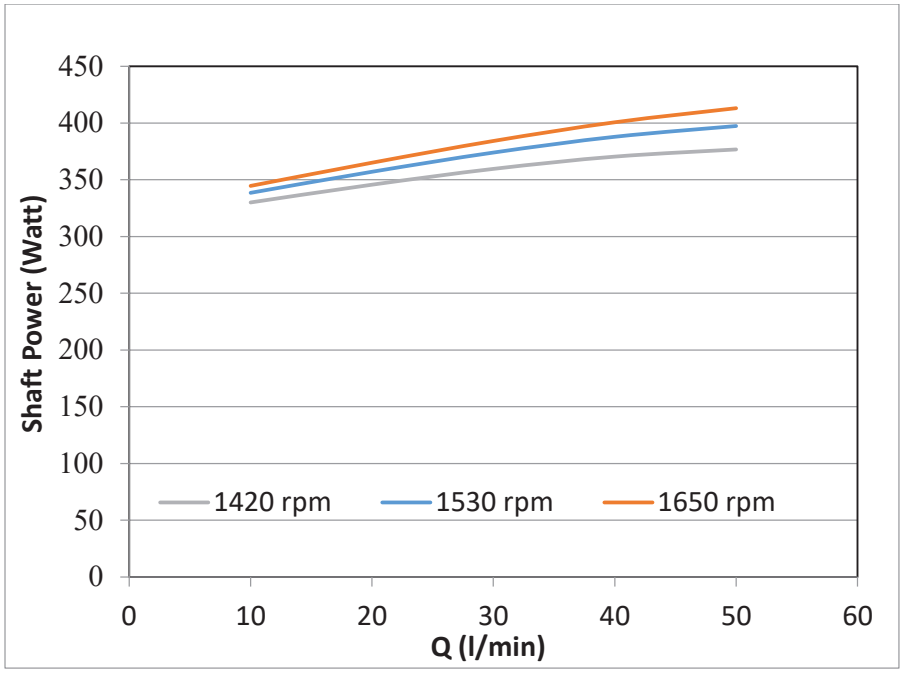

Fig.5.8 Pump rotational speed effect on shaft power with water for pump impeller (b) with 5 blades

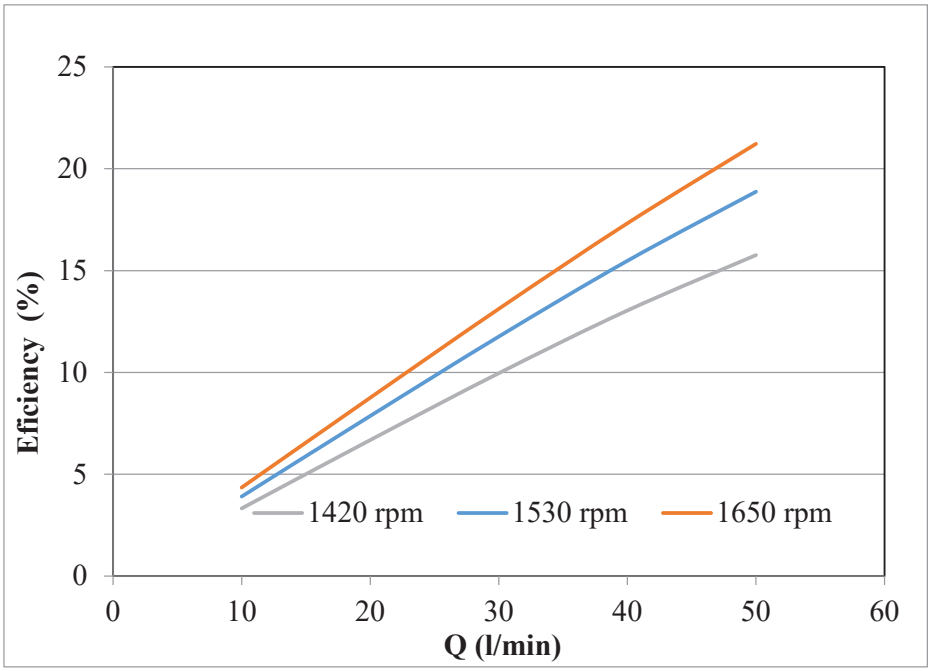

Fig.5.9 Pump rotational speed effect on pump efficiency with 0.02 unstable emulsion for pump impeller (c) with 7 blades

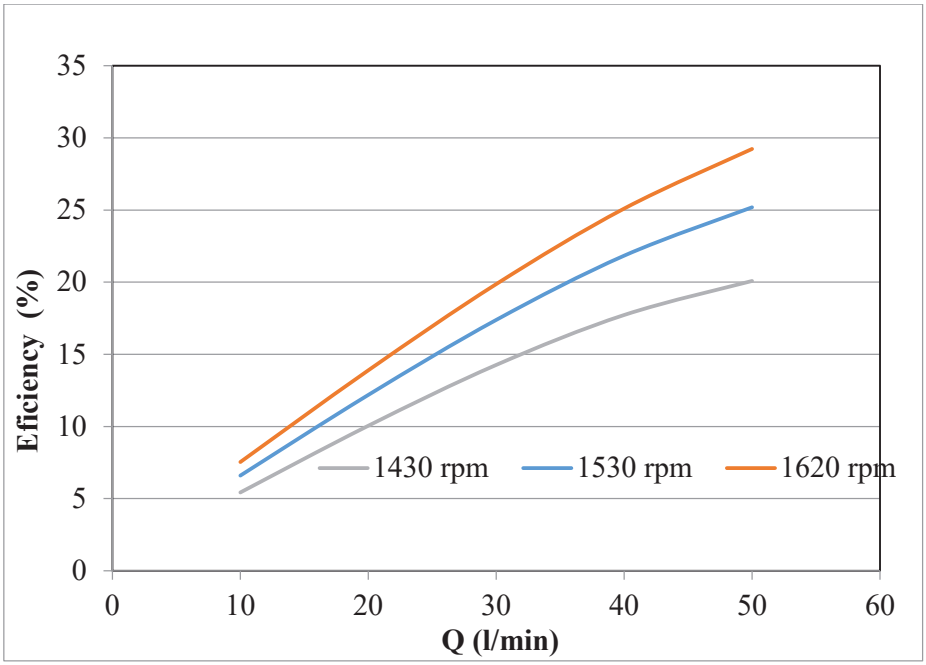

Fig.5.10 Pump rotational speed effect on pump efficiency with 0.02 stable emulsion for pump impeller (a) with 6 blades

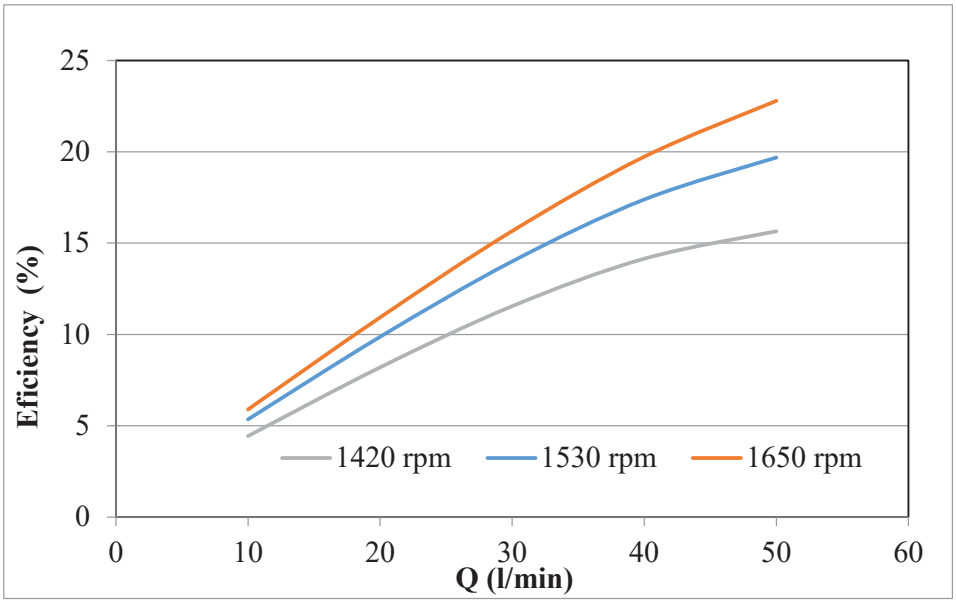

Fig.5.11 Pump rotational speed effect on pump efficiency with water for pump impeller (b) with 5 blades

The second impeller set is depicted in Figure 3.5. While the number of blades and characteristics of each impeller are the same, the blade inlet angle (β_1) varies. The inlet angles of the impellers (a), (d), and (e) are 10°, 20°, and 30°, respectively. In addition to pumping water alongside three stable and three unstable emulsions, each of the aforementioned impellers must also be evaluated at three distinct shaft rotational speeds (1420, 1530, and 1650 rpm).

Samples of the curves expressing the pump head as function of the volume flow rate with rpm as a parameter are presented in Figures 5.12 to 5.14. It can be clearly observed that the pump head decreases with increasing volume flow rate due to decreasing liquid pressure, in addition the pump head increases with increasing the pump rotational speed for the different blade inlet angels.

Figures 5.15 to 5.17 present some examples of the curves representing the shaft power as a function of the volume flow rate while also having the rpm as a parameter. It can be observed that the shaft power increase proportionally with the volume flow rate, also the shaft power increase by increasing the rpm.

Figures 5.18 to 5.20 presents three examples of the curves representing the pump efficiency as a function of the volume flow rate while also having the rpm as a parameter. It can be observed that the pump efficiency increase proportionally with the volume flow rate, it is also observed that the rotational speed of 1650 rpm showed the best pump efficiency.

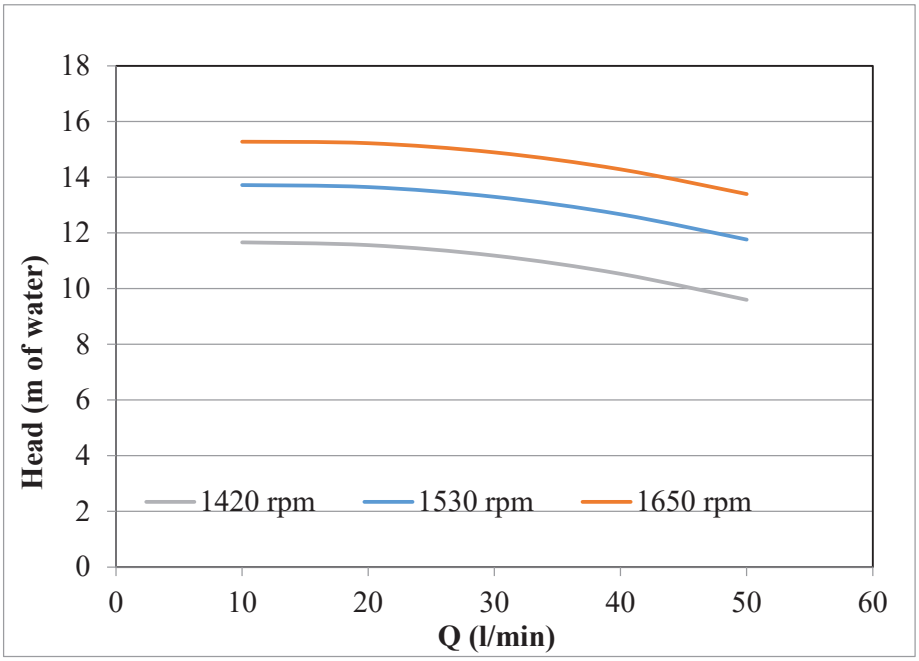

Fig.5.12 Pump rotational speed effect on head with 0.005 unstable emulsion for pump impeller (a) with inlet angle 10^{o}

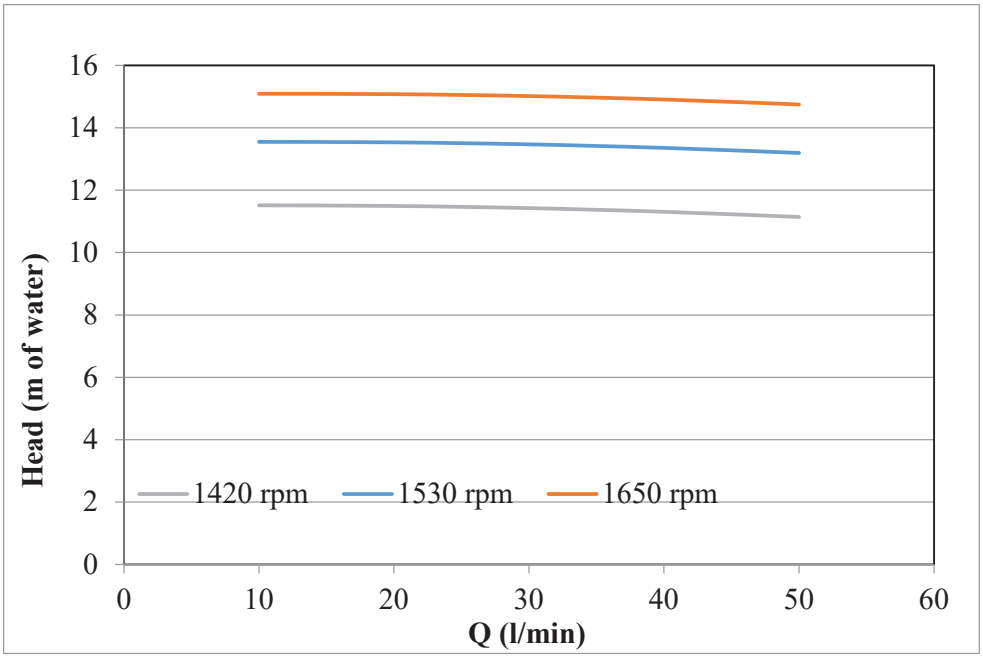

Fig.5.13 Pump rotational speed effect on head with 0.01 unstable emulsion for pump impeller (d) with inlet angle 20^{o}

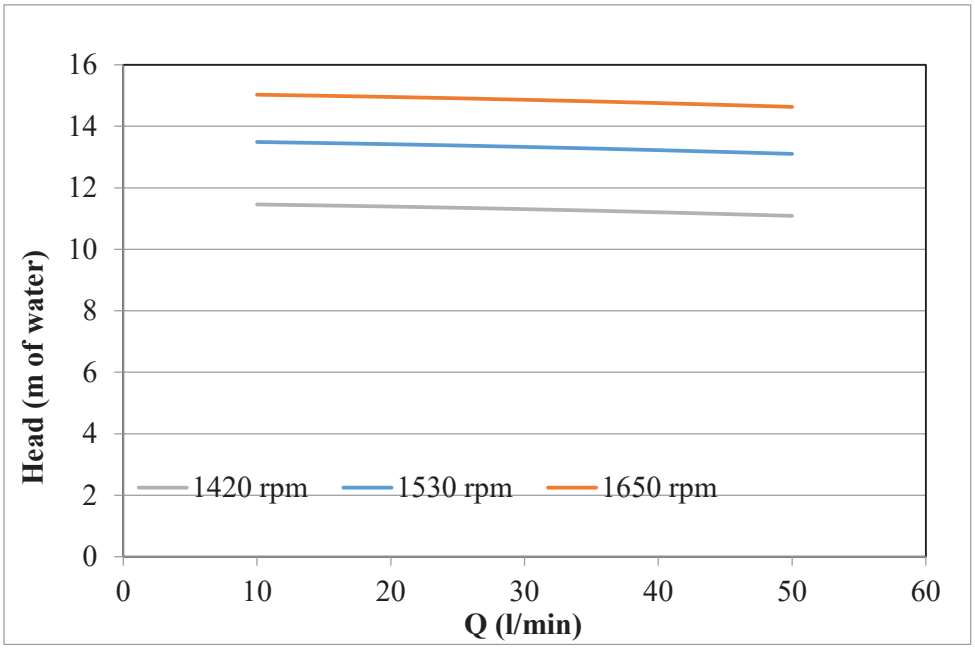

Fig.5.14 Pump rotational speed effect on head with water for pump impeller (e) with inlet angle 30°

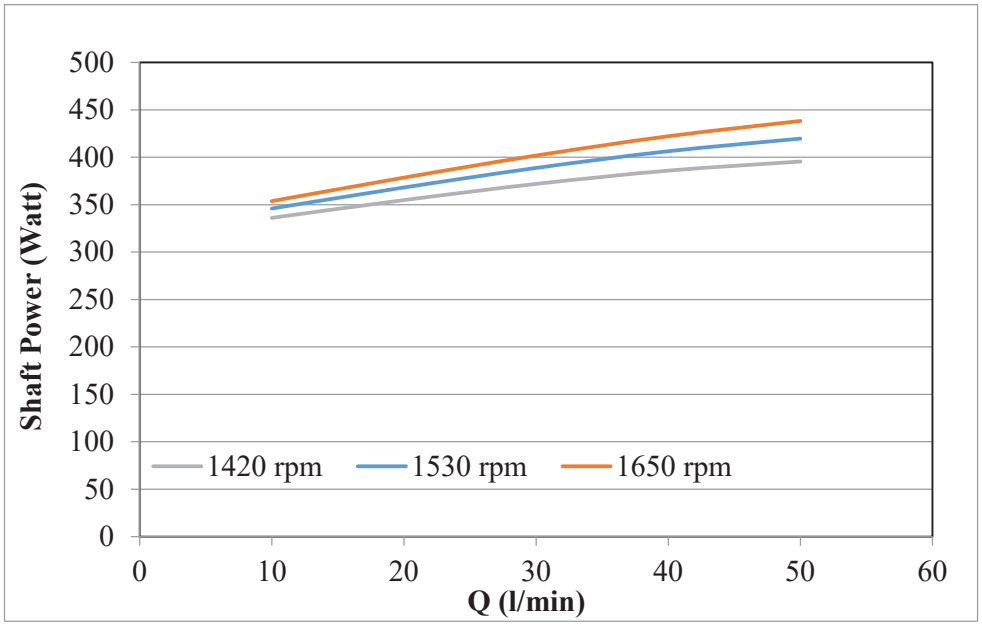

Fig.5.15 Pump rotational speed effect on shaft power with 0.005 unstable emulsion for pump impeller (a) with inlet angle 10°

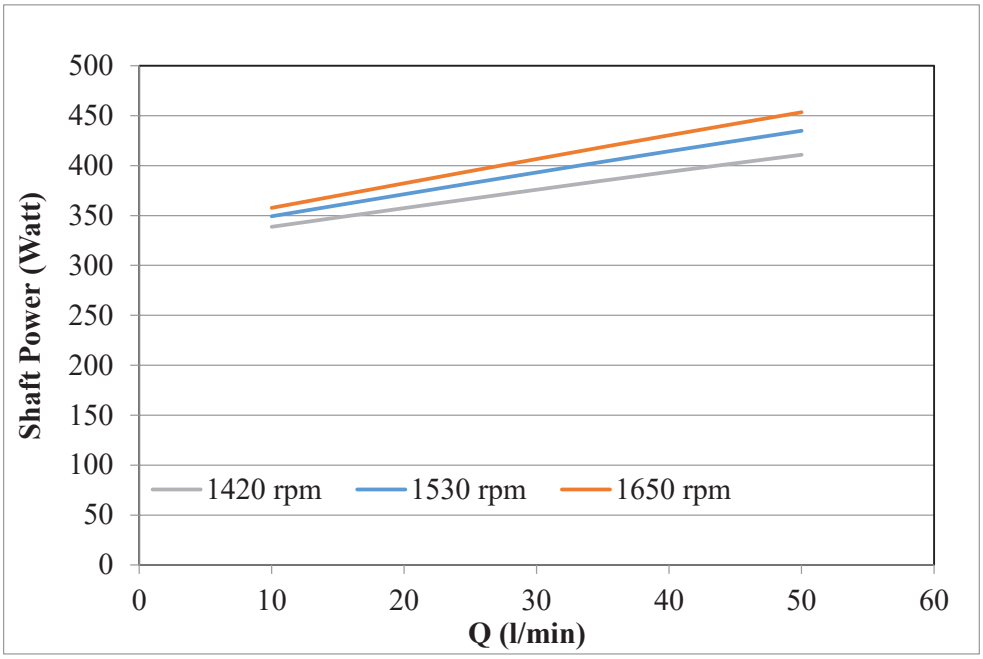

Fig.5.16 Pump rotational speed effect on shaft power with 0.01 unstable emulsion for pump impeller (d) with inlet angle 20°

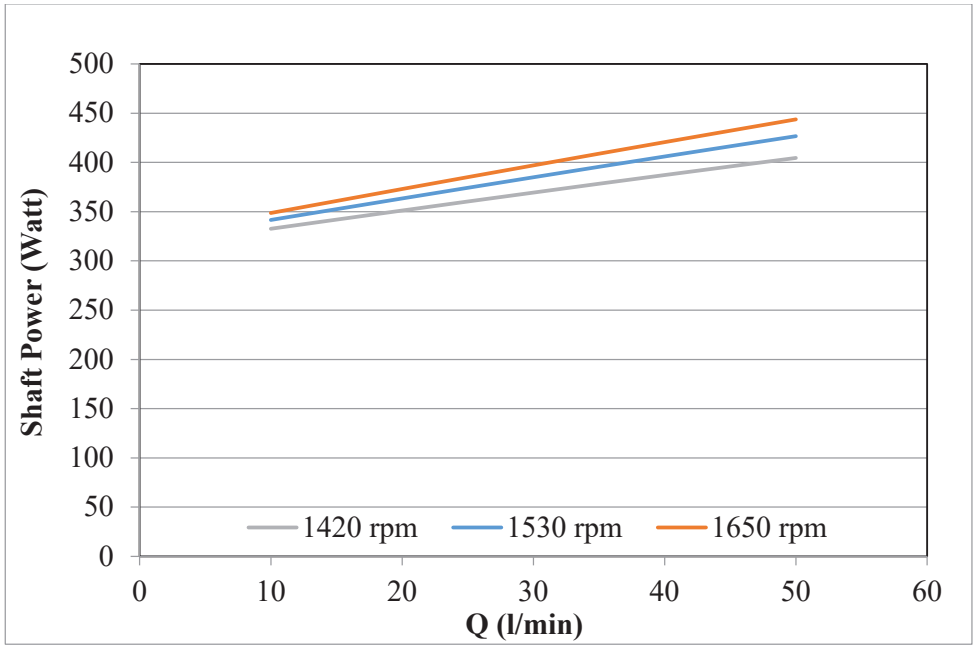

Fig.5.17 Pump rotational speed effect on shaft power with water for pump impeller (e) with inlet angle 30°

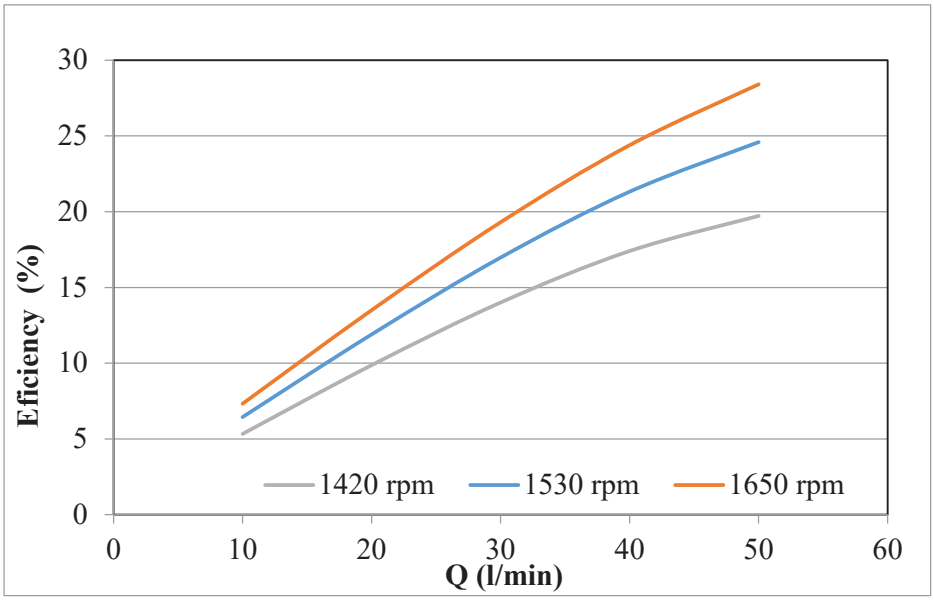

Fig.5.18 Pump rotational speed effect on pump efficiency with 0.005 unstable emulsion for pump impeller (a) with inlet angle 10º

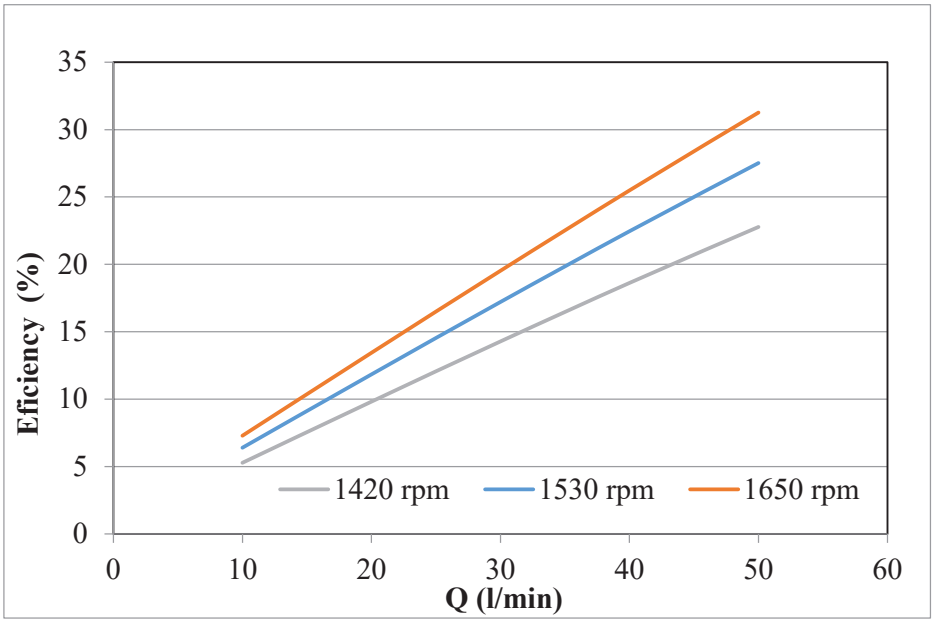

Fig. 5.19 Pump rotational speed effect on pump efficiency with 0.01 unstable emulsion for pump impeller (d) with inlet angle 20º

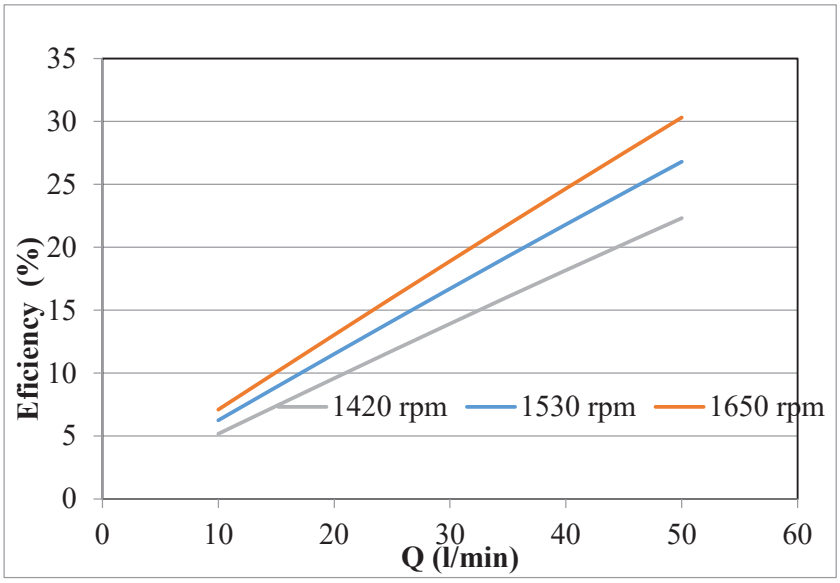

Fig.5.20 Pump rotational speed effect on pump efficiency with water for pump impeller (e) with inlet angle 30°

Figure 3.6 displays the third impeller set. With the same number of blades and same characteristics, each impeller has a distinct blade outlet angle (β_2). For example, impeller (a) has an outlet angle of 30°, impeller (f) has an outlet angle of 25°, and impeller (g) has an outlet angle of 20°. Each of the above impellers must be evaluated at three distinct shaft rotational speeds (1420, 1530, and 1650 rpm) while pumping water together with three stable and three unstable emulsions.

Illustrations of the curves expressing the pump head as function of the volume flow rate with rpm as a parameter are presented in figures 5.21 to 5.23. It can be clearly observed that the pump head decreases with increasing volume flow rate due to decreasing liquid pressure, in addition the pump head increases with increasing the pump rotational speed for the different blade outlet angels.

Figures 5.24 to 5.26 present some examples of the curves representing the shaft power as a function of the volume flow rate while also having the rpm as a parameter. It can be observed that the shaft power increase proportionally with the volume flow rate, also the shaft power increase by increasing the rpm.

Figures 5.27 to 5.29 presents three examples of the curves representing the pump efficiency as a function of the volume flow rate while also having the rpm as a parameter. It can be observed that the pump efficiency increase proportionally with the volume flow rate, it is also observed that the rotational speed of 1650 rpm showed the best pump efficiency.

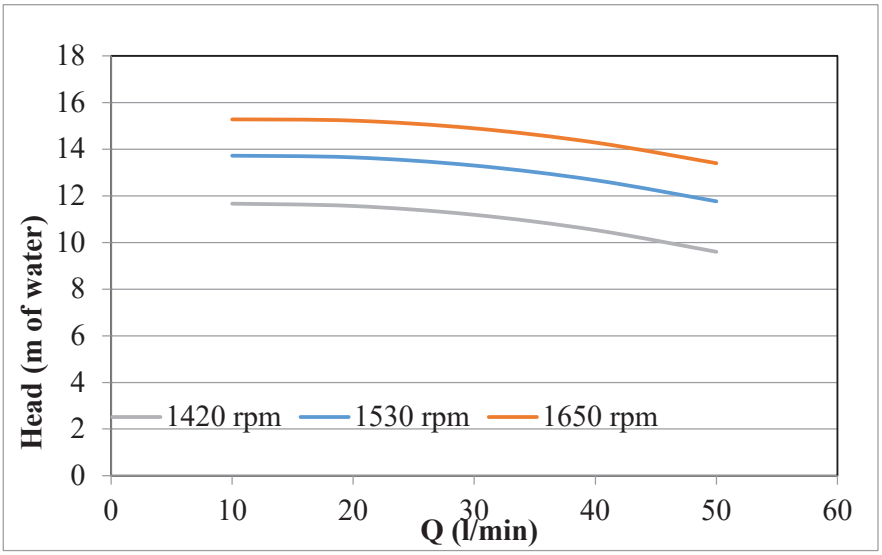

Fig.5.21 Pump rotational speed effect on head with water for pump impeller (a) with outlet angle 30°

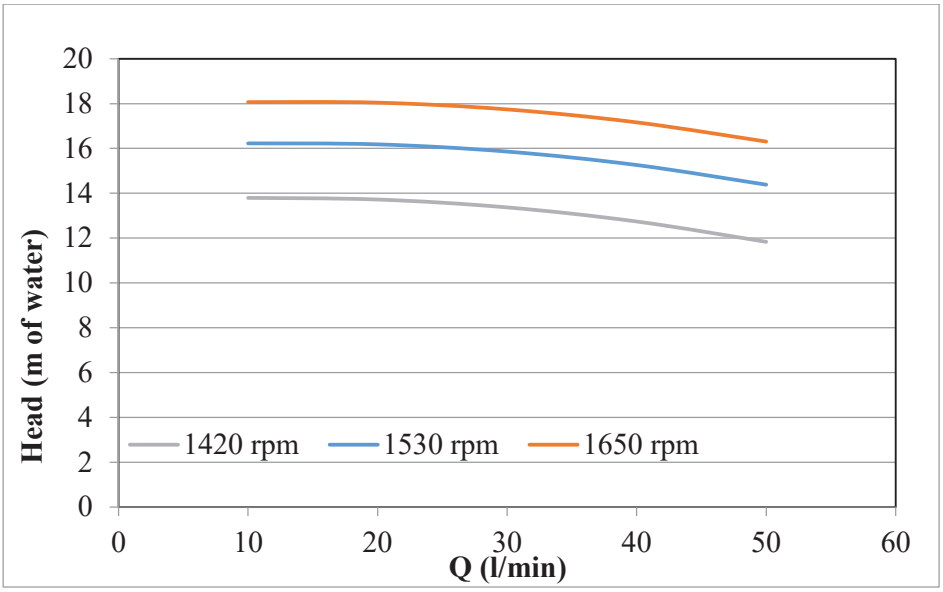

Fig.5.22 Pump rotational speed effect on head with 0.01 stable emulsion for pump impeller (f) with outlet angle 25°

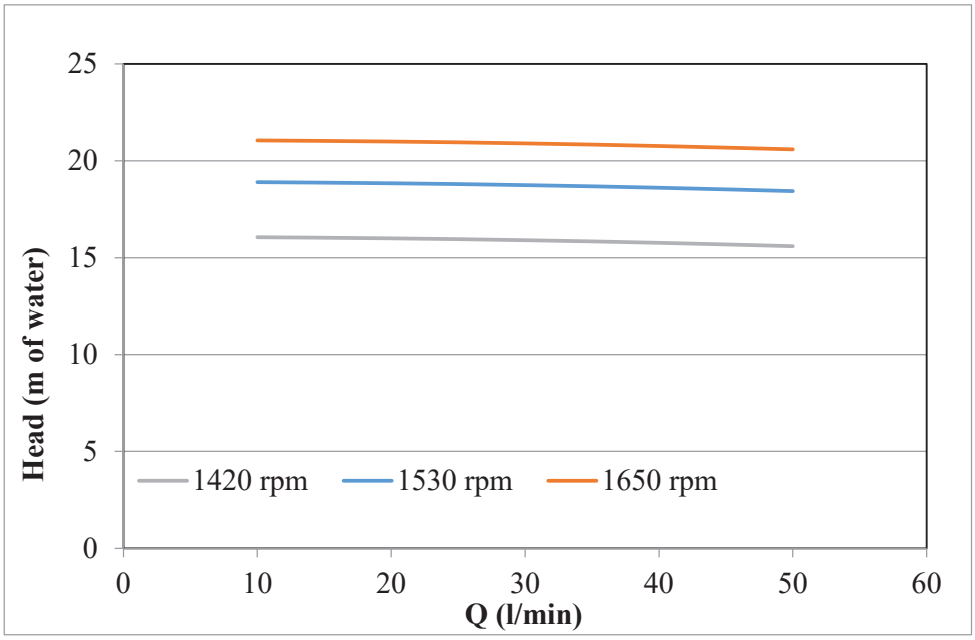

Fig.5.23 Pump rotational speed effect on head with 0.02 unstable emulsion for pump impeller (g) with outlet angle 20°

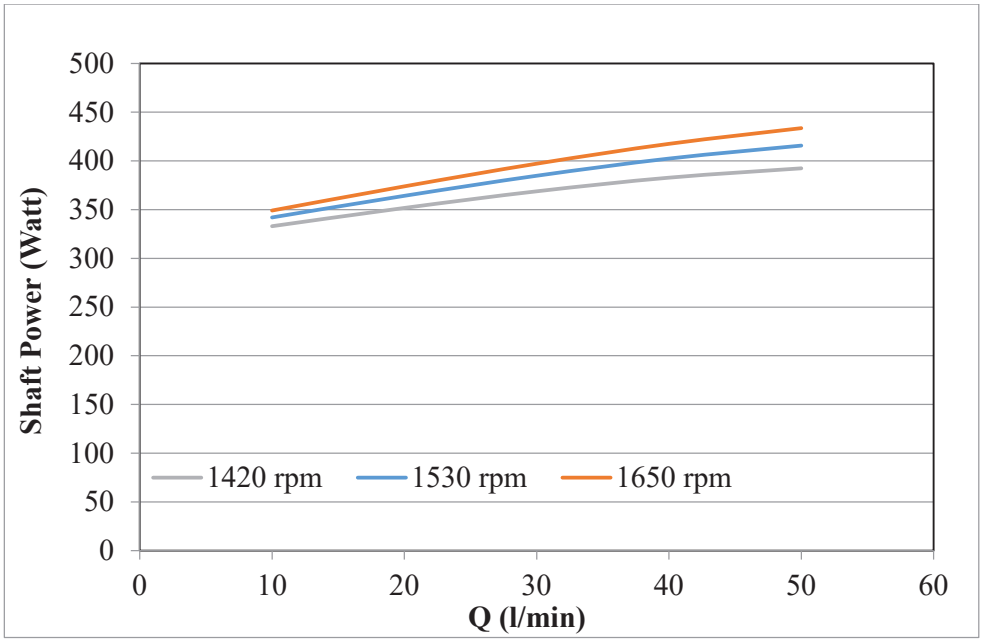

Fig.5.24 Pump rotational speed effect on shaft power with water for pump impeller (a) with outlet angle 30°

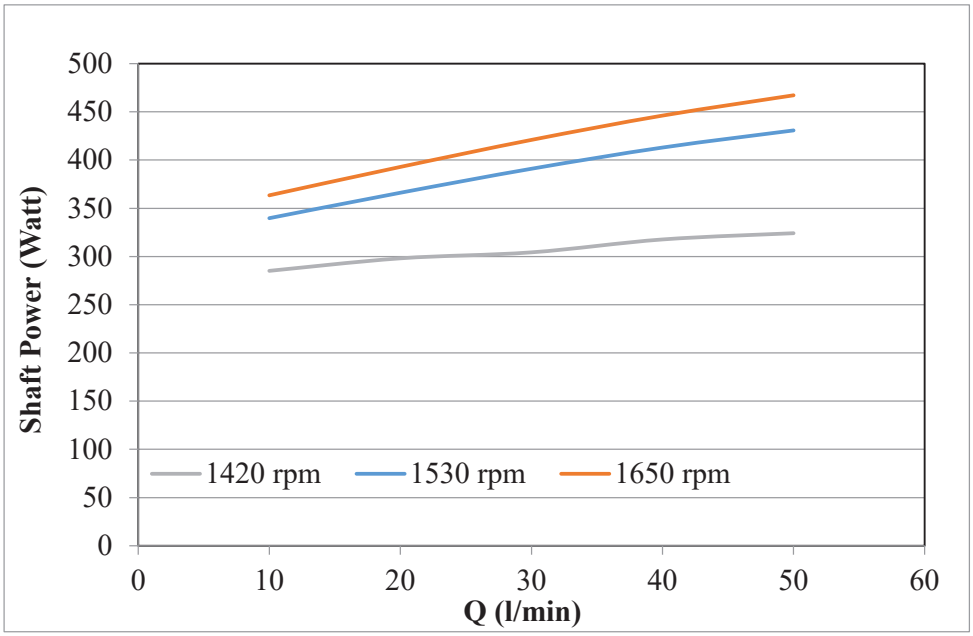

Fig.5.25 Pump rotational speed effect on shaft power with 0.01stable emulsion for pump impeller (f) with outlet angle 25°

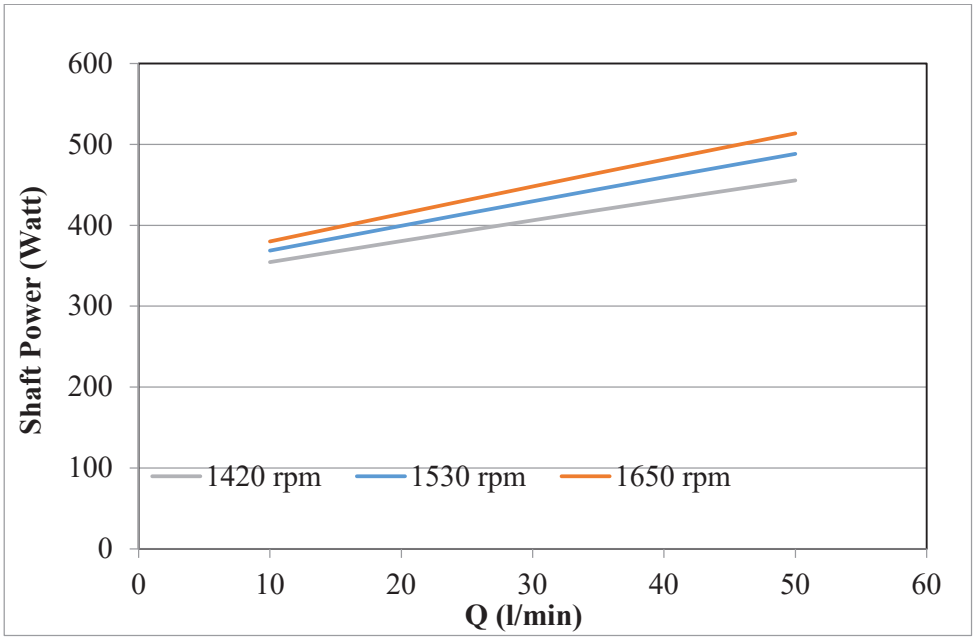

Fig.5.26 Pump rotational speed effect on shaft power with 0.02 unstable emulsion for pump impeller (g) with outlet angle 20°

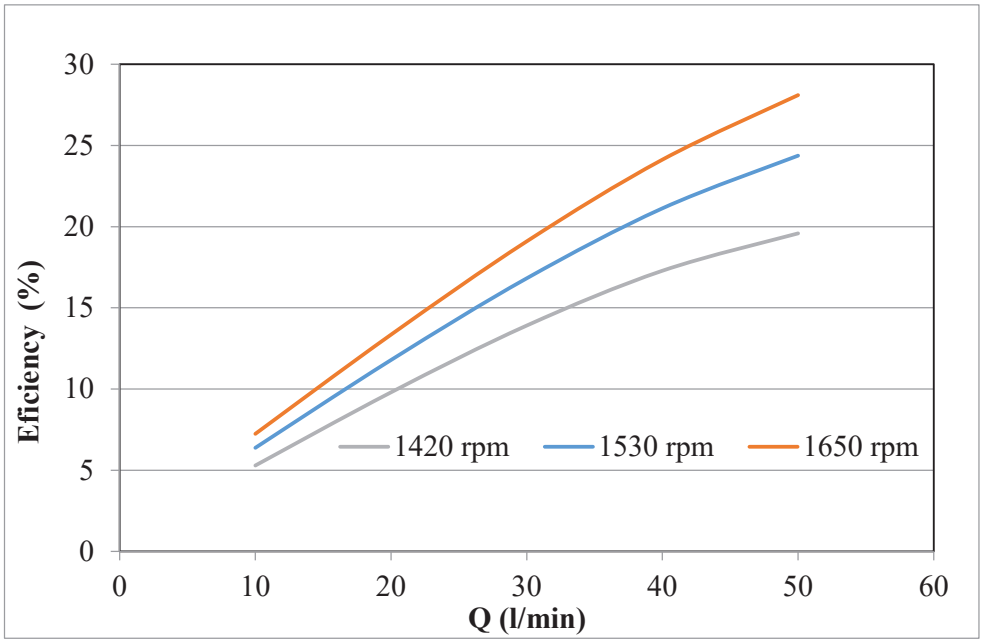

Fig.5.27 Pump rotational speed effect on pump efficiency with water for pump impeller (a) with outlet angle 30º

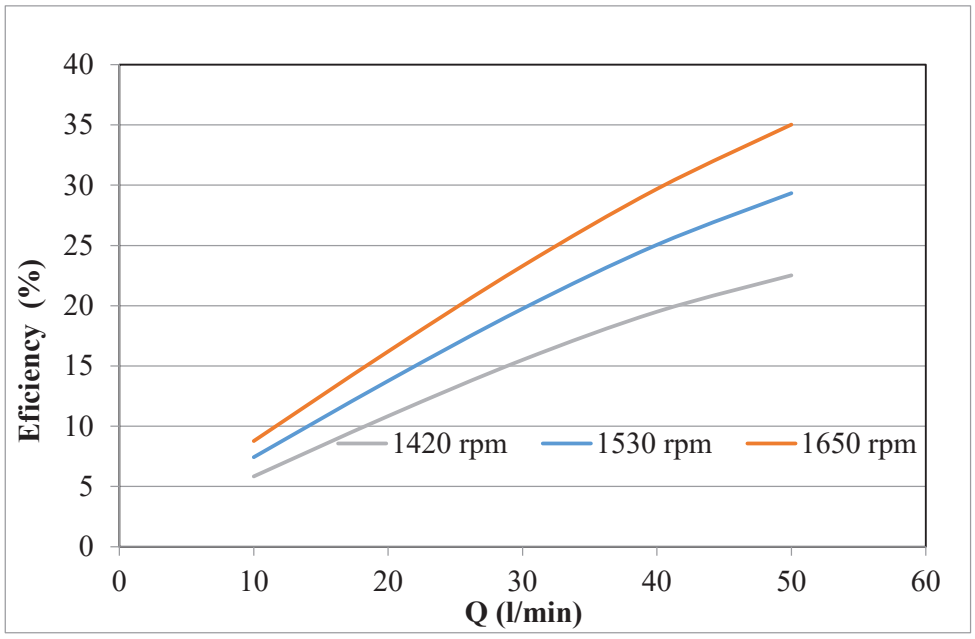

Fig.5.28 Pump rotational speed effect on pump efficiency with 0.01 stable emulsion for pump impeller (f) with outlet angle 25º

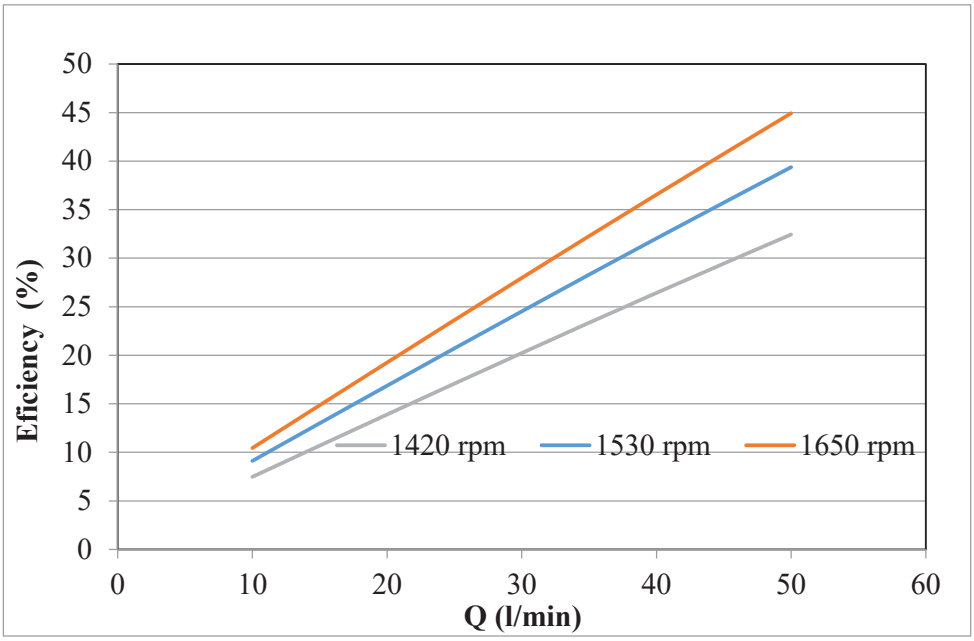

Fig.5.29 Pump rotational speed effect on pump efficiency with 0.02 unstable emulsion for pump impeller (g) with outlet angle 20°

5.4.2 Effect of Impellers blade number

In order to have a better understanding of the effect of the impellers blade number (z) on the performance of the centrifugal pump we have three different impellers, each has the same parameters except for the number of blades. Impeller (a) has 6 blades, impeller (b) has 5 blades and impeller (c) has 7 blades.

The parameters of the mentioned impellers shown in Figure 3.4 will be used in the calculations to predict the pump performance while pumping water alongside three stable emulsions and three unstable emulsions. They also are to be used at three different shaft rotational speeds (1420,1530,1650) rpm.

An example of the curves expressing the pump head as function of the volume flow rate with blade number as a parameter are presented in figure 5.30. It can be clearly observed that the pump head decreases with increasing volume flow rate due to decreasing liquid pressure, in addition the pump head increases with increasing the blade number.

Figure 5.31 presents an example of the curves representing the shaft power as a function of the volume flow rate while also having the blade number as a parameter. It can be observed that the shaft power increase proportionally with the volume flow rate.

Figure 5.32 presents an example of the curves representing the pump efficiency as a function of the volume flow rate while also having the blade number as a parameter. It can be observed that the pump efficiency increase proportionally with the volume flow rate, it is also observed that the impeller with (6) blades showed the best pump efficiency which matches the original factory optimum design.

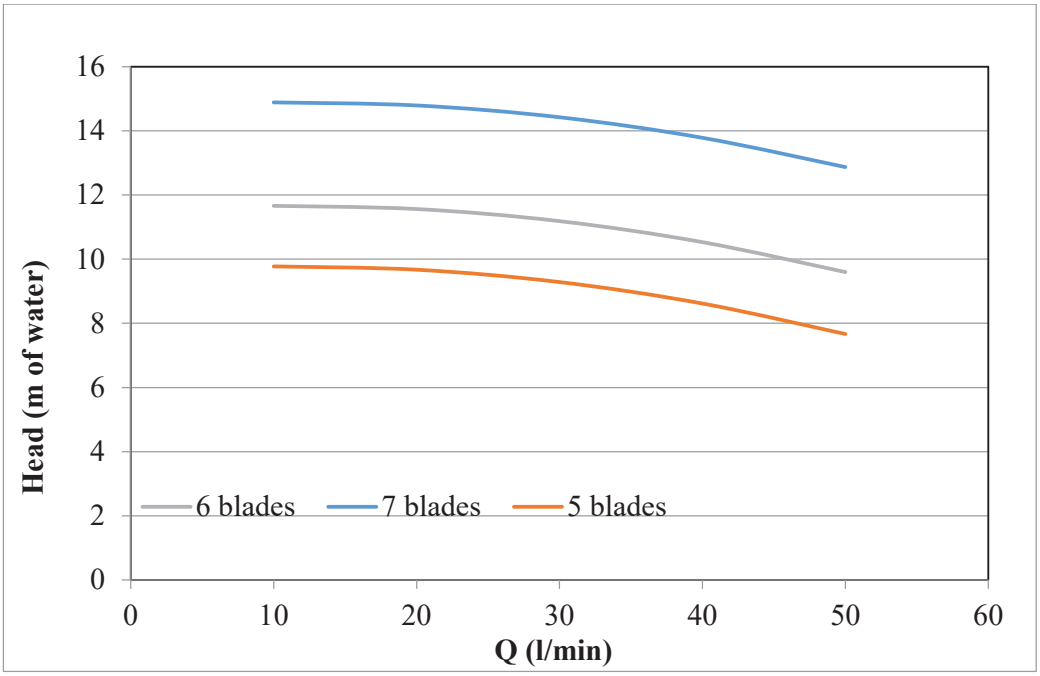

Fig.5.30 Number of blades effect on head for 0.01 stable emulsion with pump running at 1420 rpm

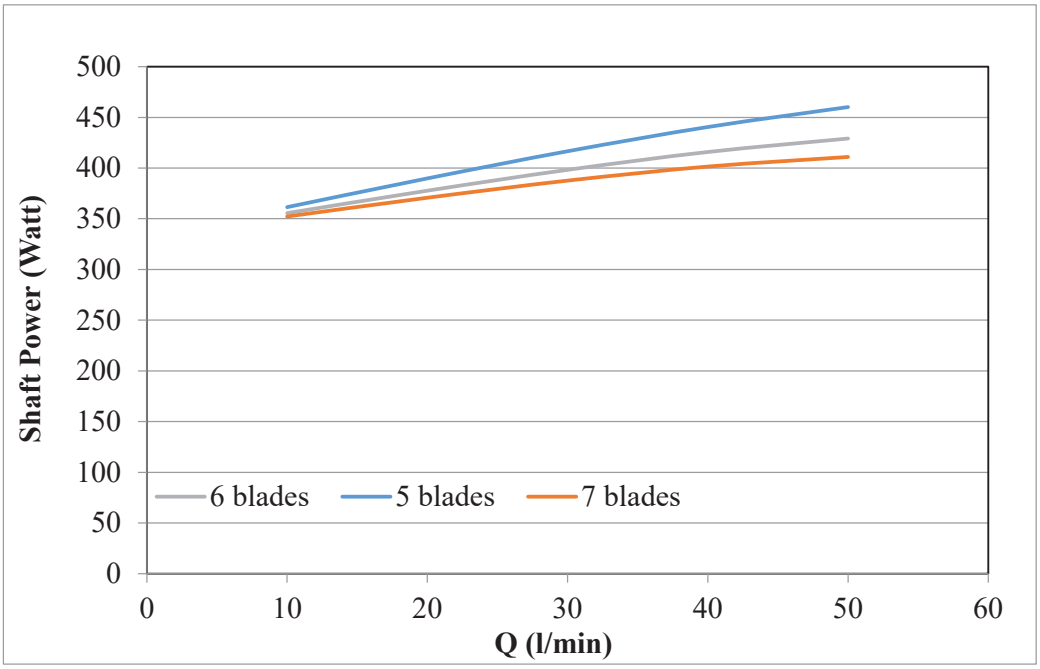

Fig.5.31 Number of blades effect on shaft power for 0.02 unstable emulsion with pump running at 1530 rpm

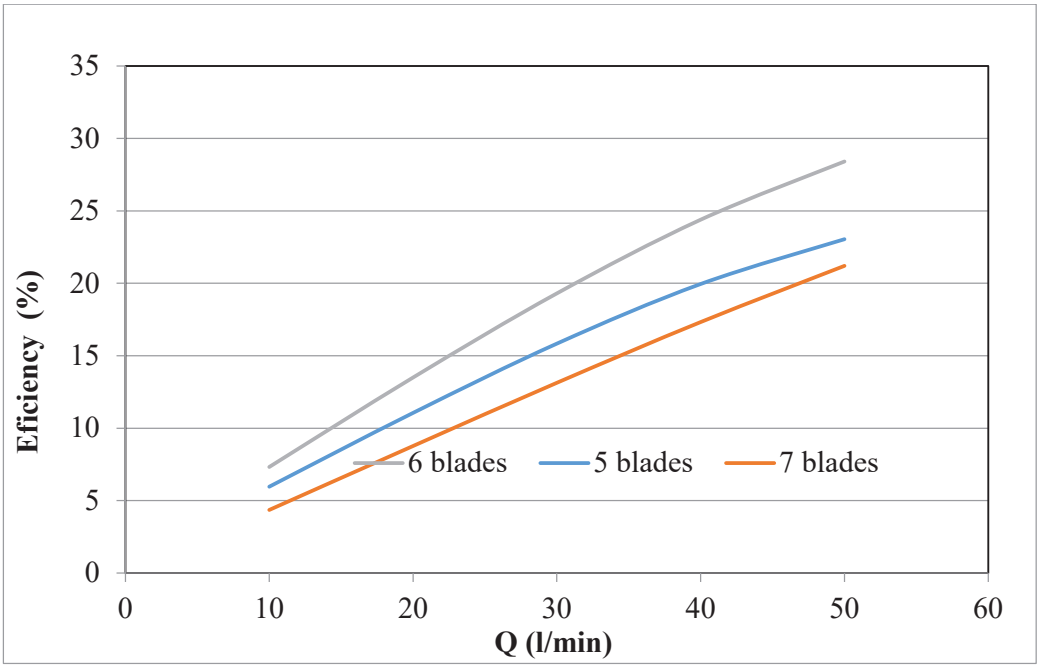

Fig.5.32 Number of blades effect on pump efficiency for 0.005 unstable emulsion with pump running at 1650 rpm

5.4.3 Effect of Impeller blade inlet angle

For the purpose of testing the effect of the impellers blade inlet angle, the same method is to be applied as well, for three different impellers, each has the same parameters with the same number of blades but with different blade inlet angle (β_1). Impeller (a) has inlet angle of (10^o), impeller (d) has inlet angle of (20^o) and impeller (e) has inlet angle of (30^o). Figure 3.5 shows the test impellers, each of the mentioned impellers is to be tested for performance while pumping water alongside three stable emulsions and three unstable emulsions, they also are to be tested at three different shaft rotational speed (1420,1530,1650) rpm.

An example of the curves expressing the pump head as function of the volume flow rate with inlet angle as a parameter are presented in figure 5.33. It can be clearly observed that the pump head decreases with increasing volume flow rate due to decreasing liquid pressure similar to the observation in the impellers with different blade number. In addition, the pump head tends to show higher values with the impeller of inlet angle ($\beta_1 = 20^o$).

Figure 5.34 presents an example of the curves representing the shaft power as a function of the volume flow rate while also having the blade inlet angle as a parameter. It can be observed that the shaft power increase proportionally with the volume flow rate, also the shaft power decreases by increasing the blade inlet angle.

Fig 5.35 Presents an example of the curves representing the pump efficiency as a function of the volume flow rate while having the blade inlet angle as a parameter. It can be observed that the pump efficiency increase proportionally with the volume flow rate, and it is also observed that the impeller with inlet angle ($\beta_1 = 10^o$) showed the best pump efficiency which matches the original factory optimum design as well.

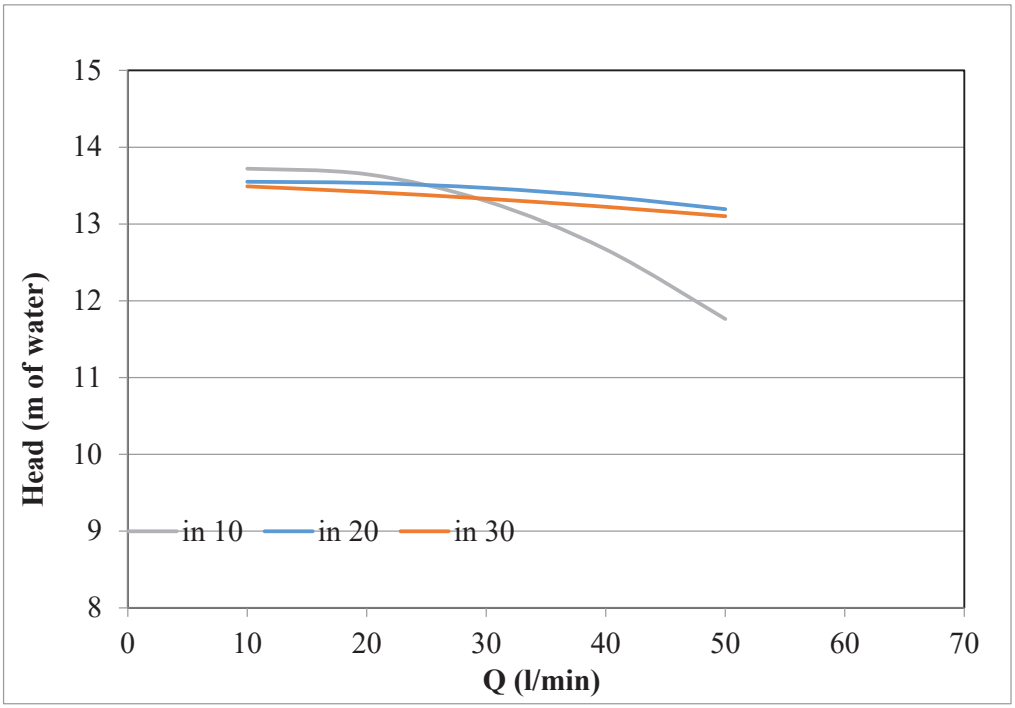

Fig.5.33 Blade inlet angle effect on head for 0.02 unstable emulsion with pump running at 1530 rpm

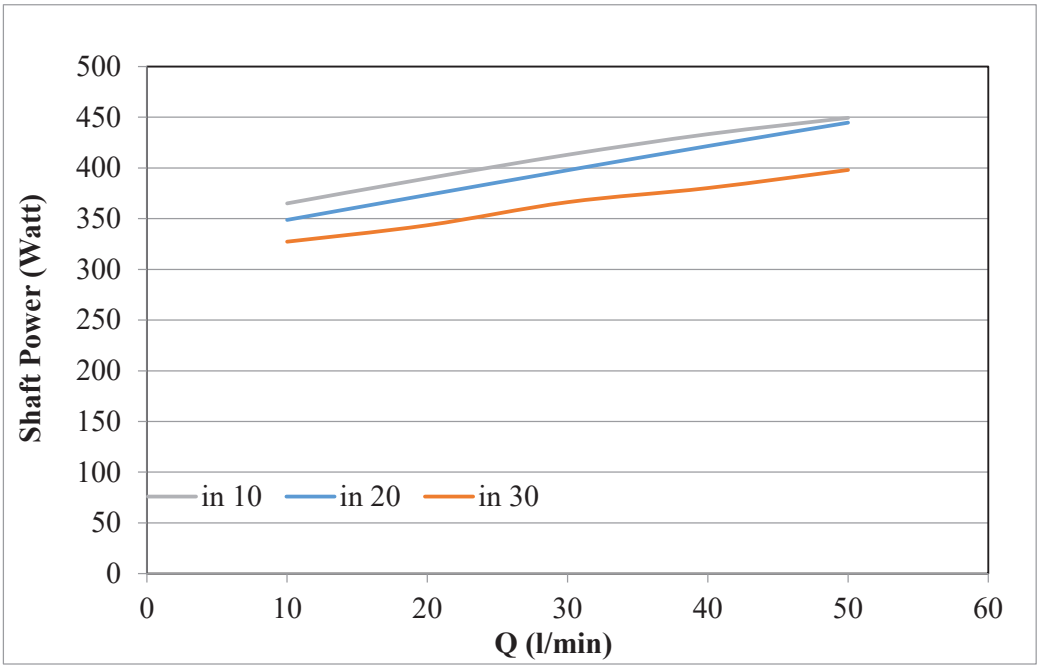

Fig.5.34 Blade inlet angle effect on shaft power for 0.005 stable emulsion with pump running at 1650 rpm

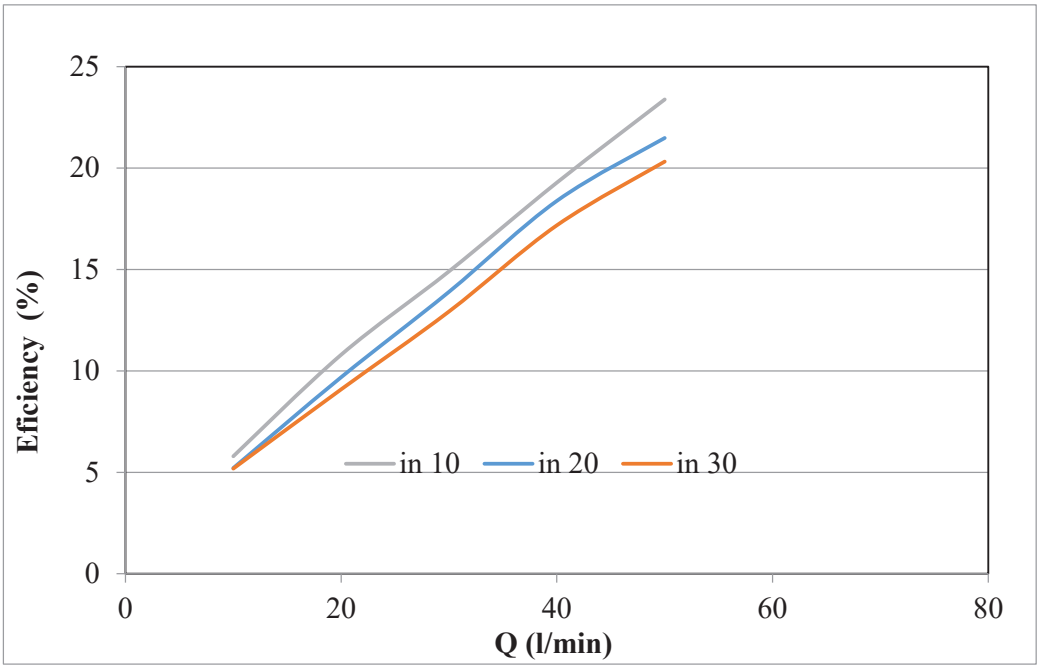

Fig.5.35 Blade inlet angle effect pump efficiency for water with pump running at 1420 rpm

5.4.4 Effect of Impeller blade outlet angle

For the purpose of testing the effect of the impellers blade outlet angle, the same method is to be applied as well with three different impellers, each has the same parameters with the same number of blades but with different blade outlet angle (β_2) impeller (a) has outlet angle of (30°), impeller (f) has outlet angle of (25°) and impeller (g) has outlet angle of (20°). Figure 3.6 shows the test impellers, each of the mentioned impellers is to be tested for performance while pumping water alongside three stable emulsions and three unstable emulsions. They are also to be tested at three different shaft rotational speed (1420,1530,1650) rpm.

An example of the curves expressing the pump head as function of the volume flow rate with inlet angle as a parameter are presented in figure 5.36. It can be clearly observed that the pump head decreases with increasing volume flow rate due to decreasing liquid pressure similar to the observation. In the impellers with different blade number. In addition, the pump head tends to show higher values with the impeller of outlet angle (β_2= 20°)

Figure 5.37 presents an example of the curves representing the shaft power as a function of the volume flow rate while also having the blade inlet angle as a parameter. It can be observed that the shaft power increases proportionally with the volume flow rate, and also the shaft power decrease by decreasing the blade outlet angle.

Figure 5.38 presents an example of the curves representing the pump efficiency as a function of the volume flow rate while having the blade inlet angle as a parameter. It can be observed that the pump efficiency increase proportionally with the volume flow rate, it is also observed that the impeller with outlet angle (β_2= 30°) showed the best pump efficiency which matches the original manufacturer's design as well.

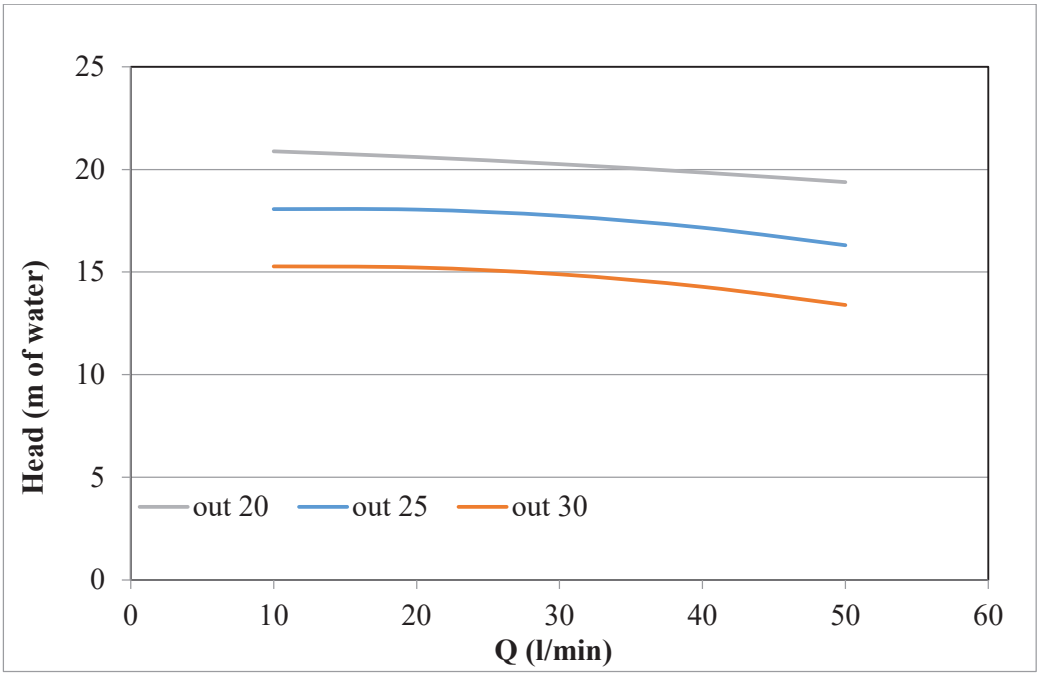

Fig.5.36 Blade outlet angle effect on head for 0.01 stable emulsion with pump running at 1650 rpm

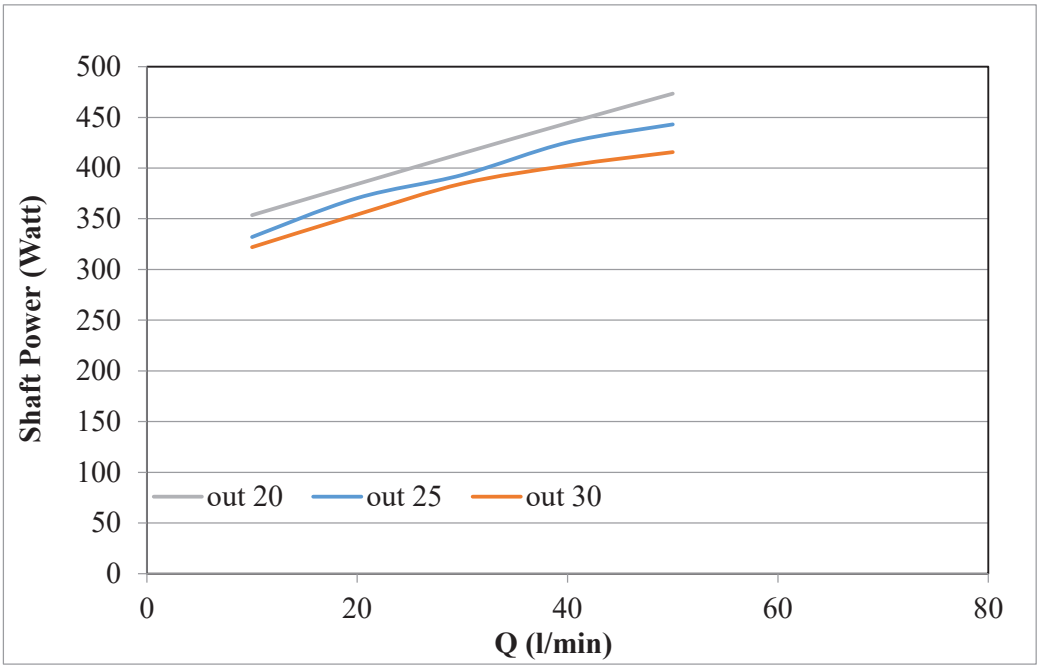

Fig.5.37 Blade outlet angle effect on shaft power for water with pump running at 1530 rpm

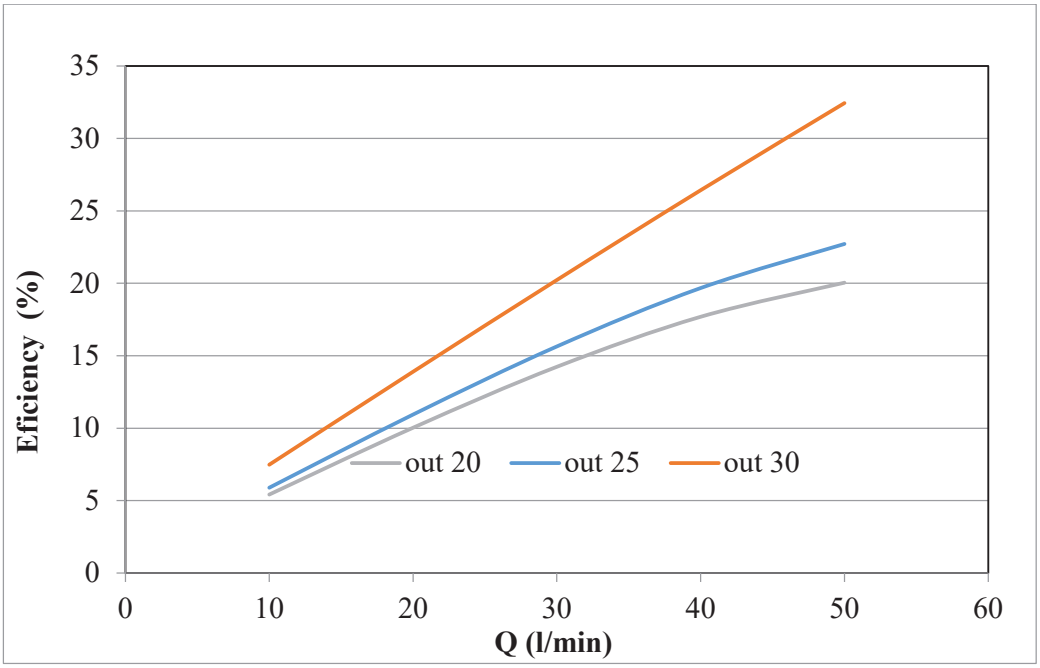

Fig.5.38 Blade outlet angle effect on pump efficiency for 0.02 unstable emulsion with pump running at 1420 rpm

5.4.5 Effect or emulsion holdup

For the purpose of understanding the effect of the emulsion holdup, water will be used as working fluid alongside 6 different (oil in water) emulsions. The emulsions are divided into two groups (stable and unstable) where each group consists of 3 emulsions with emulsion holdup Φ of (0.005, 0.01 and 0.02)

An example of the effect of the emulsion holdup on the pump head is shown on figure 5.39. It can be noted that increasing the emulsion holdup increases the pump head.

The effect of the emulsion holdup on the pump efficiency is shown in the example on figure 5.40. It shows that the pump efficiency increases with increasing the emulsion holdup. With emulsions with (Φ = 0.02) the best pump efficiency is shown in most of the cases.

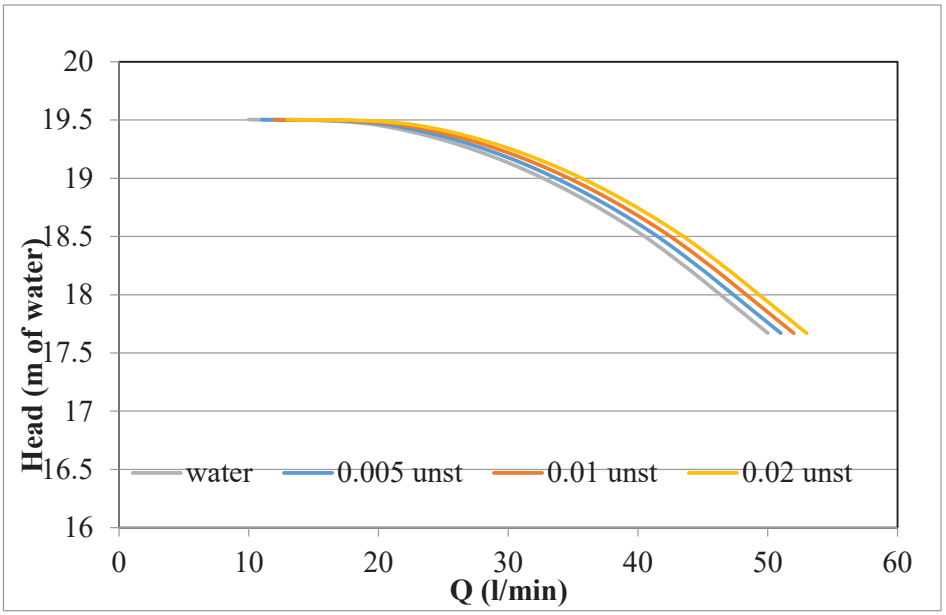

Fig.5.39 Emulsion holdup effect on head for impeller (c) with pump running at 1650 rpm (unstable emulsions)

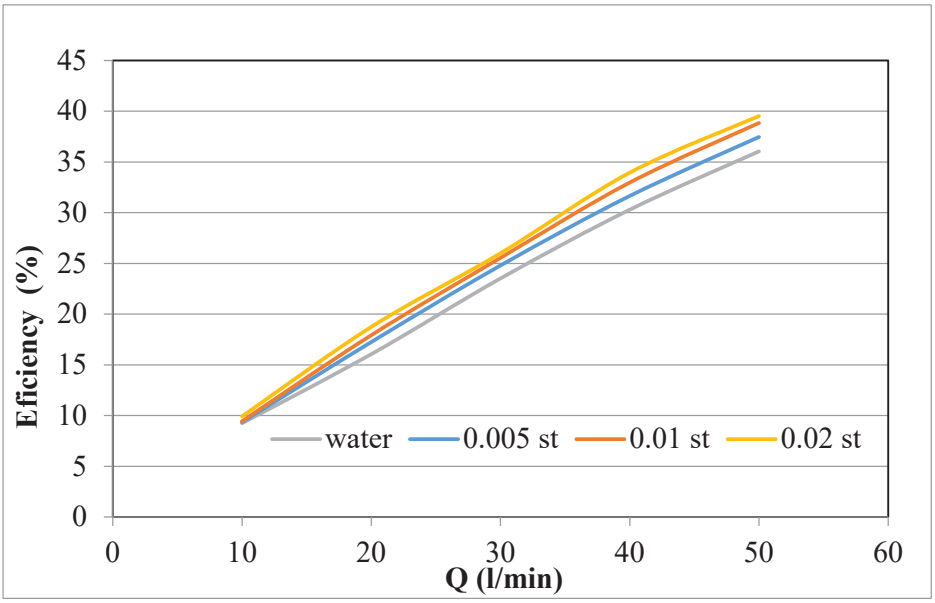

Fig.5.40 Emulsion holdup effect on pump efficiency impeller (c) with pump running at 1650 rpm (stable emulsions)

5.4.6 Effect of emulsion stability

The working fluids for the current study is to be the stable emulsions with holdup (0.005, 0.01 and 0.02) and the unstable emulsions are with holdup (0.005, 0.01 and 0.02). The emulsions performances were monitored throughout all the previous trials for parametric changes and at different rpms.The following paragraphs discus some samples of the emulsion stability effect on the pump performance.

Figures 5.41 to 5.43 show the emulsion stability effect on the pump head for some examples at different impeller design parameters, it is clear that the stable emulsions showed higher head values at different calculations.

Figures 5.44 to 5.46 show the emulsion stability effect on the pump shaft power for some examples at different impeller design parameters. It is to be noted that the stable emulsions consumed lower shaft power values at different calculations.

Figures 5.47 to 5.49 show the emulsion stability effect on the pump efficiency for some examples at different impeller design parameters. It is to be noted that the stable emulsions were related to the better pump efficiency.

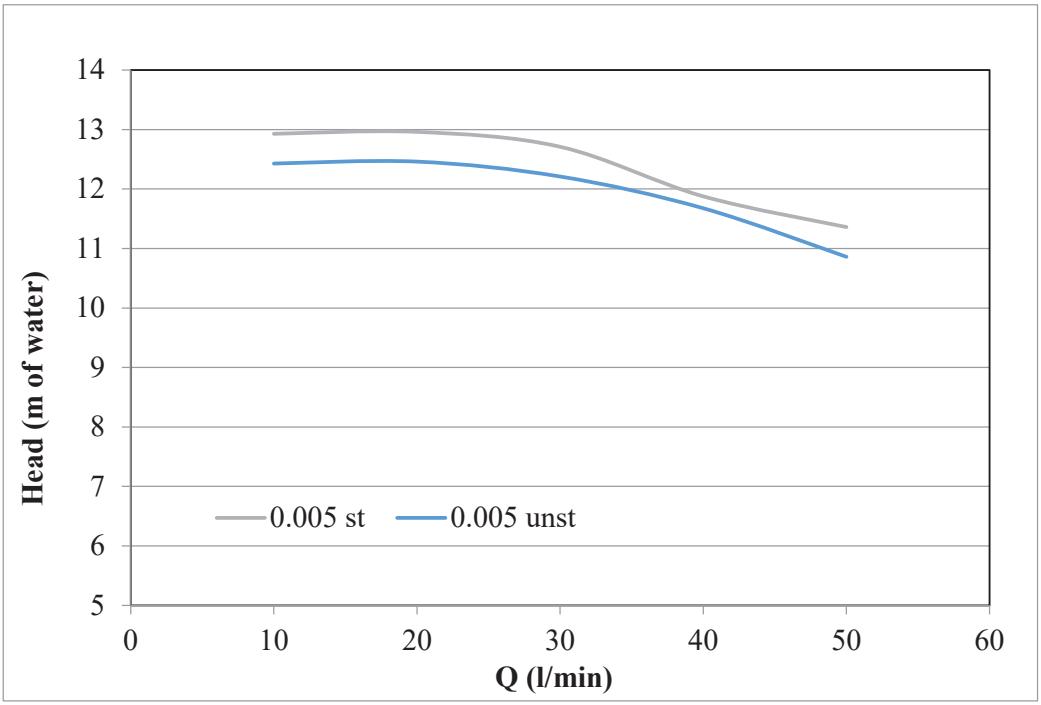

Fig.5.41 Emulsion stability effect on head for impeller (b) with blade number (5) with pump running at 1650 rpm for emulsions with holdup (Φ = 0.005)

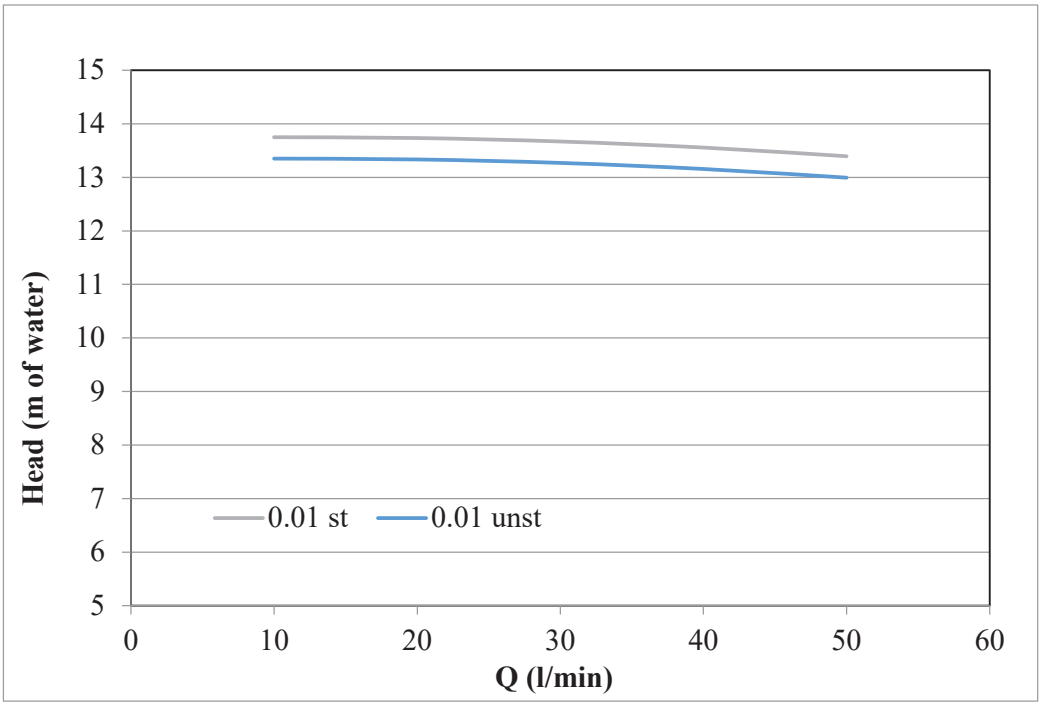

Fig.5.42 Emulsion stability effect on head for impeller (d) with blade inlet angle 20° with pump running at 1530 rpm for emulsions with holdup (Φ = 0.01)

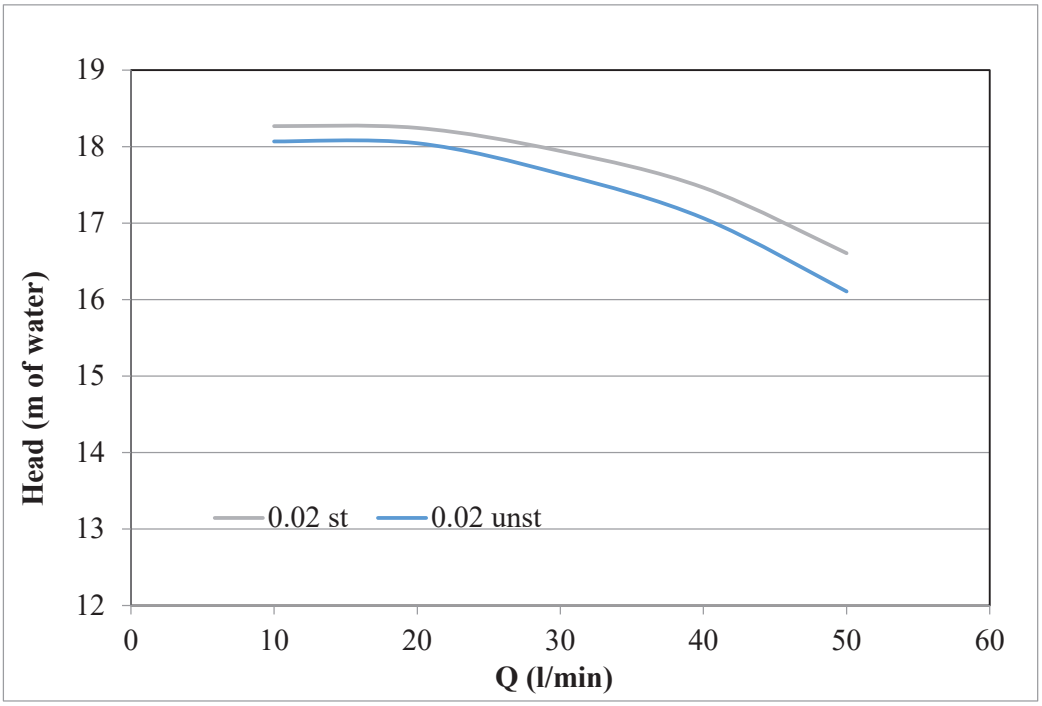

Fig.5.43 Emulsion stability effect on head for impeller (f) with blade outlet angle 25º with pump running at 1650 rpm for emulsions with holdup (Φ = 0.02)

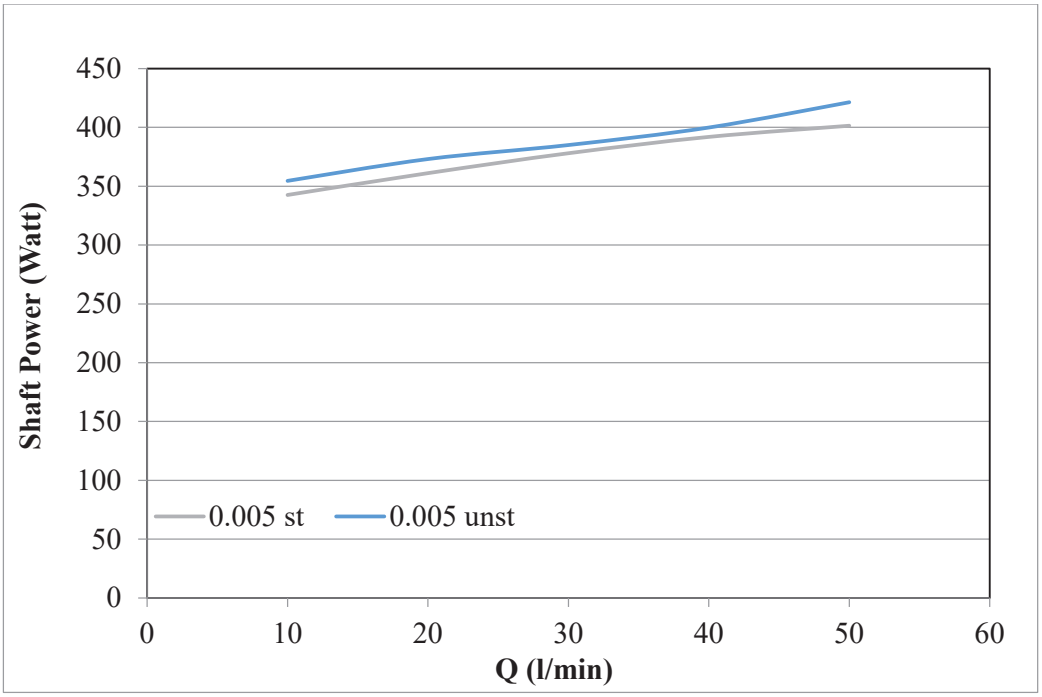

Fig.5.44 Emulsion stability effect on shaft power for impeller (b) with blade number (5) with pump running at 1530 rpm for emulsions with holdup (Φ = 0.005)

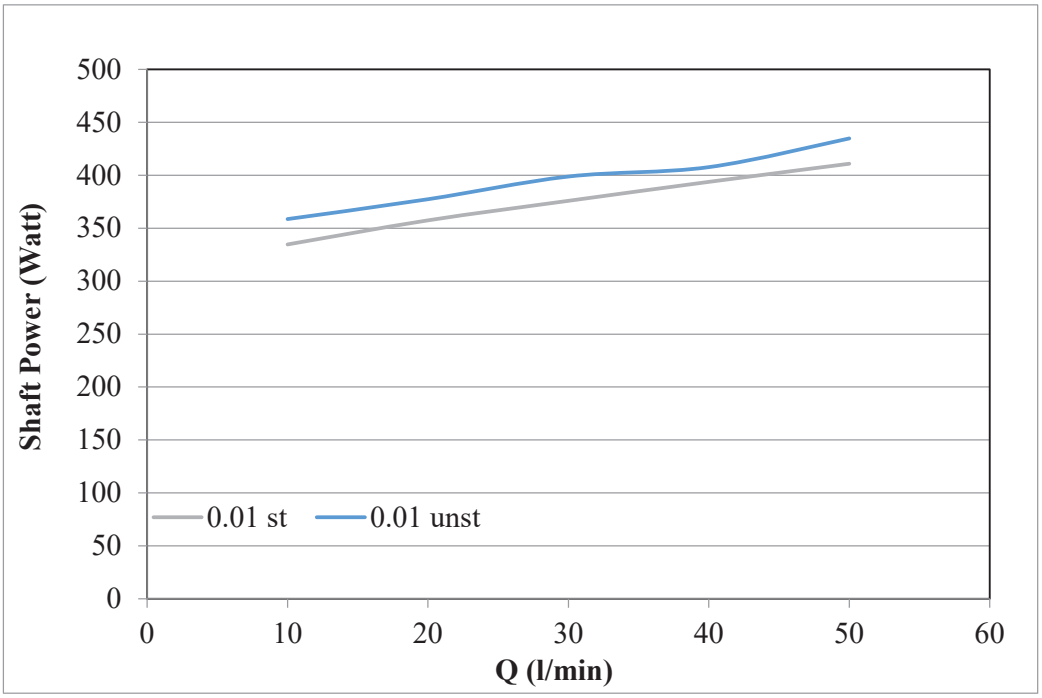

Fig.5.45 Emulsion stability effect on shaft power for impeller (d) with blade inlet angle 20^{o} with pump running at 1420 rpm for emulsions with holdup (Φ = 0.01)

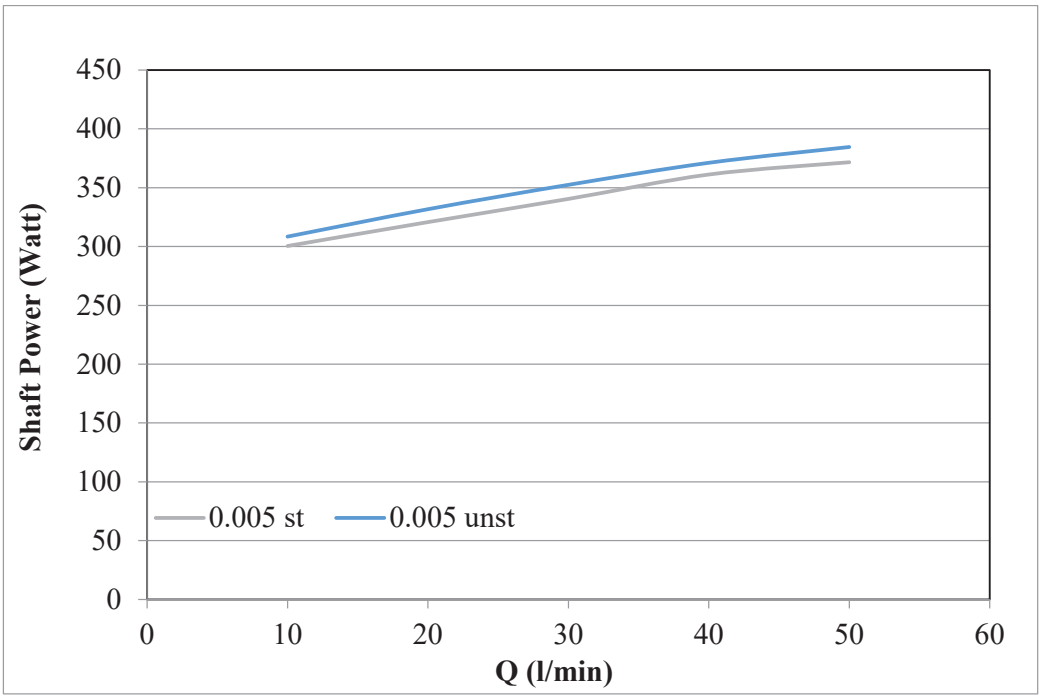

Fig.5.46 Emulsion stability effect on shaft power for impeller (f) with blade outlet angle 25^{o} with pump running at 1420 rpm for emulsions with holdup (Φ = 0.005)

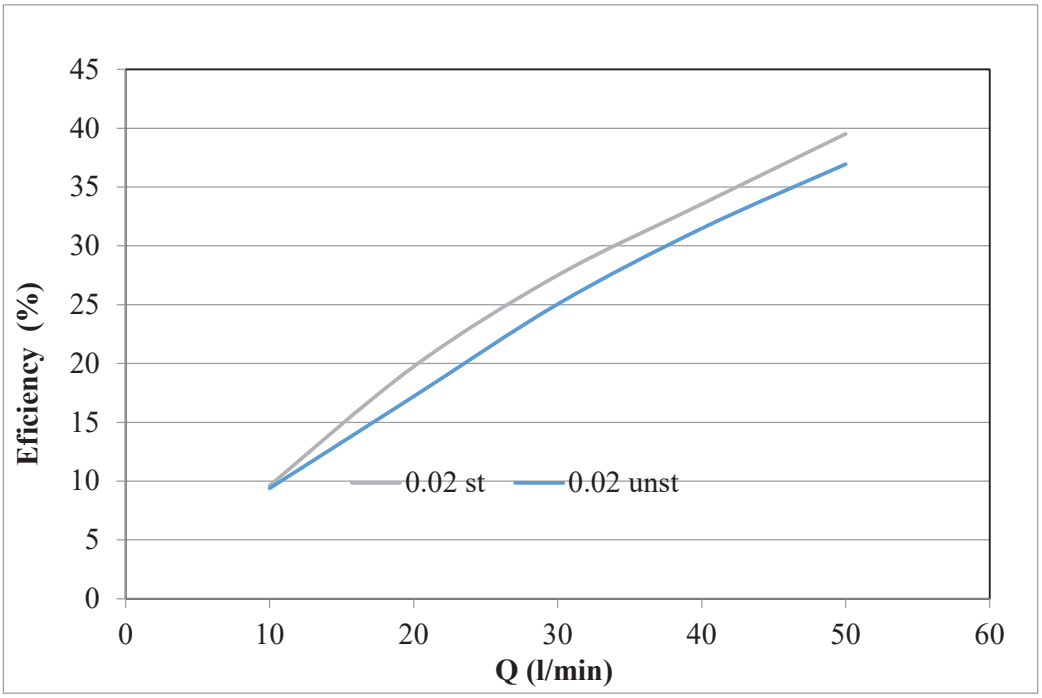

Fig.5.47 Emulsion stability effect on pump efficiency for impeller (c) with blade number (7) with pump running at 1650 rpm for emulsions with holdup (Φ = 0.02)

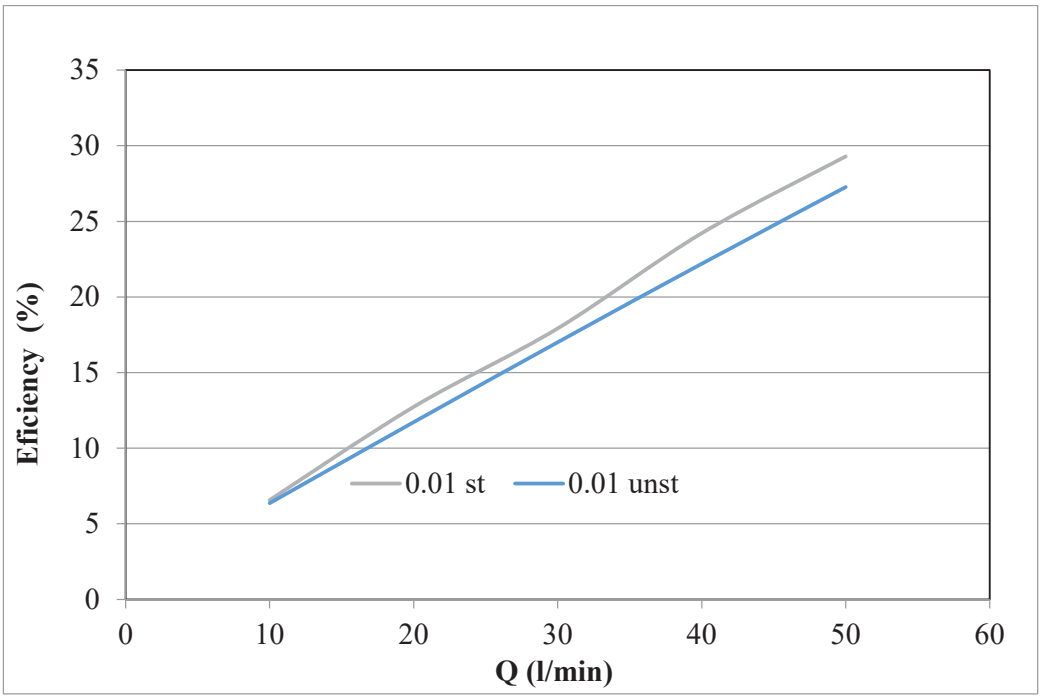

Fig.5.48 Emulsion stability effect on pump efficiency for impeller (e) with blade inlet angle 30º with pump running at 1530 rpm for emulsions with holdup (Φ = 0.01)

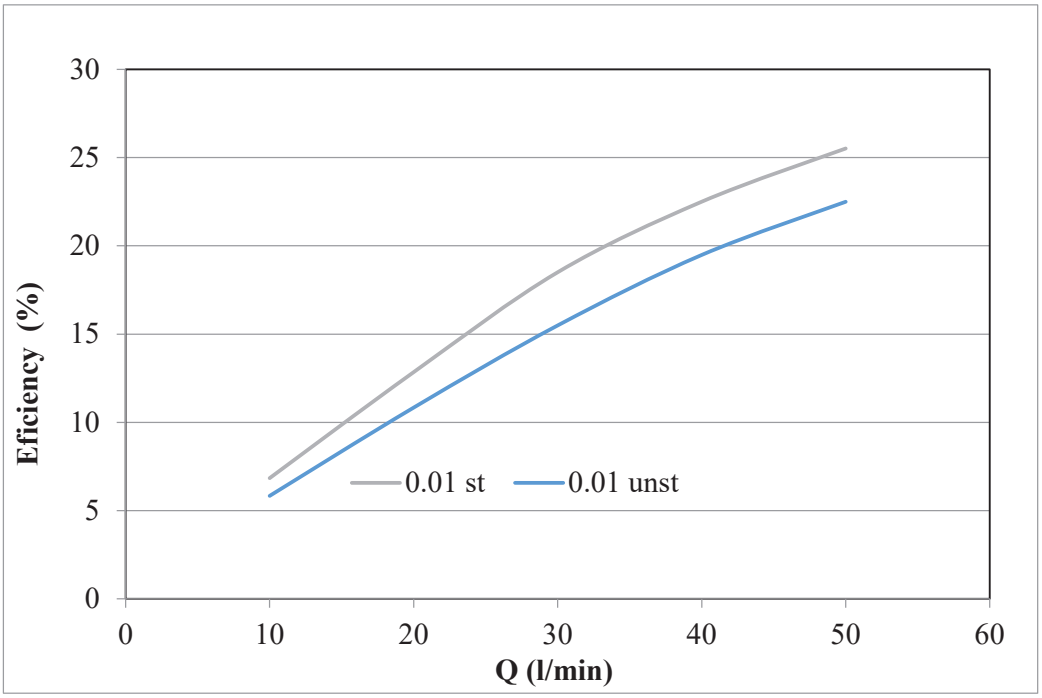

Fig.5.49 Emulsion stability effect on pump efficiency for impeller (f) with blade outlet angle 25° with pump running at 1650 rpm for emulsions with holdup (Φ = 0.01)

CHAPTER SIX

NUMERICAL ANALYSIS

CHAPTER SIX

NUMERICAL ANALYSIS

6.1 INTRODUCTION

After the test parameters were changed to closely mimic the actual conditions, the fluid flow inside the pump was simulated using ANSYS FLUENT version (R 19.1). First, as illustrated in Figs 6.1 to 6.7, SolidWorks software was used to create models that resembled the fluid inside the test impellers and the volute casing. Next, design modular software was used to identify the components of the test model so that it could be meshed using the appropriate mesh software in ANSYS Workbench software. To match the test simulation of the real experiment circumstances, the model is then placed into the ANSYS FLUENT software, and the required adjustments are made.

Table 6.1 shows the locations of each part of the model as identified by the design modular. While, Table 6.2 presents the boundary conditions identified in Fluent when sitting up the test conditions.

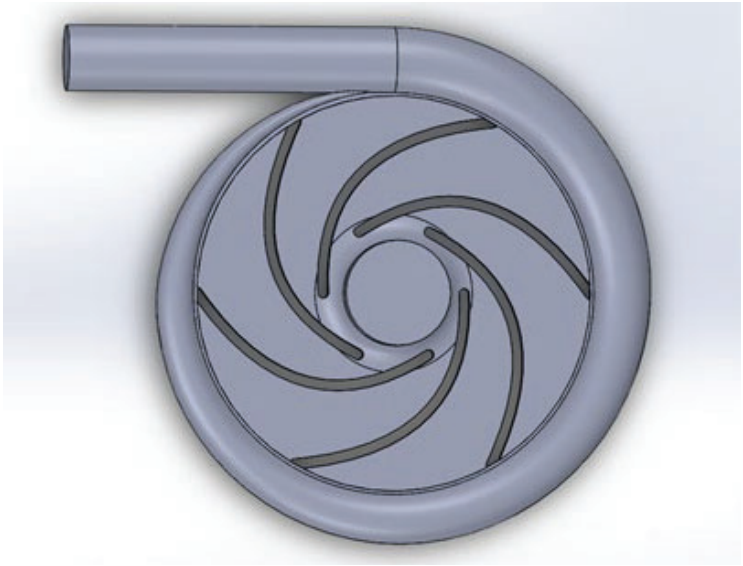

Fig. 6.1. Schematic of the fluid inside the impeller and volute used in the simulation for model with 6-blades with impeller's blade inlet angle (β_1=10^o) and impeller's blade outlet angle (β_2=30^o).

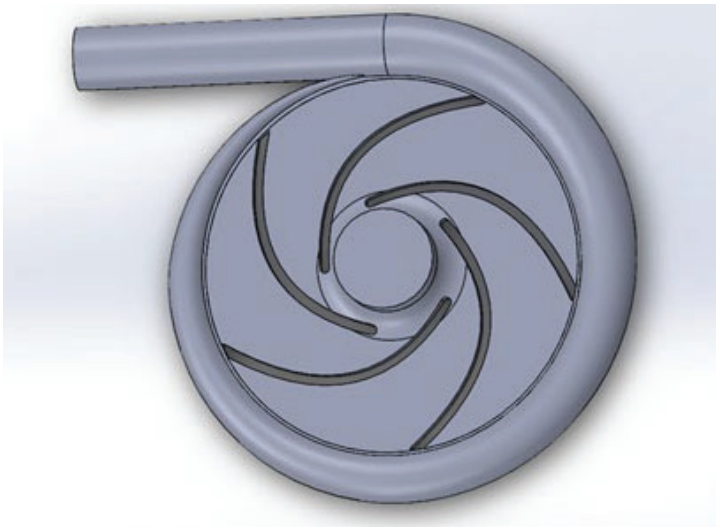

Fig. 6.2. Schematic of the fluid inside the impeller and volute used in the simulation for model with 5-blades.

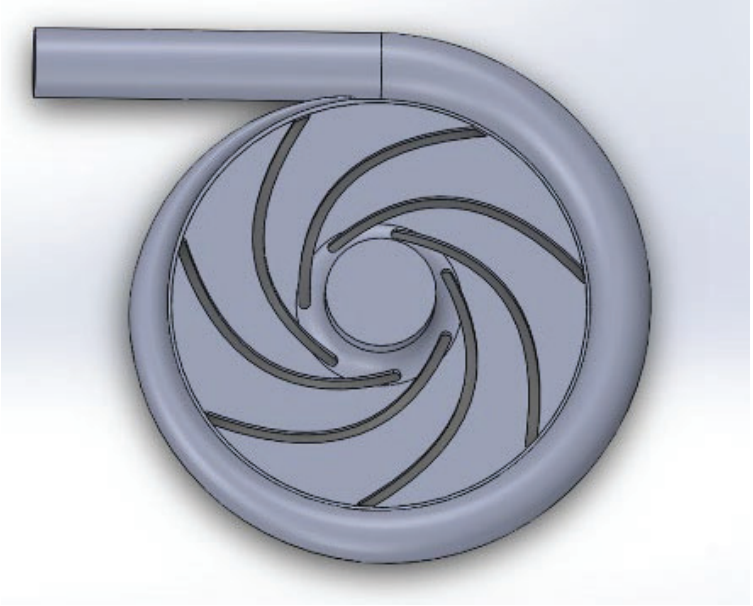

Fig. 6.3. Schematic of the fluid inside the impeller and volute used in the simulation for model with 7-blades.

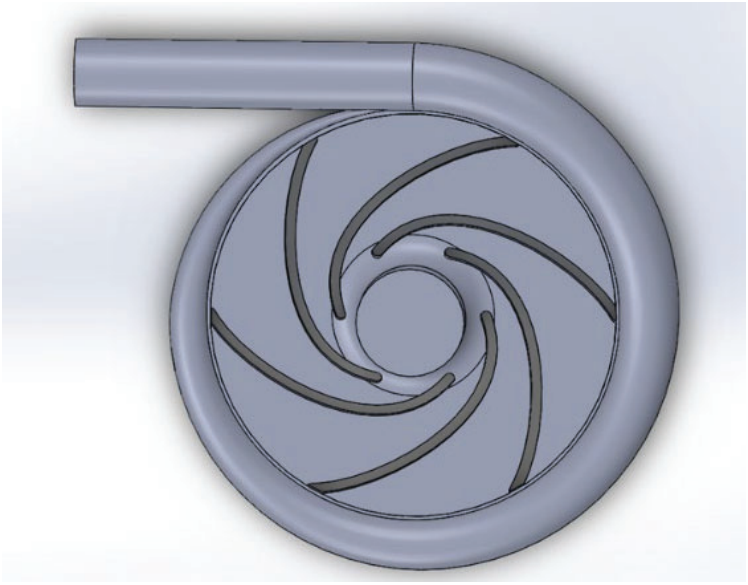

Fig. 6.4. Schematic of the fluid inside the impeller and volute used in the simulation for model with impeller's blade inlet angle (β_1=20^o).

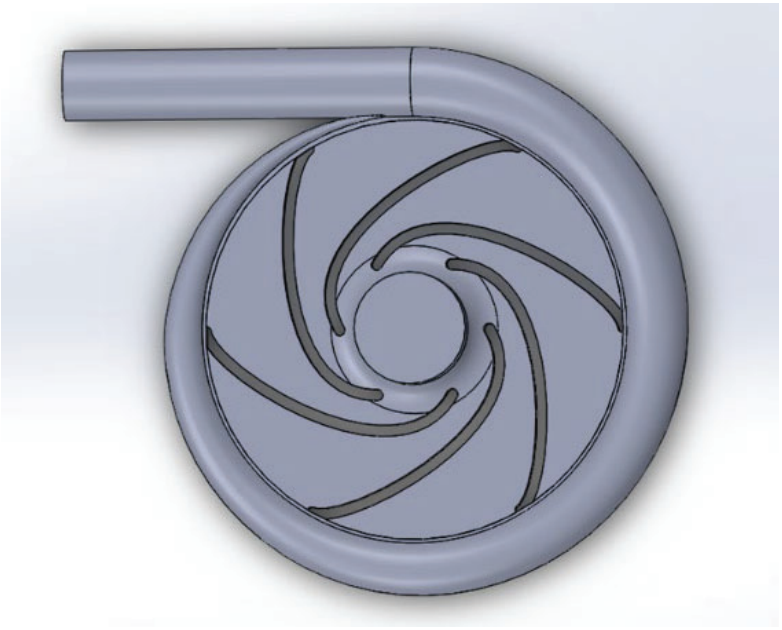

Fig. 6.5. Schematic of the fluid inside the impeller and volute used in the simulation for model with impeller's blade inlet angle (β_1=30^o).

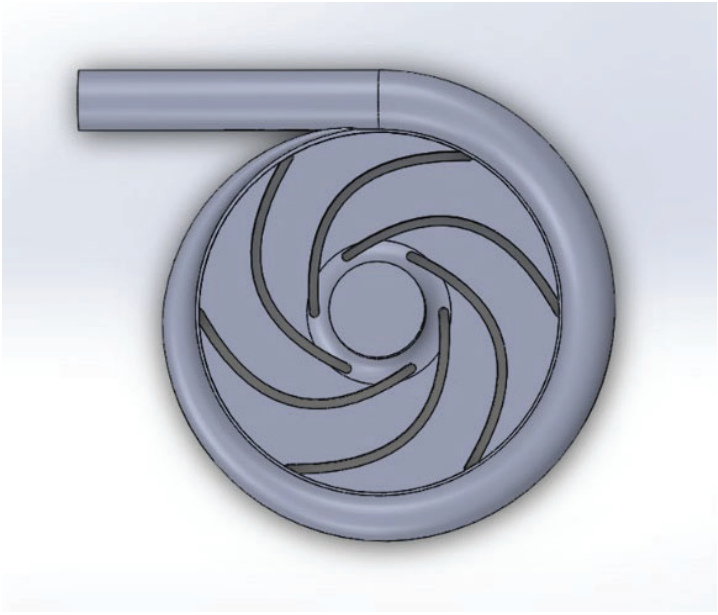

Fig. 6.6. Schematic of the fluid inside the impeller and volute used in the simulation for model with impeller's blade outlet angle (β_2=25^o).

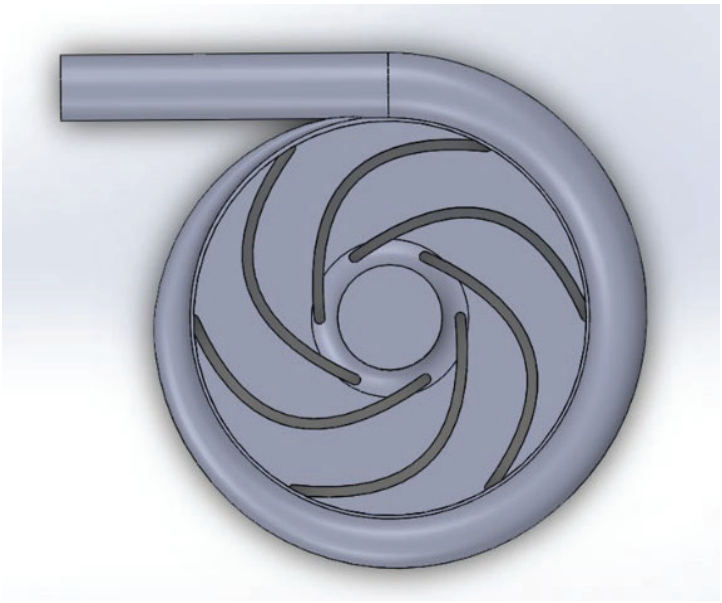

Fig. 6.7. Schematic of the fluid inside the impeller and volute used in the simulation for model with impeller's blade outlet angle (β_2=20^o).

Table 6.1. Boundar locations as identified in design modular.

Name	location
Inlet	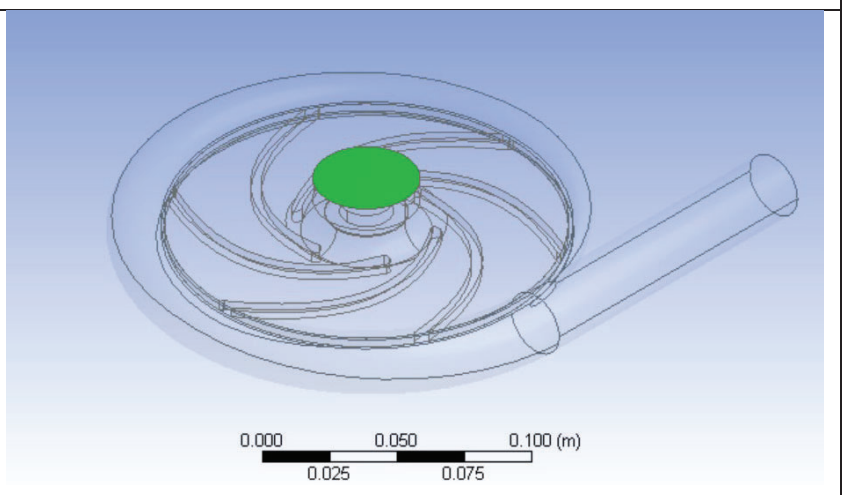
Shroud	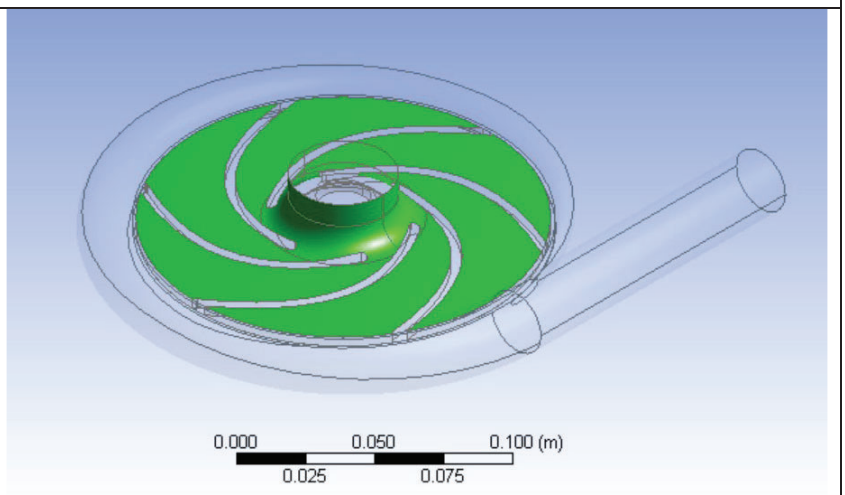
Hup	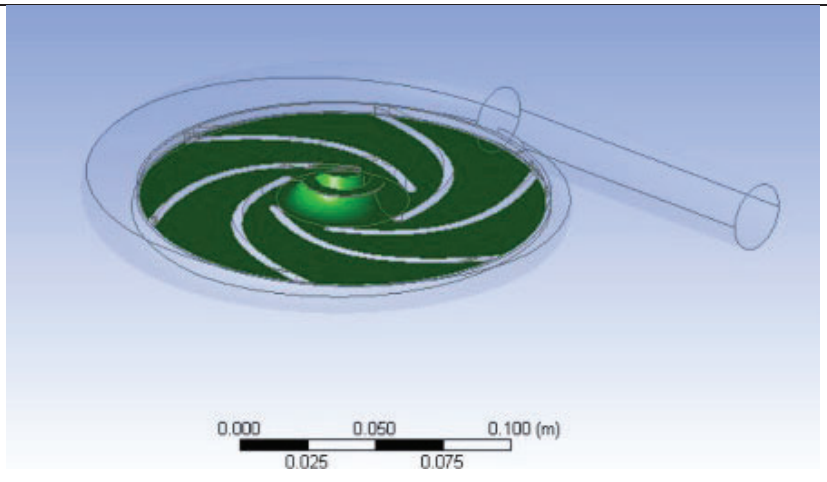

Blades	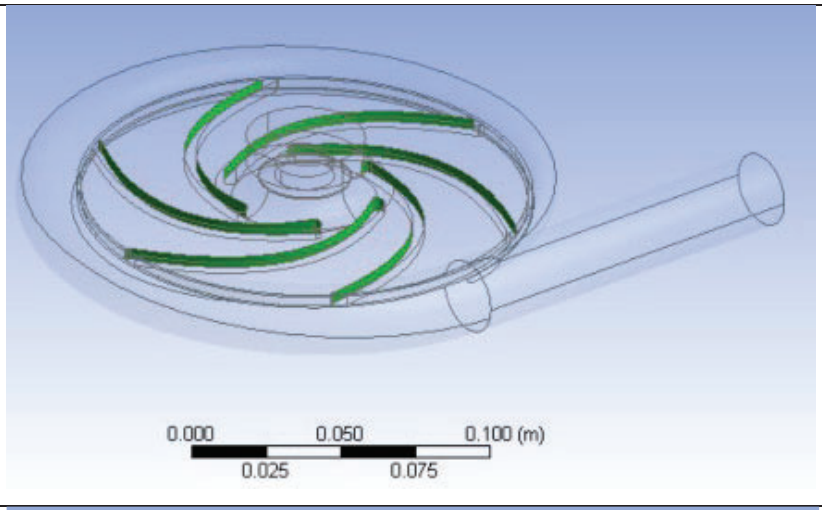
Impeller interface	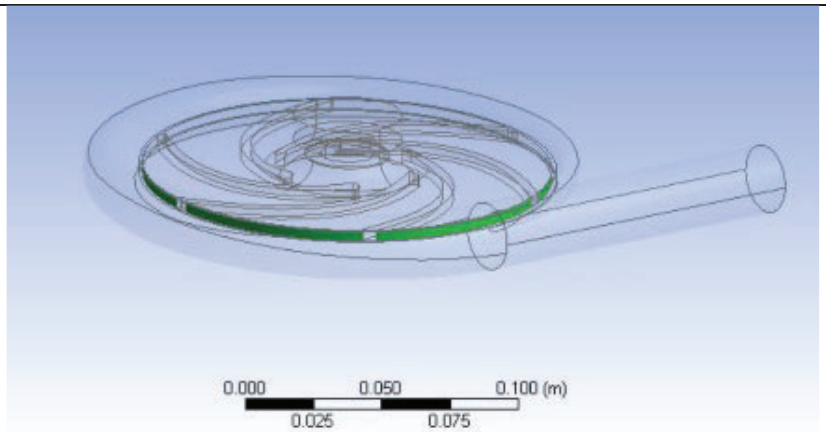
Volute interface	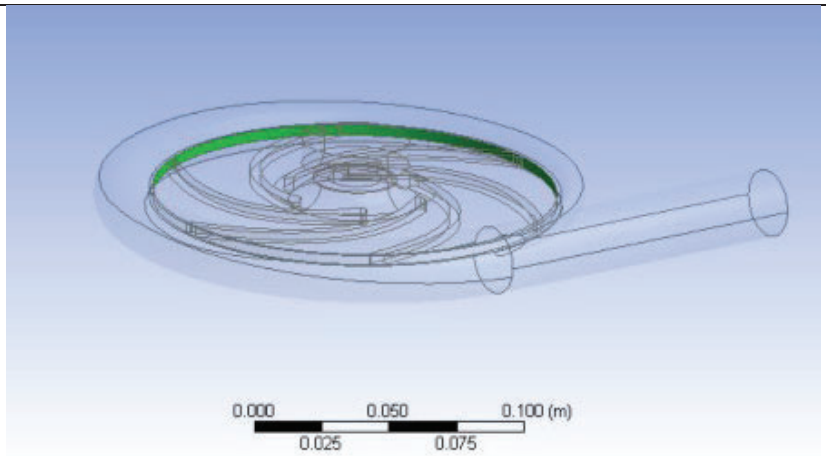

Volute casing	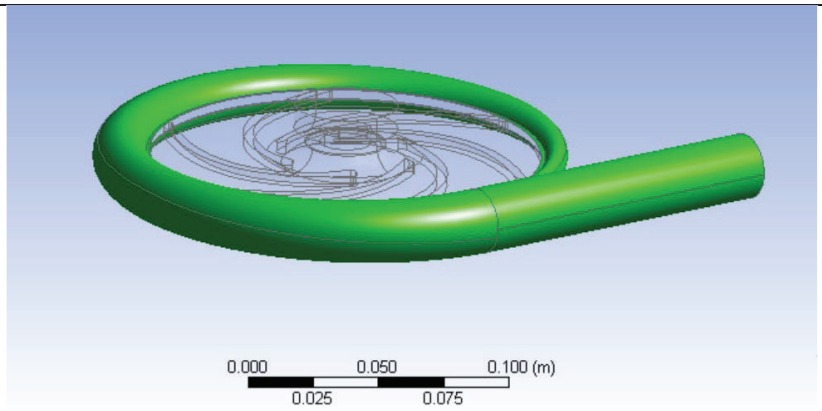
outlet	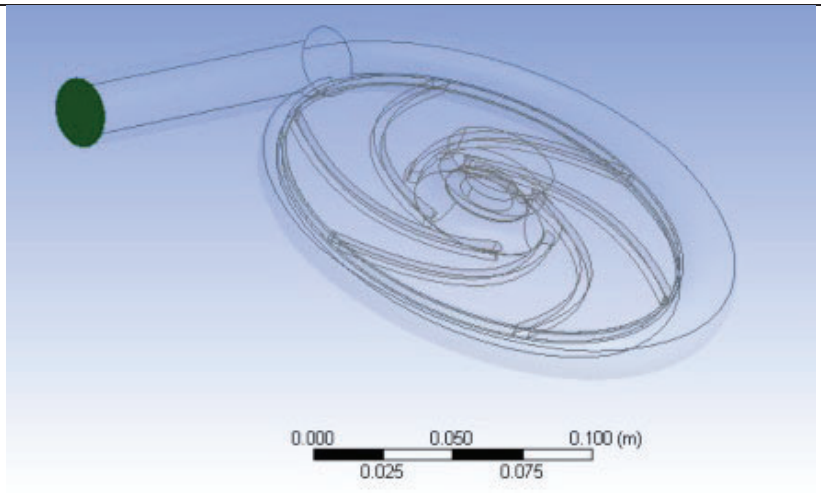

Table 6.2. Boundary Conditions.

Boundary Location	**Boundary Condition**
Shroud	Moving Wall (1530 rpm)
Hub	Moving Wall (1530 rpm)
Blade	Moving Wall (1530 rpm)
Impeller interface	Interface
Volute interface	Interface
Volute casing	Fixed wall
Outlet	Mass flowrate outlet (0.34, 0.78, 1.22, 1.7 kg/s)

ANSYS meshing software is used to generate the mesh according to the necessary criteria. In addition to making sure the contact regions are established correctly, as presented in Fig. 6.8.

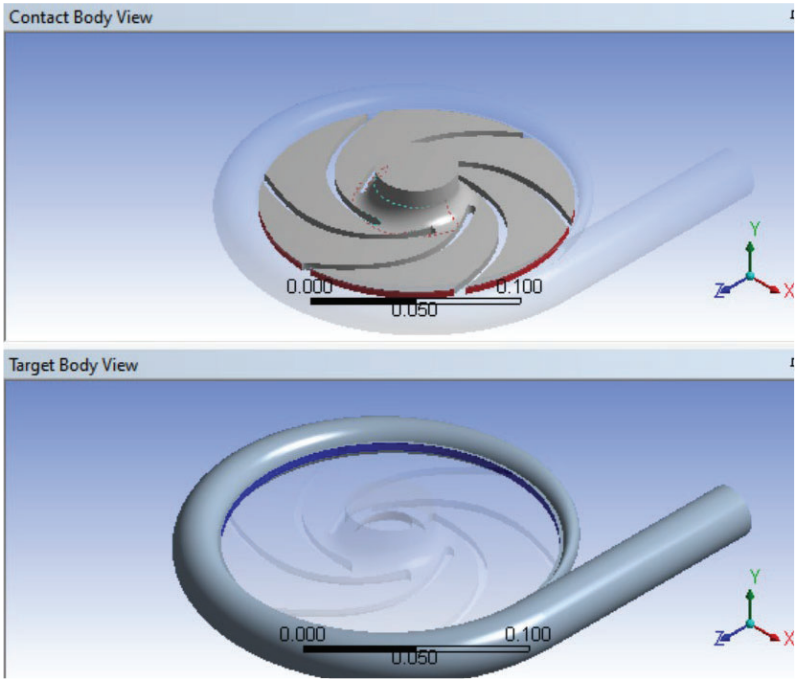

Fig. 6.8. Model Contact regions

6.2 MODELING APPROACH

The (SST k-ω) model is a two-equation eddy-viscosity model that combines the advantages of two different turbulence models. It can be applied straight down to the wall, even through the viscous sub-layer, because its formulation employs a k-ω method in the inner area of the boundary layer. This characteristic enables the SST k-ω model to function effectively as a Low-Reynolds number turbulence model without requiring any damping functions. Additionally, the SST formulation transitions to a k-ε behavior in free-stream conditions, addressing the issue with k-ω models, which is their sensitivity to the turbulence properties of the inlet free-stream. Furthermore, SST k-ω model demonstrates strong performance in situations involving adverse pressure gradients and flow separation. The transport equations for SST k-ω model are:

Turbulence kinetic energy equation

$$\frac{\partial k}{\partial t}+\overline{u}_j\frac{\partial k}{\partial x_j}=P_k-\beta^* k\omega+\frac{\partial}{\partial x_j}\left[\left(\upsilon+\sigma_k\upsilon_T\right)\frac{\partial k}{\partial x_j}\right] \tag{6.1}$$

Specific dissipation rate equation

$$\frac{\partial \omega}{\partial t}+\overline{u}_j\frac{\partial \omega}{\partial x_j}=\alpha S^2-\beta\omega^2+\frac{\partial}{\partial x_j}\left[\left(\upsilon+\sigma_w\upsilon_T\right)\frac{\partial \omega}{\partial x_j}\right]+2\left(1-F_1\right)\sigma_{w2}\frac{1}{\omega}\frac{\partial k}{\partial x_i}\frac{\partial \omega}{\partial x_i} \tag{6.2}$$

Kinematic eddy viscosity equation

$$\upsilon_T=\frac{\alpha_1 k}{\max\left(\alpha_1\omega, SF_2\right)} \tag{6.3}$$

The closure coefficients and auxiliary relations are:

$$F_2=\tanh\left\{\left[\max\left(\frac{2\sqrt{k}}{\beta^*\omega y},\frac{500\upsilon}{y^2\omega}\right)\right]^2\right\},\quad P_k=\min\left(\tau_{ij}\frac{\partial \overline{u_i}}{\partial x_j},10\beta^* k\omega\right),$$

$$F_1=\tanh\left\{\left\{\min\left[\max\left(\frac{\sqrt{k}}{\beta^*\omega y},\frac{500\upsilon}{y^2\omega}\right),\frac{4\sigma_{w2}k}{CD_{kw}y^2}\right]\right\}^4\right\},\quad CD_{kw}=\max\left(2\rho\sigma_{w2}\frac{1}{\omega}\frac{\partial k}{\partial x_i}\frac{\partial \omega}{\partial x_i},\ 10^{-10}\right),$$

$\phi=\phi_1F_1+\phi_2\left(1-F_1\right)$ (as $\phi=\alpha\ ,\beta\ ,\sigma_k,\sigma_w$, $\phi_1=\alpha_1\ ,\beta_1\ ,\sigma_{k1},\sigma_{w1}$, and $\phi_2=\ \alpha_2\ ,\beta_2\ ,\sigma_{k2},\sigma_{w2}$)

$\alpha_1=\frac{5}{9},\ \alpha_2=0.44$, $\beta_1=\frac{3}{40},\ \beta_2=0.0828$, $\beta_o^*=0.09$

$\sigma_{k1}=0.85$, $\sigma_{k2}=1$, $\sigma_{w1}=0.5$, $\sigma_{w2}=0.856$, [48]

A mesh or grid independency study is conducted to find the ideal mesh size, which is the number of elements required to find a reasonably accurate solution to the issue at the least computing effort. Mesh inflation is generated with 5 layers and 1.2 growth rate and skewness value of 0.9. The results' precision is sufficient to record all required flow characteristics, to validate the mesh's accuracy, seven models were made for the current study utilizing the design modular. The number of elements grows as the element size decreases; for the very coarse grid, the models began with 313,253 elements. The grid got finer as the number of elements increased over time. The cells of the finest grid were 4,967,209. The head value at a line segment at a constant 0.025 m distance from the model exit was calculated for each case, to compare all models and assess the grid's correctness, as shown in Fig. 6.9.

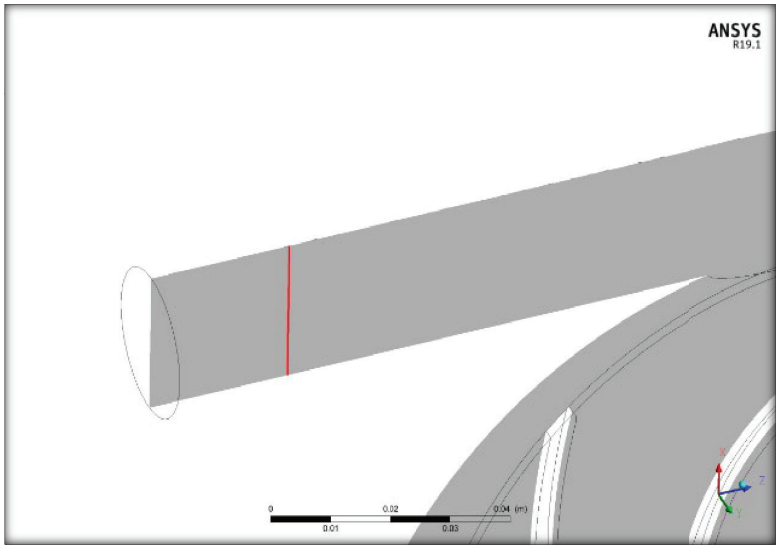

Fig. 6.9. Verification line segment location.

Results are plotted and compared, as shown in Fig. 6.10. The comparison demonstrated how the head value varies with cell count. However, there hasn't been much of a change for the last four models. Cell counts for the final four grids were (1260734, 2597278, 3524449, and 4967209).

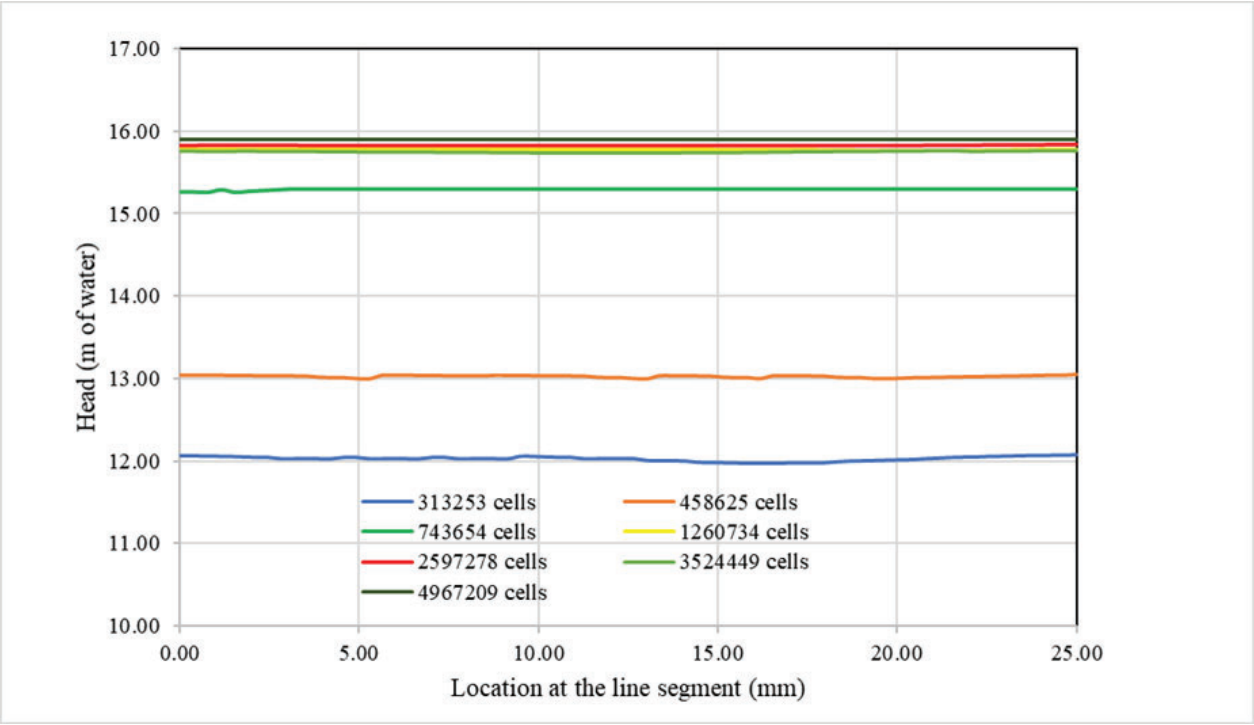

Fig. 6.10. The verification comparison plot

The grid with 2,597,278 cells will be used for the current investigation to create the remaining models. Compared to the grid with 4,967,209 cells, this grid will save calculation time while still producing correct results because of its extremely thin grid. Fig. 6.11. shows the final used mesh.

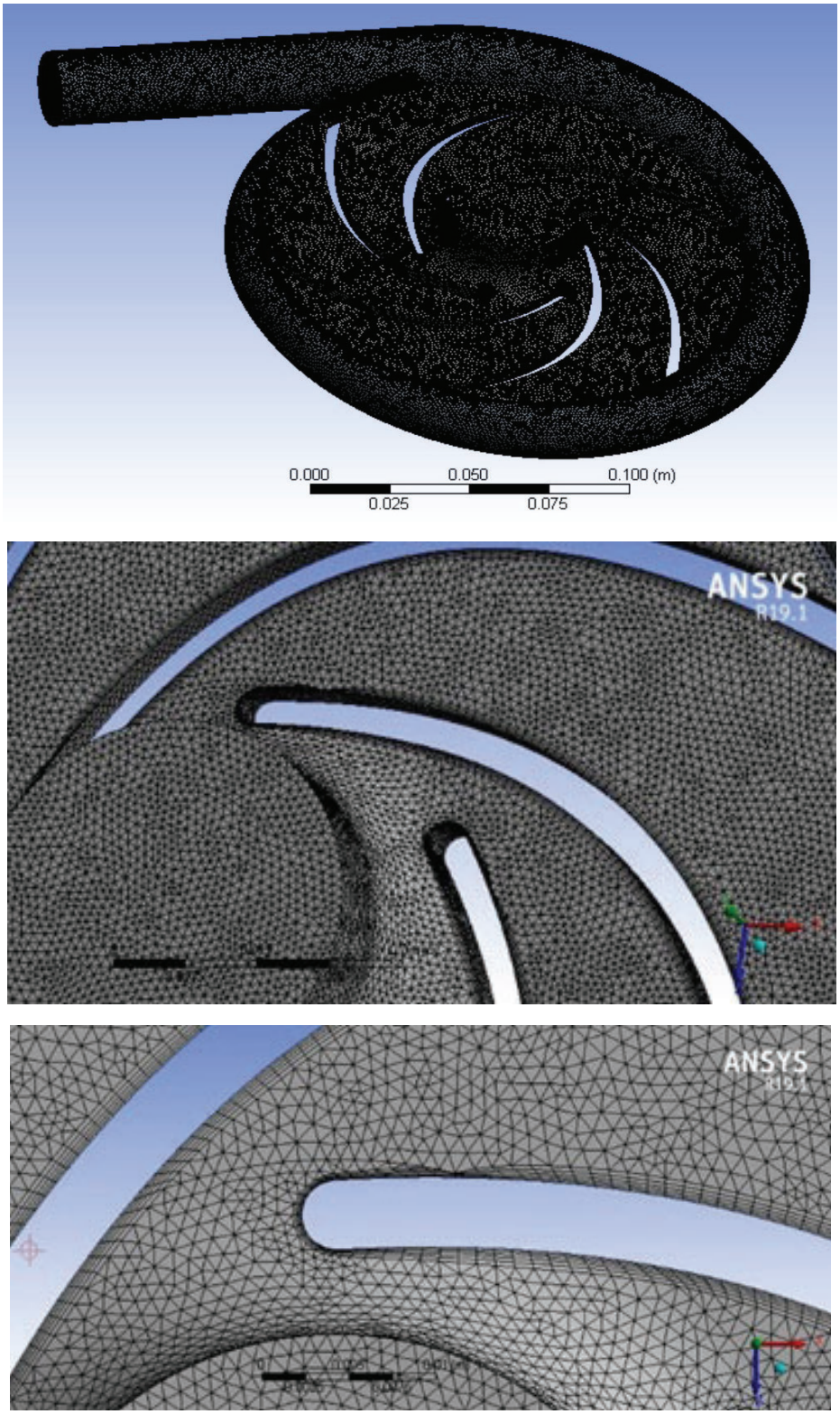

Fig. 6.11. The model meshing (a) total domain, (b) zoom in impeller (c) zoom in contact regions.

6.3 MODEL VALIDATION

A comparison was made with ongoing experimental work to ensure that the model using the SST k-ω turbulence model produces accurate results. In addition, its performance against other turbulence models (standard k-ω, standard k-ε, and realizable k-ε) was evaluated to confirm its accuracy. The convergence absolute criteria were set to (10^{-5}) for all the residuals. The validation process utilized an impeller with a blade inlet angle of $\beta_1 = 10^{o}$, operating with water at 1530 rpm, Fig. 6.12. The comparisons between experimental measurements and the predicted values from the current CFD code showed satisfactory agreement, with the SST k-ω model yielding the best results. Table 6.3 presents the average variance between results. The observed deviations may be attributed to simplifications in the numerical model, such as limitations in mesh resolution, and assumptions made about turbulence and boundary conditions. Overall, the CFD model serves as an effective solution tool, as it accurately predicts the pump performance curves.

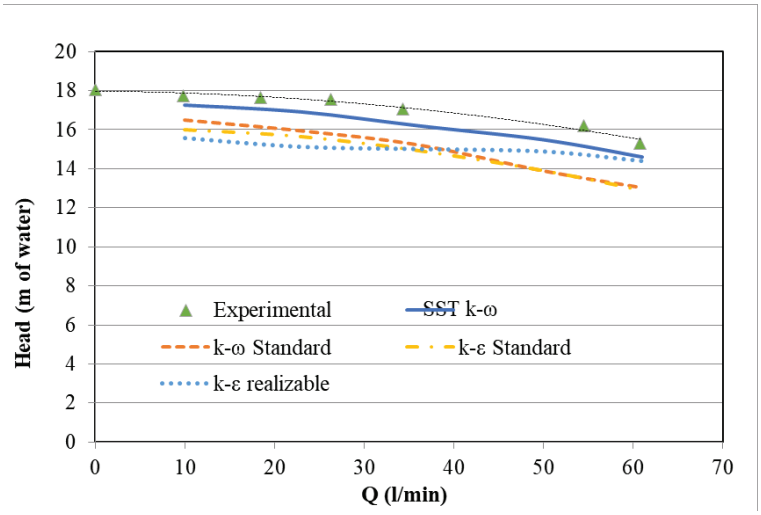

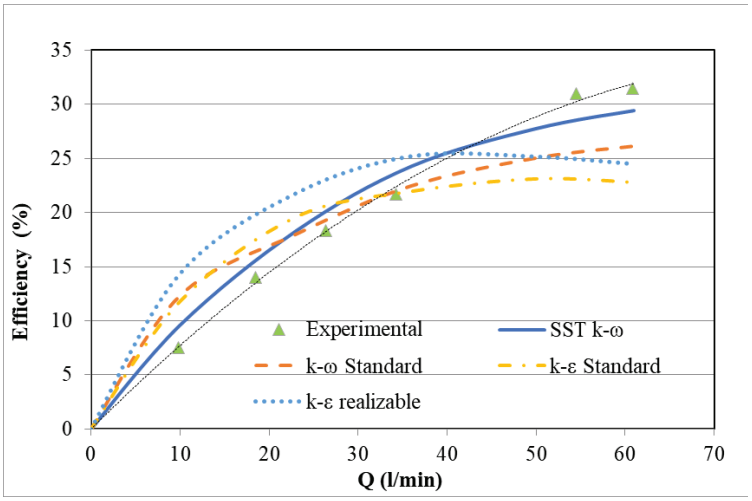

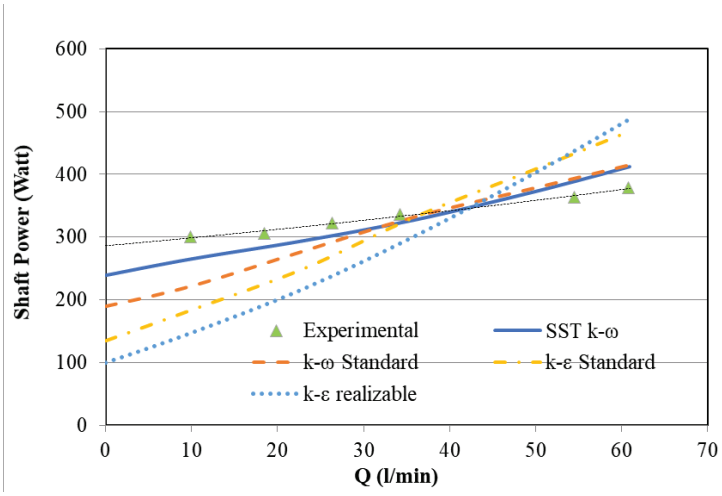

Fig. 6.12. Comparison of pump performance curves using water as working fluid a 6 blades impeller with impeller's blade inlet angle (β_1=10°) and impeller's blade outlet angle (β_2=30°), operating at 1530 rpm (a) head-flowrate (b) efficiency-flowrate (c) shaft power-flowrate.

Table 6.3 The average SST k-ω model results variations

Results	Minimum variation	Maximum variation	Average
Head	6.4%	6.8%	6.6%
Efficiency	0%	9.1%	4.46%
Shaft Power	0%	9.9%	4.95%

6.4 NUMERICAL RESULTS

6.4.1 Effect of blade number

Figure 6.13 presents the numerical results of analyzing the impact of the impellers' blade number (z) of 5,6, and 7 on the centrifugal pump's performance. The relationship across pump head, efficiency, and shaft power as functions of flow rate is illustrated, with blade number (z) as a parameter.

Figure 6.13 (a) displays the distribution of the pump head as a function of the flow rate and the blade number (z), it is evident that as the flow rate rises, the pump's head drops. Furthermore, the impeller of the blade number (z=7) tends to exhibit higher values of the pump head. The efficiency curves in Figure 6.13 (b) further show that the highest efficiency is obtained by the impeller with blade number of (z=6), Moreover, Figure 6.13 (c) presents the relevant shaft power curves as a function of volumetric flow rate, demonstrating that blade number of (z=5) angle gives the lowest shaft power value.

It is possible to identify the fluid flow features, disturbances, and places of the highest pressure by determining the pressure distribution, fluid flow velocity distribution, and streamlines inside the pump. Figures 6.14 to 6.16 display the pump fluid pressure contours, velocity contours, and streamline, results for the three-tested impellers with 5, 6, and 7-blades, respectively, at a motor speed of 1530 rpm. The obtained numerical results are consistent with the results obtained from the experimental analysis.

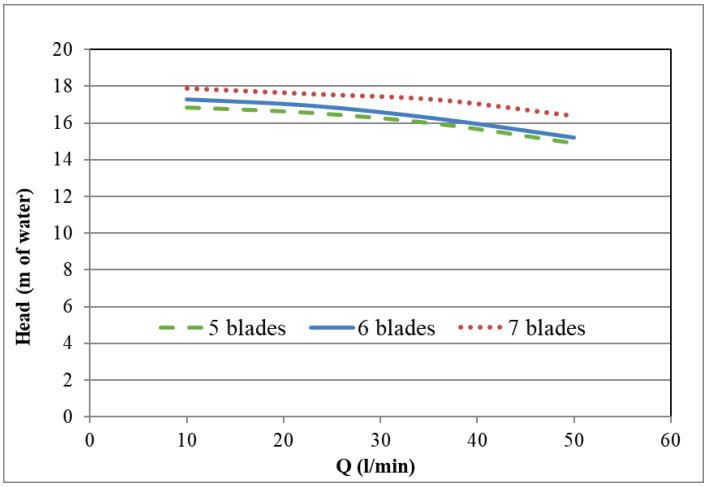

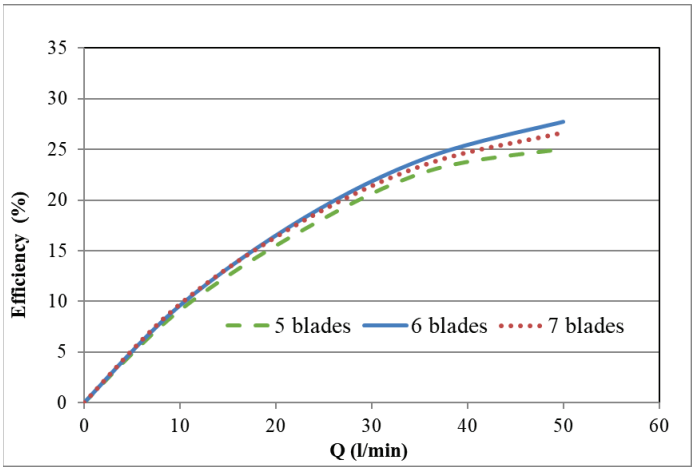

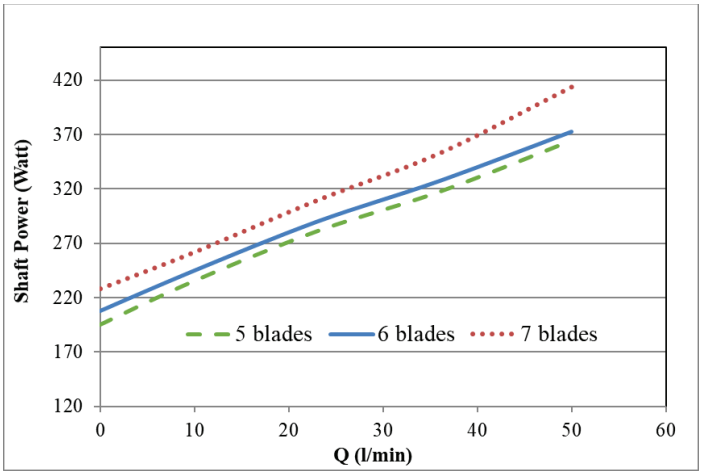

Fig. 6.13. Blade number effect on pump performance curves using water as a working fluid, with the pump running at 1530 rpm (a) head-flow rate (b) efficiency-flow rate (c) shaft power-flow rate.

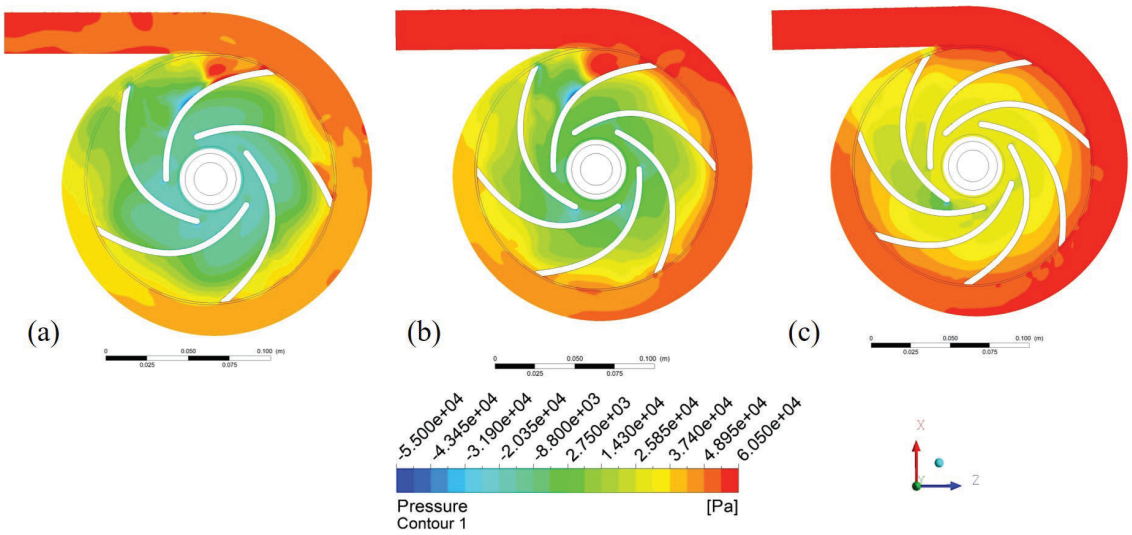

Fig. 6.14. Pressure contours inside the pump, (a) pump model with 5-blades, (b) pump model with 6-blades and (c) pump model with 7-blades.

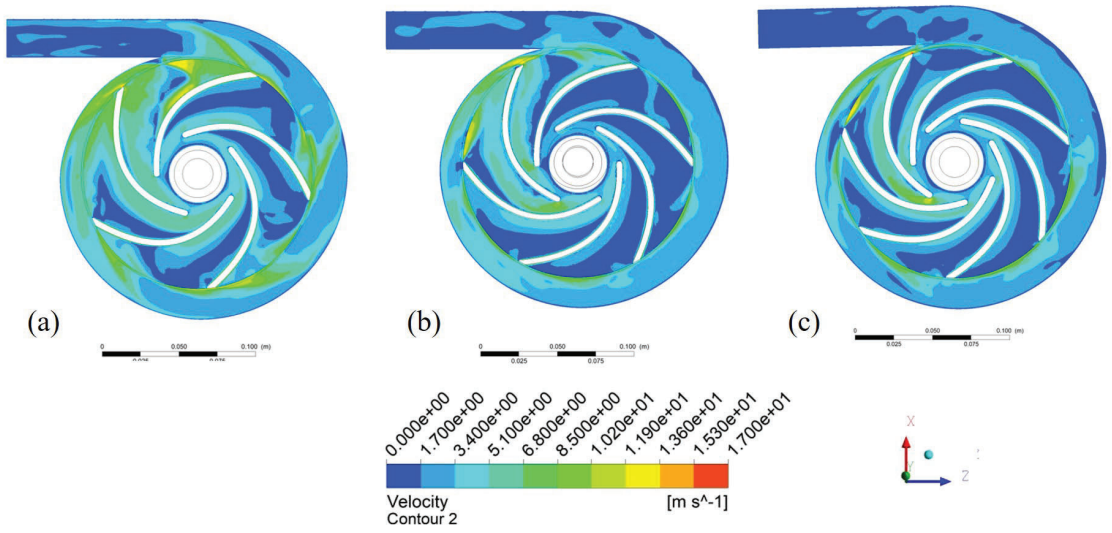

Fig. 6.15. Velocity contours inside the pump, (a) pump model with 5-blades, (b) pump model with 6-blades and (c) pump model with 7-blades.

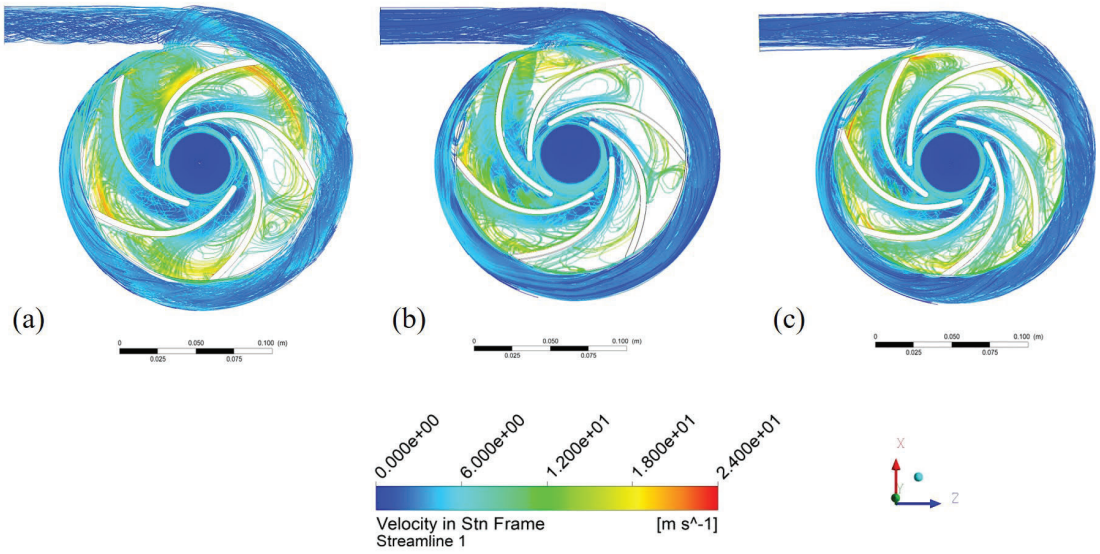

Fig.6.16. Streamlines from inlet to outlet, (a) pump model with 5-blades, (b) pump model with 6-blades and (c) pump model with 7-blades.

6.4.2 Effect of inlet blade angle

Figure 6.17 presents the numerical results of analyzing the impact of the impellers' blade inlet angle (β_1) of 10°, 20°, and 30° on the centrifugal pump's performance. The relationship across pump head, efficiency, and shaft power as functions of flow rate is illustrated, with input angle (β_1) as a parameter. Figure 6.17 (a) displays the distribution of the pump head as a function of the flow rate and the blade inlet angle (β_1), it is evident that as the flow rate rises, the pump's head drops. Furthermore, the impeller of the blade inlet angle (β_1=20°) tends to exhibit higher values of the pump head. The efficiency curves in Figure 6.17 (b) further show that the highest efficiency is obtained by the impeller with an inlet angle of (β_1=20°), Moreover, Figure 6.17 (c) presents the relevant shaft power curves as a function of volumetric flow rate, demonstrating that inlet blade angle of (β_1=20°) angle gives the lowest shaft power value.

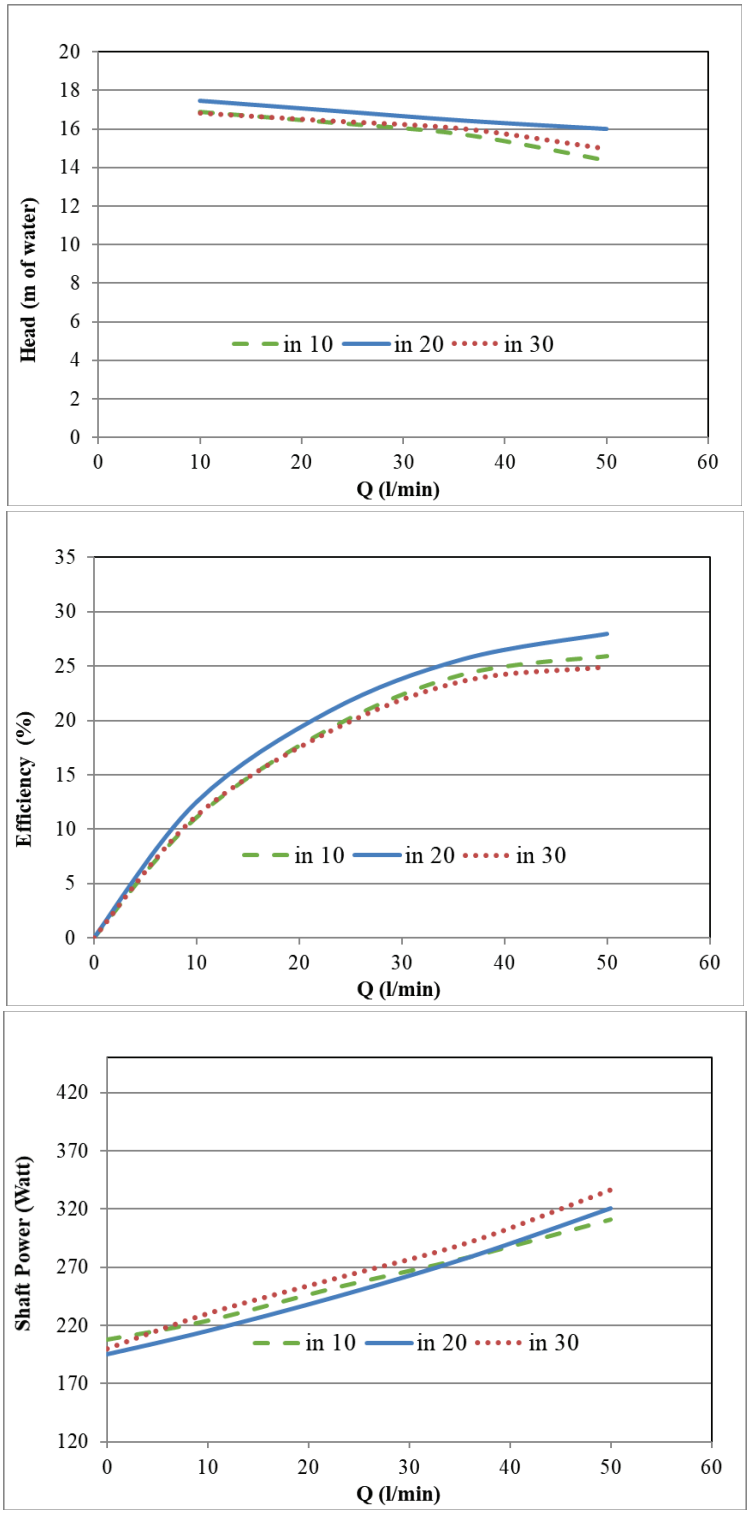

Fig. 6.17. Blade inlet angle (β_1) effect on pump performance curves using water as a working fluid, with the pump running at 1530 rpm (a) head-flow rate (b) efficiency-flow rate (c) shaft power-flow rate.

Figures. 6.18 to 6.20 present the pressure contours, fluid velocity contours, and streamlines for impeller models with inlet angle (β_1) of 10°, 20°, and 30°, respectively, at a motor speed of 1530 rpm using water as the working fluid. The numerical results that were produced align with the behavior that was seen throughout the theoretical and experimental investigation. The centrifugal pump's numerical pressure contours at Q = 23 l/min are shown in Figure 6.18. A steady pressure increases from the impeller eye toward the volute casing, Figure 6.18 (a), (b), and (c). It ranges from -55,000 Pa to around 60,500 Pa. It emphasizes how the fluid passes between the blades and converts mechanical energy into static pressure. Weak differences in pressure recovery can be seen. A more consistent high-pressure zone during the discharge is depicted in Figure 6.18 (b) for the inlet blade angle (β_1=20°).

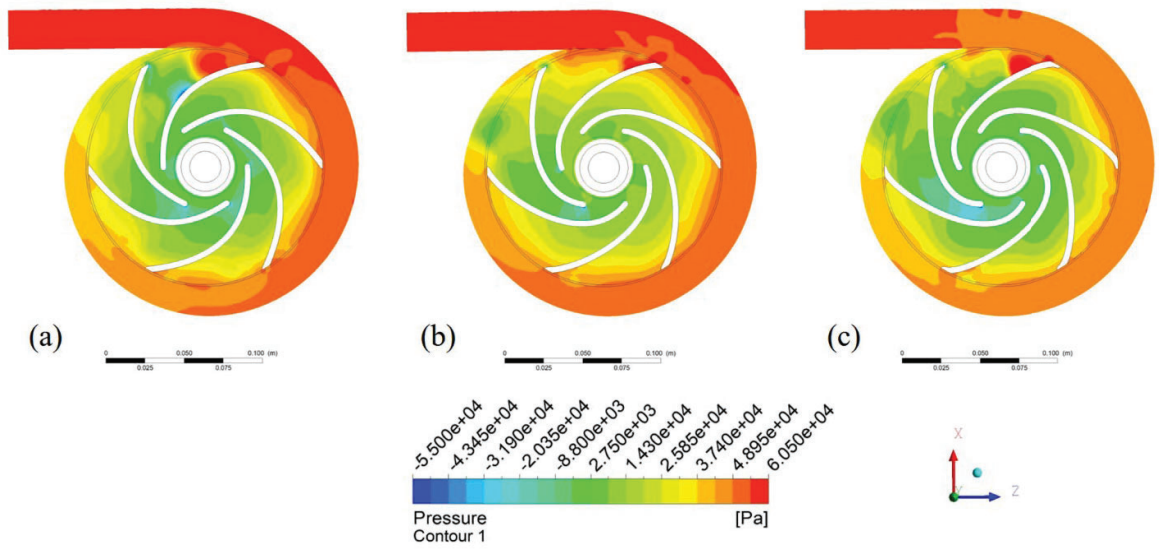

Fig. 6.18. Pressure contours inside the pump at Q = 23 l/min, (a) pump model with impeller's blade inlet angle (β_1=10°), (b) pump model with impeller's blade inlet angle (β_1=20°), and (c) pump model with impeller's blade inlet angle (β_1=30°).

Figure 6.19 shows the flow velocity contour over the impeller and volute. The velocity changes between the impeller's inlet and outlet to the volute. The velocity contours reach peak magnitudes of 17 m/s at the blade trailing edges.

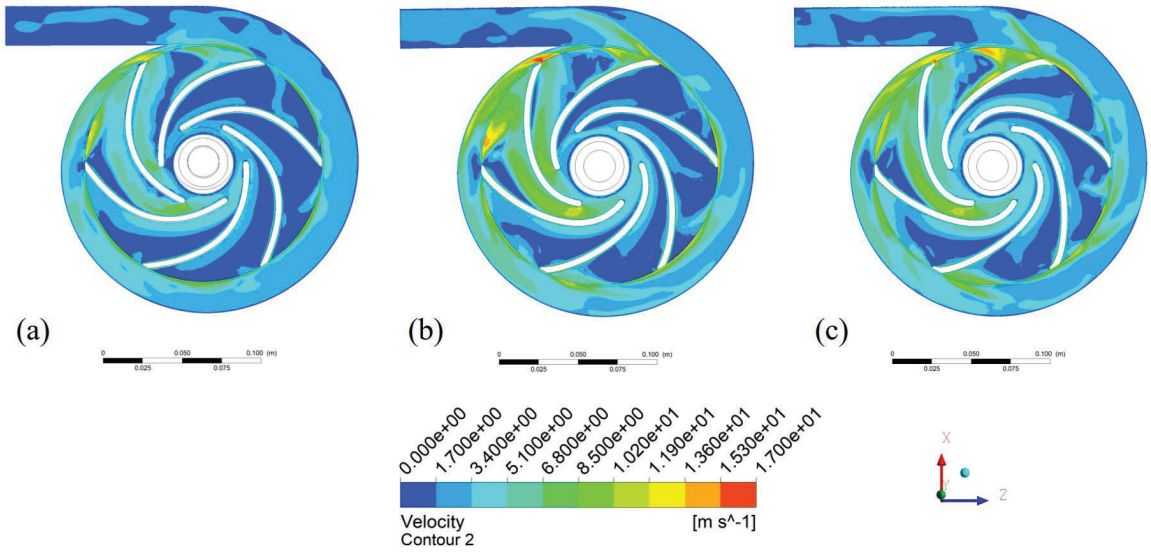

Fig. 6.19. Velocity contours inside the pump at, (a) pump model with impeller's blade inlet angle (β_1=10°), (b) pump model with impeller's blade inlet angle (β_1=20°), and (c) pump model with impeller's blade inlet angle (β_1=30°).

In the streamline analysis, Figure 6.20 shows internal flow directions and recirculation zones at speeds of up to 24 m/s. Figure 6.20 (a) and (b) clearly shows vortices and flow separation, which are usually associated with hydraulic energy losses. Moreover, Figure 6.20 (a) exhibits noticeably smoother and more connected streamlines, demonstrating its superior capacity to direct the fluid with the least amount of turbulence.

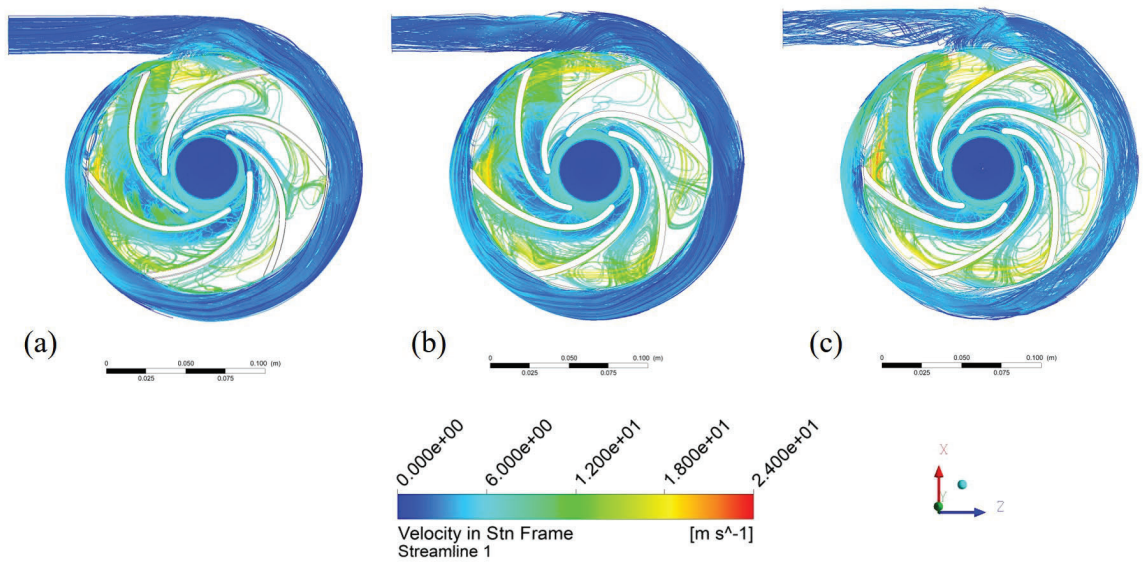

Fig. 6.20. Streamlines from inlet to outlet at, (a) pump model with impeller's blade inlet angle (β_1=10°), (b) pump model with impeller's blade inlet angle (β_1=20°), and (c) pump model with impeller's blade inlet angle (β_1=30°).

6.4.3 Effect of outlet blade angle

The performance of the centrifugal pump numerical results that observed the effect of the impeller blade outlet angle (β_2) of values (20°, 25°, and 30°) are presented in Figure 6.21. The pump head distribution as a function of flow rate and output blade angle is seen in Figure 6.21 (a). It shows that the pump head rises in conjunction with the output blade angle. This may be related to the outlet cross-section size growing in relation to the outlet blade angle, which reduces the liquid pressure drop in the flow path between the blades. The efficiency curves in Figure 6.21 (b) further demonstrate how the impeller with outlet angle β_2 = 30° gives the best efficiency. Additionally, the matching shaft power curves as a function of volume flow rate are shown in Figure 6.21 (c), which shows that shaft power rises in relation to enlarging the outlet blade angle. This is due to the increased shaft torque resulting from the bigger outlet blade angle increases.

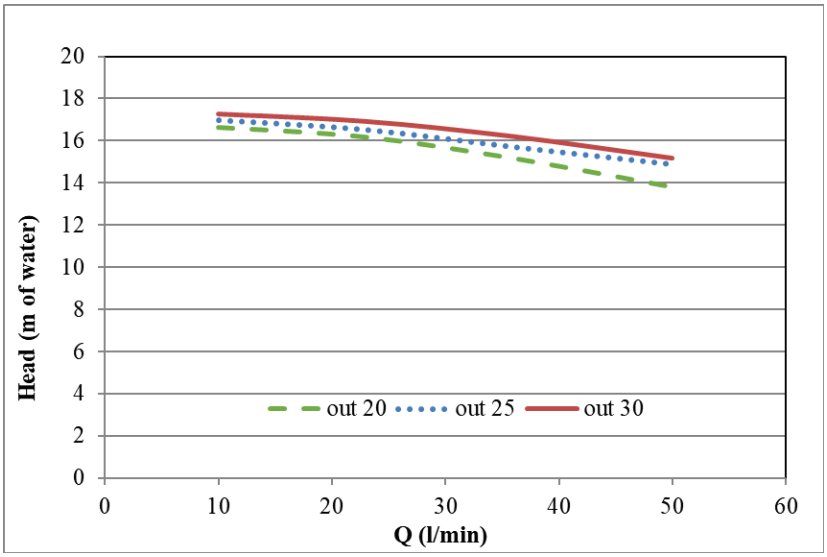

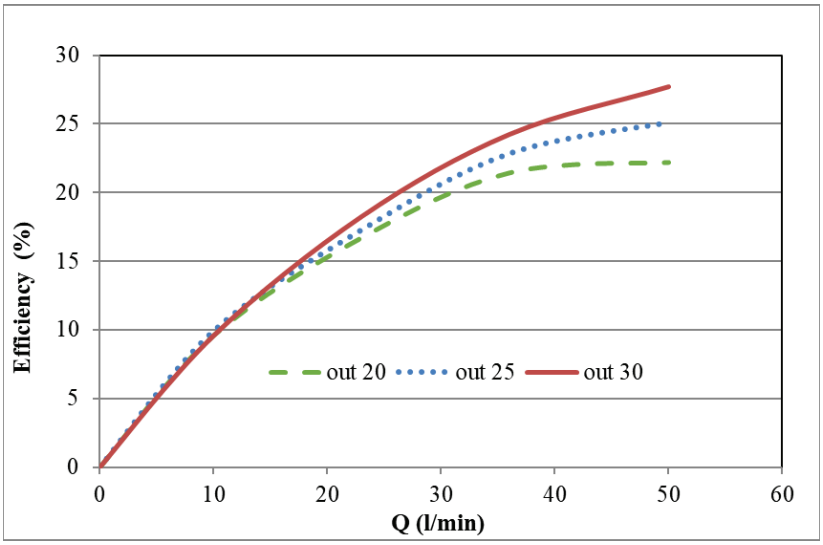

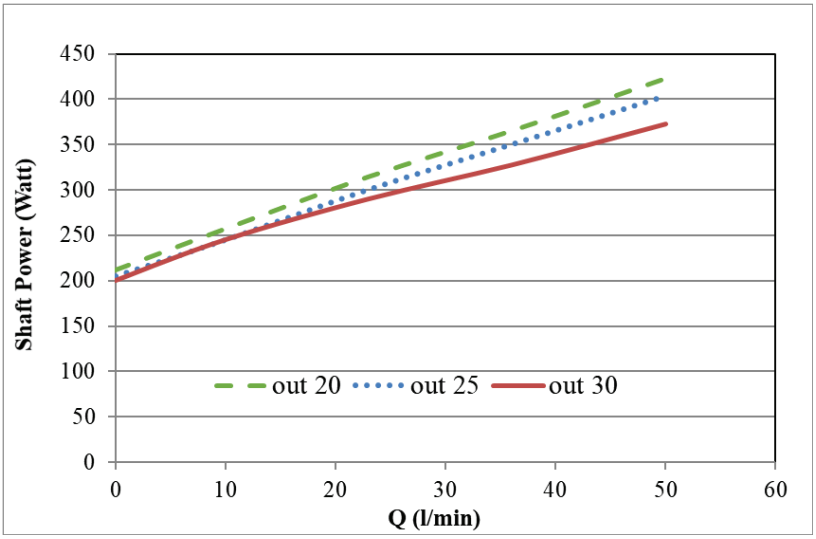

Fig. 6.21. Blade outlet angle (β_2) effect on pump performance curves using water as a working fluid, with the pump running at 1530 rpm (a) head-flow rate (b) efficiency-flow rate (c) shaft power-flow rate.

Figures 6.22 to 6.24 display the pump fluid pressure contours, velocity contours, and streamline results at Q = 23 l/min for impeller models with blade outlet angle (β_2) of values (30º, 25° and 20°), respectively. A motor speed of 1530 rpm is considered and water is the working fluid. The obtained numerical results are consistent with the behavior observed during both experimental and theoretical analysis.

Figure 6.22 (a), (b), and (c) shows that when the outlet blade angle increases, the differential pressure between the impeller inlet and outlet grows. A steady pressure increases from ranges also from -55,000 Pa to around 60,500 Pa. A higher-pressure zone during the discharge is depicted in Figure 6.22 (c) for the outlet blade angle (β_2=30º).

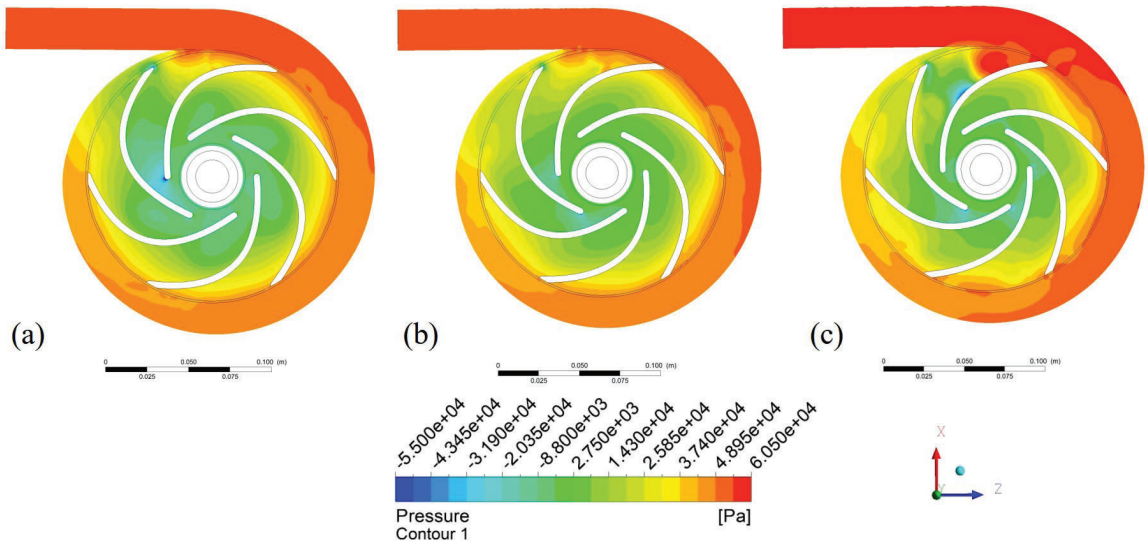

Fig. 6.22. Pressure contours inside the pump at, (a) pump model with impeller's blade outlet angle (β_2=20º), (b) pump model with impeller's blade outlet angle (β_2=25º), and (c) pump model with impeller's blade outlet angle (β_2=30º).

Figure 6.23 (a), (b), and (c) shows the flow velocity contour over the impeller and volute. The velocity changes between the impeller's inlet and outlet to the volute. In Figure 6.23 (a), the velocity contours clearly reach peak magnitudes of 17 m/s at the blade trailing edges.

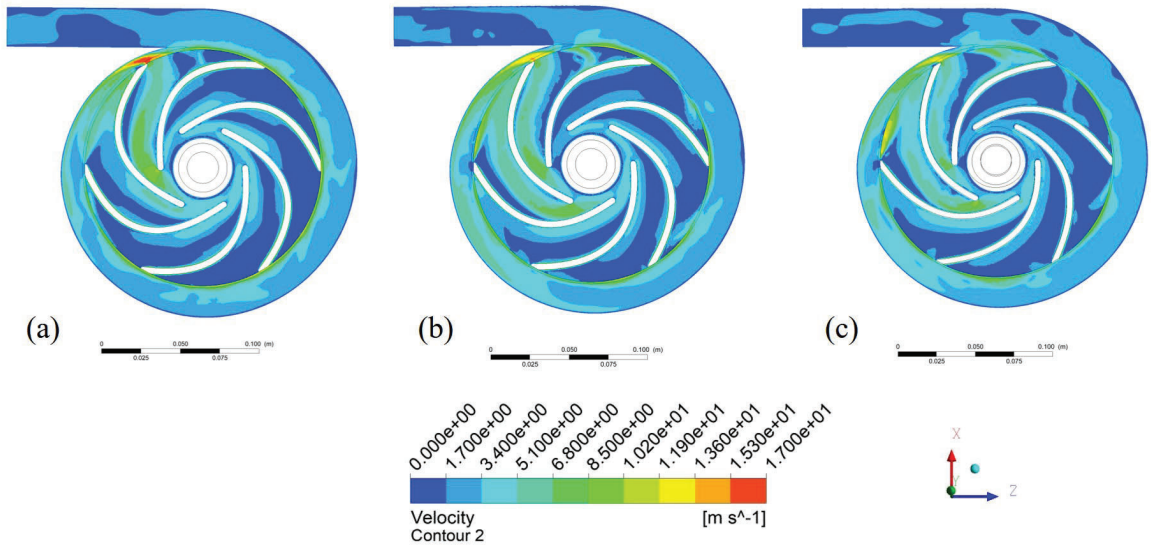

Fig. 6.23. Velocity contours inside the pump at, (a) pump model with impeller's blade outlet angle (β_2=20°), (b) pump model with impeller's blade outlet angle (β_2=25°), and (c) pump model with impeller's blade outlet angle (β_2=30°).

Figure 6.24 shows the velocity streamline at speeds of up to 24 m/s. Figure 6.24 (a) and (b) clearly shows vortices and flow separation. Moreover, Figure 6.24 (c) exhibits noticeably smoother and more connected streamlines.

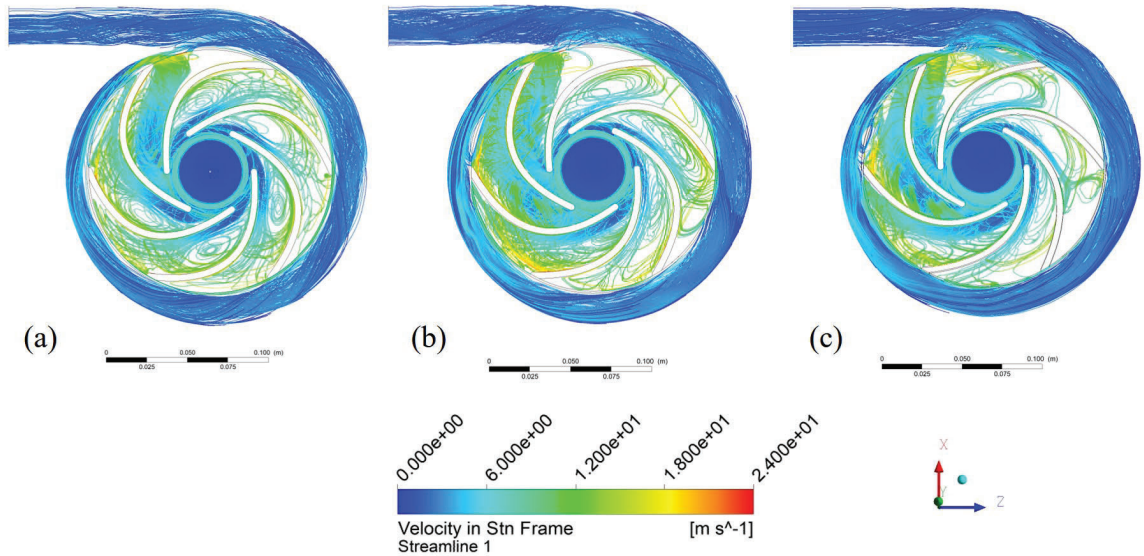

Fig. 6.24. Streamlines from inlet to outlet at, (a) pump model with impeller's blade outlet angle (β_2=30°), (b) pump model with impeller's blade outlet angle (β_2=25°), and (c) pump model with impeller's blade outlet angle (β_2=20°).

CHAPTER SEVEN

CONCLUSION AND RECOMMENDATIONS FOR FUTURE WORK

CHAPTER SEVEN

CONCLUSIONS AND RECOMMENDATIONS FOR FUTURE WORK

7.1 CONCLUSIONS

1- This thesis presents a comprehensive investigation of centrifugal pump performance when operating with water and water-oil emulsions through an integrated experimental, theoretical, and numerical framework. The combined use of controlled laboratory experiments, analytical performance modeling, and three-dimensional CFD simulations has enabled a systematic assessment of the effects of fluid properties, emulsion stability, and impeller geometric parameters on hydraulic performance.

2- Experimental results demonstrate that the presence of oil in water, even at relatively low volume fractions, leads to a measurable deterioration in pump head and hydraulic efficiency. This degradation is primarily attributed to the increase in effective viscosity and associated internal hydraulic losses. Furthermore, emulsion stability is shown to play a critical role, where stable emulsions consistently exhibit superior pump performance compared to unstable emulsions at identical oil concentrations and operating conditions.

3- The theoretical analysis based on Euler pump theory and loss modeling provides valuable insight into the influence of impeller design parameters on pump performance. Parametric studies reveal that increasing the number of impeller blades enhances the developed head due to reduced slip effects; however, excessive blade numbers increase hydraulic losses and consequently reduce efficiency. Similarly, blade inlet and outlet angles significantly affect flow incidence, internal flow structure, and energy transfer, indicating the existence of optimal geometric configurations for maximizing pump performance.

4- Numerical simulations conducted using ANSYS Fluent successfully capture the internal flow behavior within the impeller and volute. The steady-state rotating reference frame approach, combined with the SST k-ω turbulence model, yields satisfactory agreement with experimental performance curves. CFD results highlight the relationship between flow separation, velocity non-uniformity, and performance degradation, providing a detailed physical interpretation of experimentally observed trends.

5- Overall, the findings confirm that impeller geometry exerts a dominant influence on centrifugal pump performance relative to moderate variations in emulsion properties. The

integrated methodology adopted in this thesis offers a robust framework for analyzing and optimizing centrifugal pump operation under contaminated or emulsified fluid conditions.

7.2 RECOMMENDATIONS FUTURE WORK

1. Advanced Multiphase Modeling

Future studies should incorporate multiphase CFD models, such as Eulerian-Eulerian or Volume of Fluid (VOF) approaches, to explicitly capture droplet dynamics, phase interactions, and emulsion stability effects beyond effective single-phase assumptions.

2. Unsteady Flow and Transient Analysis

Transient simulations using sliding mesh techniques are recommended to investigate pressure pulsations, blade-volute interaction, and unsteady flow structures that may influence pump performance, vibration, and noise.

3. Extended Operating Conditions

The influence of rotational speed, Reynolds number, and higher oil volume fractions should be examined to assess performance scalability and operational limits under more severe contamination levels.

4. Cavitation and Thermophysical Effects

Future work may include cavitation modeling and temperature-dependent fluid properties to evaluate their combined impact on pump performance, particularly in high-load or high-temperature applications.

5. Experimental Enhancement and Uncertainty Reduction

Improved experimental diagnostics, such as high-speed visualization and particle image velocimetry (PIV), could be employed to validate CFD predictions and quantify internal flow phenomena more accurately.

6. Optimization and Design Automation

Coupling CFD simulations with optimization algorithms or machine-learning-based surrogate models could enable automated impeller design optimization for emulsified and contaminated fluid applications.

7. Industrial Scale and Long-Term Performance

Further investigations should address scale-up effects, wear mechanisms, and long-term operational stability to facilitate industrial implementation of the proposed design insights.

REFERENCES

References

1. Langevin, D., Poteau, S., Hénaut, I., Argillier, J.F., “Crude oil emulsion properties and their application to heavy oil transportation”, Oil & gas science and technology, vol. 59, issue 5, pp. 511-521, 2004.

2. Al-Wahaibi, T., Al-Wahaibi, Y., Al-Hashmi, A.R., Mjalli, F.S., Al-Hatmi, S., “Experimental investigation of the effects of various parameters on viscosity reduction of heavy crude by oil-water emulsion”, Pet. Sci., vol. 12, pp.170–176, 2015.

3. Halboose, A.T., Hussein, M.Y., Aziz., R.J., “Study of the effect of Water content and Temperature on the stability of Crude Oil/Water Emulsions”, Journal of the College of Basic Education College. Al Mustansiriyah University, vol. 20, issue 86, pp. 897-992, 2014.

4. Achour, L., Specklin, M., Belaidi, I., Kouidri, S., “Numerical study of the performance loss of a centrifugal pump carrying emulsion”, E3S Web of Conferences 321, 01010 (2021), ICCHMT, 2021.

5. Pal, R. and Rhodes, E., “Emulsion flow in pipelines”, International Journal of Multiphase Flow, 15(6): pp. 1011-1017, 1989.

6. Pal, R., “Pipeline flow of unstable and surfactant-stabilized emulsions”, AICHE Journal, 39(11): pp. 1754-1764, 1993.

7. Ismail, A., “Modeling Friction Factor and Drag Reduction Of The Unstable W/O Emulsions In Horizontal Pipe”, Al-Azhar University Engineering Journal, 8: pp. 10-24, 2005.

8. Nädler, M. and Mewes, D., “Flow-induced emulsification in the flow of two immiscible liquids in horizontal pipes”, International Journal of Multiphase Flow, 23(1): pp. 55-68,1997.

9. Khalil, M.F., Kassab, S.Z., Ismail, A.S., Elazab, I.S., “Influence of Various Parameters on the Characteristics of Stable and Unstable Oil-in-Water Emulsion”, 8th International Conference of Fluid Dynamics and Propulsion. In Proceedings of the ASME 8th International Conference of Fluid Dynamics and Propulsion, Sharm El-Shiekh, Sinai, Egypt, 2006.

10. Khalil, M. and Kassab, S.Z., “Friction Losses of Oil-in-Water Emulsions Flow through Pipes”, in Proc. Cairo 10-th Int. Conf. on Energy and Environment (EE10), 2007.

11. Turian, R., Ma, T.W., Hsu, F.L.G., Sung, D-J.M., Plackmann, G.W., “Flow of concentrated non-Newtonian slurries: 2. Friction losses in bends, fittings, valves and Venturi meters. International journal of multiphase flow”, vol. 24, issue 2, pp. 243-270, 1998.

12. Hwang, C.Y. and Pal, R., “Flow of two-phase o/w mixtures through sudden expansions and contractions”, Chemical Engineering Journal, vol. 68, issue 2, pp. 157-163, 1997.

13. Pal, R. and Hwang, C. Y., “Loss coefficients for the flow of surfactant-stabilized emulsions through pipe components”, Chemical Engineering Research and Design, vol. 77, issue 8, pp. 685-691, 1999.

14. Nasr, S., “Hydraulic Resistances”, M.Sc. Thesis, Menoufiya University, Egypt, 1988.

15. Roul, M.K. and Dash, S.K., “Two-phase pressure drop caused by sudden flow area contraction/expansion in small circular pipes”, International Journal for Numerical Methods in Fluids, vol. 66, issue 11, pp. 1420-1446, 2011.

16. Balakhrisna, T., Ghosh, S., Das, G. and Das, P.K., “Oil-water flows through sudden contraction and expansion in a horizontal pipe -Phase distribution and pressure drop”, International Journal of Multiphase Flow, vol. 36, issue 1, pp. 13-24, 2010.

17. Buhidma, A. and Pal, R., “Flow measurement of two-phase oil-in-water emulsions using wedge meters and segmental orifice meters”, The Chemical Engineering Journal and The Biochemical Engineering Journal, vol. 63, issue 1, pp. 59-64, 1996.

18. Khalil, M., Kassab, S.Z., Ismail, A.S. and Elazab, I.S., “Energy Losses of Oil-in-Water Emulsions Flow through Pipe Fittings using Image Processing”, International Review of Mechanical Engineering, vol. 5, issue 1, pp. 143-163, 2011.

19. Perissinotto, R., De Cerqueire, R., Verde, W., “Visualization of oil-water emulsion formation in a centrifugal pump stage”. Conference: 51st turbomachinery & 38th pump symposia (TPS 2022) at Huston Texas, 2022.

20. Augusto Vieira Bulgarelli, N. Luiz Biazussi, J. Monte Verde, W. Eduardo Perles, C., "Relative Viscosity Model for Oil/Water Stable Emulsion Flow within Electrical Submersible Pumps", *Chemical Engineering Science*, Vol 245,116827, 2021.

21. Zhang, R., Yun, L., Li, J. "The effect of impeller slot jet on centrifugal pump performance", Journal of Hydrodynamics, vol. 31, 2018.

22. Li, X., Gao, P., Zhu, Z., Li, Y., "Effect of the blade loading distribution on hydrodynamic performance of a centrifugal pump with cylindrical blades", Journal of Mechanical Science and Technology, vol. 32, pp. 1161-1170, 2018.

23. Barth, T. and Jespersen, D., "The design and application of upwind schemes on unstructured meshes", 27th Aerospace Sciences Meeting, American Institute of Aeronautics and Astronautics. Reno, NV, U.S.A, 1989.

24. . Chorin, A.J., "Numerical solution of the Navier-Stokes equations", Math. Comp., vol. 22, issue 104, pp. 745-762, 1968.

25. Shih, T.H., Liou, W.W., Shabbir, A., and Zhu, J., "A New k-€ Eddy-Viscosity Model for High Reynolds Number Turbulent Flows - Model Development and Validation", Comput. Fluids., vol. 24, issue 3, pp. 227-238, 1995.

26. Bai, L., Zhou, L., Han, C., Zhu, Y., and Shi, W., "Numerical Study of Pressure Fluctuation and Unsteady Flow in a Centrifugal Pump", MDPI. Processes, vol. 7, no. 3542019, 2019.

27. Nicholas Pedersen, Poul S. Larsen, "Flow in a Centrifugal Pump Impeller at Design and Off-Design Conditions Part I: Particle Image Velocimetry (PIV) and Laser Doppler Velocimetry (LDV) Measurements", Journal of Fluids Engineering, Vol. 125, pp 61-72, 2003.

28. Ning Zhang, Fankun Zheng, Xiaokai Liu, Bo Gao, and Guoping Li, "Unsteady flow fluctuations in a centrifugal pump measured by laser Doppler anemometry and pressure pulsation", Phys. Fluids 32, 125108, 2020.

29. Abo Elyamin, G.R.H., Bassily, M.A., Khalil, K.Y., Gomaa, M. S., "Effect of impeller blades number on the performance of a centrifugal pump", Alexandria Engineering Journal, vol. 58, pp. 39-48, 2019.

30. Grapsas, V., Stamatelos, F., Anagnostopoulos, J. and Papantonis, D., "Numerical Study and Optimal Blade Design of a Centrifugal Pump by Evolutionary Algorithms. Knowledge-Based Intelligent Information and Engineering Systems", 12th International Conference, KES, Zagreb, Croatia, 2008.

31. Xu, Y., Yang, A. L., Lang, D. P. and Dai, R., "Blade design loads on the flow exciting force in centrifugal pump", IOP Conf. Series: Earth and Environmental Science 15.032026, 2012.

32. Djerroud, M., Ngoma, G.D., and Ghie, W., "Numerical Identification of Key Design Parameters Enhancing the Centrifugal Pump Performance: Impeller, Impeller-Volute, and Impeller-Diffuser", International Scholarly Research Network, ISRN Mechanical Engineering, Volume 2011, 2011.

33. Li, W., ZM. H., "An experimental study on the performance of centrifugal oil pump", Fluids and Engineering. Volume 119, 1997.

34. Cheah, K.W., Lee, T. S., Winoto, S. H., and Zhao, Z.M., "Numerical Flow Simulation in a Centrifugal Pump at Design and Off-Design Conditions", International Journal of Rotating Machinery, vol. 2007, Article ID 83641, 2007.

35. Omar, A.K., Khaldi, A., and Ladouani, A., "Prediction of centrifugal pump performance using energy loss analysis", Australian Journal of Mechanical Engineering, vol. 15, issue 3, pp. 210-221, 2017.

36. Shojaeefard, M. H., Rizi, B.S., Khalkhali, A., Tahani, M., "A New Method to Calculate Centrifugal Pump Performance Parameters for Industrial Oils", JAFM, vol. 8, no. 4, pp. 673-681, 2015.

37. Tang, C., and Kim, Y.J., "Optimization for a centrifugal pump transporting brine using an orthogonal design based on CFD-DEM simulation", 2021 IOP Conf. Ser.: Mater. Sci. Eng. 1043 022061, 2021.

38. Williams, R.W., and Skelley, S. E., "Comparison of Unshrouded Impeller Analysis and Experiment", Joint Propulsion Conference and Exhibit. 37th AIAA/ASME/SAE/ ASEE. Salt Lake City, Utah. USA, 8-11, 2001.

39. Sugiyama, D., Ichinose, A., Takeda, T., Miyagawa, K., Negishi, H., Tsunoda, A., "Investigation of Internal Flow in Centrifugal Pump Diffuser using Laser Doppler

Velocimetry (LDV) and Computational Fluid Dynamics", J. Phys.: Conf. Ser. no. 1909 012075, 2021.

40. Ayada, A.F., Abdallaa, H.M., Aly, A.A., "Effect of semi-open impeller side clearance on the centrifugal pump performance using CFD", Aerospace Science and Technology, vol. 47, 2015.

41. Li., W., "Effects of flow rate and viscosity on slip factor of centrifugal pump handling viscous oils", International Journal of Rotating Machinery. Volume 2013, 2013.

42. Li., W., "Effects of blade exit angle and liquid viscosity on unsteady flow in centrifugal pumps", Journal of Power and Energy, vol. 226, 2012.

43. Li., W., "Numerical study on the behavior of a centrifugal pump when delivering viscous oils - Part 1: Performance", International Journal of Turbo and Jet Engines, vol. 25, issue 2, 2008.

44. Li., W., "Numerical Study on Behavior of a Centrifugal Pump When Delivering Viscous Oils-Part 2: Internal Flow", International Journal of Turbo and Jet Engines, vol. 25, Issue 2, 2008.

45. Shojaeefard, M.H., Tahani, M., Ehghaghi, M.B., Fallahian, M.A., Beglari, M., "Numerical study of the effects of some geometric characteristics of a centrifugal pump impeller that pumps à viscous fluid", Computers & Fluids, vol. 60, 2012.

46. Liu, Z., Ji, L., Pu, W., Li, W., Yang, Q., Zhang, X., Yang, Y., Shi, W., Tian, F., Jiang, S., "Research on Efficiency Improvement Technology of Wide Range Centrifugal Pump Based on Genetic Algorithm and Internal Flow Loss Diagnosis", Water 2024, *16*, 3402, 2024.

47. Wang, Y. Y., Zhao, W. G., Han,X. D., Fan, P. J., Liu, Z. L. and Hu., J. Q., "Effects of the Centrifugal Pump Outlet Blade Angle on Its Internal Flow Field Characteristics under Cavitation Condition", Journal of Applied Fluid Mechanics, Vol. 16, No. 2, pp. 389-399, 2023.

48. Wilcox, D. C. "Formulation of the k-ω turbulence model revisited", *AIAA Journal* 46(11), 2823-2838, 2008.

49. Munson, B. R., Young, D. F., and Okiishi, T. H., "Fundamentals of Fluid Mechanics", 7th Edition, John Wiley & Sons, Inc., 2013.

50. Dixon, S. L., and Hall, C., “Fluid Mechanics and Thermodynamics of Turbomachinery”, Burlington: Butterworth-Heinemann, 2013.

51. Gülich, J.F., “Centrifugal Pumps”, Berlin Heidelberg: Springer. 2008.

APPENDIX A

UNCERTAINTY ANALYSIS

UNCERTAINTY ANALYSIS

Actual volume flow rate

$$Q_{act} = \frac{volume}{time}$$

volume = $6\,x10^{-3} \pm 0.2\,x10^{-3}$ m^3

time = 66.9 ± 0.1 sec

$$U_{volume} = \frac{error}{reading} = \frac{0.2x10^{-3}}{6x10^{-3}} = 0.0333$$

$$U_{time} = \frac{error}{reading} = \frac{0.1}{66.9} = 0.00149$$

Uncertainty in Q at confidence level 95% can be obtained from

$$U_R = \pm\left[\left(\frac{X_1}{R}\frac{\partial R}{\partial X_1}U_{X_1}\right)^2 + \left(\frac{X_2}{R}\frac{\partial R}{\partial X_2}U_{X_2}\right)^2 + \text{---------} + \left(\frac{X_n}{R}\frac{\partial R}{\partial X_n}U_{X_n}\right)^2\right]^{1/2}$$

$$U_Q = \pm\left[\left(\frac{volume}{Q_{act}}\frac{1}{time}U_{volume}\right)^2 + \left(\frac{time}{Q_{act}}\frac{-volume}{time^2}U_{time}\right)^2\right]^{1/2}$$

$$U_Q = \pm[(U_{volume})^2 + (-U_{time})^2]^{1/2}$$

$$= \pm[(0.0333)^2 + (0.00149)^2]^{1/2}$$

$$= \pm 0.033366 = \pm 3.33\%$$

APPENDIX B

PUBLICATIONS

PUBLICATIONS

1- Noureldin, M., El-Gamal, H., Hanafy, A., Ibrahim, K., Afify, R., "**Enhancing Centrifugal Pump Performance by Varying the Pump Rotational Speed, Number of Blades, and Working Fluid Characteristics**", 10th International Conference on Advanced Technology and Applied Science (ICaTAS 2025), AASTMT, Cairo, Egypt, 21-23 October, 2025.

2- Noureldin, M., El-Gamal, H., Hanafy, A., Ibrahim, K., Afify, R., "**Assessment of impeller geometry effects on centrifugal pump performance with aqueous emulsion flows**", Journal of Engineering and Applied Science, vol. 73, no. 34 (2026). https://doi.org/10.1186/s44147-026-00884-0

تحليل أداء مضخة طرد مركزى ذات عدد شفرات وزوايا متغيرة فى ظل تدفقات مستحلب مستقرة وغير مستقرة: بإستخدام أساليب تجريبية وتحليلية ورقمية

تُعد المضخات الطاردة المركزية ضرورية لأنظمة نقل السوائل الصناعية لضمان كفاءتها فى إستهلاك الطاقة. تسد هذه الدراسة فجوة بحثية هامة من خلال دراسة تأثير شكل المروحة على المضخات التى تتعامل مع مستحلبات الزيت والماء ذات التركيز الضئيل (0.2% - 0.05%). وكان الهدف الرئيسى هو تحسين عدد الشفرات (z: 5-7)، وزاوية الدخول (β1: 10° - 30°)، وزاوية الخروج (β2: 20° - 30°) خلال مراحل استقرار المستحلب المختلفة. وقد توصلت الدراسة إلى نقطة هندسية مثالية لتحسين الأداء باستخدام تقنيات تجريبية وتحليلية ورقمية متكاملة. في الدراسة الرقمية تم استخدام برنامج Ansys CFD مع SST k-ω. كما تم تحديد نسبة عدم اليقين في معدل التدفق فى النهج التجريبى بقيمة ٣,٣% عند مستوى ثقة 95% . يعد اكتشاف أن عدد الشفرات z = 6، وزاوية الدخول β1 = 20°، وزاوية الخروج β2 = 30° تقلل بشكل ملحوظ من الفاقد الهيدروليكى مع المستحلبات منخفضة التركيز، مما يُنتج أعلى ضغط وكفاءة قصوى، اكتشافًا مبتكرًا. كما تُظهر النتائج أن المستحلبات المستقرة تُؤدى أداءً أفضل من المستحلبات غير المستقرة، وأن الكفاءة تنخفض بشكلٍ طفيف مع زيادة التركيز. تقدم هذه النتائج - التى تم التحقق من صحتها من خلال التوافق بين جميع التقنيات - رؤى عملية للصناعات الكيميائية والبترولية، ولا سيما فيما يتعلق بنقل المواد متعددة الأطوار، وأنظمة التبريد، وتحسين التشحيم.

وتتكون الرسالة من ستة أبواب بالإضافة إلى قائمة بالمراجع ويمكن تلخيصها كالتالى:-

الباب الأول:

ويشمل المقدمة الخاصة بالبحث والتي تتضمن أهمية و استخدامات المضخات المائع المستحلب (ماء + زيت) فى مجالات الحياة.

الباب الثانى:

ويشمل مراجعة شاملة للأبحاث السابقة التى تم نشرها فى مجال البحث. ثم ينتهى هذا الباب بأهم الاستنتاجات من الأبحاث السابقة وكذلك الهدف من البحث الجارى.

الباب الثالث:

ويشتمل عل وصف الجهاز المستخدم فى تنفيذ تجارب تقييم أداء المضخة وطريقة تحضير الخليط بالنسب المختلفة وخطوات رفع القياسات والأجهزة المستخدمة.

الباب الرابع:

ويشتمل على عرض وتحليل تفصيلى للنتائج المعملية التى تم الحصول عليها لكل الشفرات , وهى عبارة عن نتائج تأثير عدد الشفرات و نتائج تأثير زاوية الدخول وزاوية الخروج ونتائج تأثير نسبة تركيز الزيت فى الخليط على أداء المضخة المستخدمة فى هذا البحث. وأخيراً تم دراسة تأثير الإستقرارية وعدم الإستقرارية للخليط المستخدم على الأداء.

الباب الخامس:

ويعرض دراسة تحليلية و وصفا للنماذج الحسابية للشفرات المختلفة . كذلك يقدم دراسة للعوامل المختلفة التى تتحكم فى أدائه. كما يوضح طريقة عمل النماذج الحسابية إجراءات التحقق والتثبت المناسبة. كما يوضح كذلك نتائج تأثير نسبة تركيز الزيت فى الخليط على الأداء.

الباب السادس:

ويشتمل على عرض للطرق الحسابية فى ديناميكا الموائع (CFD) وتحليل تفصيلى للنتائج العددية التي تم الحصول عليها لكل النواشر الشفرات , وهى عبارة عن نتائج تأثير عدد الشفرات و نتائج تأثير زاوية الدخول وزاوية الخروج وتمت دراسة وتحليل خطوط السريان داخل المضخات للكشف عن اماكن حدوث الانفصال وتأثير ذلك على أداء المضخات فى ظل إستخدام الماء فقط كوسيط.

الباب السابع:

ويعرض هذا الباب ملخص نتائج البحث، حيث يحتوى على أهم الإستنتاجات التى تم استخلاصها من هذه الدراسة ونوجز أهمها فى الآتى:

- تغيير عدد الشفرات يؤثر على أداء المضخة
- زيادة زاوية الخروج للشفرة تحسن من أداء المضخة
- يعطى الخليط مستقرفى المضخة أداء أفضل من الخليط الغيرالمستقر
- وينبغى التوضيح أن النتائج والاستنتاجات التى قدمتها هذه الدراسة مفيدة للعاملين فى الصناعات الكيميائية والبترولية.

وكذلك يشتمل على طرح أفكار ومقترحات مستقبليه يمكن إجرائها فى مجال سريان مائع مستحلب خلال مضخات الطرد المركزية كما يشتمل على ما تم نشره للباحث من هذه الدراسه.

الأكاديمية العربية للعلوم والتكنولوجيا والنقل البحرى
كليـــــة الهندســـــة والتكنولوجيـــــــــــا
قسم الهندسة الميكانيكية

تحليل أداء مضخة طرد مركزى ذات عدد شفرات وزوايا متغيرة فى ظل تدفقات مستحلب مستقرة وغير مستقرة: بإستخدام أساليب تجريبية وتحليلية ورقمية

إعداد
محمد السيد محمد عبد العال نور الدين

رسالة مقدمة للأكاديمية العربية للعلوم والتكنولوجيا والنقل البحرى لاستكمال متطلبات نيل درجة

دكتوراه الفلسفة
فى
الهندسة الميكانيكية

إشراف

الأستاذ الدكتور حسن أنور الجمل
كلية الهندسة
جامعة الأسكندرية

الأستاذ الدكتور أحمد أحمد حنفى
كلية الهندسة والتكنولوجيا
الأكاديمية العربية للعلوم والتكنولوجيا
والنقل البحرى- الأسكندرية

الاستاذ الدكتور رولا سمير عفيفى
كلية الهندسة والتكنولوجيا
الأكاديمية العربية للعلوم والتكنولوجيا
والنقل البحرى- الأسكندرية

2026